Non-linear finite element modelling of reinforced concrete slabs

Mohammed Sajid Ali Abbasi

Civil Engineering

July 1991

Abstract

This research was motivated by the occurrence of premature damage in a number of concrete bridge decks in the form of severe cracking and pot hole type of failures in the Kingdom of Saudi Arabia entailing high expenses of repair and maintenance.

The primary objective of the research was to develop a generalized computer model for reinforced concrete slabs using nonlinear finite element analysis by modeling various forms of degradation in the material throughout the loading history.

The influence of several material parameters such as yield criterion of concrete, hardening of concrete, cracking of concrete, shear degradation, crushing of concrete, dowel effect and elasto-plastic behavior of steel on the failure of reinforced concrete slabs was studied. Also the structural parmeters were varied in order to study the influence of several factors on the metamorphosis in failure modes of reinforced concrete slabs.

Based on this study, the mechanisms of commonly observed failure modes including those of flexure and punching shear occurring in bridge deck slabs have been explained.

Order Number 9402445

Non-linear finite element modelling of reinforced concrete slabs

Abbasi, Mohammed Sajid Ali, Ph.D.

King Fahd University of Petroleum and Minerals (Saudi Arabia), 1991

U·M·I
300 N. Zeeb Rd.
Ann Arbor, MI 48106

NON-LINEAR FINITE ELEMENT MODELLING OF REINFORCED CONCRETE SLABS

BY

MOHAMMED SAJID ALI ABBASI

A Thesis Presented to the

FACULTY OF THE COLLEGE OF GRADUATE STUDIES

KING FAHD UNIVERSITY OF PETROLEUM & MINERALS

DHAHRAN, SAUDI ARABIA

In Partial Fulfillment of the
Requirements for the Degree of

DOCTOR OF PHILOSOPHY

In

CIVIL ENGINEERING

July 1991

KING FAHD UNIVERSITY OF PETROLEUM & MINERALS

DHAHRAN, SAUDI ARABIA

This Dissertation, written by **Mohammed Sajid Ali Abbasi** *under the direction of his Dissertation Advisor and approved by his Dissertation committee, has been presented to and accepted by the Dean of the College of Graduate Studies, in partial fulfillment of the requirements for the degree of* DOCTOR OF PHILOSOPHY IN CIVIL ENGINEERING

Dissertation Committee

Chairman (Prof. Mohammed H. Baluch)

Co-Chairman (Prof. Abul K. Azad)

Member (Dr. Ghazi J. Al-Sulaimani)

Member (Dr. Hamdan N. Al-Ghamdi)

Member (Dr. Mohammed A. El-Gebeily)

14-1-92

Dr. Ghazi J. Al-Sulaimani
Department Chairman

Dr. Ala H. Al-Rabeh
Dean College of Graduate Studies

Date : July, 1991.

This dissertation is dedicated

to

my parents

ACKNOWLEDGEMENT

Firstly, I thank ALLAH, All the Praise is for Him, the All Kind and Merciful, Who bestowed me with the strength to complete the work. Then acknowledgement is due to King Fahd University of Petroleum and Minerals for supporting this research work.

I acknowledge my deep gratitude and appreciation to my major advisor Prof. M. H. Baluch for providing me with inspiration, encouragement and continuous guidance all the way. I am also indebted to co-advisor of dissertation committee Prof. A. K. Azad for his valuable comments throughout this work. I am also grateful to the other committee members Dr. G. J. Al-Sulaimani, Dr. H. N. Ghamdi and Dr. M. A. Al-Gebeil for their valuable suggestions and comments they made to improve the work.

I must acknowledge the computer support offered by Data Processing Centre of KFUPM that made the research work possible.

I once again thank Dr. G. J. Al-Sulaimani who as a Chairman of Civil Engineering Department lent considerable help and encouragement. It is a pleasure to acknowledge the company provided by Mr. Ziraba Y. N. during this work, which made it enjoyable.

Finally I thank my parents and my wife who, through their moral support, have permitted me to indulge my passion for the long task of completing this work.

TABLE OF CONTENTS

LIST OF TABLES

LIST OF FIGURES

DISSERTATION ABSTRACT

NAME OF STUDENT	*: MOHAMMED SAJID ALI ABBASI*
TITLE OF STUDY	*: NON-LINEAR FINITE ELEMENT MODELLING OF REINFORCED CONCRETE SLABS*
MAJOR FIELD	*: CIVIL ENGINEERING*
DATE OF DEGREE	*: JULY, 1991*

This research was motivated by the occurrence of premature damage in a number of concrete bridge decks in the form of severe cracking and pot hole type of failures in the kingdom of Saudi Arabia entailing high expenses of repair and maintenance.

The primary objective of the research was to develop a generalized computer model for reinforced concrete slabs using nonlinear finite element analysis by modeling various forms of degradation in the material throughout the loading history.

The influence of several material parameters such as yield criterion of concrete, hardening of concrete, cracking of concrete, shear degradation, crushing of concrete, dowel effect and elasto-plastic behavior of steel on the failure of reinforced concrete slabs was studied. Also the structural parameters were varied in order to study the influence of several factors on the metamorphosis in failure modes of reinforced concrete slabs.

Based on this study, the mechanisms of commonly observed failure modes including those of flexure and punching shear occurring in bridge deck slabs have been explained.

DOCTOR OF PHILOSOPHY

KING FAHD UNIVERSITY OF PETROLEUM AND MINERALS

Dhahran , Saudi Arabia

July 1991

خلاصة الرسالة

اسم الطالب : محمد ساجد علي عباسي .

عنوان الرسالة : نموذج أجزاء محدودة غيرخطي لبلاطات الخرسانة المسلحة .

التخصص : هندسة مدنية .

تاريخ الدرجة : يوليو ١٩٩١م .

إن هذا البحث كان محفزاً بسبب تضرر بلاطات عدد من الجسور الخرسانية في المملكة العربية السعودية رغم قصر عمرها . هذا الضرر يكون بشكل تشققات وحفر دائرية مما يجعل عملية الاصلاح والصيانة باهظة التكاليف .

والهدف الأساسي من هذا البحث هو تطوير نموذج حاسب آلي عام لبلاطات الخرسانة المسلحة باستخدام التحليل غير الخطي بالأجزاء المحدودة عن طريق عدة نماذج لتآكل أو تضاعف المواد طوال تاريخ التحميل .

هذا وقد تمت دراسة تأثير عدة عوامل على تحطم بلاطات الخرسانة المسلحة مثل نظرية حد المرونة والتصلب والتشقق وانخفاض مستوى قوى القص بالاضافة إلى التهشم أو التفتت بالنسبة للخرسانة ، كذلك أخذ في الحسبان التأثير الوتدي والسلوك المرن - اللدن للحديد . بالاضافة إلى ذلك فقد اعتبرت عدة متغيرات انشائية حتى يتبين تأثير تلك العوامل على التحول في طريقة سقوط بلاطات الخرسانة المسلحة .

واعتماداً على هذه الدراسة ، فقد حاولنا أن نشرح آلية طرق السقوط أو التحطم الشائعة في واقعنا مثل التهشم الانثنائي والقص الثقبي .

دكتوراة الفلسفة

جامعة الملك فهد للبترول والمعادن

الظهران ، المملكة العربية السعودية

يوليو ١٩٩١م

Chapter 1

INTRODUCTION

1.1 BACKGROUND TO THE PROBLEM

A number of concrete bridge decks suffered premature damage in the form of severe cracking and pot hole type of failures in the kingdom of Saudi Arabia entailing high expenses of repair and maintenance. In view of this, a national research project [1] was sponsored by King Abdulaziz City for Science and Technology (KACST) to investigate the cracking of bridge decks in Saudi Arabia. In this project a series of experiments were conducted in order to study pattern of crack formation, crack growth and overall failure modes of girder-slab type reinforced concrete (R/C) concrete panels. Although this thesis is not formally a part of that research program, the motivation behind the work reported herein is to develop a parallel nonlinear computational model based on finite element methodology in order to study the flexure/shear response of R/C slabs by modelling various damage components.

It has been observed that due to in plane compressive forces induced by support restraints the flexural capacity is enhanced considerably. This behavior is often referred to as arching action or compressive membrane action. In view of the evidence of existence of the favourable influence of membrane forces Ontario Bridge Code [2] has

introduced an empirical design method using 0.3% isotropic steel at both top and bottom faces of the slab. This approach is based on the assumption that the most likely mode of failure is the flexural mode of failure and the possibility of failure precipitated by other localized mechanism under occasional heavy repetitive wheel loads precluded. Experiments [3] made it evident that progressive crack nucleation impairs the punching capacity and forms a closed envelop creating in effect a surface of separation leading to premature punching failure. Such a metamorphosis in failure modes from global failure to localized failure calls for comprehensive non-linear computational analysis in order to assess the contribution of various damage components and to find the actual collapse mechanism.

There are several aspects to the nonlinear analysis of such structural problems. The major aspect is the constitutive modelling of the material as it degrades throughout the load history. Other aspects include the development of the computational model to analyze a structure subjected to certain loads and the numerical solution of the nonlinear problem. Finite element technique has been evolved to be the most powerful computational model to analyze such structural problems.

1.2 SCOPE AND OBJECTIVES

The scope of this thesis is the static nonlinear finite element analysis of R/C slabs subjected to distributed patch loading. Attention is focussed on rectangular R/C slabs, which are treated using layered, 9-node Lagrangian element formulation. Displacements are small and

temperature, creep and shrinkage effects are out of scope of this work. Also bond behavior is assumed to be perfect. Experimental data on flexure/shear behavior of R/C slabs as available in the literature is used to verify the computational model developed.

The primary objectives of the proposed research are as follows:

1. To develop a generalized computer model using nonlinear finite element analysis for the prediction of flexure and shear response of R/C concrete slabs by modelling various forms of degradation in the material throughout the loading history.
2. To use this software to implement some of the existing elasto-plastic constitutive models for concrete. The software would be written in a modular form, rendering it convenient to accommodate new developments in constitutive modelling of concrete.
3. To present the full range sensitivity study of various components of material model on the response of R/C slabs.
4. To explain the mechanisms of various failure modes of R/C slabs such as flexural, flexure-shear and punching shear.
5. To study the influence of several factors on the metamorphosis in failure modes of R/C slabs.

The various components of the nonlinear model are chosen so as to reflect :

1. yielding of concrete according to an appropriate stress yield criterion with hardening.
2. cracking of concrete with tension stiffening
3. shear degradation of cracked concrete.
4. elasto-plastic yielding of steel.

4. crushing of concrete according to a strain criterion.

1.3 LITERATURE REVIEW

There exists voluminous literature addressing the flexural response of slabs, especially pertaining to enhancement of slab strength due to compressive membrane action [4-7], with a worldwide consensus on its behavior. As far the shear and shear/flexure interactive failures are concerned there appears to be a lack of consensus on the role of the various characteristic parameters influencing such failures. This is reflected in the conservative approach adopted by the design codes, with the American Concrete Institute (ACI 318-83) Code not reflecting the beneficial effect of main reinforcement on punching resistance, and both British Standards (BS 8110 : 1985) and ACI neglecting any contribution of edge restraint to punching capacity. Also the punching shear capacity is proportional to the square root of the concrete strength in ACI whereas in BS 8110 the shear capacity of the concrete is proportional to cube root of the concrete strength. Moreover in the design codes the punching shear strength of a concrete slab is usually checked by considering a cylindrical surface around the loaded area (column section) at a distance equal to the effective slab depth or a fraction of it as the critical punching section whilst the actual failure surface is by no means cylindrical as borne out from the experiments.

In order to overcome the limitations of empirical design methods, theoretical approaches were tried. There have been three main types of theoretical approaches. One is the rotational model introduced by

Kinnunen and Nylander [8,9], the second is from the application of perfect plasticity theory by Nielsen et al [10] and the last is based on a truss model developed by Andra [11] and Van Dusen [12]. All these methods have divergence features making their general acceptance difficult. The Kinnunen and Nylander approach seems to give the best account of both slab behavior and the factors affecting punching resistance, but involves various assumptions of questionable validity. In this model the slab is considered to be divided into rigid segments each bounded by two radial crack lines. Hewitt and Batchelor [13] used Kinnunen and Nylander model and incorporated effect of edge restraint. Shehata and Regan [14] improved the Kinnunen and Nylander model in many ways. They assumed that at near failure a rigid wedge element, bounded by the internal inclined crack and the initial circumferential crack, is detached from each radial segment and rotates independently around the center of rotation. These models include the effect of ratio of reinforcement and its yield strength, effect of ratio of slab radius to its thickness and the influence of concrete strength on punching resistance.

Expressions for punching collapse load using plasticity theory have been presented by Braestrup, M. W., et al [15], Nielsen,M.P. [10]. A modified Mohr-Coulomb was used as the failure criterion for concrete. Braestrup M. W. [15] suggested parabolic failure envelope combined with a circular tension cut-off. More recently, Jiang and Shen [16] presented a similar model using a second-degree parabola to simulate the Mohr-Coulomb failure locus. Bortolotti [17] included strain softening of concrete in the form of failure surface generatrix.

The application of plasticity theory for punching failure modelling was questioned by Bazant and Cao [18] in view of its brittle mode of failure. The reason presented is that concrete does not exhibit a horizontal yield plateau after reaching the failure envelope, but exhibits a strain softening. Consequently, the limit states are not reached simultaneously at various points of the failure surface in concrete. Rather, they are reached in sequence, so the failure zone propagates. Further they added that there is evidence of size effect on the punching shear stress which is the well established phenomenon for brittle fracture type behavior. Thus plastic limit analysis could be applicable only to very small specimens, such that the slab thickness is only a few maximum aggregate sizes. Then, however, the slab is no longer a homogeneous continuum and the applicability of continuum analysis is questionable.

Furthermore the models based on plastic theory completely ignore both dowel and membrane actions of flexural reinforcement. For slabs where the slab diameter is relatively large with respect to punching diameter, as in the general case, the outer part of the slab that surrounds the punching cone does not remain undeformed (rigid disk) while the punching cone has its relative vertical displacement. Also the degree of homogeneity is largely affected by the extensive cracking in radial and tangential directions along the failure surface. These considerations lead to the conclusion that punching resistance of slabs can not be estimated by limit analysis.

Alexander and Simmonds [19] extended the concepts of Van Dusen's [12] truss model and proposed a model consists of a three dimensional

space truss composed of concrete compressive struts and steel tension ties. The reinforcing steel and concrete compressive fields are broken down into individual bar strut units. The compressive struts are assumed of two types: one parallel to the plane of the slab (anchoring struts) and the other at some angle to the plane of the slab (shear struts). They assumed that punching shear failure could be represented by a truss analogy and that failure is due to the concrete cover failing to contain the out-of-plane component of force between the reinforcement and the concrete compressive struts.

Analytical procedures based on experimental data were attempted to predict the punching capacity of slab at interior columns by Long and Bonds [20], Long [21], Gesund and Dikshit [22] and Yitzhaki [23].

Extensive experimental data was produced in the last forty years by many researchers in the realm of punching shear study of R/C slabs: Richart and Kluge [24], Elstner and Hagnested [25], Scordelis et. al [26], Kinnunen and Nylander [8], Moe [27], Anderson [28], Kinnunen [9], Taylor and Hayes [29], Mowrer and Vanderbilt [30], Corley and Hawkins [31], Criswell [32], Gerber and Burns [33], Masterson [34], Aoki and Seki [35], Nylander et. al [36], Kinnunen, Nylander and Tolf [37], Shehata [38], Regan [39,40], Narayan [41], Bazant and Cao [18], Gardner [42] and Dragosavic and Reukel [43], The test results of Taylor and Hayes [29] reflected an interesting phenomenon that the beneficial effect of edge restraint on the failure load, identified as punching, appeared to taper off as the main reinforcement percentage was increased.

In the work presented thus far, the one serious limitation appears

to be the lack of definition of what constitutes a punching failure, and its true failure mechanism at macrocrack level. All the procedures discussed thus far have certain limitations with regard to incorporation of all the effects contributing to the punching capacity and no method includes these effects comprehensively. An alternate, sophisticated and rational procedure is called for in order to clearly understand the mechanism of punching failure explaining how various factors affect such a failure.

To an increasing degree, computational modelling of R/C structures is finding its way as an essential tool towards understanding the comprehensive behavior of these structures considering the complex interactive effects of various parameters. Finite element modelling is one of the most promising method as applied to R/C structures. The earliest published application of the finite element method to R/C structure was by Ngo and Scordelis in March 1967 [44]. Since then enormous amount of work has been done on the material modelling of concrete with the advancement of finite element technique due to development of high speed computers. State of the art papers which review much of research done in North America and Europe from 1967 to 1976 have been published by Scordelis [45], Schnobrich [46,47] and Wegner [48]. From 1977 to 1985 several important events and publications occurred, which gave a strong impetus to research in this field. A state-of-the-art report [49] was published in 1982 by the Task committee of the American Society of Civil Engineers. Recent developments up to 1985 in the realm of non-linear finite element analysis of R/C structures is presented in the state-of-the-art seminars sponsored by Japan Society for

Promotion of Science/U.S. National Science Foundation [50].

Attempts to apply finite element method to punching shear problem have been reported only sporadically. Masterson and Long [51] used this method for punching problem when the complexities in the concrete material were not recognised yet fully. Recently de Borst and Nauta [52] simulated the punching shear in circular slabs by using an axisymmetric model. They used the non-orthogonal cracks within the smeared crack concept. The concrete in compression is modelled as elastic-perfectly plastic using Mohr-Coulomb yield surface. Similar effort has been done by Gonzalez-Vidosa F. et al. [53] in which they also simulated the effect of punching using axisymmetric non-linear finite element modelling and finally presented the mechanism of failure of slabs with and without stirrups in view of the distribution of radial and tangential cracking.

In [52] and [53], the problem is formulated axisymmetrically which is appropriate exclusively for circular slabs in the two dimensional frame work. Such a model can not be applied to rectangular slabs specially when precise modelling of boundary restraint in terms of displacements and rotations are desired in order to see the effect of restraint on punching capacity. Moreover, the perfectly plastic models are used for concrete while it is evident from experiments that concrete exhibits hardening behavior in compression even at lower level of stress. Also the interactive effect of cracking with bond between steel and concrete, known as tension stiffening is completely ignored which has been proven to be an important aspect of modelling of R/C structures.

Considering these limitations of the past work, a nonlinear elasto-

plastic finite element model for R/C slabs using plate bending formulations under generalized triaxial conditions is presented.

1.4 ORGANIZATION OF THESIS

Chapter Two contains the behavior of concrete and a literature review of some of the existing constitutive models for multiaxial behavior of concrete. A yield criterion has been proposed which is simple and reflects most of the characteristics of concrete failure envelope. Also the elasto-plastic formulation of concrete is presented for computer implementation. Modelling of other components such as cracking of concrete with tension stiffening in conjunction with shear degradation, elasto-plastic steel, and crushing of concrete is presented.

In Chapter Three, the finite element model is described. Standard formulations for degenerate plate element are given. Some other aspects of this formulation such as types of elements, layered model, numerical integration are discussed.

A finite element program FATIMA for nonlinear elasto-plastic analysis of R/C slabs is described in Chapter Four. A detailed discussion of important subroutines is presented. The correction of stresses for yielding concrete and steel, cracking and crushing concrete is elaborated.

Chapter Five consists of the verification of the developed computational model as applied to some square and rectangular slabs from literature.

Chapter Six presents a parametric variation study of material, structural, geometrical and finite element parameters on the behavior of R/C slabs. Mechanism of failure modes is presented in the perspective of the influence of reinforcement ratio and support restraint on the metamorphosis of failure modes.

Chapter Seven presents conclusions, suggestions and future scope of the work.

Chapter 2

MATERIAL MODELLING

2.1 INTRODUCTION

With the advancement of finite element technique and availability of high speed computers, there has been a demand for refined and sophisticated models in order to trace the response of reinforced concrete structures in the nonlinear post-cracking and post-yield range. The limitations of linear elastic, plastic and ultimate load theories necessitate the nonlinear analysis by a computational model such as finite element method. Linear elastic theory can never predict the failure stress and the true factor of safety is never determined. To overcome this objection, plastic methods and ultimate load theories have been developed. Since determination of the actual failure stress distribution and collapse mechanism is not straightforward due to complex geometry of structures and loading, these methods can not be relied for important structures. Moreover there is no consideration in these methods for several other factors such as: inplane behavior, failure mechanism of localized failures, effect of load history, etc.

Although the use of finite element technique for R/C structures is highly promising, yet the task of modelling the material behavior was and remains a great challenge. Ever since this method was applied to

R/C structures, concrete material modelling has become a very active area of research. Although a great deal of progress has been made by researchers as seen in the state-of-the-art reports [49,50], continuing research work is still attempting to resolve some of the difficult issues. These include: nonlinear behavior, tension cracking, biaxial stiffening and strain softening phenomenon, modelling of post fracture behavior and interaction effect between the concrete and reinforcing bars. For the development of a mathematical model, the typical experimental data is used for concrete under uniaxial, biaxial and triaxial states of stress in order to simulate the material behavior and to determine the various material constants in the mathematical model.

To model the nonlinear response of concrete as a continuum, four distinct approaches have been employed i.e., nonlinear elasticity based models [54-59], plasticity-based models [60-63], plastic-fracturing models [64,65], and endochronic theory [66-69]. A complete evaluation of these approaches was given in state-of-the-art report [49].

In the nonlinear elasticity based models, nonlinear deformational response of concrete is simulated incrementally as a piecewise linear elastic material with variable moduli. These models have the capability of producing repeated, hysteretic effects in cyclic loading. However, experimental data under reversed loading is still very scarce, thus limiting further developments. Also variable moduli approach does not model accurately the behavior of concrete at high stress levels and it may have the continuity problem when stress paths are on or near neutral loading.

The strain-hardening plasticity models can be considered as a generalization of elastic perfectly plastic models and they satisfy all the basic principles of continuum mechanics such as the requirements of uniqueness and continuity of stress near neutral loading paths. These models use strain-hardening theory of plasticity with an associated flow rule for plastic concrete before fracture. An initial discontinuous surface or elastic limit surface is described similar to the failure surface for uniform hardening. When the material is stressed beyond the initial discontinuous surface, a subsequent new discontinuous surface called the loading surface is developed. This new surface replaces the initial discontinuous surface. If the material is unloaded from and reloaded within this subsequent loading surface, no additional irrecoverable deformation will occur until this new surface is reached. If straining is continued beyond this surface, further discontinuity and additional irrecoverable deformation results. In other words, at each stage of the history of loading there exists a loading surface in stress space containing all states of stress which can be reached by elastic changes and any straining beyond this surface is accompanied by the irrecoverable plastic deformation. Beyond the elastic limit, the normality condition or the so-called associated flow rule is assumed to govern the post yielding stress-strain relations for concrete. Once the loading surface is defined, constitutive equations based on the concept of flow rule can be derived. The stress failure surface in terms of stresses is defined as the outermost extreme of the loading surface similar to that of perfectly plastic yield surface. Crushing surface is expressed in terms of strains to mark the eventual collapse of the yielded material. Once the stress failure surface is reached, the concrete begins to flow under

constant stress.

The theory of incremental plasticity does not take into account microfracturing, which in contrast to plastic phenomena, is accompanied by a degradation of elastic moduli. Plastic theory does not reflect the change in elastic moduli, but rather it accounts only for the plastic slip which is true for the conditions of very high hydrostatic pressure. If the unloading slopes for various points of the stress-strain diagram are known, these two contributions to inelastic behavior can be rigorously distinguished [64]. In contrast to plastic phenomena, the fracturing phenomena are better characterized in terms of a loading surface that depends on strains rather than stresses. Since stress decrease is impossible for strictly plastic behavior, it is the fracturing which is responsible for the strain-softening, i.e., the decline of stress at increasing strain. The fact that the loading surface that governs fracturing should depend on strains rather than stresses may be also concluded from the need to distinguish unloading from loading. If we consider a state on the strain-softening branch, whereas both loading and unloading involve decreasing stress, unloading is distinguished by strain decrease in contrast to loading which registers a strain increase on the softening branch.

Endochronic theory of inelasticity has been proposed to develop a continuous model which may not require the existence of a yield condition, and to be thus free from the cumbersome hardening rules. The endochronic theory was proposed in 1971 by Valanis [70] for the description of mechanical behavior of metals. Valanis showed that by employing a pseudo-time scale, the intrinsic time, a constitutive

equation in integral or differential form can successfully be used to describe metal behaviors including strain hardening, unloading and reloading, cross-hardening and continued cyclic straining. The theory does not require the specific definitions of yielding and hardening. Using Valanis' concept, Bazant and his co-workers have extended the theory to describe behavior of plain concrete and reinforced concrete under various conditions [66-69]. They have also shown that the new constitutive formulations have the capability of correctly predicting the nonlinear effect, creep behavior and concrete response subjected to cyclic loadings. Although some fundamental questions of the theory seem to need further studies, it appears to have remarkable potential of practical applications. One of the main advantages for employing an inelastic theory without a yield condition is its tractability in the numerical analysis of two-dimensional or three-dimensional problems, particularly when the problem involves complicated cyclic loading histories. Further research in refining this theory is needed in order to circumvent the limitations of the theory to satisfy the basic principles of continuum mechanics and to reduce the number of material constants without sacrificing accuracy. Despite the obvious generality of this theory, it is not used as a widely accepted modelling tool.

In addition to the nonlinear stress strain response, concrete cracking is one of the major contributing factors to material nonlinearities. Generally, two types of crack models, i.e., a discrete model and a smeared model, have been employed by the analysts; the latter became popular for purposes of application. Reinforced concrete is considered as a composite material. On the macroscopic level, it consists of two

major components: steel reinforcement and concrete. In the modelling of its stress-strain behavior, a general approach is to treat the response of each component separately, then obtain the combined effects by imposing the conditions of material continuity. In the present work the behavior assumed for steel is extrapolated from an idealized one dimensional bilinear elasto-plastic curve. The steel reinforcement is assumed as a smeared layer in the direction of rebars. Modelling of concrete cracking is further complicated by the interaction effects between the cracked concrete and the steel reinforcements. These include tension stiffening, shear transfer due to dowel action, and bond slip. Several techniques in the modelling of tension stiffening have been suggested by various researchers [71-74]. It was recognized that the overall nonlinear response of a reinforced concrete structure is significantly affected by tension stiffening. Another important aspect in the analysis of reinforced concrete structures is the consideration of shear transfer behavior. Shear can be transferred through aggregate interlock and dowel action across the cracked concrete sections [75]. In the finite element analysis, such effect can be treated either using elastic spring elements [76], or by reducing the shear stiffness of cracked concrete [77]. Due to its simplicity, the latter approach is more useful for computational purpose. The post-cracking softening of concrete and tension stiffening due to bond effects between steel bars and concrete are accounted in this model. The cracked concrete is modeled to lose shear stiffness gradually as the cracks become wider and with the closure of cracks the shear stiffness is assumed to resume its full value.

To account for the effect of steel reinforcement in stiffness calcula-

tions, three alternative approaches can be used: smeared model, embedded model and discrete model. A review of these methods is given in [49]. In the smeared model, the reinforcement is assumed to be distributed uniformly over the element. Assuming perfect bonding between concrete and reinforcement, the constitutive relations can be derived from the composite theory. On the other hand, when the rebars are sparsely located in the reinforced concrete member, either the embedded or discrete model becomes more effective. In the embedded model, the stiffness of reinforcement is evaluated individually in the element in conjunction with isoparametric shape function. Thus, the reinforcement need not be distributed uniformly. Also, their location and orientation can be arbitrary. In the discrete model [44], a one-dimensional bar element is superimposed on the two-dimensional elements. In spite of its simplicity of concept, the discrete model has one disadvantage in that the finite element mesh patterns are restricted by the locations of reinforcements. Numerically, it is less efficient than the embedded and smeared approach.

2.2 BEHAVIOR OF CONCRETE

Some typical experimental data for concrete under uniaxial, biaxial and triaxial states of stress are reviewed. These data provide guidance in the development of the computational model and also help determine the various material constants to describe the model.

2.2.1 Uniaxial Compression

The uniaxial stress-strain curves in compression are shown in Fig.2.1 for low-, normal-, and high-strength concretes. The normal-strength concrete has a linearly elastic behavior up to about 30% of its maximum compressive strength f'_c. In the present work, the uniaxial stress-strain curve is employed for the modelling of strain-hardening behavior of multiaxial state of stress. In the present model linear elastic behavior is assumed up to stress equal to $0.3f'_c$ and beyond this level a parabolic stress-strain relationship is assumed with strain corresponding to peak stress equal to $2f'_c/E_o$ for normal concrete where E_o is initial modulus of elasticity (Fig.2.2). Beyond this peak, the stress is assumed to be constant at increasing strain until crushing failure occurs at some ultimate strain ε_u.

2.2.2 Uniaxial Tension

The typical stress-strain curve in tension is linear up to a relatively high stress level of around 60% of its maximum tensile strength f'_t. In the model adopted herein, the curve is assumed linearly elastic up to its maximum tensile strength f'_t with a descending softening branch (will be discussed in detail in 2.7.1). The tensile strength f'_t is calculated using either split-cylinder tensile strength $6\sqrt{f'_c}$ or the modulus of rupture $7.5\sqrt{f'_c}$, with the latter being more appropriate for flexural modes of failures.

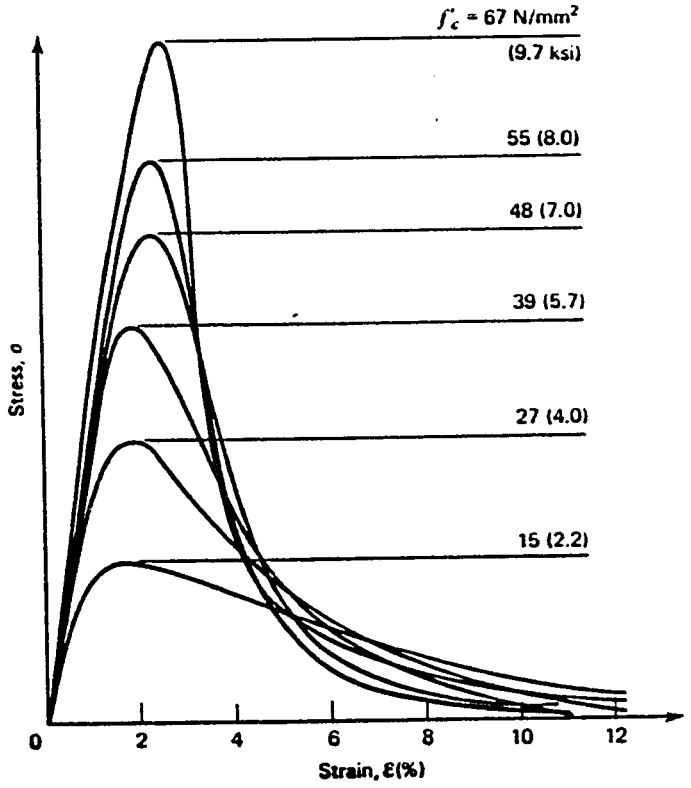

Fig. 2.1 Uniaxial compressive stress-strain curves for concrete [78]

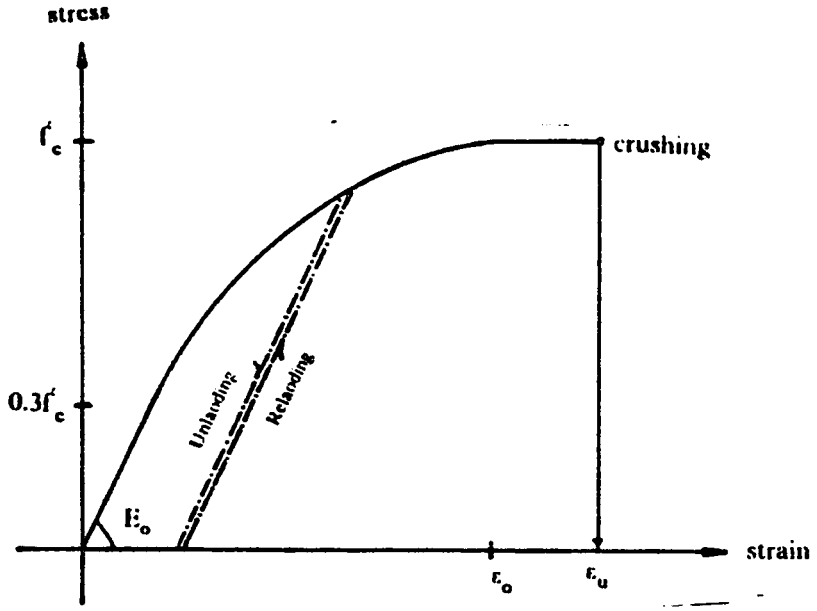

Fig. 2.2 Uniaxial compressive stress-strain curve used in the model

2.2.3 Biaxial Behavior

Biaxial test results of Kupfer [79] for concrete are shown in Fig.2.3. The maximum compressive stress increases for biaxial compressive state which is known to be the biaxial stiffening effect. A maximum strength increase of approximately 25% is achieved at a stress ratio of 0.5 and about 16% at an equal biaxial compressive state.

Many important classes of structures can be approximated as being in the state of plane stress, such as beams, panels, and thin shells. In modelling such structures, test results for concrete under biaxial states of stress are very useful.

2.2.4 Triaxial Behavior

Fig.2.4 shows typical stress-strain curves from the tests by Richart et al. [80]. Their tests were conducted at low or moderate confining pressures. It is seen that under higher confining stresses the unstable strain softening portion gradually vanishes. This is because under higher confining stresses the possibility of bond cracking is greatly reduced and the failure mode shifts from cleavage to crushing of cement paste.

Under triaxial loading, concrete has a fairly consistent failure surface that is a function of the three principal stresses [81]. If isotropy of concrete is assumed, the elastic limit, subsequent yielding and failure limit all can be represented as surfaces in three-dimensional principal stress space (Fig.2.5). These surfaces are closely associated with

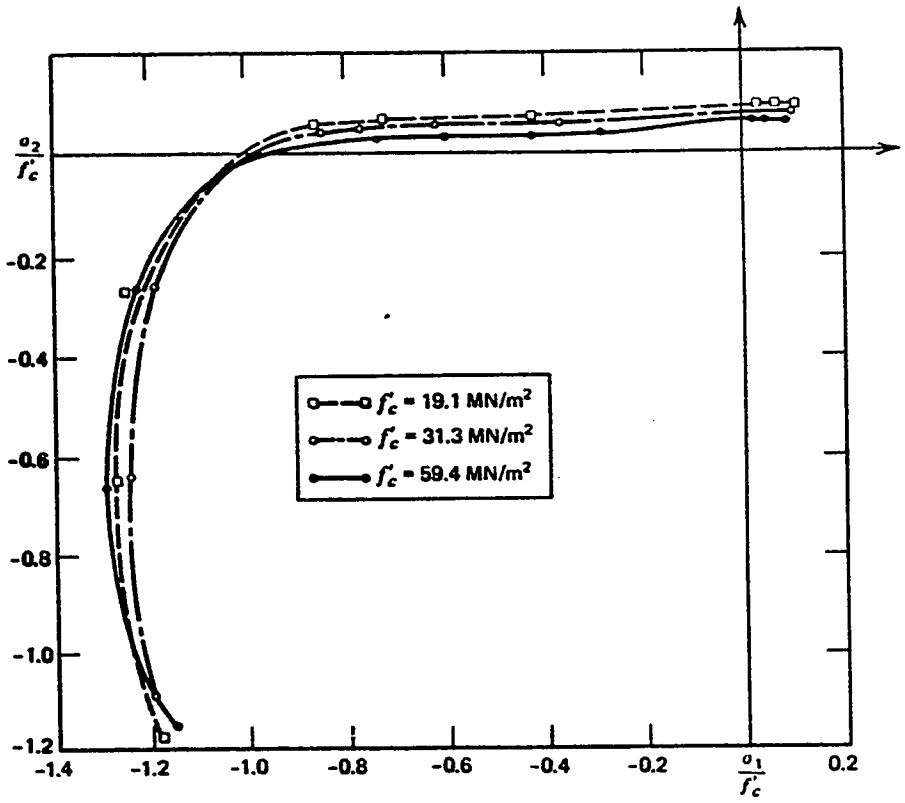

Fig. 2.3 Biaxial strength envelope of concrete [79]

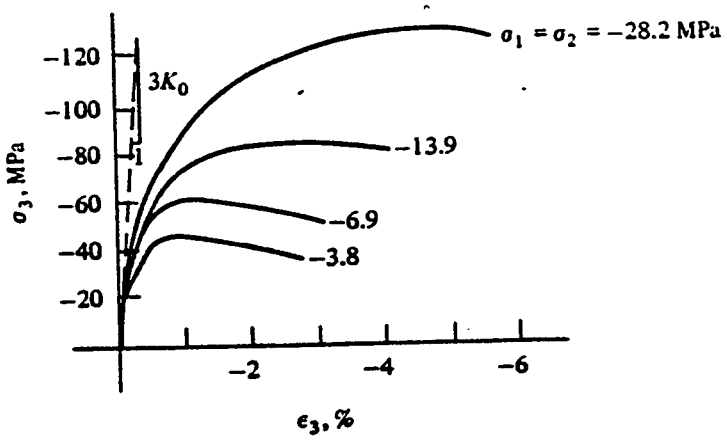

Fig. 2.4 Triaxial stress-strain relationship for concrete [80]

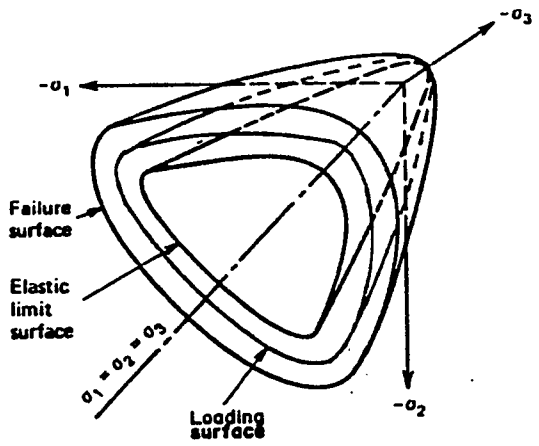

Fig. 2.5 Elastic limit, loading and failure surfaces of concrete in three dimensional principal stress space

the mechanism of internal progressive microcracking. The surface corresponding to elastic limit and often referred to as initial yield surface marks the onset of stable crack propagation. Within this surface, the available energy is less than the energy required to create new microcrack surfaces. The subsequent loading surfaces are associated with stable crack propagation until the failure surface is reached which marks the onset of unstable crack propagation and the material starts softening unstably. Eventually the fracture surface in terms of strains marks the complete disruption of the material often referred to as crushing.

2.2.5 Characteristics of Failure Surfaces

The yield criterion $F(I_1 , J_2 , J_3 , \chi) = 0$ is generally represented by first stress invariant I_1, second and third deviatoric stress invariants J_2 , J_3 and hardening parameter χ. Alternatively it is also defined by variables ξ , ρ and θ in the σ_1 , σ_2 , σ_3 coordinate system as the cylindrical geometric coordinates of the surface in the three-dimensional principle stress σ_i space (Fig.2.5), where

$$\xi = I_1/\sqrt{3}$$

$$\rho = \sqrt{2J_2}$$

and

$$\sin 3\theta = -\frac{3\sqrt{3}}{2} J_3/J_2^{3/2} \qquad -\frac{\pi}{6} \le \theta \le \frac{\pi}{6} \tag{2.1}$$

With these definitions, the principal stresses can be expressed as fol-

lows:

$$\begin{Bmatrix}\sigma_1\\ \sigma_2\\ \sigma_3\end{Bmatrix} = \frac{\xi}{\sqrt{3}}\begin{Bmatrix}1\\1\\1\end{Bmatrix} + \frac{\rho}{\sqrt{3}}\begin{Bmatrix}\sin(\theta+2\pi/3)\\ \sin\theta\\ \sin(\theta+2\pi/3)\end{Bmatrix} \qquad -\frac{\pi}{6} \le \theta \le \frac{\pi}{6} \tag{2.2}$$

The general shape of the yield/failure surface can be best described by its cross sectional shapes in the deviatoric planes (Fig.2.6) and its meridians in the meridian planes (Fig.2.7). Experimental results indicate that for concrete the failure curve (trace of the failure surface) in the deviatoric plane is smooth, convex, nearly triangular for tensile and small compressive stresses and almost circular for high compressive stress [82].

Two failure curves in the meridian planes are identified as tensile ($\theta=-30$) and compressive meridians ($\theta=30$). These meridians are also smooth, convex and depend on the hydrostatic component of stress, I_1 or ξ i.e., ρ increases for increasing hydrostatic pressure.

The general characteristics of the failure surface described above provide the necessary guidelines required in the development of failure models for concrete materials. A brief review of the proposed yield and failure criteria for concrete materials is presented now.

2.3 YIELD CRITERIA FOR CONCRETE

A multiaxial constitutive relationship is an essential component in any finite element nonlinear analysis of reinforced concrete structures.

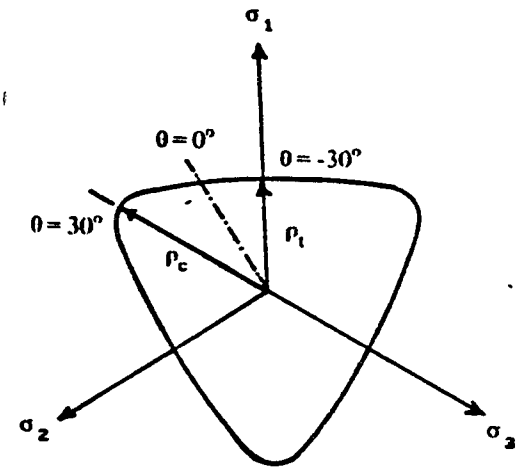

Fig. 2.6 Trace of failure surface in the deviatoric plane

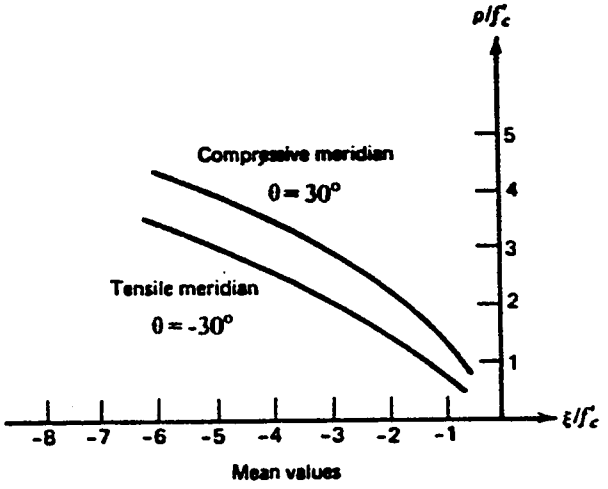

Fig. 2.7 Trace of failure surface in the meridian plane [82]

Early proposed models were simple one- and two-parameter models when the true behavior of concrete was not known. With the advent of computer technology, and as more test data have become available, three-, four- and five-parameter models have been formulated. Recent review papers on the failure criteria of concrete have been made by Argyris et al. [83], Eibl and Ivanyi [84], Paul [85], Chen [86], and Chen and Saleeb [82]. A brief review of the failure criteria for concrete materials is presented now.

Early finite element applications utilized one parameter models such as Rankine's maximum tensile stress criterion in terms of tension cut-off to account for brittle fracture of concrete. This criterion is still used extensively in combination with other models for modelling of crack initiation. For ductile failure, von Mises and Tresca yield criteria were used. Tresca criterion neglects the effect of the intermediate principal stress, σ_2, and cannot represent the increase in strength under biaxial compression. And both von Mises and Tresca criteria are found to be independent of hydrostatic states of stress, and thus are not considered adequate for describing the actual behavior of concrete.

Thus pressure dependent two parameter models are proposed for use in the computational model to be developed herein. For simplicity and convenience, these models have assumed that all the deviatoric cross-sections are geometrically similar; the only effect of the pressure is to adjust the size of the cross section. The simplest and most commonly used two parameter models of this type are the Mohr-Coulomb and Drucker-Prager failure criteria, whose meridians depend linearly on the

hydrostatic stress component ξ (Fig.2.8). These models are used in combination with a maximum tensile strength cut-off. As is evident from the shapes of Mohr-Coulomb, the trace of Mohr-Coulomb surface in the deviatoric plane is an irregular hexagon with corners. These corners are characteristic of models which are independent of intermediate principal stress σ_2. Tresca and Mohr-Coulomb are examples of such models. Since these corners are not numerically convenient, Drucker and Prager [87], have suggested a smooth approximation to the Mohr-Coulomb surface by a simple modification of the von Mises criterion (Fig.2.8). As is evident from the shapes of Mohr-Coulomb and Drucker Prager failure surfaces, Mohr-Coulomb is a good predictor model at low and moderate pressures with non-circular deviatoric section while the Drucker Prager is the appropriate one at high hydrostatic pressures with the circular deviatoric cross section.

To overcome the basic shortcoming of two-parameter models which is the existence of a linear relationship between ξ and ρ and that the deviatoric sections are not appropriate, three-parameter models have been developed. The three-parameter models replaced the two parameter models in two ways: first by assuming a parabolic dependence of ρ on ξ but retaining the circular cross section and as a second approach by retaining the linear $\rho-\xi$ relation but letting the deviatoric sections exhibit θ dependence.

Following the first approach, Bresler and Pister [88], proposed a three-parameter failure criterion. On the other hand, the second approach has been used by Willam and Warnke [89], to develop a three-

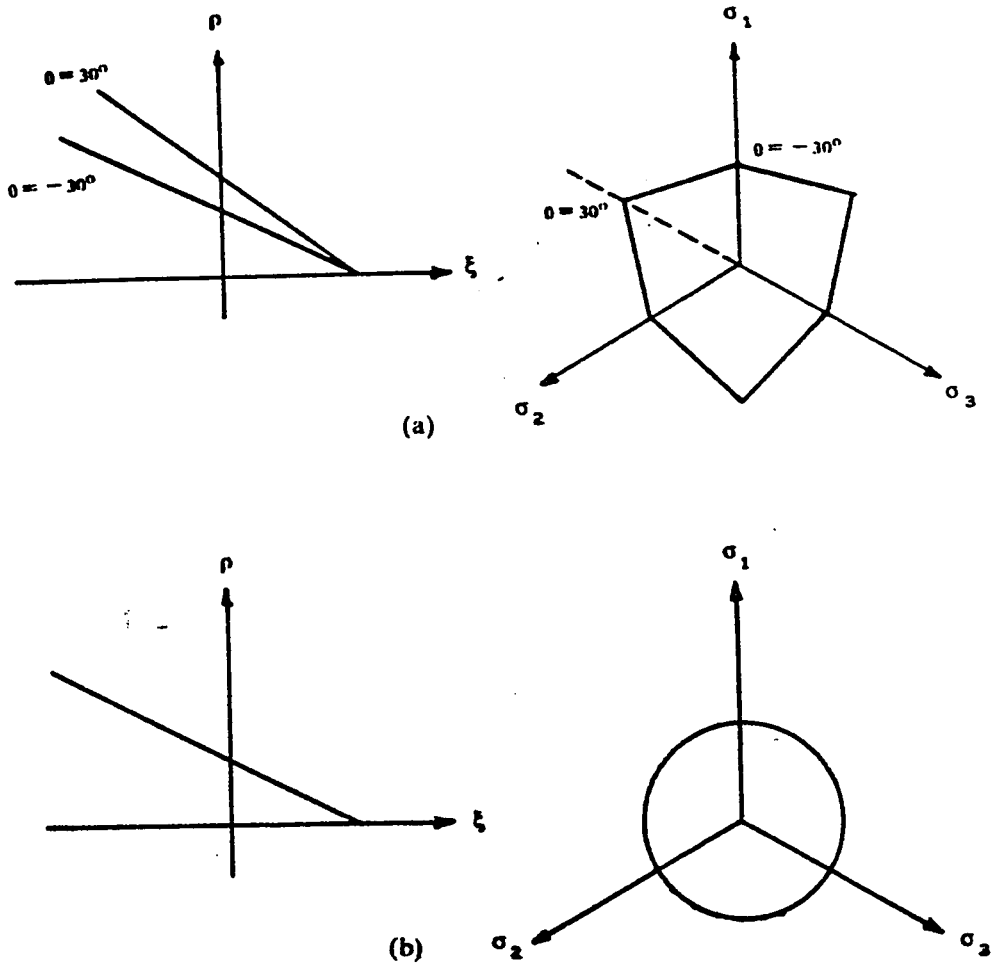

Fig. 2.8 Meridian and deviatoric sections for (a) Mohr-Coulomb criterion (b) Drucker Prager criterion

parameter failure surface for concrete in the tension and low compression regime.

Attempts have been made to develop models that exhibit both curved meridians and noncircular deviatoric sections. Reimann [90], and Ottosen [91], proposed four parameter models to meet these requirements. Later Willam and Warnke [89] developed a five parameter criterion which has elliptic deviatoric sections and parabolic meridians. The model meets the required characteristics concerning smoothness, convexity and symmetry for all stress combinations.

Failure models are used as perfectly plastic models. A failure model can be rendered to an isotropic strain-hardening model by replacing the failure stress f'_c by the effective stress σ_o which is function of strain hardening parameter χ. The strain hardening models are expressed explicitly such as

$$f(I_1 , J_2 , J_3) = \sigma_o(\chi) \tag{2.3}$$

Initial and subsequent loading surfaces are assumed to retain the same shape as the failure surface but with different size depending upon the level of hardening. In order to use any proposed failure model as a strain hardening model, it should be expressed in the explicit form as equation 2.3.

Unfortunately the refined three-, four- and five-parameter models are presented in implicit form such as

$$f(I_1 , J_2 , J_3, f'_c) = f'_c \tag{2.4}$$

with f'_c lying on both sides of the equation. Reduction of equa-

tion(2.4) to the explicit form further complicates the equation and in the calculation of the flow vector as required in the numerical implementation. Consequently the computer implementation either becomes too complicated to use or computationally it becomes too expensive. Thus sophisticated models are practical for the most part only as perfectly plastic models. Since the use of perfectly plasticity is questionable for a material such as concrete, there is a tendency to use models that can be modified readily use as strain hardening models. Therefore in this work attention is focussed on two and three parameter models.

2.3.1 Drucker Prager Criterion

Drucker-Prager criterion is expressed as

$$F(I_1,J_2) = \alpha I_1 + \sqrt{J_2} - k = 0 \qquad (2.5)$$

where k and α are material constants. Using the uniaxial and biaxial test results ($f'_{cb} = 1.2f'_c$ [79]) these constants can be evaluated and shown to be $\alpha = .08$, $k = 0.5f'c$. The criterion can then be expressed as

$$F(I_1,J_2) = 0.08I_1 + \sqrt{J_2} - 0.5f'_c = 0 \qquad (2.6)$$

which can be rewritten as:

$$F(I_1,J_2) = 0.16I_1 + 2\sqrt{J_2} - f'_c = 0 \qquad (2.7)$$

2.3.2 Mohr-Coulomb Criterion

Mohr-Coulomb yield criterion has been used successfully for shear

critical reinforced concrete structures [77]. The Mohr-Coulomb failure criterion is described as

$$|\tau| = c - \sigma\tan\varphi \tag{2.8}$$

where τ and σ are shear and normal stresses on any plane at a point in a concrete material. c and φ are material constants. This equation may be written in the alternative form in terms of principal stresses as :

$$\sigma_1 \frac{(1 + \sin\varphi)}{2c\ \cos\varphi} - \sigma_3 \frac{(1 - \sin\varphi)}{2c\ \cos\varphi} = 1 \tag{2.9}$$

or in terms of invariants using the equations(2.2)

$$F(I_1, J_2, 0) = \frac{1}{3} I_1 \sin\varphi + \sqrt{J_2}\sin(0 + \frac{\pi}{3}) + \sqrt{J_2/3}\ \cos(0 + \frac{\pi}{3})\sin\varphi - c\ \cos\varphi = 0 \tag{2.10}$$

or in terms of the variables ρ, ξ and 0

$$f(\xi, \rho, 0) = \sqrt{2}\xi\sin\varphi + \sqrt{3}\rho\sin(0 + \frac{\pi}{3}) + \cos(0 + \frac{\pi}{3})\sin\varphi - \sqrt{6}c\ \cos\varphi = 0 \tag{2.11}$$

In these expressions φ is the angle of internal friction for concrete and taken as 37^{o} [16]. The constant c is obtained in terms of concrete compressive strength by making the Mohr-Coulomb envelope touch the circle corresponding to the uniaxial compressive test. The value of c is then evaluated as :

$$c = \frac{f'_c(1-\sin\varphi)}{2\cos\varphi} \tag{2.12}$$

Now equation (2.10) can be rewritten as :

$$F(\sigma_{ij}) = \frac{2}{(1-\sin\ \varphi)} \left[\frac{I_1}{3} \sin\ \varphi + \sqrt{J_2}\left(\cos\ \theta - \frac{1}{\sqrt{3}} \sin\ \theta \sin\ \varphi\right)\right] - f'_c = 0 \tag{2.13}$$

The casting of the Mohr-Coulomb criterion in the form of equation 2.13

renders convenient the adaptability of the formulation to either perfectly plastic model or to strain-hardening model, where $f_c^{'}$ can be replaced by the effective stress σ_o.

2.3.3 Parabolic Mohr-Coulomb Criterion

Parabolic Mohr-Coulomb failure envelope combined with circular tension cut-off was originally presented by Braestrup [15], as an improvement over the ordinary Mohr-Coulomb envelope. Jiang and Shen [16] presented the same model with the intrinsic curve (Fig.2.9), to reflect the convexity of failure envelope. In their analytical work they used perfectly plastic theory to arrive at the punching collapse load using parabolic Mohr-Coulomb failure envelope expressed as :

$$\frac{\sigma_n}{f_t} + \frac{1}{K}\left(\frac{\tau_{nt}}{2f_t}\right)^2 = 1 \qquad (2.14)$$

where K is defined as:

$$K = \frac{1}{4}[m + 2(1 - \sqrt{m+1})] \qquad (2.15)$$

and

$$m = \frac{f_c}{f_t} = \frac{\nu_c f'_c}{\nu_t f'_t} \qquad (2.16)$$

where ν_c and ν_t are effectiveness factors and f_c and f_t are effective strengths corresponding to full compressive and tensile strengths f'_c and f'_t.

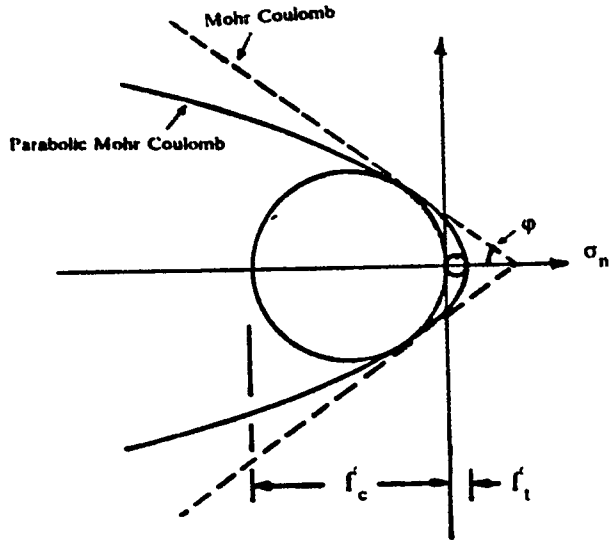

Fig. 2.9 Mohr-Coulomb and Parabolic Mohr-Coulomb envelopes [16]

The computational model developed herein tested the suitability of the parabolic Mohr-Coulomb failure law by recasting it in a form suitable for use in isotropic hardening description of concrete state of stress by first rewriting equation 2.14 in terms of principal stresses.

$$\frac{1}{f_t}\left[\left[\frac{\sigma_1-\sigma_3}{2}\right]\sin\alpha + \frac{\sigma_1+\sigma_3}{2}\right] + \frac{1}{K}\frac{1}{4f_t^2}\cos^2\alpha\left[\frac{\sigma_1-\sigma_3}{2}\right]^2 = 1 \qquad (2.17)$$

where α is defined as

$$\tan\alpha = \frac{2Kf_t}{\tau_{nt}} \qquad (2.18)$$

In terms of invariants, equation 2.17 is expressed as a yield criterion (by making use of equation 2.2 which expresses the principal stresses in terms of stress invariants) in the form

$$F(\sigma_{ij}) = \frac{m}{v_c(K-1)}\left\{\frac{\sqrt{J_2}\sin\theta}{\sqrt{3}} - \frac{J_2\cos^2\theta\, m}{4Kv_c f'_c} - \frac{I_1}{3}\right\} = f'_c \qquad (2.19)$$

Application of parabolic Mohr-Coulomb criterion resulted in divergence after the first few load increments. The obvious reason found was that the term (K-1) in equation 2.19 happens to be very small for certain experimental values of f'_c, f'_t, v_c and v_t causing singularity. Moreover the values of v_c and v_t used were somewhat arbitrary and did not have any experimental basis. Considering these shortcomings of this criterion, a new model with different parameters is proposed.

2.3.4 Proposed Yield Criterion

In order to remove the serious defects of the parabolic Mohr-Coulomb yield criterion a new model is proposed using form similar to equation 2.19 with a new set of parameters as:

$$F(I_1, J_2, 0) = A\sqrt{J_2}\sin 0 + B\frac{J_2\cos^2 0}{f'_c} + CI_1 = f'_c \qquad (2.20)$$

The values of A, B and C can be determined from three tests on concrete such as uniaxial compression, biaxial compression and high compression on tensile meridian as follows:

(i) Uniaxial compression:

The point corresponding to uniaxial compression test lies on the compressive meridian (Fig. 2.10) with angle of similarity 0 equal to 30°. For this test, $I_1 = -f'_c$ and $\sqrt{J_2} = f'_c/\sqrt{3}$.

(ii) Biaxial compression:

The point corresponding to biaxial compression test lies on the tensile meridian (Fig. 2.10) with angle of similarity 0 equal to -30°. For this test, $I_1 = -2f'_{bc}$ and $\sqrt{J_2} = f'_{bc}/\sqrt{3}$, where f'_{bc} is the biaxial compressive strength and it's value is $1.18f'_c$ [89].

(iii) High compressive stress point on the tensile meridian:

The corresponding point for this test lies on the tensile meridian (Fig. 2.10) with angle of similarity 0 equal to -30°.

with $I_1 = -11.01f'_c$ and $\sqrt{J_2} = 2.37f'_c/\sqrt{3}$ [89].

Using the values for I_1, J_2 and 0 for these tests in equation 2.20 yields

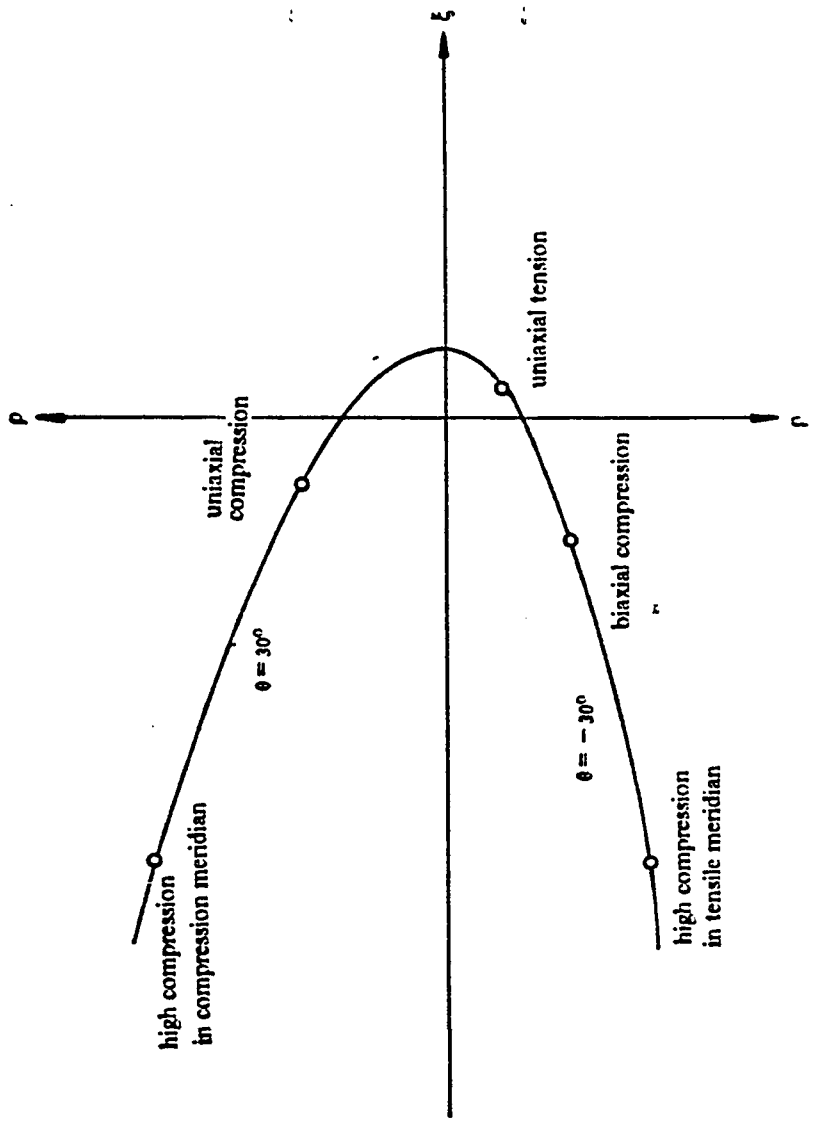

Fig. 2.10 Tests of concrete [89]

the values of A, B and C as follows:

A = 1.7288

B = -1.6812

C = -0.9212

Equation 2.20 can be rewritten in terms of $\xi = I_1/\sqrt{3}$ and $\rho = \sqrt{2\bar{J}_2}$ as:

$$F(\xi,\rho,\theta) = A\frac{\rho}{\sqrt{2}}\sin\theta + B\rho^2\frac{\cos^2\theta}{2f'_c} + \sqrt{3}C\xi = f'_c \qquad (2.21)$$

Equation 2.21 describes the geometry of the proposed yield criterion in the deviatoric and meridian planes. For $\theta = 30^\circ$ and $\theta = -30^\circ$ the tensile and compressive meridians are drawn and shown in Fig. 2.11. The meridians are curved conforming to the characteristics of concrete failure envelope. For ordinary Mohr-Coulomb and Drucker Prager yield criteria the meridians are straight lines. The deviatoric cross section is shown in Fig. 2.12. The cross sections are non-circular and convex with corners at $\theta = \pm 30^\circ$. The flow vector can be found out at corners using the explicit expression of yield function at $\theta = \pm 30^\circ$. The ratio of values of ρ corresponding to tensile and compressive meridians ρ_t and ρ_c is found to be 1.13 at $\frac{\xi}{f'_c} = 10$. As it is evident from Fig. 2.11 that very limited yielding is predicted in tension zone. By fitting points corresponding to other data of concrete tests the model parameters can be readily modified.

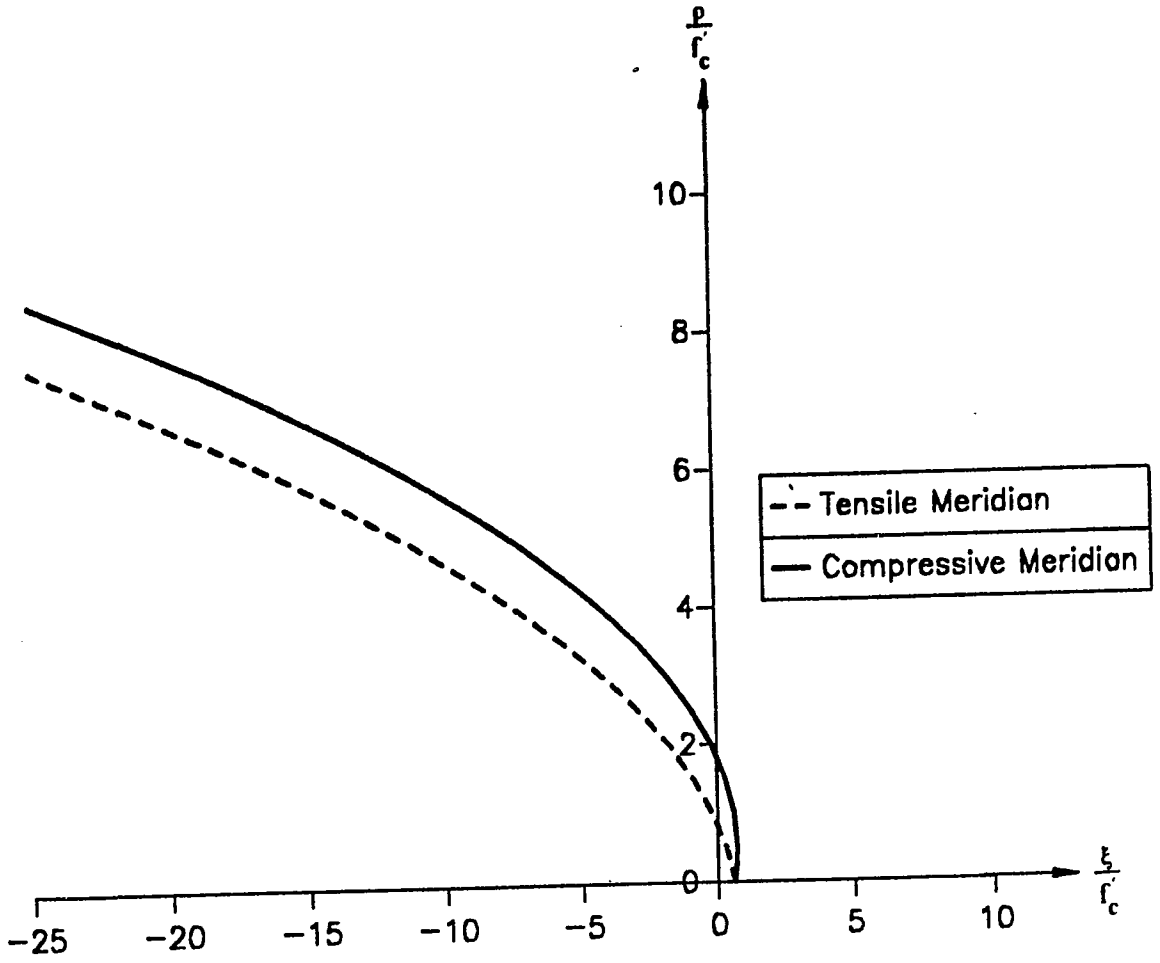

Fig. 2.11 Compressive and tensile meridians of proposed yield criterion

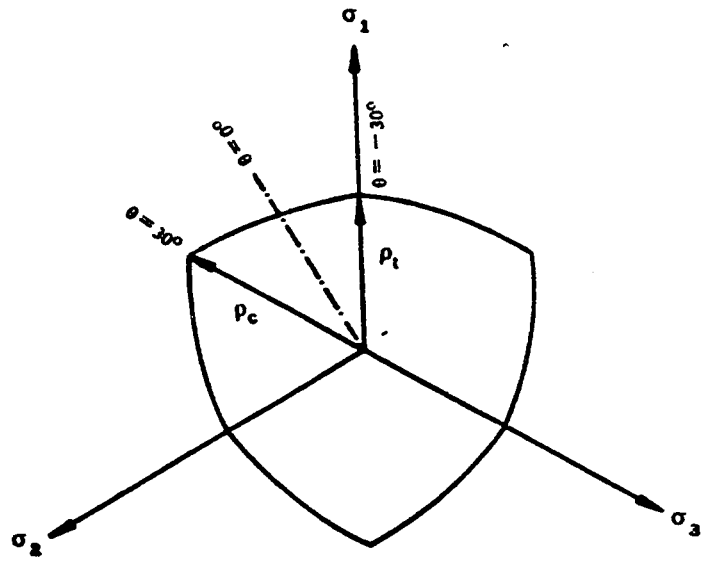

Fig. 2.12 Deviatoric representation of the proposed yield criterion

2.4 FLOW AND HARDENING RULE

In order to apply the incremental theory of plasticity to concrete, four basic assumptions must be made:

1. The initial yield surface that defines the beginning of plastic flow;
2. The failure condition that sets the upper bound in stress space;
3. The hardening rule that describes the evolution of the subsequent loading surface; and
4. The flow rule that is related to a plastic potential function and gives an incremental plastic stress-strain relation.

2.4.1 Flow Rule

To construct the stress-strain relationship in the plastic range, the concept of plastic potential function $G(\sigma_{ij})$ is introduced. This helps in writing the equation of plastic flow in the form

$$d\varepsilon_{ij}^{p} = d\lambda \frac{\partial G}{\partial \sigma_{ij}} \tag{2.22}$$

where $d\lambda$ is a positive scalar factor of proportionality which determines the magnitude of the plastic strain increment, and the gradient $\partial G/\partial \sigma_{ij}$ called flow vector defines direction of plastic strain increment to be perpendicular to the plastic potential function. For simplicity an associated flow rule is assumed i.e., F = G , or the plastic strain increment is assumed to be perpendicular to the yield surface. The case of G when different from F is referred to as the non-associated rule. Thus

$$d\varepsilon_{ij}^{p} = d\lambda \frac{\partial F}{\partial \sigma_{ij}} \tag{2.23}$$

2.4.2 Hardening Rule

The hardening rule defines the motion of the subsequent yield surface (the loading surfaces) during plastic deformation. There are four types of hardening rules; isotropic, kinematic, mixed and non-uniform hardening. Kinematic hardening is employed to depict the so-called Baushinger's effect found in metals during cyclic loading. Recently Han and Chen [92] proposed nonuniform hardening plasticity of concrete in order to differentiate the response of concrete in the compressive region from that of tension region. However, since in this work a parallel model for cracking of concrete exists, the use of isotropic hardening is sufficient for the present model. The isotropic hardening is extrapolated from the uniaxial compression stress-strain curves(Fig.2.1). For simplicity, these curves are assumed to be parabolic [93] in the post-linear elastic range and post-yield stress-strain relationship is assumed as follows:

$$\sigma = E_o\varepsilon - 0.5\frac{E_o}{\varepsilon_o}\varepsilon^2 \qquad 0.3f'_c < \sigma \leq f'_c \tag{2.24}$$

where

E_o = the initial elasticity modulus

ε = the total strain

ε_o = the total strain at peak stress f'_c

For normal concrete with f'_c of around 4 ksi (Fig.2.1) ε_o is equal to

$2f'_c/E_o$.

Decomposing the total strain in equation 2.24 in elastic and plastic strain components and substituting the elastic strain component $\varepsilon_e = \sigma/E_o$ in equation 2.24 and then solving for σ yields :

$$\sigma = -E_o\varepsilon_p + \sqrt{2E^2{}_o\varepsilon_o\varepsilon_p} \; ; \qquad 0.3f_c' < \sigma \leq f_c' \tag{2.25}$$

where ε_p is the plastic strain component.

Differentiating equation 2.25 with respect to ε_p, yields the hardening parameter as :

$$\frac{d\sigma}{d\varepsilon_p} = H' = -E_o + E_o\sqrt{\varepsilon_o/2\varepsilon_p} \tag{2.26}$$

Equations 2.25 and 2.26, give the current yield stress σ and the current hardening parameter H', respectively, corresponding to the current loading surface at current level of effective plastic strain.

For strain hardening model the yield criterion is expressed explicitly as

$$f(\sigma_{ij}) = k(\varepsilon_p) \tag{2.27}$$

while the perfect plasticity model is expressed as

$$f(\sigma_{ij}) = k \; ; \text{ a constant} \tag{2.28}$$

Strain softening for post-peak behavior has been tried in a quite refined way recently by Han and Chen [65] using the plastic and fracture degradation concepts. However in view of the behavior of concrete in confined triaxial compression where the unstable strain softening part vanishes(Fig.2.4), a perfect plastic model is used in the

post-peak region till crushing surface is reached.

2.5 ELASTO-PLASTIC STRESS-STRAIN RELATIONS

In the post-linear elastic range, the increment of strain during an infinitesimal increment of stress σ_{ij} is divided into elastic and plastic components.

$$d\varepsilon_{ij} = d\varepsilon^{e}_{ij} + d\varepsilon^{p}_{ij} \tag{2.29}$$

The elastic strain increment is related to stress increment as follows:

$$d\varepsilon^{e}_{ij} = \frac{ds_{ij}}{2G} + \frac{(1-2\nu)}{E}\delta_{ij}d\sigma_{kk} \tag{2.30}$$

where s_{ij} is stress deviatoric tensor.

Using equations 2.23 and 2.30 in equation 2.29 the complete stress-strain relationship can be written as follows:

$$d\varepsilon_{ij} = \frac{ds_{ij}}{2G} + \frac{(1-2\nu)}{E}\delta_{ij}d\sigma_{kk} + d\lambda\frac{\partial f}{\partial \sigma_{ij}} \tag{2.31}$$

The yield function defined in (2.27) can be rewritten as

$$F(\sigma_{ij},\chi) = f(\sigma_{ij}) - \sigma_{o}(\chi) = 0 \tag{2.32}$$

where χ is the hardening parameter which governs the expansion of the yield surface. The total differential of equation 2.32 yields

$$dF = \frac{\partial F}{\partial \{\sigma\}}d\{\sigma\} + \frac{\partial F}{\partial \chi}d\chi = 0, \tag{2.33}$$

or

$$\{a\}^{T}d\{\sigma\} - Ad\lambda = 0, \tag{2.34}$$

with the definitions

$$\{a\}^T = \frac{\partial F}{\partial \{\sigma\}} = \left\{\frac{\partial F}{\partial \sigma_x}, \frac{\partial F}{\partial \sigma_y}, \frac{\partial F}{\partial \sigma_z}, \frac{\partial F}{\partial \sigma_{xy}}, \frac{\partial F}{\partial \sigma_{xz}}, \frac{\partial F}{\partial \sigma_{yz}}\right\}, \qquad (2.35)$$

and

$$A = -\frac{1}{d\lambda}\frac{\partial F}{\partial \chi}d\chi. \qquad (2.36)$$

The vector {a} is termed the flow vector. Equation 2.31 can be rewritten in the matrix form as:

$$d\{\varepsilon\} = |D|^{-1}d\{\sigma\} + d\lambda\frac{\partial F}{\partial \{\sigma\}}, \qquad (2.37)$$

where |D| is the matrix of elastic constants. Premultiplying both sides of equation 2.37 by $\{a\}^T|D|$ and eliminating $\{a\}^T d\{\sigma\}$ by use of equation 2.34, one may show the plastic multiplier $d\lambda$ to be

$$d\lambda = \frac{1}{A+\{a\}^T|D|\{a\}}\{a\}^T|D|\{\varepsilon\}. \qquad (2.38)$$

Substituting equation 2.38 into equation 2.37 yields the complete elasto-plastic incremental stress-strain relationship to be

$$d\{\sigma\} = |D|_{ep}d\{\varepsilon\}. \qquad (2.39)$$

where

$$|D_{ep}| = |D| - \frac{|D|\{a\}\{a\}^T|D|}{A + \{a\}^T|D|\{a\}} \qquad (2.40)$$

Now A is evaluated as outlined in [94] using work hardening hypothesis given by :

$$d\chi = \{\sigma\}^T d\{\varepsilon_p\} \qquad (2.41)$$

For uniaxial case work hardening hypothesis results in :

$$d\chi = \sigma_y d\bar{\varepsilon}_p \qquad (2.42)$$

where σ_y is uniaxial yield stress and $\bar{\varepsilon}_p$, uniaxial plastic strain.

Equating equations 2.41 and 2.42 and using normality rule (equation 2.21) yields :

$$\sigma_y d\bar{\varepsilon}_p = \{\sigma\}^T d\{\varepsilon_p\} = d\lambda \{a\}^T d\{\sigma\} \tag{2.43}$$

Using equation 2.32 in equation 2.36 we get :

$$A = \frac{1}{d\lambda} \frac{d\sigma_y}{d\chi} d\chi. \tag{2.44}$$

Applying Euler's theorem on homogeneous functions - equation 2.32 we have :

$$\frac{\partial f}{\partial \{\sigma\}} \{\sigma\} = \sigma_y \tag{2.45}$$

Now substituting equations 2.26 and 2.45 into equations 2.43 and 2.44 we get :

$$d\lambda = d\bar{\varepsilon}_p$$

$$A = H'. \tag{2.46}$$

Substituting equation 2.46 into equation 2.40 we get :

$$|D_{ep}| = |D| - \frac{|D| \{a\} \{a\}^T |D|}{H' + \{a\}^T |D| \{a\}} \tag{2.47}$$

The linear elastic constitutive matrix |D| is given as :

$$\begin{Bmatrix} \sigma_x \\ \sigma_y \\ \tau_{xy} \\ \tau_{xz} \\ \tau_{yz} \end{Bmatrix} = \begin{bmatrix} E/(1-\nu^2) & E/(1-\nu^2) & 0 & 0 & 0 \\ \nu E/(1-\nu^2) & \nu E/(1-\nu^2) & 0 & 0 & 0 \\ 0 & 0 & G & 0 & 0 \\ 0 & 0 & 0 & 5G/6 & 0 \\ 0 & 0 & 0 & 0 & 5G/6 \end{bmatrix} \begin{Bmatrix} \varepsilon_x \\ \varepsilon_y \\ \gamma_{xy} \\ \gamma_{xz} \\ \gamma_{yz} \end{Bmatrix} \tag{2.48}$$

wherein shear correction factor of 5/6 is applied to transverse shear terms.

2.5.1 Flow Vector

For yield function $F=F(I_1, J_2, 0)$, the flow vector $\frac{\partial F}{\partial \sigma_{ij}}$ can be evaluated following the procedure given in [46] as :

$$|a|^T = \frac{\partial F}{\partial \{\sigma\}} = \frac{\partial F}{\partial I_1}\frac{\partial I_1}{\partial \{\sigma\}} + \frac{\partial F}{\partial \sqrt{J_2}}\frac{\partial \sqrt{J_2}}{\partial \{\sigma\}} + \frac{\partial F}{\partial 0}\frac{\partial 0}{\partial \{\sigma\}} \tag{2.49}$$

Eliminating 0 in terms of J_2 and J_3, equation 2.49 may be recast in the form

$$|a| = C_1|a_1| + C_2|a_2| + C_3|a_3| \tag{2.50}$$

where

$$|a_1|^T = \frac{\partial I_1}{\partial \{\sigma\}} = \{1,\ 1,\ 0,\ 0,\ 0\} \tag{2.51}$$

$$|a_2|^T = \frac{\partial \sqrt{J_2}}{\partial \{\sigma\}} = \frac{1}{2\sqrt{J_2}}\{\sigma_{x'},\ \sigma_{y'},\ 2\tau_{xy},\ 2\tau_{xz},\ 2\tau_{yz}\} \tag{2.52}$$

$$\begin{aligned} |a_3|^T = \frac{\partial J_3}{\partial \{\sigma\}} = \Big|\Big[\sigma_{y'}\sigma_{z'} - \tau_{yz}^2 + \frac{J_2}{3}\Big],\ \Big[\sigma_{x'}\sigma_{z'} - \tau_{xz}^2 + \frac{J_2}{3}\Big],\ \cdot \\ 2(\tau_{yz}\tau_{xz} - \sigma_{z'}\tau_{xy}),\ 2(\tau_{xy}\tau_{yz} - \sigma_{y'}\tau_{xz}), \\ .2(\tau_{xz}\tau_{xy} - \sigma_{x'}\tau_{yz})\Big] \end{aligned} \tag{2.53}$$

and

$$C_1 = \frac{\partial F}{\partial I_1} \tag{2.54}$$

$$C_2 = \frac{\partial F}{\partial \sqrt{J_2}} - \frac{\tan 30}{\sqrt{J_2}} \frac{\partial F}{\partial 0} \tag{2.55}$$

$$C_3 = -\frac{\sqrt{3}}{2\cos 30} \frac{1}{J_2 \sqrt{J_2}} \frac{\partial F}{\partial 0} \tag{2.56}$$

with the primed stresses being deviatoric stresses.

The expressions for C_1, C_2 and C_3 for different yield criteria were evaluated and are as noted :

2.5.1.1 Drucker Prager

Using equations 2.54 - 2.56 in equation 2.7, the values of C_1, C_2 and C_3 may be shown to be :

$$C_1 = 0.16$$
$$C_2 = 2.0 \tag{2.57}$$
$$C_3 = 0.0$$

2.5.1.2 Mohr-Coulomb

Using equations 2.54 - 2.56 in equation 2.13, C_1, C_2 and C_3 for Mohr-Coulomb are found to be :

$$C_1 = \frac{2\sin\varphi}{3(1-\sin\varphi)}$$

$$C_2 = \frac{2}{1-\sin\varphi} \cos 0 \{(1 + \tan 0 \tan 30) + \sin\varphi(\tan 30 - \tan 0)/\sqrt{3}\}$$

(2.58)

$$C_3 = \frac{2}{1-\sin\varphi}(\sqrt{3}\sin 0 + \cos 0 \sin\varphi)/(2J_2 \cos 30)$$

2.5.1.3 Parabolic Mohr-Coulomb

Since equation 2.19 has f'_c on both sides, it needs to be reduced to explicit form in order to use it as a strain-hardening model. Equation 2.19 is rewritten as

$$F(I_1,J_2,0) = \frac{m}{2\nu_c(K-1)}\left|\left(\sqrt{J_2}\frac{\sin 0}{\sqrt{3}}-\frac{I_1}{3}\right)-\sqrt{\left(\sqrt{J_2}\frac{\sin 0}{\sqrt{3}}-\frac{I_1}{3}\right)^2-\frac{K-1}{K}J_2\cos^2 0}\right| \tag{2.59}$$

Using equations 2.54 - 2.56 in equation 2.59, the values of C_1, C_2 and C_3 for parabolic Mohr-Coulomb are given by :

$$C_1 = \frac{A}{3}(B/\sqrt{R}-1)$$

$$C_2 = F_2 - \frac{\tan 30}{\sqrt{J_2}}F_\theta \tag{2.60}$$

$$C_3 = -\frac{\sqrt{3}}{2\cos 30}\frac{1}{J_2\sqrt{J_2}}F_\theta$$

where

$$F_2 = \frac{\partial F}{\partial\sqrt{J_2}} = A\left|\frac{\sin 0}{\sqrt{3}}-\frac{1}{\sqrt{R}}\left\{B\frac{\sin 0}{\sqrt{3}}-\frac{K-1}{K}\sqrt{J_2}\cos^2 0\right\}\right|$$

$$F_\theta = \frac{\partial F}{\partial 0} = A\left|\sqrt{J_2/3}\cos 0-\frac{1}{\sqrt{R}}\left\{B\sqrt{J_2/3}\cos 0+\frac{K-1}{K}J_2\sin 0\cos 0\right\}\right|$$

$$A = \frac{m}{2v_c(K-1)}$$

$$B = \sqrt{J_2}\frac{\sin\theta}{\sqrt{3}} - \frac{I_1}{3}$$

$$R = B^2 - \frac{K-1}{K}J_2\cos^2\theta$$

2.5.1.4 Proposed Yield Criterion

Since equation 2.20 has f'_c on both sides, it needs to be reduced to explicit form in order to use it as a strain-hardening model. Equation 2.20 is rewritten as

$$F(I_1, J_2, \theta) = \frac{1}{2}\left|A\sqrt{J_2}\sin\theta + CI_1 + \sqrt{\left(A\sqrt{J_2}\sin\theta + CI_1\right)^2 + 4BJ_2\cos^2\theta}\right| \tag{2.61}$$

In order to calculate the flow vector defined in equations 2.49 and 2.50 C_1, C_2 and C_3 are evaluated using equations 2.54 - 2.56 in equation 2.61

$$C_1 = \frac{C}{2}\left(\frac{X}{\sqrt{R}}+1\right)$$

$$C_2 = F_2 - \frac{\tan 30}{\sqrt{J_2}}F_\theta \tag{2.62}$$

$$C_3 = -\frac{\sqrt{3}}{2\cos 30}\frac{1}{J_2\sqrt{J_2}}F_\theta$$

where

$$F_2 = \frac{\partial F}{\partial \sqrt{J_2}} = \frac{1}{2}\left| A\sin\theta + \frac{1}{\sqrt{R}}\left\{ AX\sin\theta + 4B\sqrt{J_2}\cos^2\theta \right\} \right|$$

$$F_\theta = \frac{\partial F}{\partial \theta} = \frac{1}{2}\left| A\sqrt{J_2}\cos\theta + \frac{1}{\sqrt{R}}\left\{ AX\sqrt{J_2}\cos\theta - 4BJ_2\sin\theta\cos\theta \right\} \right|$$

$$X = A\sqrt{J_2}\sin\theta + CI_1$$

$$R = X^2 + 4BJ_2\cos^2\theta$$

2.5.2 Singular Points on the Yield Surface

For the yield surfaces which are independent of intermediate principal stress, it is found that their surfaces in three dimensional stress space possess some corners. The flow vector can not be uniquely defined for certain stress combinations (at the corners). For example this case arises for Tresca, Mohr-Coulomb and parabolic Mohr-Coulomb yield criteria at corners located by $\theta = \pm 30^\circ$. This difficulty can be overcome by rewriting the original expressions of yield criteria for the explicit values of $\theta = \pm 30^\circ$. Then the expressions for C_1, C_2 and C_3 can be derived from the θ- independent forms of yield criteria.

For Mohr-Coulomb, parabolic Mohr-Coulomb and proposed yield criteria, the expressions for C_1, C_2 and C_3 at points of singularity can be shown to be :

2.5.2.1 Mohr-Coulomb

For $\theta = \pm 30^{\circ}$ equation 2.13 will have the form:

$$F(I_1, J_2) = \frac{2}{(1-\sin\varphi)} \left| \frac{I_1}{3} \sin\varphi + \sqrt{J_2} \left(\frac{\sqrt{3}}{2} \mp \frac{1}{2\sqrt{3}} \sin\varphi \right) \right| \quad (2.63)$$

$$C_1 = \frac{2\sin\varphi}{3(1-\sin\varphi)}$$

$$C_2 = \frac{2}{1-\sin\varphi} \left\{ \sqrt{3}/2 \mp \sin\varphi/2\sqrt{3} \right\} \quad (2.64)$$

$$C_3 = 0$$

2.5.2.2 Parabolic Mohr-Coulomb

Equation 2.59 can be explicitly written for $\theta = \pm 30^{\circ}$ as follows:

$$F(I_1, J_2) = \frac{m}{2v_c(K-1)} \left| \pm\sqrt{J_2}/2\sqrt{3} - \frac{I_1}{3} - \sqrt{\left(\pm\sqrt{J_2}/2\sqrt{3} - \frac{I_1}{3} \right)^2 - 3\frac{K-1}{4K} J_2} \right| \quad (3.65)$$

The values of C_1, C_2 and C_3 for $\theta = \pm 30^{\circ}$ are given as follows:

$$C_1 = \frac{A}{3} \left(B_1/\sqrt{R_1} - 1 \right)$$

$$C_2 = A \left| \pm\frac{1}{2\sqrt{3}} - \frac{1}{2\sqrt{R_1}} \left\{ \pm\frac{B_1}{\sqrt{3}} - \frac{3(K-1)}{2K}\sqrt{J_2} \right\} \right| \quad (2.66)$$

$$C_3 = 0$$

where

$$A = \frac{m}{2v_c(K-1)}$$

$$B_1 = \pm\frac{\sqrt{J_2}}{2\sqrt{3}} - \frac{I_1}{3}$$

$$R_1 = B_1^{\,2} - \frac{3(K-1)}{4K}J_2$$

2.5.2.3 Proposed Yield Criterion

At corners ($\theta = \pm 30^{\circ}$), the expression for yield criterion is rewritten for the explicit values of $\theta = \pm 30^{\circ}$. Then the expressions for C_1, C_2 and C_3 can be derived from the θ independent form of yield criteria.

Equation 2.21 can be explicitly written for $\theta = \pm 30^{\circ}$ as follows:

$$F(I_1, J_2) = \frac{1}{2}\left[\pm A\sqrt{J_2}/2 + CI_1 + \sqrt{\left(\pm A\sqrt{J_2}/2 + CI_1\right)^2 + 3BJ_2}\right] \qquad (2.67)$$

The values of C_1, C_2 and C_3 for $\theta = \pm 30^{\circ}$ are given as follows:

$$C_1 = \frac{C}{2}\left(X_1/\sqrt{R_1} + 1\right)$$

$$C_2 = \frac{1}{2}\left[\pm\frac{A}{2} + \frac{1}{\sqrt{R_1}}\left\{\pm A\frac{X_1}{2} + 3B\sqrt{J_2}\right\}\right] \qquad (2.68)$$

$$C_3 = 0$$

where

$$X_1 = \pm A\frac{\sqrt{J_2}}{2} + CI_1$$

$$R_1 = X_1^2 + 3BJ_2$$

2.6 CRUSHING OF CONCRETE

The post-peak behavior of concrete under multiaxial compression either exhibit limited perfect plasticity or strain softening depending upon the degree of confinement of the material, with eventual crushing of concrete. The crushing type of concrete fracture is a strain-controlled phenomenon. Thus an appropriate strain criterion is developed in terms of strain invariants. Usually the strain criterion is obtained by simply converting the yield criterion described in terms of stresses directly into strains as follows:

$$f(\varepsilon_{ij}) = \bar{\varepsilon} - \varepsilon_u \tag{2.69}$$

where ε_u is an ultimate total strain extrapolated from uniaxial test results and taken as 0.0035. The loading function has the same form as stress loading function. The same material parameters used in the stress failure criterion are used in the crushing criterion. When $\bar{\varepsilon}$ reaches the value specified as the ultimate strain ε_u, the material is assumed to lose all its characteristics of strength at a specific Gauss point. Hence the incremental and total stresses are respectively given by the relationships

$$d\{\sigma\} = [\ 0\ ]\, d\{\varepsilon\} \tag{2.70}$$

and

$$\{\sigma\} = [\ 0\ ]\{\varepsilon\} \tag{2.71}$$

Usually von Mises strain criterion is used to define the equivalent

crushing strain for simplicity. In this work the equivalent crushing strain $\bar{\varepsilon}$ is evaluated using Drucker Prager strain criterion. This criterion reflects the effect of high confinement under which concrete strength increases. Using equation 2.7 with stress invariants replaced by strain invariants and f'_c by ε_u, the crushing condition is given by :

$$0.16(\varepsilon_x+\varepsilon_y)+2.0\left|\varepsilon_x^2 + \varepsilon_y^2 - \varepsilon_x\varepsilon_y + 0.75\left(\gamma_{xy}^2 + \gamma_{yz}^2 + \gamma_{zx}^2\right)\right|^{1/2} = \varepsilon_u \tag{2.72}$$

2.7 CRACKING BEHAVIOR OF CONCRETE

In addition to the elasto-plastic stress strain response, concrete cracking is one of the major contributing factors to material nonlinearities. Generally, two types of crack models, i.e., a discrete model and a smeared model, have been employed by the analysts. In the early stage of modelling, concrete cracking was represented by the discrete approach with a predefined crack pattern [44]. Although the discrete model can indeed trace the detail features of concrete cracking, the application of this approach has received only limited acceptance due to two reasons: difficulty in redefining the crack topology , and excessive computational efforts. Thus, an alternative approach, i.e., the so called 'smeared model', has become more popular in application. This approach, originally introduced by Rashid [95], has the advantage of permitting automatic crack propagation with a relatively small computational cost. Also, it offers complete generality in predicting crack directions, independent of the mesh configuration and element type used

in the analysis [96,97]. In lieu of its simplicity of application, the smeared crack approach has nevertheless a drawback in the dependence of finite element mesh sizes, as pointed out by Bazant and Cedolin [98-100]. In their study, they investigated the objectivity requirement of the smeared crack model. From the analysis of a cracked panel with the fracture mechanics concept, it was found that the use of a strength criterion in the finite element analysis is not objective and may yield incorrect solution. For the analysis of large-scale concrete structures, e.g., nuclear containment vessels, the mesh size of the finite element model may become fairly large. Then, the objectivity requirement for the cracking criterion may have a serious effect on the analysis results. In this case, a modification of the cracking criterion was recommended [100] to account for the effect of element size. In this work smeared crack model is used with corrections made in order to restore objectivity. Constitutive equations for cracked concrete are given now for plate bending applications.

The smeared crack representation implies that cracks are not discrete but distributed across a region of finite element. The main features of the present cracking model when applied to the layered plate may be summarized as follows:

1. Different crack direction is allowed for each Gauss point in each layer
2. Tension stiffening and reduced shear modulus are included in the model
3. Cracks are allowed to open or close during the load increment
4. Cracking in one or two directions is allowed and

5. Partial or full closing of the already formed cracks is allowed upon unloading.

The response of concrete under tensile stresses is assumed to be linear elastic until the cracking surface is reached and then follows the softening branch of the stress-strain curve. The isotropic linear elastic relations for uncracked concrete are given in equation 2.48. The tensile type of fracture or cracking is governed by a maximum tensile stress criterion (tension cut-off). Cracks are assumed to form in planes perpendicular to the direction of maximum principal tensile stresses of the in-plane stress components. The principal stresses are calculated as:

$$\sigma_{1/2} = \frac{\sigma_x + \sigma_y}{2} \pm \sqrt{\left(\frac{\sigma_x - \sigma_y}{2}\right)^2 + \tau_{xy}^2} \qquad (2.73)$$

Thus cracks are assumed to form in planes perpendicular to the structural plane (layer). The concrete at any Gauss point may crack in one direction if σ_1 reaches the specified concrete tensile strength f'_t. The second crack orthogonal to the first crack may occur simultaneously or subsequently depending upon the value of σ_2. Since the cracks are orthogonal, only one direction is required to be stored. The angle α between the first principal stress σ_1 and the x-axis may be calculated as follows:

$$\tan 2\alpha = \frac{2\tau_{xy}}{\sigma_x - \sigma_y} \qquad (2.74)$$

The direction of principal crack with respect to x-axis is then given by the angle 0 as follows:

$$\theta = \alpha + \pi/2 \tag{2.75}$$

After cracking the Poisson's effect is neglected due to the lack of interaction between the two orthogonal cracks and the material will be treated as an orthotropic one with material axes parallel and normal to the crack direction after cracking.

2.7.1 Tension Stiffening

To improve the realism of the representation of cracking, 'tension stiffening' has been added to this model. Fig.2.13 shows the physical situation in the vicinity of a crack in a R/C member. Fig.2.13 indicates that only at crack location, the full load is carried by the reinforcement, whereas the load between the cracks is shared between steel and concrete. This ability of concrete between cracks to share the tensile load with the reinforcement is termed 'tension stiffening'. Thus, while the concrete stress is zero at the cracks, the average stress over a cracked region is not zero. However, as the load is increased and the stress in the concrete between cracks reaches the ultimate strength, the concrete will then rupture and a further crack forms between the main cracks. Therefore, the average concrete stress over the cracked region will progressively decreases with loading. A gradual release of the concrete stress component normal to the cracked plane is adopted in this work. The process of unloading and reloading of cracked concrete is assumed to follow the linear behavior shown with a fictitious elasticity modulus E_1 (Fig.2.14), given by

$$E_1 = \alpha f'_t(1-\varepsilon_{imax}/\varepsilon_m)/\varepsilon_{imax} \; ; \qquad \varepsilon_t \le \varepsilon_{imax} \le \varepsilon_m \tag{2.76}$$

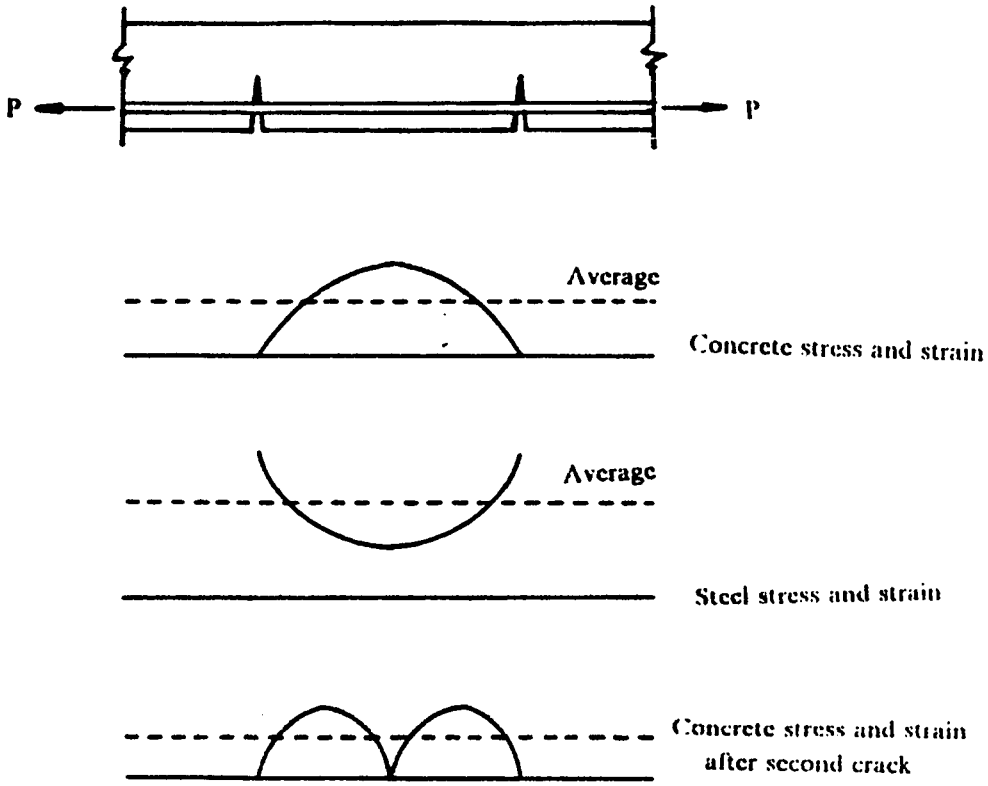

Fig. 2.13 Stress distribution in cracked reinforced concrete

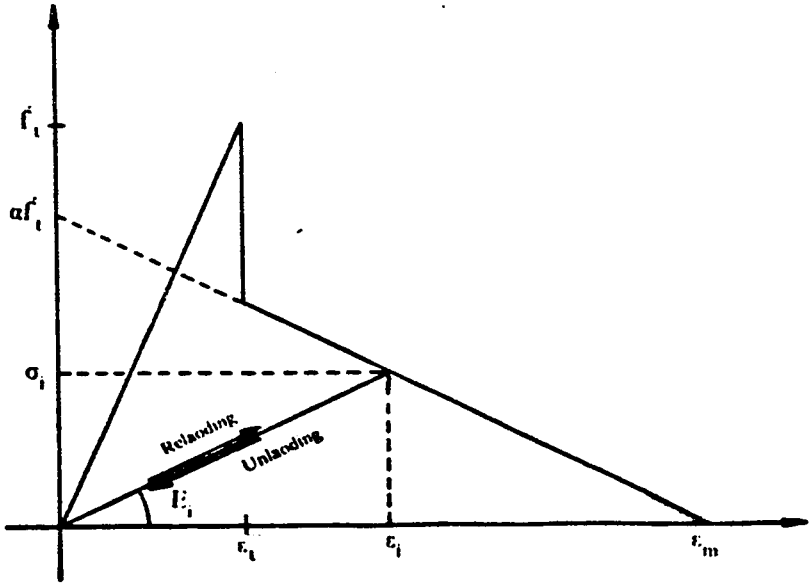

Fig. 2.14 Tension stiffening behavior in cracked concrete [93]

where α and ε_m are tension stiffening parameters and ε_{imax} is the maximum value ever reached by the tensile strain at the Gauss point under consideration. The normal stress σ_l is obtained by the following expression

$$\sigma_l = E_l \varepsilon_l, \qquad \varepsilon_t \leq \varepsilon_l \leq \varepsilon \tag{2.77}$$

where ε_l is the current tensile strain in the cracked direction l. If the strain component normal to the crack plane becomes zero or negative, the crack is assumed to close and the concrete acquires the uncracked behavior in the corresponding direction but the crack direction and the maximum tensile strain continue to be stored. Further reloading curve follows the modulus E_l depending upon ε_{imax}, i.e., the greatest strain reached at that point. This tension stiffening constitutive law is essentially as that considered by Owen and Figueiras [93].

2.7.2 Shear Degradation of Concrete

Experimental results indicate that a considerable amount of shear stress can be transferred across the rough surfaces of cracked concrete [101,102] due to the rough nature and due to dowel action of steel bars. These tests show that the primary variable in the shear transfer mechanism is the crack width. In smeared cracking model, the best way to account for aggregate interlock and dowel action is to use a reduced shear modulus G^c . This is equivalent to introducing a number of springs parallel to the crack to represent the effect of aggregate interlock and to some extent the dowel action. Hand et al [103] used a con-

stant value for G^c throughout the analysis. Later, Cedolin and Poli [77] adopted a value for G_c which is decreasing linearly with the strain normal to crack. Al-Mahaidi [76] has suggested a hyperbolic variation of G^c with the strain normal to the crack. Depending upon how the structure is shear critical, an appropriate model can be used. In the present work an approach similar to that used in [77] for R/C beams and later extended to slabs by Owen and Figueiras [93] is adopted, where the cracked shear modulus is assumed to be a function of the current tensile strain. For singly cracked concrete (Fig.2.15):

$$G^c_{12} = 0.25 \times G(1-\varepsilon_1/0.004) \; ; \quad G^c_{12} = 0 \text{ if } \varepsilon_1 \geq 0.004$$

$$G^c_{13} = G^c_{12} \tag{2.78}$$

where 1,2 refer to the directions normal and parallel to the crack and direction 3 is the global z direction. G is the uncracked concrete shear modulus and ε_1 is the tensile strain in the 1 direction. For singly cracked case G_{23} is left intact with a value of 5G/6.

For concrete cracked in two directions(Fig.2.16):

$$G^c_{13} = 0.25 \times G(1-\varepsilon_1/0.004) \; ; \; G^c_{13} = 0 \text{ if } \varepsilon_1 \geq 0.004$$

$$G^c_{23} = 0.25 \times G(1-\varepsilon_2/0.004) \; ; \; G^c_{23} = 0 \text{ if } \varepsilon_2 \geq 0.004 \tag{2.79}$$

$$G^c_{12} = 0.5 \times G^c_{13} \; ; \text{ or } G^c_{12} = 0.5 \times G^c_{23} \text{ if } G^c_{23} < G^c_{13}$$

If the crack closes the uncracked shear modulus is again resumed in the corresponding direction.

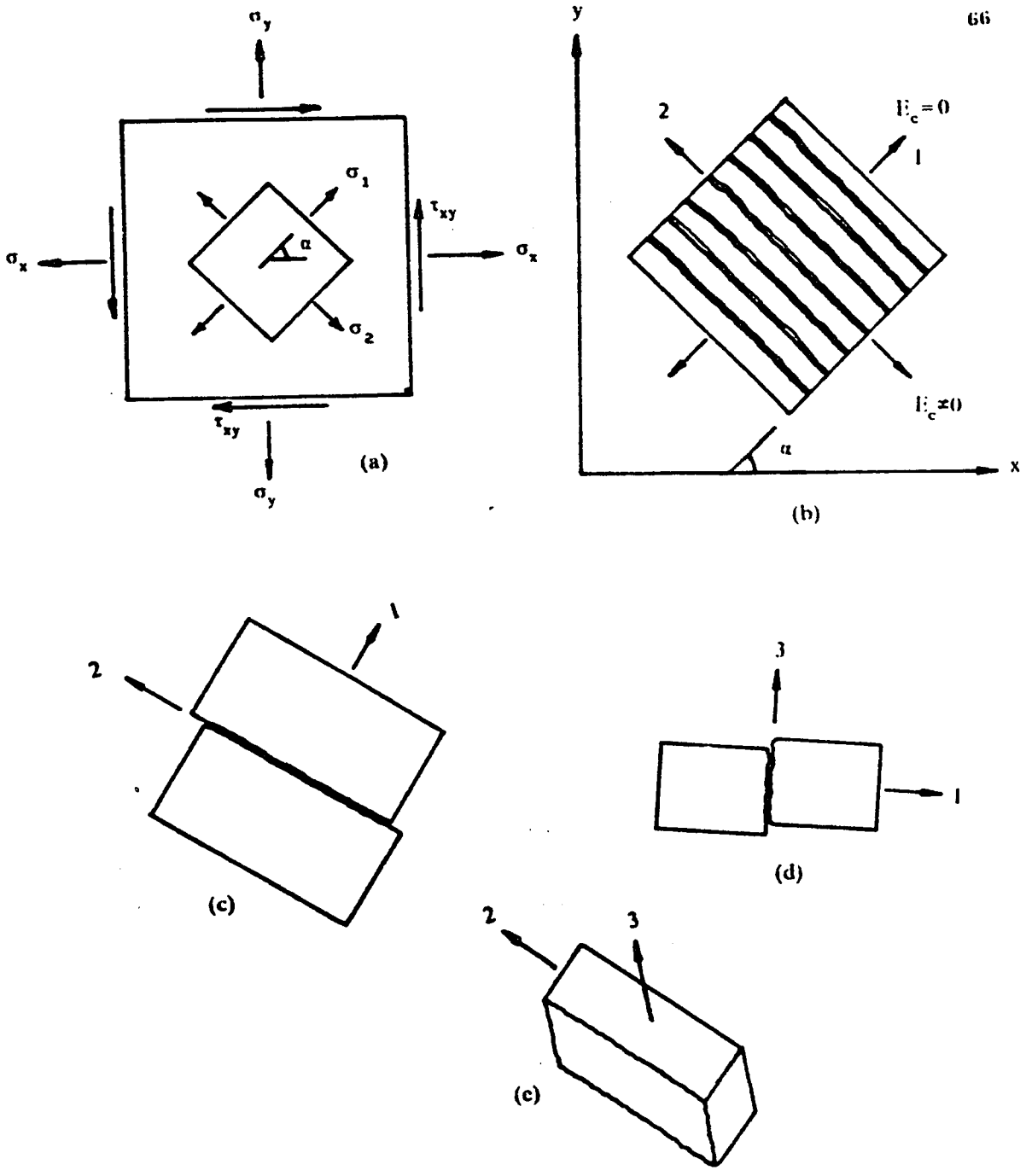

Fig. 2.15 Cracked concrete in one direction (a) Directions of principal axes (b) Direction of smeared cracks in one direction (c) Shear stiffness reduction in cracked material plane 12 (d) Shear stiffness reduction in cracked material plane 13 (e) Intact shear stiffness in plane 23

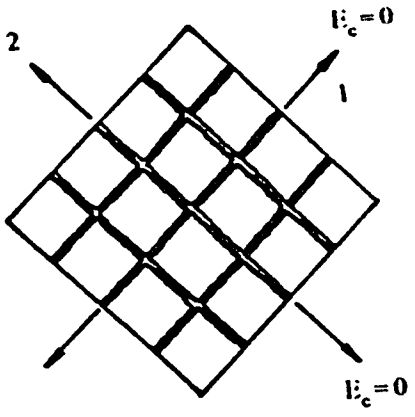

Fig. 2.16 Cracked concrete in two directions

2.7.3 Constitutive Matrix for Cracked Concrete

The total stresses at any Gauss point at the onset of cracking are given with respect to the local material coordinate system 1,2 and 3 as follows, with direction 3 coinciding with the global z-axis (Fig.2.15). For singly cracked concrete by virtue of σ reaching f'_t, the stress-strain relations are given by

$$\begin{Bmatrix} \sigma_1 \\ \sigma_2 \\ \tau_{12} \\ \tau_{13} \\ \tau_{23} \end{Bmatrix} = \begin{bmatrix} E_1 & 0 & 0 & 0 & 0 \\ 0 & E & 0 & 0 & 0 \\ 0 & 0 & G^c_{12} & 0 & 0 \\ 0 & 0 & 0 & G^c_{13} & 0 \\ 0 & 0 & 0 & 0 & 5G/6 \end{bmatrix} \begin{Bmatrix} \varepsilon_1 \\ \varepsilon_2 \\ \gamma_{12} \\ \gamma_{13} \\ \gamma_{23} \end{Bmatrix} \tag{2.80}$$

And if σ_2 also reaches f'_t, a second crack is assumed to occur normal to the direction of σ_2 i.e., orthogonally to the first crack. For doubly cracked concrete the stress-strain relations are as follows:

$$\begin{Bmatrix} \sigma_1 \\ \sigma_2 \\ \tau_{12} \\ \tau_{13} \\ \tau_{23} \end{Bmatrix} = \begin{bmatrix} E_1 & 0 & 0 & 0 & 0 \\ 0 & E_2 & 0 & 0 & 0 \\ 0 & 0 & G^c_{12} & 0 & 0 \\ 0 & 0 & 0 & G^c_{13} & 0 \\ 0 & 0 & 0 & 0 & G^c_{23} \end{bmatrix} \begin{Bmatrix} \varepsilon_1 \\ \varepsilon_2 \\ \gamma_{12} \\ \gamma_{13} \\ \gamma_{23} \end{Bmatrix} \tag{2.81}$$

where E_i and E_1 are equal to zero for loading whilst for unloading and reloading, it has nonzero value according to equation 2.76. And the shear moduli G^c_{12}, G^c_{13}, and G^c_{23} are degraded according to equation 2.78 or 2.79.

2.7.4 Transformation of Constitutive Matrix

The global stresses are calculated using the transformed cracked material constitutive matrix. To derive this global constitutive matrix, the stress and strains are first transformed. Considering the rotation of xy plane about z axis (Fig.2.15), the stresses in the cracked direction are expresses as follows:

$$\{\sigma^m\} = [A]\{\sigma^g\} \tag{2.82}$$

and

$$\{\varepsilon^m\} = [B]\{\varepsilon^g\} \tag{2.83}$$

where m and g refer to the cracked material and the global directions respectively. [A] and [B] are given as:

$$[A] = \begin{bmatrix} [A_1] & 0 \\ 0 & [A_2] \end{bmatrix} \quad ; \quad [B] = \begin{bmatrix} [B_1] & 0 \\ 0 & [A_2] \end{bmatrix} \tag{2.84}$$

where

$$[A_1] = \begin{bmatrix} \cos^2\theta & \sin^2\theta & 2\sin\theta\cos\theta \\ \sin^2\theta & \cos^2\theta & -2\sin\theta\cos\theta \\ -\sin\theta\cos\theta & \sin\theta\cos\theta & \cos^2\theta - \sin^2\theta \end{bmatrix} \tag{2.85}$$

$$[A_2] = \begin{bmatrix} \cos\theta & \sin\theta \\ -\sin\theta & \cos\theta \end{bmatrix} \tag{2.86}$$

$$[B_1] = \begin{bmatrix} \cos^2\theta & \sin^2\theta & \sin\theta\cos\theta \\ \sin^2\theta & \cos^2\theta & -\sin\theta\cos\theta \\ -2\sin\theta\cos\theta & 2\sin\theta\cos\theta & \cos^2\theta - \sin^2\theta \end{bmatrix} \tag{2.87}$$

And finally the global constitutive matrix is given as:

$$[D^g] = [A]^{-1}[D^m][B] \quad ; \text{ where } \quad [A]^{-1} = [B]^T \tag{2.88}$$

2.8 BEHAVIOR OF STEEL

A smeared model is used in the present work wherein the reinforcing bars are considered as steel layers of equivalent thickness. The dowel effect is incorporated by adding the shear stiffness in the direction of steel bar. For steel in x-direction and in y-direction, the shear stiffnesses G_{xz} and G_{yz} are introduced, respectively. For the steel in direction i the constitutive matrix is shown as follows:

$$|D_s| = \begin{bmatrix} E_{is} & 0 & 0 & 0 & 0 \\ 0 & 0 & 0 & 0 & 0 \\ 0 & 0 & 0 & 0 & 0 \\ 0 & 0 & 0 & G_{iz} & 0 \\ 0 & 0 & 0 & 0 & 0 \end{bmatrix} \quad (2.89)$$

where E_{is} and G_{iz} are modulus of elasticity and shear stiffness of steel in the direction of steel i, respectively. Transformation is then performed in order to get the global constitutive matrix using equation 2.88. The stress correction for elasto-plastic steel is performed in a generalized triaxial sense using the flow and hardening rules with von Mises yield criterion. The element stiffness matrix is simply evaluated by adding the contributions from concrete and steel layers together.

$$|K|^e = |K_c|^e + |K_s|^e \quad (2.90)$$

For the case when dowel effect is not to be considered each steel layer is assumed to have a uniaxial behavior resisting, only the axial force in the bar direction with a bilinear elasto-plastic idealization.

Chapter 3

FINITE ELEMENT MODEL

3.1 INTRODUCTION

A computer code 'FATIMA' has been developed for reinforced concrete plates using the eight/nine node quadrilateral elements derived from the degeneration of a three dimensional element. Five degrees of freedom are specified at each nodal point, corresponding to three displacements and two rotations of the normal at that node. The five degrees of freedom element allows for modelling of in-plane stretching of shear deformable or Mindlin plates, which is essential in investigating the influence of support restraint on punching resistance of reinforced concrete slabs. This approach may be considered as a generalization of the classical Mindlin plate formulation, in which three degrees of freedom at each nodal point are used corresponding to two rotations of the normal and the transverse displacement. In this formulation and in the Mindlin plate formulation shear deformations are accounted for, and these have the advantage of only requiring C(0) continuity of the displacement and rotation fields of normals.

A layered model is used in order to observe progressive damage through the thickness. Stresses, strains and change in the characteristics of material are monitored at Gauss integration points in each

layer. Any material represented at a Gauss point may remain elastic, crack, yield or crush. It is possible that the material may crack in one direction whilst yielding (under combined shear and tension) at the same time. Selective integration scheme is employed using normal 3 x 3 integration rule for bending and membrane energy terms and 2 x 2 integration rule for shear terms.

In this chapter the governing equilibrium equations are derived by using minimization of the total potential energy, and the finite element discretization is presented for 8-node Serendipity, 9-node Lagrangian and Heterosis elements. Finally, the selective integration scheme in the context of layered model is elaborated.

3.2 FINITE ELEMENT FORMULATION

The governing equilibrium equations are derived by minimizing the total potential energy of the system.

3.2.1 Total Potential Energy of the System

If the structural system is subjected to a set of body forces {b} and boundary tractions {t} over the volume and surface of the domain Ω and Γ, respectively, then the total potential energy can be written as :

$$\Pi = \frac{1}{2}\int_{\Omega}\{\varepsilon\}^{T}\{\sigma\}d\Omega - \int_{\Omega}\{u\}^{T}\{b\}d\Omega - \int_{\Gamma}\{u\}^{T}\{t\}d\Gamma \qquad (3.1)$$

where {u} is the global displacement vector.

Discretizing the vectors {u} and {ε} globally as :

$$\{u\} = |N|\ \{d\} \tag{3.2}$$

$$\{\varepsilon\} = |B|\ \{d\} \tag{3.3}$$

Equation 3.1 can now be expressed as

$$\Pi = \frac{1}{2}\int\{d\}^T\ |B|^T\ \{\sigma\}d\Omega - \int\{d\}^T\ |N|^T\ \{b\}d\Omega - \int\{d\}^T\ |N|^T\{t\}d\Gamma \tag{3.4}$$

Further, using

$$\{\sigma\} = |D|\{\varepsilon\} \tag{3.5}$$

(|D| being elastic or elasto-plastic) and minimizing total potential energy with respect to nodal displacements

$$\frac{d\Pi}{d\{d\}} = 0 \tag{3.6}$$

yields

$$\int|B|^T|D||B|\{d\}d\Omega - \int|N|^T\{b\}d\Omega - \int|N|^T\{t\}d\Gamma = 0 \tag{3.7}$$

Equation 3.7 may now be recast in the form

$$|K|\{d\} = \{f\} \tag{3.8}$$

where :

$$|K| = \int|B|^T|D||B|d\Omega \tag{3.9}$$

is the global stiffness matrix

{d} is the global displacement vector

and

$$\{f\} = \int|N|^T\{b\}d\Omega + \int|N|^T\{t\}d\Gamma \tag{3.10}$$

is the global load vector.

3.2.2 Element Stiffness Matrix

In order to determine the global stiffness matrix and the global load vector of the system, the contribution to them from each element needs to be determined. Expression 3.4 for the total potential energy of the plate can be written as the sum of the contributions Π_e from each element

$$\Pi = \sum_{e-1}^{n} \Pi^e \tag{3.11}$$

Minimization of the total potential energy with respect to global displacements implies minimization of potential energy of every element with respect to the corresponding element displacement vector $\{d^e\}$.

Equation 3.6 implies that for each element

$$\frac{d\Pi^e}{d\{d^e\}} = 0 \tag{3.12}$$

and this yields the element stiffness matrix

$$[K^e] = \int [B^e]^T [D^e][B^e] d\Omega^e \tag{3.13}$$

and element load vector

$$\{f^e\} = \int [N^e]^T \{b^e\} d\Omega^e + \int [N^e]^T \{t\} d\Gamma^e \tag{3.14}$$

where $[N^e]$ and $[B^e]$ are the element shape matrix and element strain matrix respectively, described in the next section of this chapter. $[D^e]$ is the element constitutive matrix.

For ease of numerical computation, a typical submatrix of $[K^e]$ link-

ing nodes i and j may be expressed as:

$$|K^e_{ij}|_{5\times5} = \int |B^e_i|^T |D^e| |B^e_j| d\Omega^e \simeq \iiint |B^e_i|^T |D^e| |B^e_j| \det J \, d\xi d\eta d\zeta \qquad (3.15)$$

3.3 DEGENERATE PLATE ELEMENT FORMULATION

The approach of discretizing the three dimensional equations of continuum mechanics for plates and shells was originally introduced by Ahmed et al. [104] for the linear analysis of moderately thick shells. In this approach independent rotational and displacement degrees of freedom are employed, by degenerating the three dimensional stress and strain conditions to plate/shell behavior.

3.3.1 Basic Assumptions

Two basic assumptions are adopted in this process :

(i) The stress normal to the mid-surface of the plate is constrained to be zero in the constitutive equations.

(ii) Normals to the mid-surface before deformation remain straight but not necessarily normal to the mid-surface after deformation.

3.3.2 Finite Element Discretization

3.3.2.1 Element Geometry

In the isoparametric formulation the coordinates of a point within the element are obtained by applying the element shape functions to the nodal coordinates. The coordinates in the z- direction are obtained by using a normalized coordinate ζ varying from -1 to +1 corresponding to bottom and top points in the plate in order to facilitate the location of different layers and Gauss integration points through the thickness (Fig 3.1). For defining element geometry, 8-node Serendipity or 9-node Lagrangian shape functions may be used.

$$\begin{Bmatrix} x \\ y \\ z \end{Bmatrix} = \sum_{k=1}^{n} N_k \begin{Bmatrix} x_k \\ y_k \\ z_k \end{Bmatrix}_{mid} + \frac{h}{2}\zeta \begin{Bmatrix} 0 \\ 0 \\ 1 \end{Bmatrix} \tag{3.16}$$

3.3.2.2 Displacement Field

The displacement field $\{u\}=[u,v,w]^T$ at any point in the plate in direction x,y and z respectively, is defined by the five degrees of freedom at each nodal point corresponding to its three displacements and the two rotations of the normal at the node. The definition of the independent rotational and displacement degrees of freedom permits transverse shear deformation to be taken into account. The displacements of a point on the normal resulting from the two rotations are cal-

culated as illustrated in Fig.3.2. In view of the small incremental rotations, a linear relationship is assumed. The displacements δ_{1k} and δ_{2k} due to two rotations β_{1k}, β_{2k} are given as:

$$\delta_{1k} = h\beta_{1k}$$

$$\delta_{2k} = -h\beta_{2k} \tag{3.17}$$

Note that with assumed positive directions of rotations, displacement due to rotation β_{2k} would be in the negative y-direction. The element displacement field can then be expressed as

$$\begin{Bmatrix} u \\ v \\ w \end{Bmatrix} = \sum_{k-1}^{n} N_k \begin{Bmatrix} u_k \\ v_k \\ w_k \end{Bmatrix}_{mid} + \sum_{k-1} N_k \frac{h}{2}\zeta \begin{Bmatrix} \beta_{1k} \\ -\beta_{2k} \\ 0 \end{Bmatrix} \tag{3.18}$$

The use of normalized coordinates in z directions provides great convenience in defining different material layer thicknesses and their position through the depth.

The contribution to the global displacements from a given node k is

$$\begin{Bmatrix} u \\ v \\ w \end{Bmatrix} = \begin{bmatrix} N_k & 0 & 0 & N_k\zeta\frac{h}{2} & 0 \\ 0 & N_k & 0 & 0 & -N_k\zeta\frac{h}{2} \\ 0 & 0 & N_k & 0 & 0 \end{bmatrix} \begin{Bmatrix} u_k \\ v_k \\ w_k \\ \beta_{1k} \\ \beta_{2k} \end{Bmatrix} \tag{3.19}$$

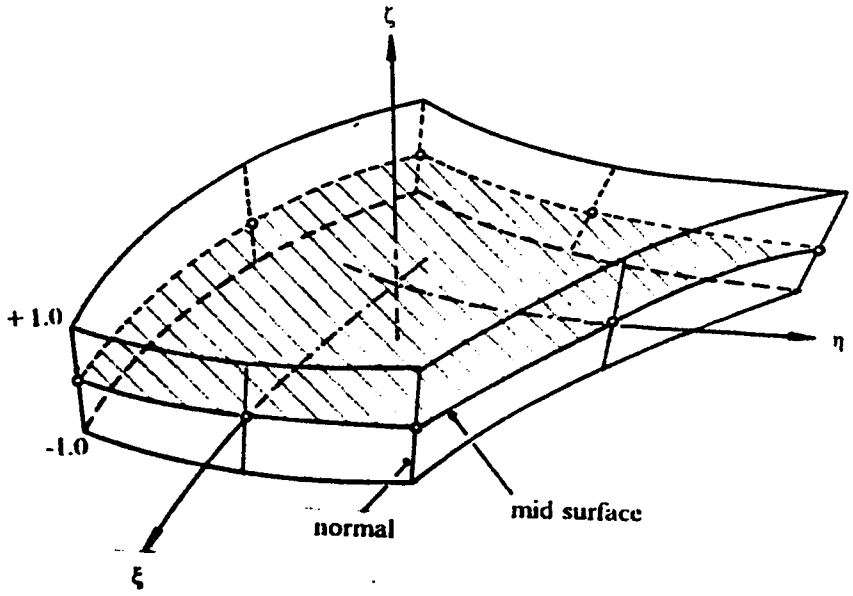

Fig.3.1 Degenerate plate element

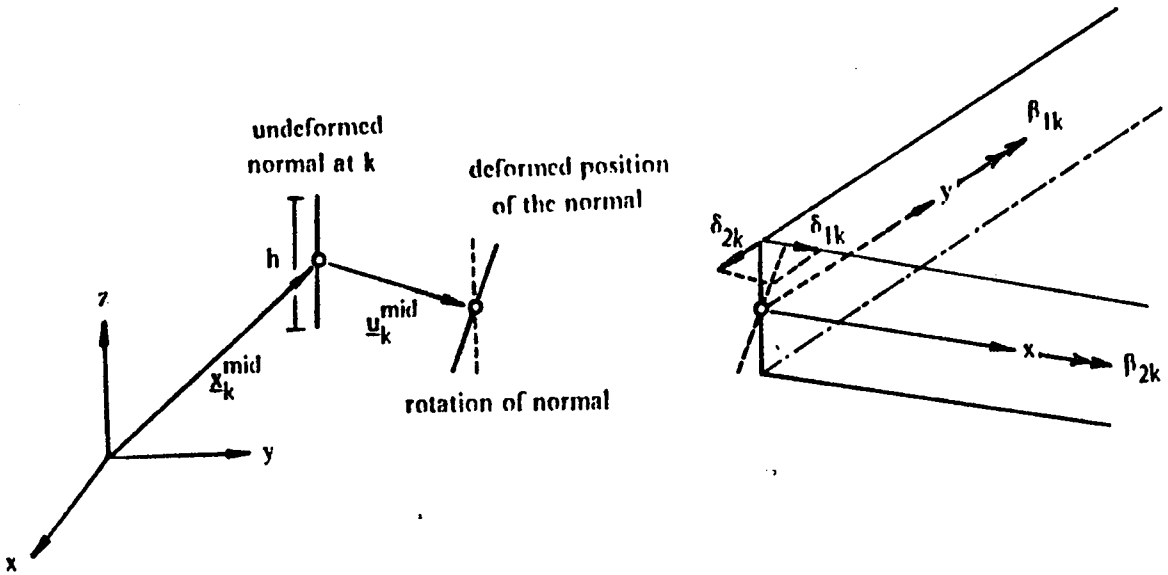

Fig. 3.2 Displacement of a point on the normal at node k

or

$$\underline{u}_k = \underline{N}_k \underline{\delta}_k \tag{3.20}$$

For the complete element, the displacement field is

$$\underline{u}^e = \sum_{k-1}^{n} \underline{N}_k(\xi,\eta)\underline{\delta}_k \tag{3.21}$$

where n is the number of nodes in the element.

3.3.3 Plate Elements

A brief review of the quadratic elements used in this work is presented. The elements considered are the 8-node Serendipity, the 9-node Lagrangian and the Heterosis element (Fig.3.3).

3.3.3.1 8-node Serendipity

The 8-node Serendipity has been the simplest element of the quadratic quadrilateral isoparametric family. The shape functions are given as follows:

for corner nodes i=1,3,5,7

$$N_i^e = \frac{1}{4}(1+\xi\xi_i)(1+\eta\eta_i)(\xi\xi_i+\eta\eta_i-1) \tag{3.22a}$$

for mid side nodes i=2,4,6,8

$$N_i^e = \frac{\xi_i^2}{2}(1+\xi\xi_i)(1-\eta^2)+\frac{\eta_i^2}{2}(1+\eta\eta_i)(1-\xi^2) \tag{3.22b}$$

The results obtained with this element by using a normal integration

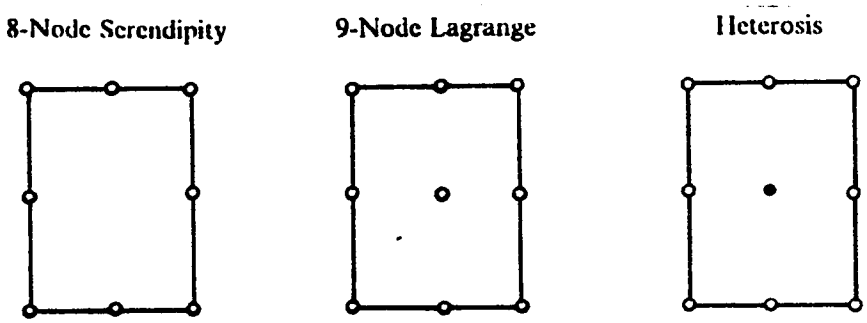

Fig. 3.3 Nodal configuration of the three quadratic plate elements

rule (3x3) showed that the solution becomes increasingly stiff as the plate thickness is reduced [104]. This is called locking and is exhibited by this element even in moderately thin situations. A great improvement of the results was achieved by using a reduced integration rule (2x2). However, for very thin situations the results given by 8-node Serendipity element with reduced integration exhibited locking again [105,106].

3.3.3.2 9-node Lagrangian

Experiments carried out by Pugh et al. [107] with linear, quadratic and cubic elements of the Serendipity and Lagrangian families showed that the 9-node Lagrangian element is nearly optimal as a general plate element. The shape functions are given as follows:

for corner nodes i=1,3,5,7

$$N_i^e = \frac{1}{4}(\xi^2 + \xi\xi_i)(\eta^2 + \eta\eta_i) \tag{3.23a}$$

for mid side nodes i=2,4,6,8

$$N_i^e = \frac{1}{2}\eta_i^2(\eta^2 - \eta\eta_i)(1-\xi^2) + \frac{1}{2}\xi_i^2(\xi^2 - \xi\xi_i)(1-\eta^2) \tag{3.23b}$$

and for central node the bubble Lagrangian function is used

$$N_i^e = (1-\xi^2)(1-\eta^2) \tag{3.23c}$$

The performance exhibited by Lagrangian elements appeared to be superior to Serendipity elements when reduced or selective integration

was adopted. However a serious problem may arise with this element when reduced integration is employed; the stiffness matrix exhibits rank deficiency which causes the appearance of spurious mechanisms [107-110]. These communicable mechanisms may result in very erratic solutions, specially when the restraints imposed by the boundary conditions are minimal.

3.3.3.3 Heterosis Element

The shortcomings pointed out above (locking and spurious mechanism) led to the development of the Heterosis element. This 9-node quadrilateral element employs Serendipity shape functions for the transverse displacements u,v and w of the middle surface and Lagrangian shape functions for the rotations β_1, β_2 [111]. The Heterosis element exhibits improved characteristics when compared with each of the previous quadratic elements. When selectively integrated, its stiffness matrix possesses correct rank and the element doesn't lock in very thin situations.

3.3.4 Strain Displacement Relationship

Using small deformation theory and noting that the strain normal to the mid-surface ε_z is zero since displacement w is taken to be independent of z, the five significant strains are expressed as:

$$\{\varepsilon\} = \begin{Bmatrix} \varepsilon_x \\ \varepsilon_y \\ \gamma_{xy} \\ \gamma_{xz} \\ \gamma_{yz} \end{Bmatrix} = \begin{bmatrix} \frac{\partial u}{\partial x} \\ \frac{\partial v}{\partial y} \\ \frac{\partial u}{\partial y} + \frac{\partial v}{\partial x} \\ \frac{\partial u}{\partial z} + \frac{\partial w}{\partial x} \\ \frac{\partial v}{\partial z} + \frac{\partial w}{\partial y} \end{bmatrix} \tag{3.24}$$

Substituting equation 3.18 in equation 3.24 gives the strain-displacement relationship for an element e as follows:

$$\begin{Bmatrix} \varepsilon_x \\ \varepsilon_y \\ \gamma_{xy} \\ \gamma_{xz} \\ \gamma_{yz} \end{Bmatrix} = \begin{bmatrix} \sum_{k-1}^{n} \frac{\partial N_k}{\partial x} & 0 & 0 & \sum_{k-1}^{n} \frac{\partial N_k}{\partial x}\zeta\frac{h}{2} & 0 \\ 0 & \sum_{k-1}^{n} \frac{\partial N_k}{\partial y} & 0 & 0 & -\sum_{k-1}^{n} \frac{\partial N_k}{\partial y}\zeta\frac{h}{2} \\ \sum_{k-1}^{n} \frac{\partial N_k}{\partial y} & \sum_{k-1}^{n} \frac{\partial N_k}{\partial x} & 0 & \sum_{k-1}^{n} \frac{\partial N_k}{\partial y}\zeta\frac{h}{2} & -\sum_{k-1}^{n} \frac{\partial N_k}{\partial x}\zeta\frac{h}{2} \\ 0 & 0 & \sum_{k-1}^{n} \frac{\partial N_k}{\partial x} & \sum_{k-1}^{n} N_k & 0 \\ 0 & 0 & \sum_{k-1}^{n} \frac{\partial N_k}{\partial y} & 0 & -\sum_{k-1}^{n} N_k \end{bmatrix} \begin{Bmatrix} u_k \\ v_k \\ w_k \\ \beta_{1k} \\ \beta_{2k} \end{Bmatrix} \tag{3.25}$$

$$\{\varepsilon\}^e = \sum_{1}^{e} [B_i^e]\{\delta_i^e\} \tag{3.26}$$

Contribution from a node to the element strain matrix $[B]^e$ is

$$[B_i]^e = \begin{bmatrix} \frac{\partial N_i}{\partial x} & 0 & 0 & \frac{\partial N_i}{\partial x}\zeta\frac{h}{2} & 0 \\ 0 & \frac{\partial N_i}{\partial y} & 0 & 0 & -\frac{\partial N_i}{\partial y}\zeta\frac{h}{2} \\ \frac{\partial N_i}{\partial y} & \frac{\partial N_i}{\partial x} & 0 & \frac{\partial N_i}{\partial y}\zeta\frac{h}{2} & -\frac{\partial N_i}{\partial x}\zeta\frac{h}{2} \\ 0 & 0 & \frac{\partial N_i}{\partial x} & N_i & 0 \\ 0 & 0 & \frac{\partial N_i}{\partial y} & 0 & -N_i \end{bmatrix} \tag{3.27}$$

The Cartesian shape function derivatives $\frac{\partial N_i^e}{\partial x}$ and $\frac{\partial N_i^e}{\partial y}$ in the strain matrix may be obtained by using the chain rule of partial differentiation:

$$\begin{aligned} \frac{\partial N_i^e}{\partial \xi} &= \frac{\partial N_i^e}{\partial x}\frac{\partial x}{\partial \xi} + \frac{\partial N_i^e}{\partial y}\frac{\partial y}{\partial \xi} \\ \frac{\partial N_i^e}{\partial \eta} &= \frac{\partial N_i^e}{\partial x}\frac{\partial x}{\partial \eta} + \frac{\partial N_i^e}{\partial y}\frac{\partial y}{\partial \eta} \\ \frac{\partial N_i^e}{\partial \zeta} &= \frac{\partial N_i^e}{\partial z}\frac{\partial z}{\partial \zeta} \end{aligned} \tag{3.28}$$

In matrix form:

$$\begin{Bmatrix} \frac{\partial N_i^e}{\partial \xi} \\ \frac{\partial N_i^e}{\partial \eta} \\ \frac{\partial N_i^e}{\partial \zeta} \end{Bmatrix} = \begin{bmatrix} \frac{\partial x}{\partial \xi} & \frac{\partial y}{\partial \xi} & 0 \\ \frac{\partial x}{\partial \eta} & \frac{\partial y}{\partial \eta} & 0 \\ 0 & 0 & \frac{\partial z}{\partial \zeta} \end{bmatrix} \begin{Bmatrix} \frac{\partial N_i^e}{\partial x} \\ \frac{\partial N_i^e}{\partial y} \\ \frac{\partial N_i^e}{\partial z} \end{Bmatrix} \tag{3.29}$$

or

$$\begin{Bmatrix} \frac{\partial N_i^e}{\partial \xi} \\ \frac{\partial N_i^e}{\partial \eta} \\ \frac{\partial N_i^e}{\partial \zeta} \end{Bmatrix} = |J_i^e| \begin{Bmatrix} \frac{\partial N_i^e}{\partial x} \\ \frac{\partial N_i^e}{\partial y} \\ \frac{\partial N_i^e}{\partial y} \end{Bmatrix} \tag{3.30}$$

where $|J^e|$ is the Jacobian matrix given by

$$|J^e| = \begin{bmatrix} \frac{\partial x}{\partial \xi} & \frac{\partial y}{\partial \xi} & 0 \\ \frac{\partial x}{\partial \eta} & \frac{\partial y}{\partial \eta} & 0 \\ 0 & 0 & \frac{\partial z}{\partial \zeta} \end{bmatrix} = \begin{bmatrix} \sum_{i=1}^{n} \frac{\partial N_i^e}{\partial \xi} x_i & \sum_{i=1}^{n} \frac{\partial N_i^e}{\partial \xi} y_i & 0 \\ \sum_{i=1}^{n} \frac{\partial N_i^e}{\partial \eta} x_i & \sum_{i=1}^{n} \frac{\partial N_i^e}{\partial \eta} y_i & 0 \\ 0 & 0 & \frac{h}{2} \end{bmatrix} \tag{3.31}$$

The Cartesian derivatives $\frac{\partial N_i^e}{\partial x}$ and $\frac{\partial N_i^e}{\partial y}$ are now calculated as:

$$\begin{Bmatrix} \frac{\partial N_i^e}{\partial x} \\ \frac{\partial N_i^e}{\partial y} \\ \frac{\partial N_i^e}{\partial z} \end{Bmatrix} = |J_i^e|^{-1} \begin{Bmatrix} \frac{\partial N_i^e}{\partial \xi} \\ \frac{\partial N_i^e}{\partial \eta} \\ \frac{\partial N_i^e}{\partial \zeta} \end{Bmatrix} \tag{3.32}$$

The discretized elemental volume is given in the isoparametric formulation as

$$dv = dx.dy.dz = \det J \; d\xi d\eta d\zeta \tag{3.33}$$

3.3.5 Strain Displacement Relationship for Heterosis Element

Heterosis element formulation is achieved by using Serendipity shape functions for mid-plane displacements u, v and w and Lagrangian shape functions for the rotations β_1, β_2. If N_k^s and N_k^l denote Serendipity and Lagrangian shape functions respectively, then the element displacement field can be expressed by

$$\begin{Bmatrix} u \\ v \\ w \end{Bmatrix} = \sum_{k=1}^{n} N_k^s \begin{Bmatrix} u_k \\ v_k \\ w_k \end{Bmatrix}_{mid} + \sum_{k=1}^{n} N_k^l \frac{h}{2}\zeta \begin{Bmatrix} \beta_{1k} \\ -\beta_{2k} \\ 0 \end{Bmatrix} \tag{3.34}$$

The contribution to the global displacements from a given node k is

$$\begin{Bmatrix} u \\ v \\ w \end{Bmatrix} = \begin{bmatrix} N_k^s & 0 & 0 & N_k^l \zeta \frac{h}{2} & 0 \\ 0 & N_k^s & 0 & 0 & -N_k^l \zeta \frac{h}{2} \\ 0 & 0 & N_k^s & 0 & 0 \end{bmatrix} \begin{Bmatrix} u_k \\ v_k \\ w_k \\ \beta_{1k} \\ \beta_{2k} \end{Bmatrix} \tag{3.35}$$

And the strain displacement relationship for an element can be written as follows:

$$\begin{Bmatrix} \varepsilon_x \\ \varepsilon_y \\ \gamma_{xy} \\ \gamma_{xz} \\ \gamma_{yz} \end{Bmatrix} = \begin{bmatrix} \sum_{k=1}^{n} \frac{\partial N_k^s}{\partial x} & 0 & 0 & \sum_{k=1}^{n} \frac{\partial N_k^l}{\partial x}\zeta\frac{h}{2} & 0 \\ 0 & \sum_{k=1}^{n} \frac{\partial N_k^s}{\partial y} & 0 & 0 & -\sum_{k=1}^{n} \frac{\partial N_k^l}{\partial y}\zeta\frac{h}{2} \\ \sum_{k=1}^{n} \frac{\partial N_k^s}{\partial y} & \sum_{k=1}^{n} \frac{\partial N_k^s}{\partial x} & 0 & \sum_{k=1}^{n} \frac{\partial N_k^l}{\partial y}\zeta\frac{h}{2} & -\sum_{k=1}^{n} \frac{\partial N_k^l}{\partial x}\zeta\frac{h}{2} \\ 0 & 0 & \sum_{k=1}^{n} \frac{\partial N_k^s}{\partial x} & \sum_{k=1}^{n} N_k^l & 0 \\ 0 & 0 & \sum_{k=1}^{n} \frac{\partial N_k^s}{\partial y} & 0 & -\sum_{k=1}^{n} N_k^l \end{bmatrix} \begin{Bmatrix} u_k \\ v_k \\ w_k \\ \beta_{1k} \\ \beta_{2k} \end{Bmatrix} \quad (3.36)$$

In order to determine the Cartesian derivatives based on the mixed Serendipity and Lagrangian formulations, two Jacobian matrices are evaluated using Serendipity and Lagrangian shape functions separately. Note that while using the Serendipity shape functions the summation is over n (nine) nodes by including the shape function for the 9th node as Lagrangian bubble function in order to avoid any singularity.

A second approach is adopted in [93], wherein the Serendipity shape functions are defined for the eight nodes on the boundary and Lagrangian bubble function is used for 9th central node and the mid-plane displacements u, v and w are constrained for the 9th node. This approach resulted in stiff results and is not recommended for adoption.

3.4 NUMERICAL INTEGRATION

Numerical integration of isoparametric plate bending element is an important aspect of the element efficiency. In through thickness

direction, the integration is simplified with the use of layered model. At any layer mid-surface (ζ = constant) the normal (full) integration rule consists of m x m Gauss integration points where m is the number of nodes along each element side. Nevertheless the normal integration exhibits shear and membrane locking [107-110]. Reduced and selective integration schemes have been suggested to overcome the locking phenomenon. The reduced integration technique introduced first by Zienkiewics et al [105] of using (m-1) x (m-1) Gauss points was proven to be absolutely essential for lower order elements. However for higher order elements, uniform application of reduced integration led to spurious zero energy modes in the global stiffness matrix. An alternative procedure of selective integration has been proposed. In the selective integration scheme, bending and membrane terms are integrated using normal rule, while the shear terms are computed using the reduced integration rule. The process involves the following three steps [93].

(i) shear terms in the strain matrix B are computed at the four Gauss points I,II, III and IV of the 2 x 2 reduced integration rule.

(ii) Using the shape functions $N_r(\xi,\eta)$, the terms of the B matrix computed in (i) are extrapolated to the nine Gauss points of the 3 x 3 integration rule.

$$B(\xi,\eta)_n = \sum_{r=1}^{4} N_r(\xi,\eta)_n B(\xi,\eta)_r \qquad (3.37)$$

where $(\xi,\eta)_n$ and $(\xi,\eta)_r$ correspond to Gauss point positions in the normal and reduced integration rules respectively. The four shape functions $N_r(\xi,\eta)$ are defined by

Table 3.1 Constants for selective integration rule

Point Number	Shape Function	ξ_r	η_r
I	N_1	-1.0/0.57735	-1.0/0.57735
II	N_2	-1.0/0.57735	+1.0/0.57735
III	N_3	+1.0/0.57735	-1.0/0.57735
IV	N_4	+1.0/0.57735	+1.0/0.57735

$$N_r(\xi,\eta) = 1/4(1+\xi\xi_r)(1+\eta\eta_r) \qquad (3.38)$$

where ξ_r and η_r are determined so that each of the N_r shape functions takes a unit value at the corresponding Gauss point (2 x 2 rule) and is zero at the other three positions. The values of ξ_r and η_r are given in Table 3.1

(iii) The bending and membrane terms of B matrix are computed at the nine Gauss points of the normal integration rule.

3.5 LAYERED MODEL

If the plate is built up from a series of layers of different materials such as the case of reinforced concrete, fiber reinforced, and overlay structure, an appropriate integration through the thickness has to be carried out, since the stresses are discontinuous function of ε. In non-linear material problems, the stress profile in the thickness direction should be known at a reasonable number of points where the constitutive laws are satisfied. In reinforced concrete plate problems, the nonlinear behavior of concrete in compression, cracked concrete and reinforcement need a convenient representation across the structure thickness. In the present finite element model all these cases are accommodated in a simple and effective manner by using a layered approach wherein a mid-point integration scheme is adopted for each layer.

Layers are numbered sequentially, starting at the bottom surface of plate. Each layer contains Gauss integration points on its mid surface. The stress components are computed at each Gauss point of every layer

and assumed to be constant over the thickness of each layer, so that the actual stress distribution of the plate is modelled by a piecewise constant approximation as shown in Fig.3.4. Layers of different thicknesses can be employed, as well as different number of layers per element. The specification of the layer thickness in terms of nondimensional coordinate ζ permits the variation of layer thickness.

From equation (3.15), the element stiffness matrix for an element can be written as:

$$|k^e| = \int_{-1}^{+1} \int |B^e|^T |D^e| |B^e| \det J \, dA \, d\zeta = \int_{-1}^{+1} |X| d\zeta \tag{3.39}$$

and equivalent internal nodal force vector (used in the calculation of residual force vector) can be written as:

$$|p^e| = \int_{-1}^{+1} \int |B^e|^T \{\sigma\} \det J \, dA \, d\zeta = \int_{-1}^{+1} |Y| d\zeta \tag{3.40}$$

In equations 3.41 and 3.42, integrands |X| and |Y| are obtained by the integration on layer mid-surface at ζ corresponding to that layer. Later these are summed up over the layers as follows.

$$|k^e| = \sum_{i=1}^{l} |X|^i \Delta\zeta^i \tag{3.41}$$

and

$$|p^e| = \sum_{i=1}^{l} |Y|^i \Delta\zeta^i \tag{3.42}$$

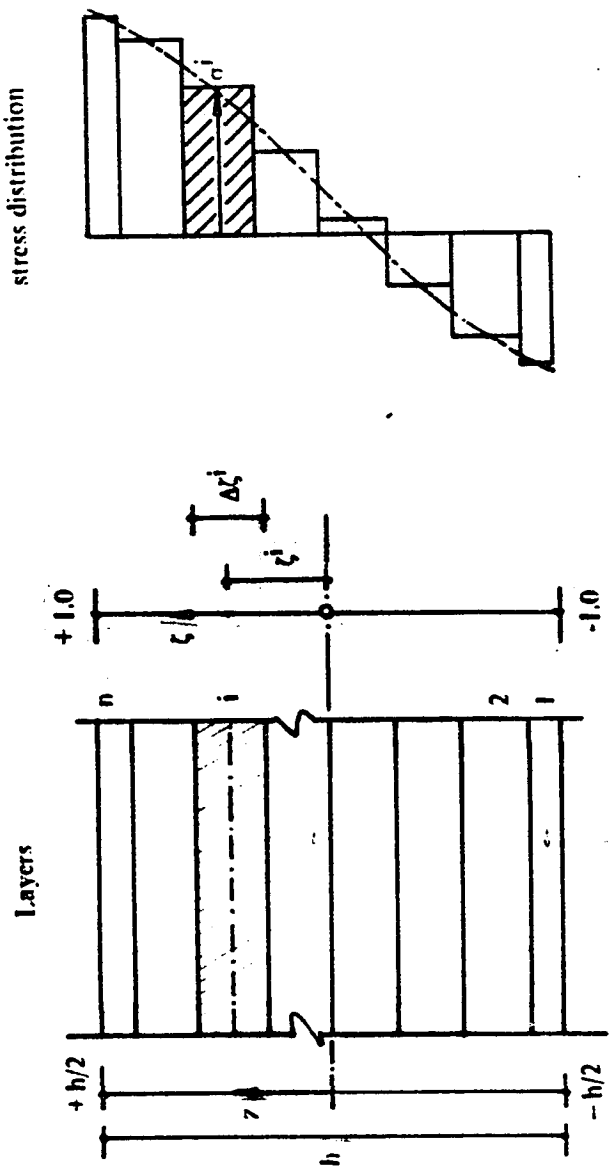

Fig. 3.4 Layered model

Chapter 4

FINITE ELEMENT IMPLEMENTATION

4.1 INTRODUCTION

This Chapter presents a detailed discussion regarding the implementation of the material model and the finite element model discussed in Chapters 2 and 3 respectively. Program FATIMA is written in FORTRAN code in a modular form consisting of various subroutines called from the master and from within themselves. This program is written along the same format as outlined by Prof. Owen and Hinton at University College of Swansea in their books on finite element modelling [93,94]. In this chapter, a general description of the program is presented.

FATIMA has many interesting features that make it very flexible and versatile. For instance, it offers dynamic dimensioning, choice of convergence criteria, variety of options in the material model, element types, integration scheme, solution algorithm, and selective output for graphical postprocessing . Such a flexibility makes it a useful tool for research purposes. Furthermore, the program has also been provided with a restart facility which enables the nonlinear analysis to be broken into a series of separate distinct computer runs. The program generates data in a suitable format such that the postprocessing graphical

representation of results is achieved,including material degradation in a sectional view through the thickness, cracking pattern in the bottom of the slab and plots of distribution of stresses and strains at a desired layer.

In the following sections, the various options, the structure and the description of the functions of various subroutines are presented.

4.2 PROGRAM FATIMA (OPTIONS)

Program FATIMA has variety of options making it very comprehensive and flexible. These options can be classified under two classes:

(i) Finite element parameters

(ii) Material parameters

4.2.1 Finite Element Parameters

(a) Type of elements including:

- 8-node Serendipity
- 9-node Lagrangian
- Heterosis

(b) Solution Algorithm

- Initial stiffness method
- Tangential stiffness calculation at first iteration of the increment
- Tangential stiffness calculation at second iteration of the increment

(c) Integration scheme

- Normal integration
- Reduced integration
- Selective integration

(d) Layered Model

- Different elements can have different number of layers of different thicknesses and of different materials

(e) Load cases

- Gravity
- Concentrated
- Uniformly distributed
- Centrifugal

(f) Output of Converged/Unconverged results at different intervals of increments.

- Only displacements
- Displacements and reactions
- Displacements, reactions, stresses, stress resultant and material status

(g) The boundary conditions can be precisely defined using 5 degrees of freedom which include the mid-plane displacements u, v, w, and the two rotations about x and y axes

(h) Restart facility: The analysis can be restarted at any intermediate increment of load.

(i) Convergence criteria

- Displacement norm
- Residual force norm
- Both displacements and rotations

(j) Maximum number of iterations and tolerance for convergence

(k) Post processing for plotting

- Deformed sectional view
- Load deflection curve
- Material state in the sectional view
- Cracking pattern in the bottom view
- Stress and strain distribution in a given layer.

4.2.2 Material Based Parameters

(l) Yield criterion for concrete

- Drucker Prager
- Mohr-Coulomb
- Parabolic Mohr-Coulomb

(m) Concrete hardening

- Perfectly plastic
- with isotropic hardening

(n) Shear degradation

- Normal
- Full
- No degradation

(o) Crushing of concrete

- No crushing
- Crushing with von Mises strain criterion
- Crushing with Drucker Prager strain criterion

(p) Tension stiffening

- No tension stiffening

- Tension stiffening with given variable parameters

(q) Elasto-plastic steel

- Perfectly plastic

- Bilinear elasto-plastic

4.3 FLOW OF OPERATIONS

Fig.4.1 illustrates the flow of operations for the nonlinear incremental-iterative procedure schematically.

4.4 METHODOLOGY

The main features of the nonlinear incremental-iterative solution are presented as follows:

Before entering the increment loop, all the arrays of stresses, strains, effective stresses, effective plastic strains and directions of cracks are initialized to zero in subroutine ZERO. The material status is initialized as elastic for steel and for concrete Gauss points. If the analysis has to be restarted after certain number of increments, then all the information at the last converged increment is read from TAPE 12 and subsequent load increment is applied. On TAPE 12, all the necessary information is written as per instruction in subroutine RESTAR after convergence is achieved at the end of each increment.

At the beginning of the r^{th} load increment, the displacements $\{d\}^{r-1}$ and the stresses $\{\sigma\}^{r-1}$ are known, as well as the unbalanced nodal

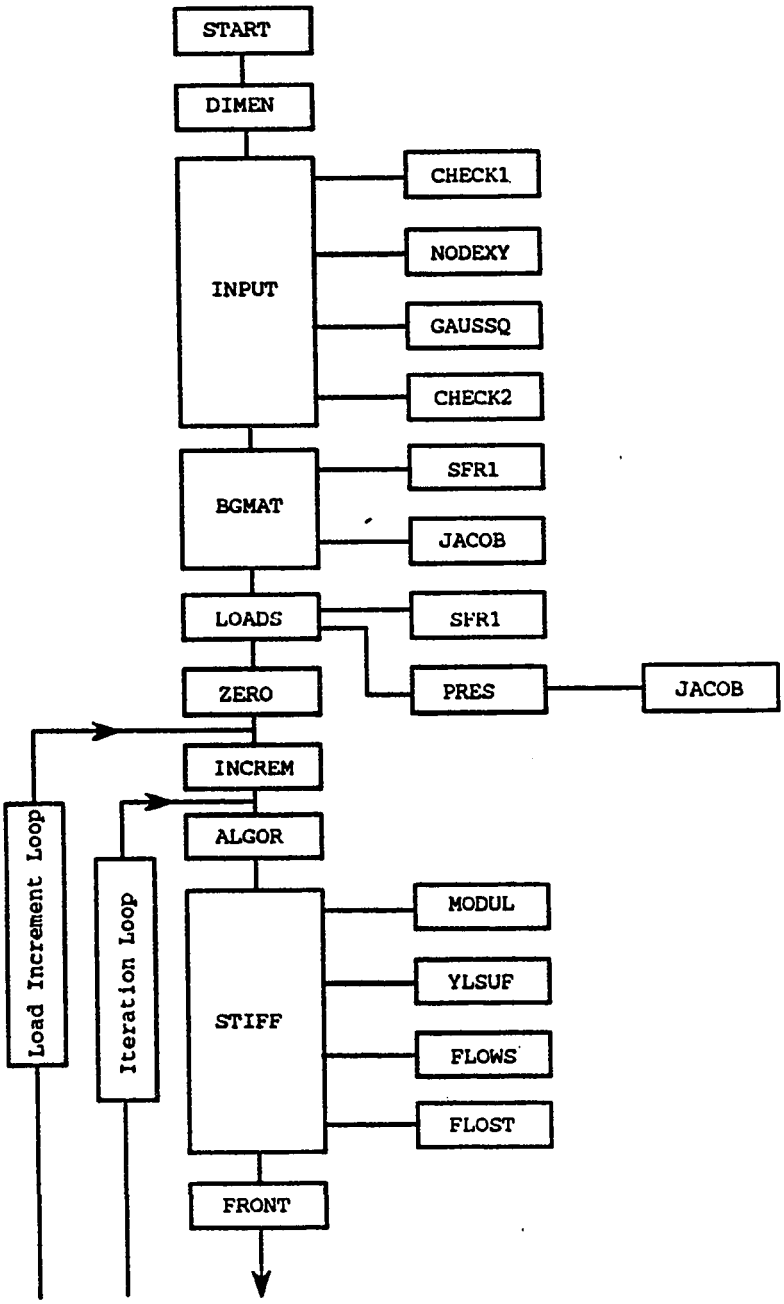

Fig.4.1 Flow of Operations (Contd.)

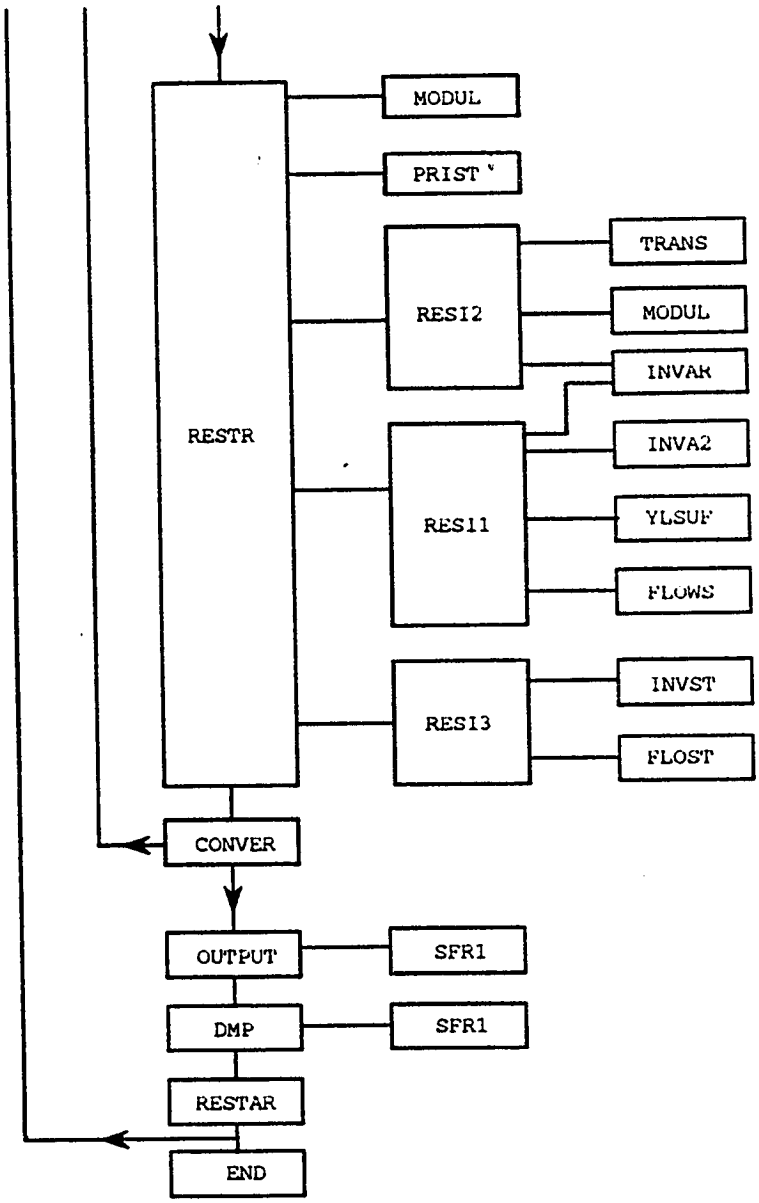

Fig.4.1 Flow of Operations

forces $\{\psi\}^{r-1}$ resulting from the previous load increment. The incremental nodal forces are as follows :

$$\{\psi\}^{r} = \{\psi\}^{r-1} + \{df\}^{r} \tag{4.1}$$

where $\{df\}^{r}$ is the r^{th} load increment. The iterative process is performed with the following steps for a generic iteration, i :

1. The stiffness matrix [K] is updated or not according to the solution algorithm adopted. This algorithm is directed from subroutine ALGOR

2. The incremental displacements $\{\Delta d\}^{i}$ are evaluated using the equilibrium equations

$$\{\Delta d\}^{i} = - [K]^{-1} \{\psi\}^{i-1} \tag{4.2}$$

where $\{\psi\}^{i-1}$ are the unbalanced nodal forces resulting from the previous iteration. The total displacement vector $\{d\}^{i}$ is then updated,

$$\{d\}^{i} = \{d\}^{i-1} + \{\Delta d\}^{i} \tag{4.3}$$

3. The incremental strains $\{d\varepsilon\}^{i}$ and the total strains $\{\varepsilon\}^{i}$ are evaluated,

$$\{d\varepsilon\}^{i} = [B] \{\Delta d\}^{i} \tag{4.4}$$

$$\{\varepsilon\}^{i} = [B] \{d\}^{i} \tag{4.5}$$

where |B| is the strain matrix at a Gauss point.

4. The incremental stresses $\{d\sigma\}^i$ and the total stresses $\{\sigma\}^i$ are calculated,

$$\{d\sigma\}^i = |D| \{d\varepsilon\}^i \tag{4.6}$$

$$\{\sigma\}^i = \{\sigma\}^{i-1} + \{d\sigma\}^i \tag{4.7}$$

where |D| is the elasticity matrix taken as:

- either the elastic matrix of uncracked concrete or the corresponding matrix of cracked concrete for concrete layers
- or the elastic matrix for steel layers.

5. The stresses are corrected according to the material constitutive equations (elaborated in more detail in section 4.6) :

4.4.1 Concrete Layers

- Using the total stresses $\{\sigma\}^i$ the maximum principal stress σ_1 , acting in the structural plane(layer), is calculated.
- If $\sigma_1 > f_t'$ or, if the concrete is already cracked, the stresses are updated according to tension stiffening and shear degradation.
- Using $\{\sigma\}^i$ or the stresses updated in the previous step, the effective stress $\bar{\sigma}$ is calculated according to the yield function.
- If $\bar{\sigma}$ is greater than the initial yield stress of if the Gauss point

has already yielded, the stresses are corrected according to the elasto-plastic behavior.

4.4.2 Steel Layers

- Using the total stresses $\{\sigma\}^i$,the effective stress in the reinforcement $\bar{\sigma}$ is obtained according to von Mises yield criterion.
- If $\bar{\sigma}$ is greater than the steel yield stress f_y or if the Gauss point has already yielded, the stresses are treated elasto-plastically.

6. The equivalent internal nodal forces $\{p\}^i$ are evaluated using numerical integration, as

$$\{p\}^i = \int_V [B]^T \{\sigma\}^i dV \tag{4.8}$$

where $\{\sigma\}^i$ are the total stress components corrected according to the constitutive equations.

7. The out of balance forces $\{\psi\}^i$ are calculated,

$$\{\psi\}^i = \{f\}^i - \{p\}^i \tag{4.9}$$

where $\{f\}^i$ is the current external nodal force vector.

8. The convergence of the process is checked:

- If convergence is achieved proceed to the next load increment

- If the convergence criterion is not satisfied restart the iterative cycle from step 1.

4.5 DESCRIPTION OF SUBROUTINES

A detailed discussion now follows of the function of major subroutines of FATIMA

4.5.1 Dynamic Dimensioning

For any given problem the maximum dimensions are first calculated by program DIMENC and required storage is specified in the top of the program. And in subroutine DIMEN within the program, the maximum dimensions are defined and passed to all subroutines as arguments. This approach has the advantage that the maximum dimensions can be updated in a very simple and straightforward manner. This helps in saving a considerable amount of core space and results in the optimum use of core storage with minimal chance of errors related to dimensions.

4.5.2 Input and Output Module

The subroutine INPUT first reads the control parameters defining various options, element and layer discretization(geometry), material properties and boundary conditions. It calls NODEX for generation of coordinates of midside and middle nodes using the given coordinates of corner nodes. It also reads Gauss point locations and their weights through subroutine GAUSSQ. After reading all the data this subroutine

calls two diagnostic subroutines CHECK1 and CHECK2 for verification of the data already read for any possible errors before going for expensive runs. If the error is diagnosed then the rest of the data is echoed by subroutine ECHO and the program terminates.

Subroutine LOADS reads first the control parameters to identify the types of loading applied. Then it calculates the consistent nodal forces due to each type the of given loading. Subroutine PRES is called when the given loading is uniformly distributed over certain elements.

Subroutine OUTPUT displays the output selectively depending upon the options given as control parameters in subroutine INCREM. In INCREM, the load factors, values of tolerance for convergence and maximum number of iterations required for convergence for each increment are provided.

A selective data is written on different files in subroutine DMP in a way that the graphical postprocessing of the data is handled later by plotting programs.

4.5.3 Data Management

Program FATIMA deals with voluminous data which has to be transferred through different subroutines; thus the use of scratch files (magnetic tapes) becomes inevitable. This helps reducing in central core storage dramatically. Unfortunately this is achieved at the expense of the time required for operating these devices (rewinding, reading and writing). The full description of the function of each

device and the flow of data using tapes between different parts of the program are given in Fig.4.2.

4.5.4 Stiffness and Solution Module

Before entering the incremental and iterative loops the strain matrix [B] is evaluated in subroutine BGMAT at each Gauss integration point of each layer of all elements. In subroutine BGMAT the shear terms are evaluated at four Gauss points and then these are extrapolated to nine Gauss points. It is then written on TAPE 8 in the sequence of elements and layers so that this need not be evaluated every time.

In STIFF, the strain matrix [B] for each Gauss point is read and [D] at that Gauss point is evaluated depending upon the state of material as elastic, cracked or elasto-plastic. Using [B] and [D] matrices the element stiffness matrix $[K^e]$ is evaluated by performing numerical integration within the layers and summation through the thickness over all layers. It is then written on TAPE 1 in the sequence of elements.

In FRONT, equations of equilibrium are then assembled and variables are eliminated at the same time using the frontal technique introduced by Irons [112]. In this technique, as soon as the coefficients of an equation are completely assembled from the contributions of all relevant elements, the corresponding variable can be eliminated. A detailed description of this technique is outlined in [113].

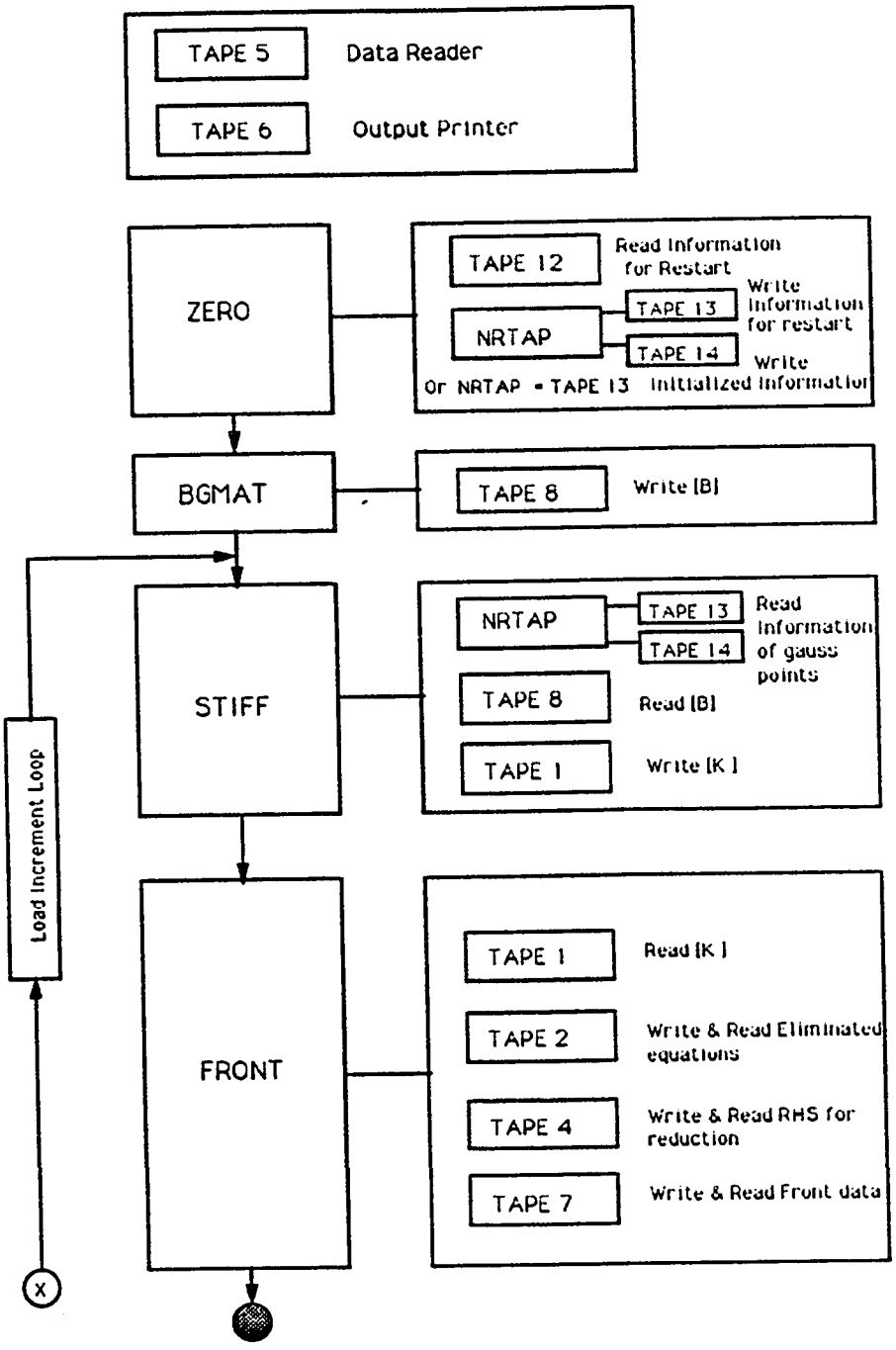

Fig.4.2 Data Management through TAPES (Contd.)

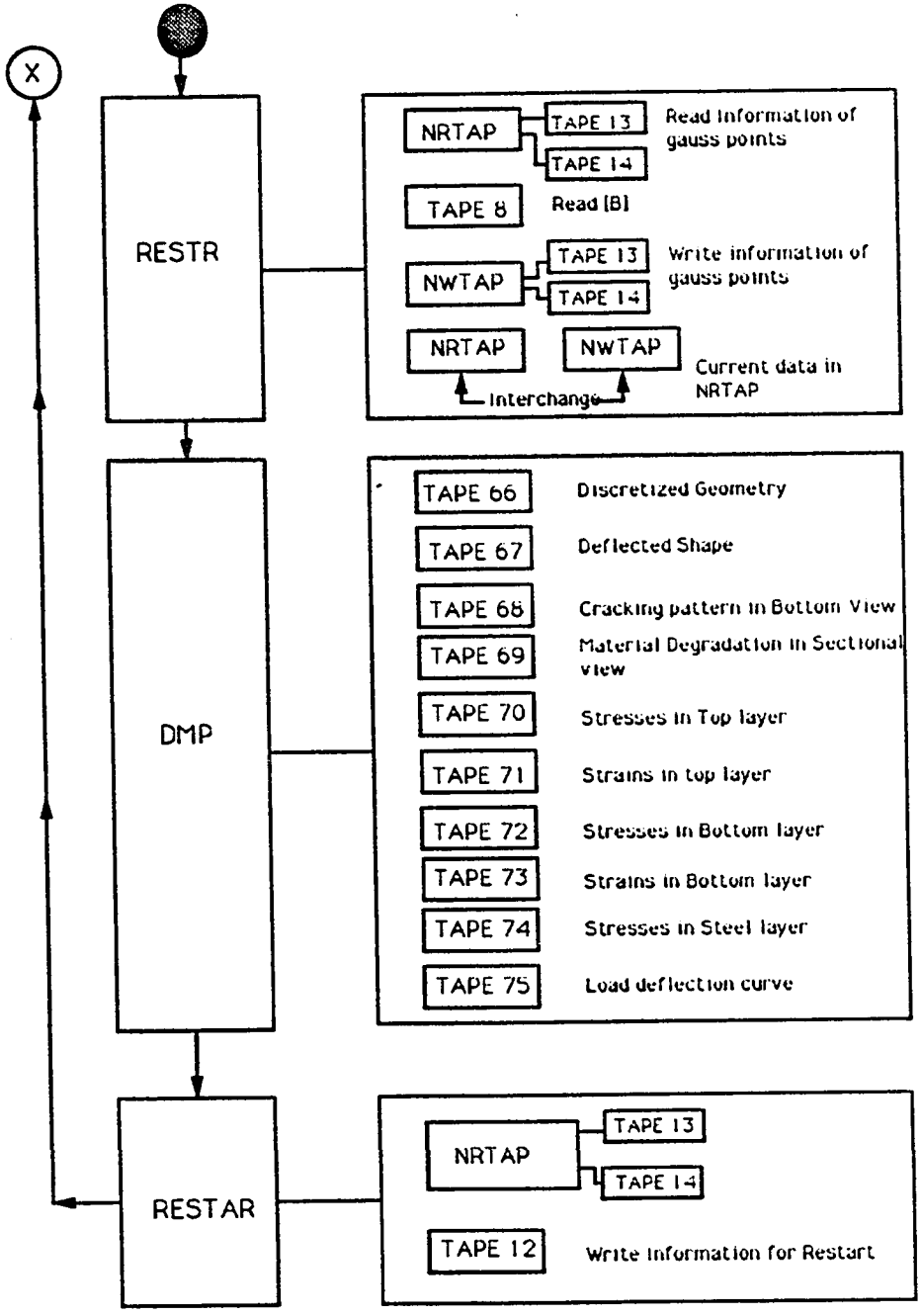

Fig.4.2 Data Management through TAPES

4.5.5 Subroutine MODUL

This subroutine is called frequently in many subroutines such as STIFF, RESTR, RESI1, RESI2 and RESI3. It evaluates mainly elastic constitutive matrix [D] for cracked and uncracked concrete and steel.

4.5.6. Subroutine SFR1 and JACOB

These are frequently called subroutines. Subroutine SFR1 calculates the shape functions and their derivatives at any given value of natural coordinates at sampling points. Subroutine JACOB calculates the Cartesian derivatives and the Jacobean matrix and its derivative by using the information obtained from SFR1.

4.6 CORRECTION OF STRESSES

Subroutine RESTR is the most important component of the nonlinear elasto-plastic iterative-incremental computational algorithm. During the application of an increment of load a Gauss point of an element may yield whilst other Gauss points may remain elastic, crack or crush. Also it is possible that a Gauss point may crack in one direction whilst also yielding (in combined tension/shear) overall. At the end of every iteration, at each Gauss point the status of the material, direction of cracking and the greatest cracking strain ever reached for a cracked Gauss point, stresses, strains, plastic strains and effective stresses are stored on TAPE NRTAP (alternating between TAPE 13 and TAPE 14). At the subsequent iteration, all the previous information is read and

updated by satisfying the criteria of material degradation. Eventually in this subroutine nodal forces are evaluated which are statically equivalent to the corrected stress field. The difference of applied nodal loads and these equivalent nodal loads gives the residual forces which are reduced in successive iterations to a tolerable value to meet the desired degree of convergence in subroutine CONVER.

4.6.1 Correction of Stresses for Yielding Gauss points

Stresses at the Gauss points that are yielding are corrected by satisfying the elasto-plastic conditions such as yield criterion, flow and hardening rules. The following are the steps used for the correction of yielding Gauss points in steel and concrete layers in the generalized multiaxial frame work.

(a) At the beginning of any generic i^{th} iteration the residual forces are $\{\psi\}^{i-1}$, which give rise to incremental displacement $\{\Delta d\}^{i}$. Then using the strain matrix at a Gauss point, incremental strains $\{d\varepsilon\}^{i}$ are evaluated.

(b) Using the elastic- uncracked or cracked $|D|$ matrix, the elastic increment of stresses $\{d\sigma_e\}^{i}$ are evaluated.

(c) The total stresses are accumulated for each Gauss point as

$$\{\sigma_e\}^{i} = \{\sigma\}^{i-1} + \{d\sigma\}^{i}$$

where $\{\sigma\}^{i-1}$ are the corrected stresses for iteration i-1.

(d) The next step depends on whether or not yielding took place at

the Gauss point during the r^{i-1} iteration. Therefore it is checked if $\bar{\sigma}^{i-1} \leq \sigma_y^{i-1}$, where $\bar{\sigma}^{i-1}$ is the effective stress at previous iteration and σ_y^{i-1} is the previous yield stress. For the elastic state of stress the σ_y^{i-1} is taken as σ_{yo}, the initial yield stress. For subsequent yielding, the yield stress is modified by using the hardening parameter as obtained from the result of a uniaxial test.

** If $\bar{\sigma}^{i-1} < \sigma_y^{i-1}$, then the Gauss point had not yielded previously. Now it is checked to see if $\bar{\sigma}_e^{\,i} > \sigma_{yo}$, where $\bar{\sigma}_e^{\,i}$ is the effective stress corresponding to $\{\sigma_e\}^i$

*** If the answer is NO, then the Gauss point is still elastic and therefore go directly to Step g.

*** If the answer is YES, the Gauss point had yielded during application of load corresponding to this iteration as shown in Fig.4.3. The portion of stress greater than the yield value must be reduced to the yield surface. The reduction factor R is given to be:

$$R = \frac{AB}{AC} = \frac{\bar{\sigma}_e^{\,i} - \sigma_y^{i-1}}{\bar{\sigma}_e^{\,i} - \bar{\sigma}^{i-1}} \qquad (4.10)$$

Go to Step e.

** If $\bar{\sigma}^{i-1} = \sigma_y^{i-1}$, then the Gauss point had yielded previously. Now it is checked to see if $\bar{\sigma}_e^{\,i} > \bar{\sigma}^{i-1}$

*** If the answer is NO, then the Gauss point is unloading

elastically and therefore go directly to Step g.

*** If the answer is YES, the Gauss point had yielded previously and the stress is still increasing. Therefore all excess stress $\{\sigma_e\}^i - \{\sigma\}^{i-1}$ must be reduced to the yield surface as indicated in Fig. 4.4. Therefore the factor R which defines the portion of stress which must be corrected to satisfy the yield criterion is equal to 1.

(e) Compute the portion of the total stress which satisfies the yield criterion as $\{\sigma\}^{i-1} + (1-R)\{d\sigma_e\}^i$

(f) The remaining portion of stress $R\{d\sigma_e\}^i$ corresponding to BA in Fig 4.3 must be effectively eliminated by satisfying the yield criterion, normality condition and hardening rule.

In the post-yield range the elasto-plastic stress increment is given by:

$$\{d\sigma_{ep}\}^i = |D_{ep}|\{d\varepsilon_{ep}\}^i$$

Using equation 2.40

$$\{d\sigma_{ep}\}^i = \left[|D| - \frac{|D|\ \{a\}\ \{a\}^T\ |D|}{A + \{a\}^T\ |D|\ \{a\}}\right]\{d\varepsilon_{ep}\}^i \qquad (4.11)$$

$$\{d\sigma_{ep}\}^i = |D|\{d\varepsilon_{ep}\}^i - \left[\frac{|D|\ \{a\}\ \{a\}^T\ |D|}{A + \{a\}^T\ |D|\ \{a\}}\right]\{d\varepsilon_{ep}\}^i \qquad (4.12)$$

Using equation 2.38 in equation 4.12

$$\{d\sigma_{ep}\}^i = |D|\{d\varepsilon_{ep}\}^i - |D|\ \{a\}\ d\lambda \qquad (4.13)$$

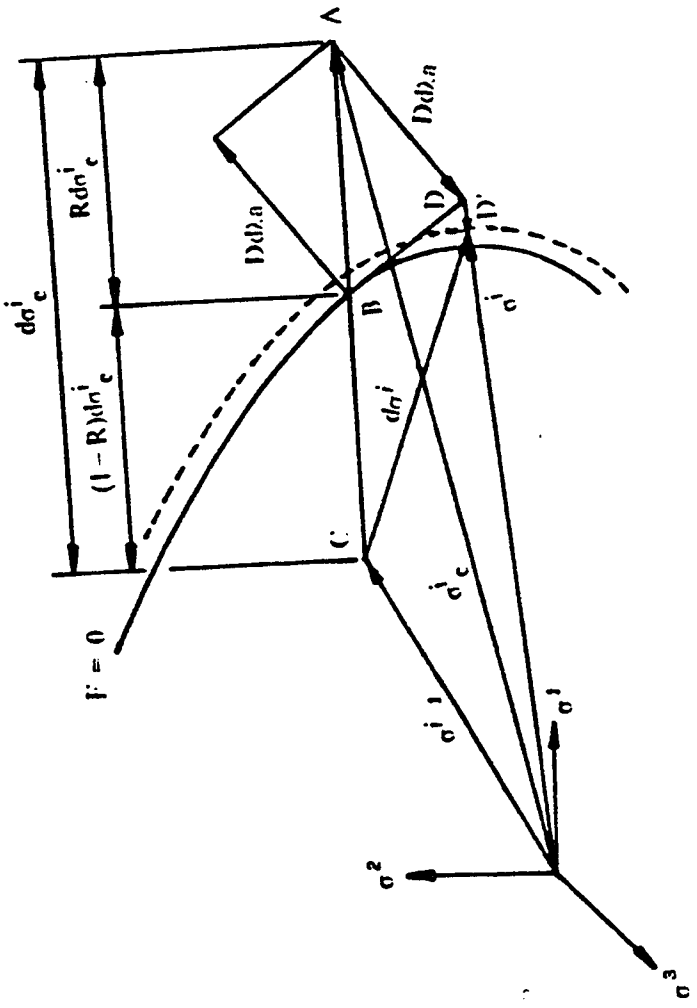

Fig. 4.3 Correction of stresses for yielding Gauss points for R < 1

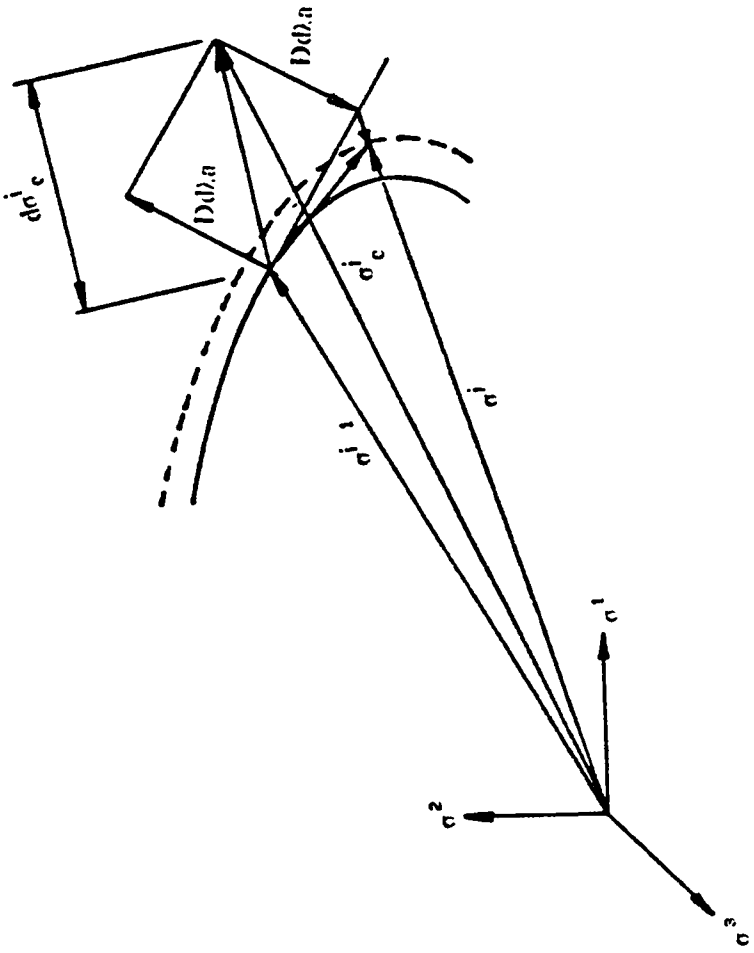

Fig. 4.4 Correction of stresses for yielding Gauss points for R = 1

Now using relations

$$\{d\varepsilon_{ep}\}^i = R\{d\varepsilon\}^i \tag{4.14}$$

and

$$[D]\{d\varepsilon\}^i = \{d\sigma_e\}^i \tag{4.15}$$

in equation 4.13, results in

$$\{d\sigma_{ep}\}^i = R\{d\sigma_e\}^i - [D]\{a\}\, d\lambda \tag{4.16}$$

Equation 4.16 gives the elasto-plastic increment satisfying the elasto-plastic conditions wherein the first term corresponds to BA and the second term corresponds to AD in Fig. 4.3. The second term is obtained by satisfying the normality condition at B. Therefore the total stresses corresponding to point D are given as:

$$\{\sigma\}^i = \{\sigma\}^{i-1} + (1-R)\{d\sigma_e\}^i + \{d\sigma_{ep}\}^i \tag{4.17}$$

Using equation 4.13 in equation 4.17 it yields the form:

$$\{\sigma\}^i = \{\sigma\}^{i-1} + (1-R)\{d\sigma_e\}^i + R\{d\sigma_e\}^i - [D]\{a\}\, d\lambda\{d\sigma_{ep}\}^i \tag{4.18}$$

The effective plastic strain is evaluated by considering the work hardening hypothesis given by:

$$d\chi = \{\sigma\}^{iT} d\{\varepsilon_p\}^i = \bar{\sigma} d\bar{\varepsilon}_p^i \tag{4.19}$$

which yields

$$d\bar{\varepsilon}_p^{\,i} = \frac{\{\sigma\}^{iT} d\{\varepsilon_p\}^i}{\bar{\sigma}} \tag{4.20}$$

where $d\{\varepsilon_p\}^i$ is calculated using the normality rule (equation 2.21). The current effective plastic strain is now computed by adding

increment $d\bar{\varepsilon}_p^{\,i}$ to the previous effective plastic strain $\bar{\varepsilon}_p^{\,i-1}$

$$\bar{\varepsilon}_p^{\,i} = \bar{\varepsilon}_p^{\,i-1} + \{\sigma\}^{iT} d\lambda \frac{\{a\}}{\bar{\sigma}} \tag{4.21}$$

However in order to satisfy the hardening law the new point D has to be corrected by scaling the vector $\{\sigma\}^i$ as

$$\{\sigma\}^i = \{\sigma\}^i \left[\frac{\sigma_y^i}{\bar{\sigma}^i}\right] \tag{4.22}$$

where σ_y^i is obtained by uniaxial hardening law corresponding to $\bar{\varepsilon}_p^i$ from the idealized uniaxial stress-strain curve. $\bar{\sigma}^i$ is the effective stress corresponding to total stresses $\{\sigma\}^i$ obtained by using the yield criterion. Thus the newly corrected point at D' is on the new yield surface.

Further refinement in the correction process is achieved by dividing the excess stress $R\{d\sigma_e\}^i$ in several steps, especially when large load increment sizes are to be permitted and/or the final point D' is in the vicinity of a region of large curvature on the yield surface. For greater accuracy the excess stress is divided into several parts and each increment is reduced to the yield surface in turn. In Fig.4.5 the two step reduction is demonstrated and it is seen that the final point E' is appreciably different from point D'. An additional refinement which can be made is to scale the stress point to the yield surface after the reduction process for each cycle and not after the final cycle as shown in Fig.4.5. The criterion of choosing the number of steps m (nearest integer)

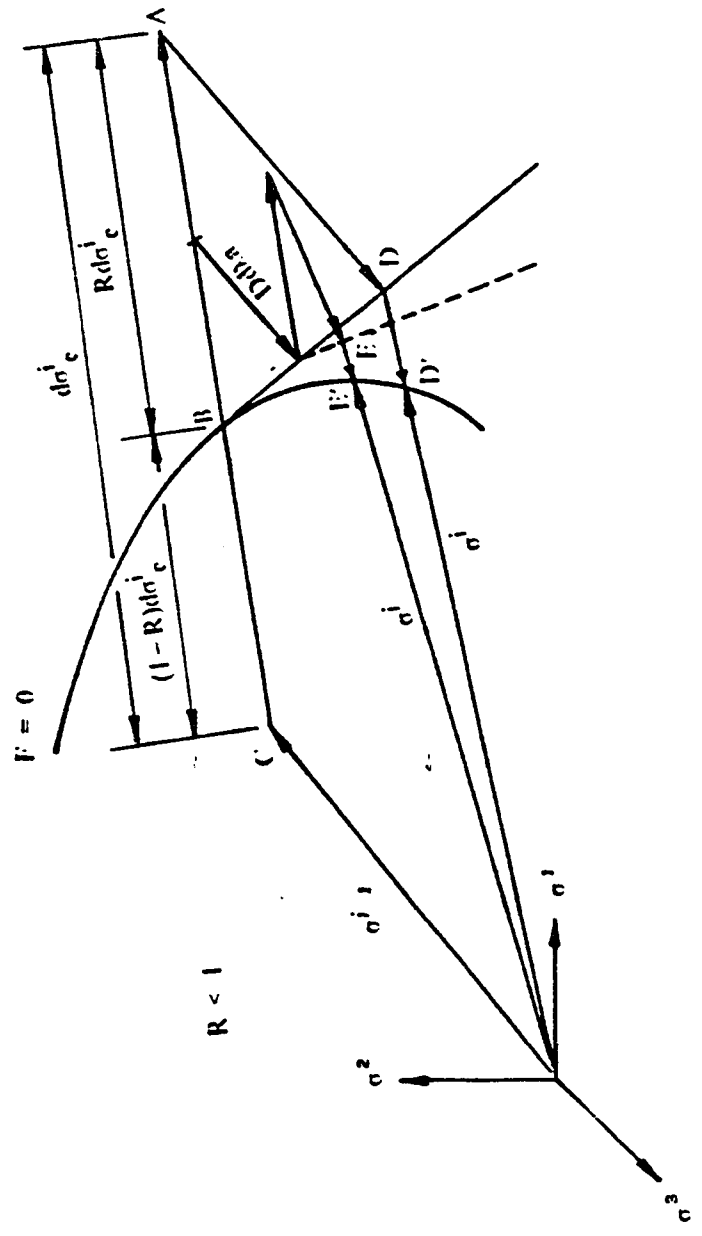

Fig. 4.5 Correction of stresses in steps for yielding Gauss points for perfectly plastic case

adopted in this work is [94]:

$$m < \left[\frac{\bar{\sigma}_e^i - \sigma_y^r}{\sigma_{yo}}\right] * 8 + 1 \qquad (4.23)$$

where $\bar{\sigma}_e^i - \sigma_y^r$ gives measure of excess stress AB. For the Gauss points already yielded in the previous iteration (Fig.4.4), the above equations are valid with R=1.

(g) For elastic Gauss points only:

$$\{\sigma\}^i = \{\sigma\}^{i-1} + d\{\sigma_e\}^i \qquad (4.24)$$

(h) Finally, calculate the equivalent nodal forces from the element stresses according to

$$\{f^e\}^i = \int_\Omega [B^e]^T \{\sigma_e\} d\Omega \qquad (4.25)$$

For the yielding concrete Gauss points, the stresses are corrected in subroutine RESI1 wherein the subroutine INVAR is called for the calculation of effective stress corresponding to a state of stress and subroutine FLOWS for the calculation of flow vector. Subroutine YLSUF is also called in RESI1 to calculate the yield stress and hardening parameter H' at a level of effective plastic strain. For steel yielding Gauss points stresses are corrected in RESI3 wherein subroutine INVST and FLOST are called for the calculation of effective stress and flow vector, respectively.

4.6.2 Correction of Stresses for Cracking Gauss Points

In subroutine RESTR, the principal stresses are evaluated for con-

crete Gauss points in a layer using in-plane stresses in order to check for possible cracking by calling subroutine PRIST. If the principal stress exceeds the tensile strength of concrete, then subroutine RESI2 is called for the reduction of stresses. In subroutine RESI2 stresses normal to the crack are first initialized to zero and then updated according to the tension stiffening (equation 2.71) and shear degradation laws (equations 2.72 and 2.73). After the stresses are corrected, they are transformed to the global directions using transformation as defined in subroutine TRANS.

4.6.3 Correction of Stresses for Crushing Gauss Points

The Gauss points which yield under compression experience increasing strains under a limiting constant yield stress, are assumed to loose all stiffness eventually after meeting the crushing strain criterion, activated from subroutine INVA2. On crushing, all stress components are reduced to zero at the Gauss point in question and the stiffness set to zero for further increments of load.

Chapter 5

VERIFICATION OF MODEL

5.1 INTRODUCTION

In order to verify the nonlinear finite element model developed in this work for prediction of response of reinforced concrete slabs, numerical results in terms of ultimate load, load deflection curves and strains in steel versus load were compared with existing experimental data for corresponding quantities as reported in the literature. Five test examples were chosen, four from the well known series of slabs used by Taylor and Hayes [29] and one as used by Kareem [3].

5.2 GEOMETRY AND MATERIAL PROPERTIES

The slabs used by Taylor and Hayes in their experimental work were adopted for simulation. The slabs were 864 x 864 x 76 mm (34 x 34 x 3 in) and the experimental loads and load deflection curves were presented for total steel percentages of ρ = 1.57 and ρ = 3.14. The slabs were tested as pairs - one unrestrained and simply supported, with the other of the pair being restrained along the edges. For each replica, the size of the platen through which the load was applied was varied from two inches square to six inches square. Four slabs of this

series were adopted for simulation in this work. Three of these were reinforced with a total steel ratio of $\rho = 1.57$ and these were simply supported with platen sizes of 2 inch, 4 inch and 6 inch (2S2, 2S4 and 2S6). The fourth slab was also simply supported and loaded by 2 in platen having reinforcement ratio of $\rho = 3.14$ (3S2).

The slab geometry and finite element discretization of slab loaded by 2 in. platen (2S2 and 3S2) is shown in Fig. 5.1 with slab being subdivided into eight concrete layers. Steel of equal amount was placed in two orthogonal layers. The material properties used in the numerical analysis are shown in Table 5.1 for all five slabs. The finite element discretization and geometry of slabs 2S4 and 2S6 are shown in Figs. 5.2 and 5.3, respectively. The slab used by Kareem [3] is a two panel, girder supported slab (A-31) and loaded on one panel at a time by patch load. This slab was modelled as being restrained on two opposite edges and free on the other two sides. The geometry and discretization of this slab is shown in Fig. 5.4.

In all the slabs chosen for simulation, the Mohr-Coulomb yield criterion was used with strain hardening which was assumed to start at $0.3f'_c$. Dowel effect was included in all the slabs, treating the stresses in steel in a multiaxial frame work. Tangential stiffness matrix was calculated at every second iteration of each increment. The maximum number of iterations allowed for convergence was 20 with a convergence tolerance of one percent when both displacement and rotation residual norms were used for convergence. Isoparametric Lagrangian element was used together with a selective integration scheme. In the slabs

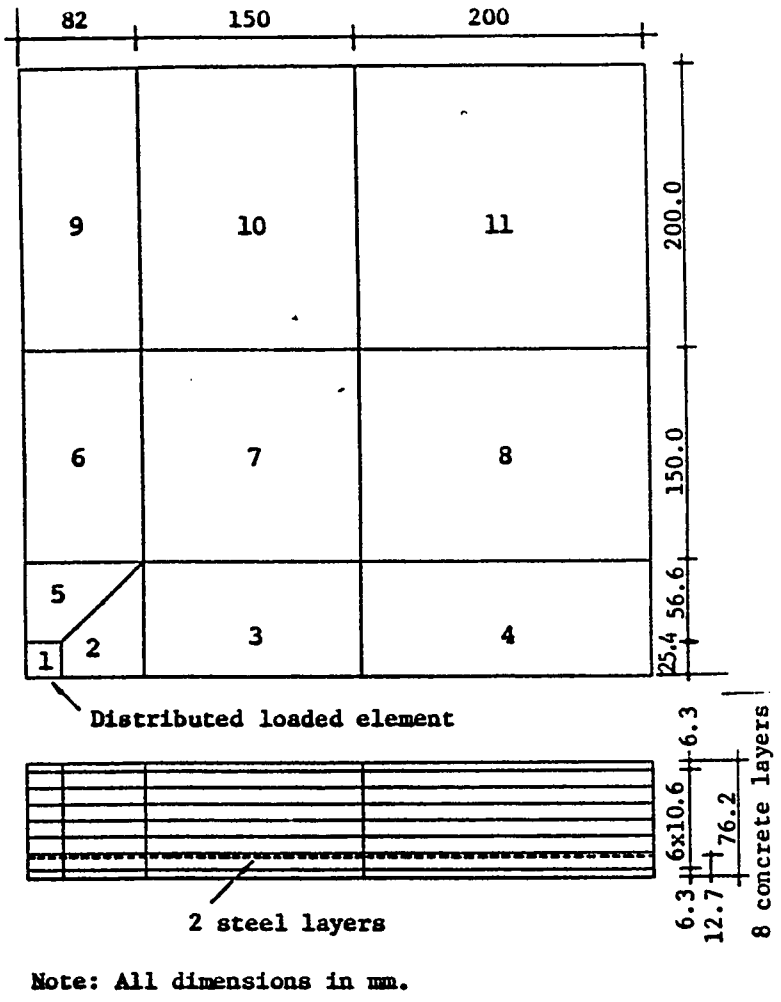

Fig. 5.1 Finite Element Discretization of slab 2S2 & 2S3 [29]

Table 5.1 Slab geometry and material properties

Slab Ref	Material Properties						Reinforcement Ratio (%)		Plate size (mm)	Support Condition
	Given		Assumed							
	f'_c(MPa)	f_y(Mpa)	f'_t(Mpa)	E_c(Mpa)	E_s(Mpa)	E'_s(Mpa)	Layer 1	Layer 2		
2S2	32.4	375.8	3.50	28460.0	200,000	3,500.0	0.785	0.785	50.8 × 50.8	ss all around
3S2	28.5	375.8	2.66	26683.0	200,000	3,500.0	1.570	1.570	50.8 × 50.8	ss all around
2S4	29.0	375.8	2.68	26906.8	200,000	3,500.0	0.785	0.785	101.6 × 101.6	ss all around
2S6	23.0	375.8	2.39	23958.5	200,000	3,500.0	0.785	0.785	152.4 × 152.4	ss all around
A-31	28.7	550.8	2.67	26800.0	200,000	3,500.0	0.976	0.635	150.0 × 75.0	Restrained on two edges ,other two edges free

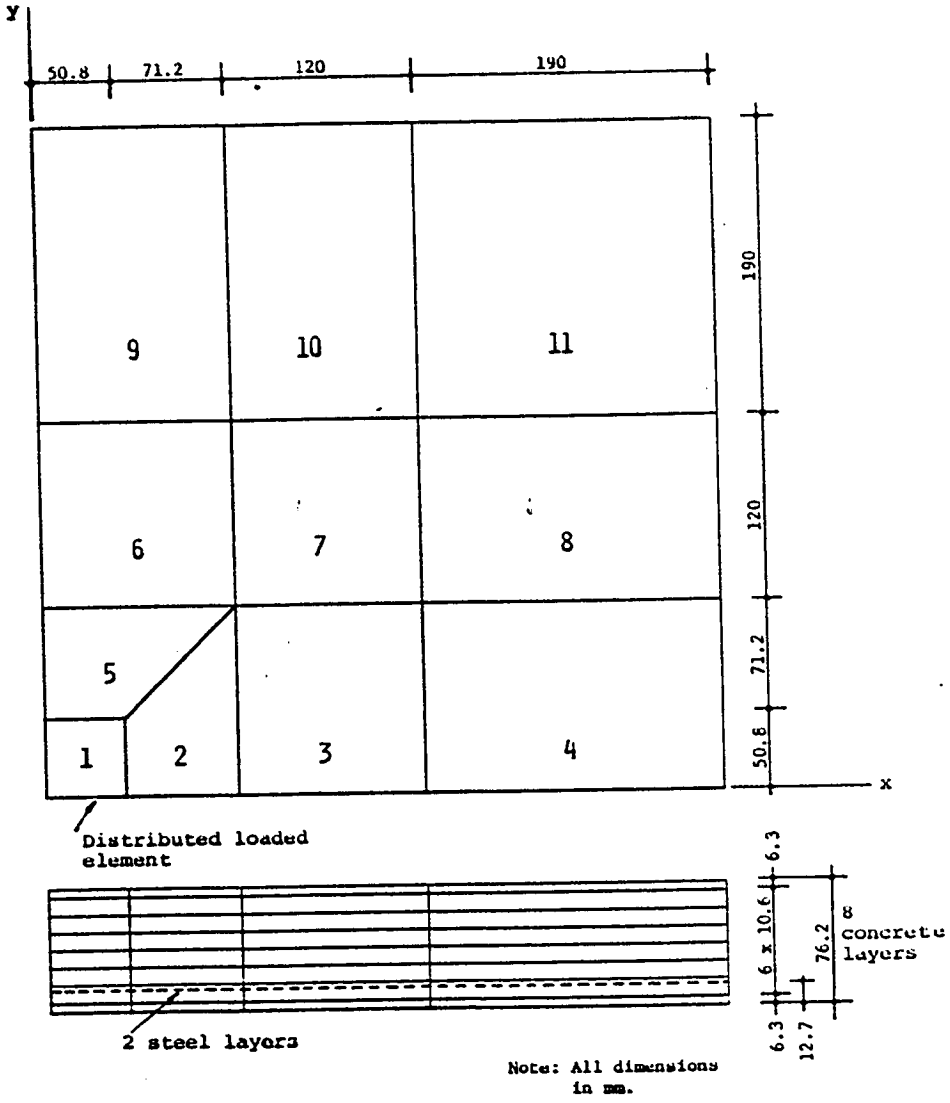

Fig. 5.2 Finite Element Discretization of slab 2S4 [29]

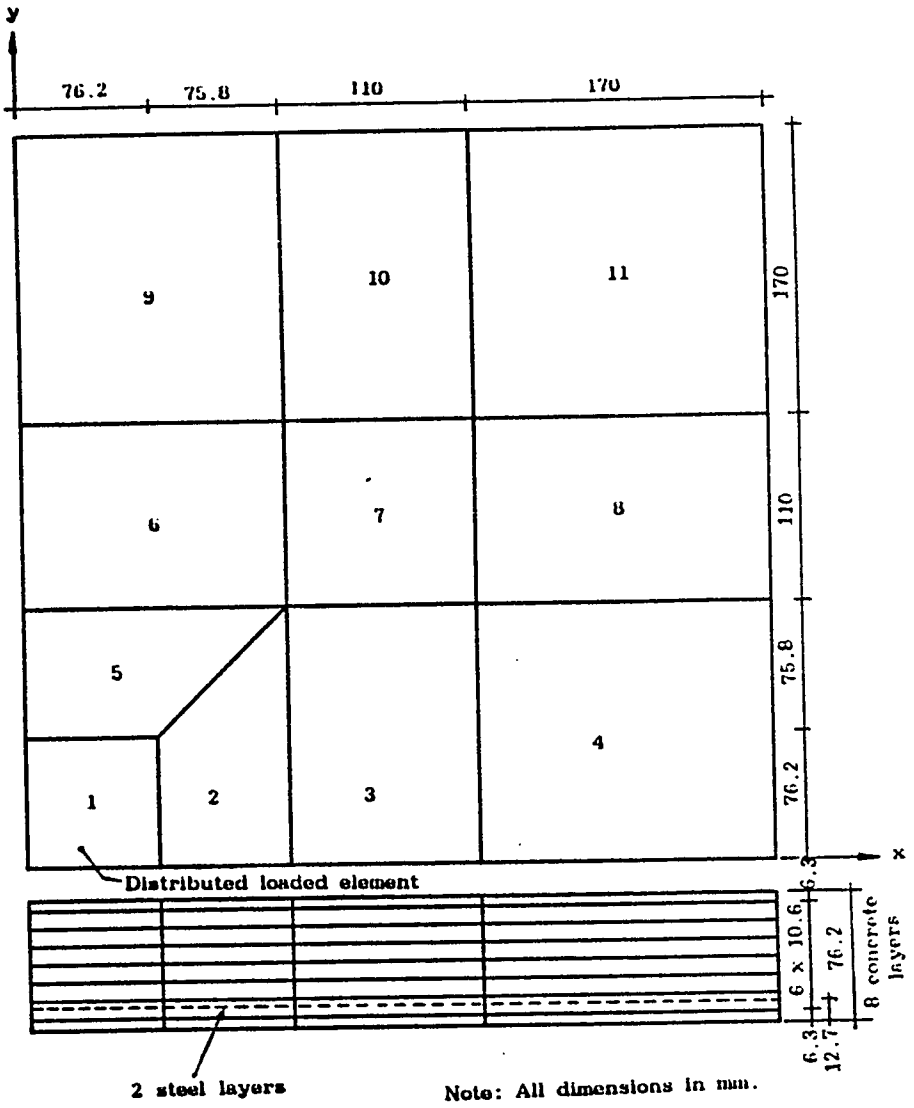

Fig. 5.3 Finite Element Discretization of slab 2S6 [29]

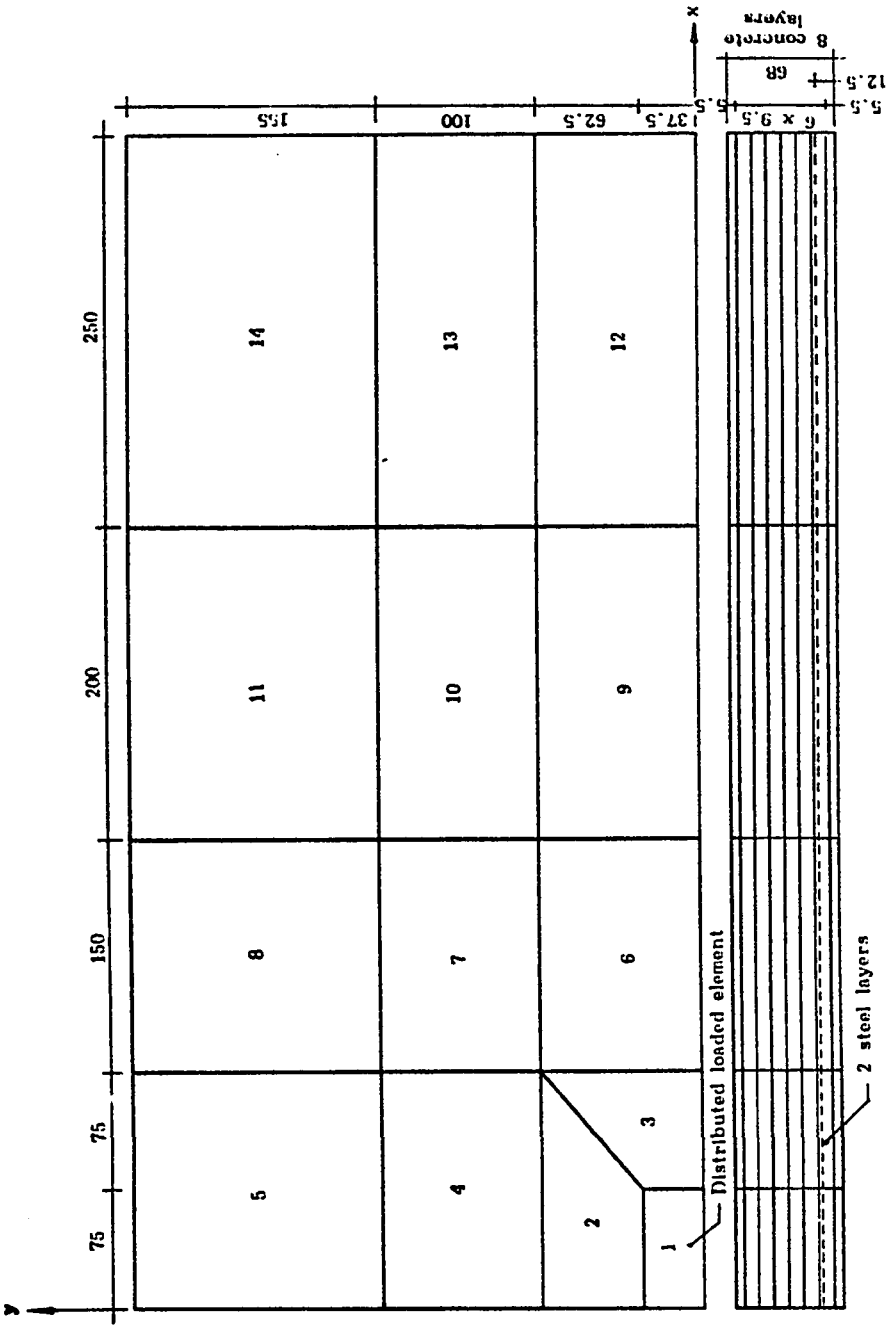

Note: All dimensions in mm.

Fig. 5.4 Finite Element Discretization of slab A-31 [3]

considered by Kareem [3], compression reinforcement was provided and the numerical model reflected a proportionate increase in the ultimate load due to the presence of this reinforcement.

The material properties related to material modelling such as crushing, tension stiffening and shear degradation were taken for all slabs as follows:

Crushing strain $\varepsilon_u = 0.0035$

Cracking strain parameter ε_c (influencing shear degradation) = 0.005

Cracking strain for tension stiffening $\varepsilon_m = 0.002$

Tension stiffening parameter $\alpha = 0.7$

5.3 RESULTS

The experimental and the predicted results are compared in Table 5.2 and in Figs. 5.5 to 5.10.

5.3.1 Failure Loads

Table 5.2 shows that there is an excellent agreement between the experimental and predicted collapse loads for the various cases considered.

5.3.2 Load-Deflection (P − Δ) Curves

The load deflection curves (Figs. 5.5 to 5.9) indicate that the initial

Table 5.2 Comparison of failure loads

Slab	Material Properties		Reinforcement ratio %		Loaded area	P_u (kN)		
Ref	f'_c(MPa)	f_y(Mpa)	Longitudinal	Transverse	(mm*mm)	Test	FEM	FEM Test
2S2	32.4	375.8	0.785	0.785	50.8 × 50.8	72.2	64	0.89
3S2	28.5	375.8	1.570	1.570	50.8 × 50.8	79.7	83	1.04
2S4	29.0	375.8	0.785	0.785	101.6 × 101.6	87.2	86	0.99
2S6	23.0	375.8	0.785	0.785	152.4 × 152.4	98.1	95	0.96
A-31	28.7	375.8	0.635	0.976	150.0 × 75.0	97.0	98	1.01

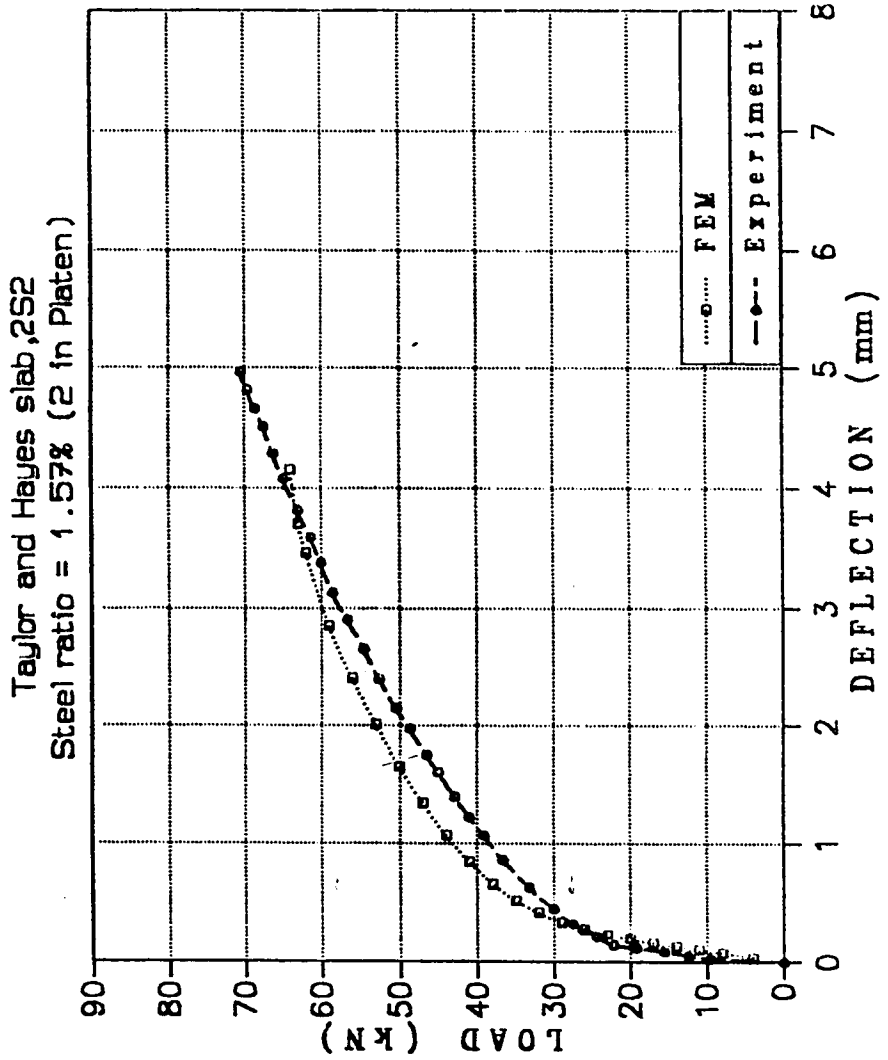

Fig.5.5 Load Deflection curve for slab 2S2

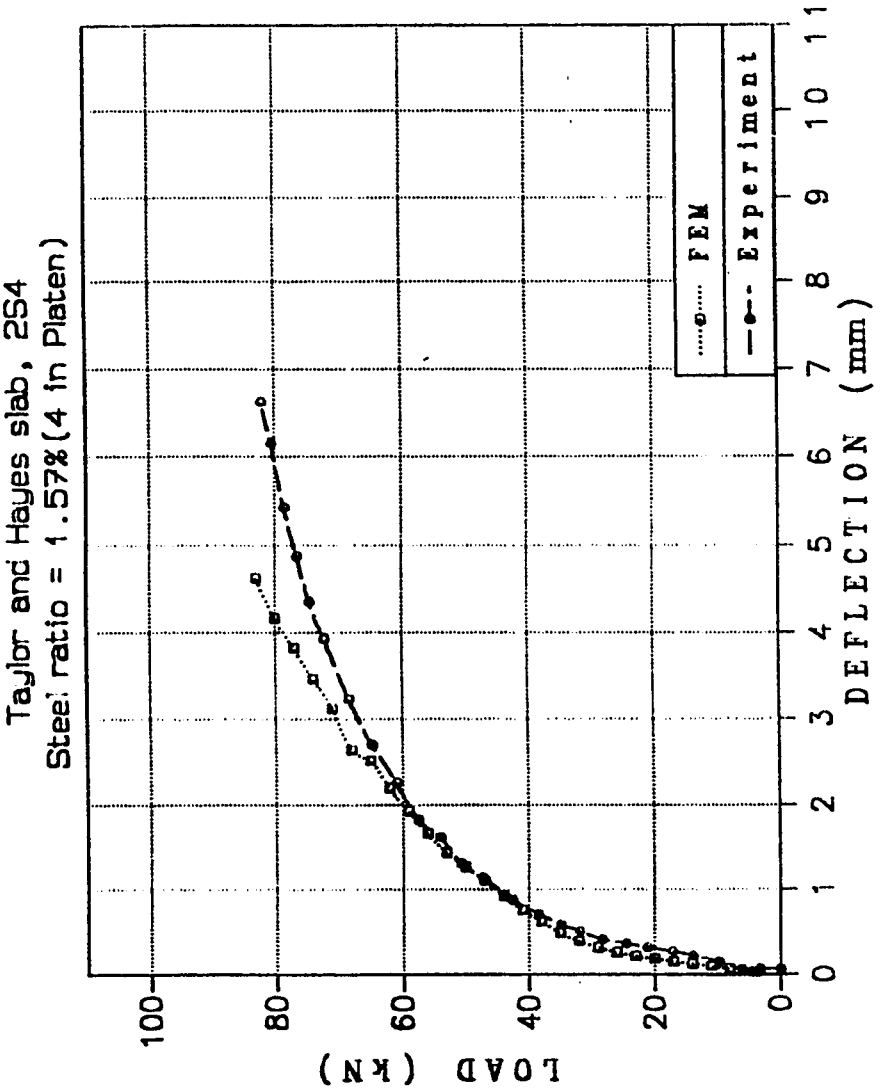

Fig.5.6 Load Deflection curve for slab 2S4

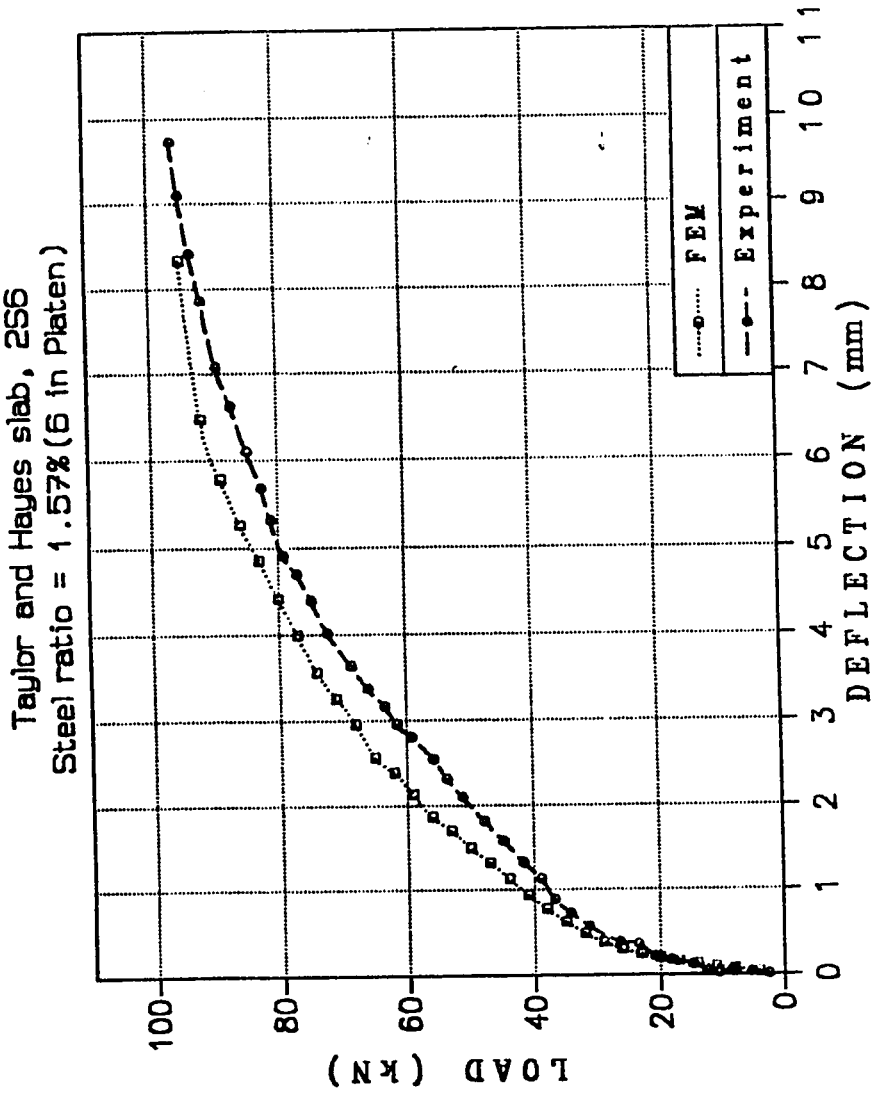

Fig.5.7 Load Deflection curve for slab 2S6

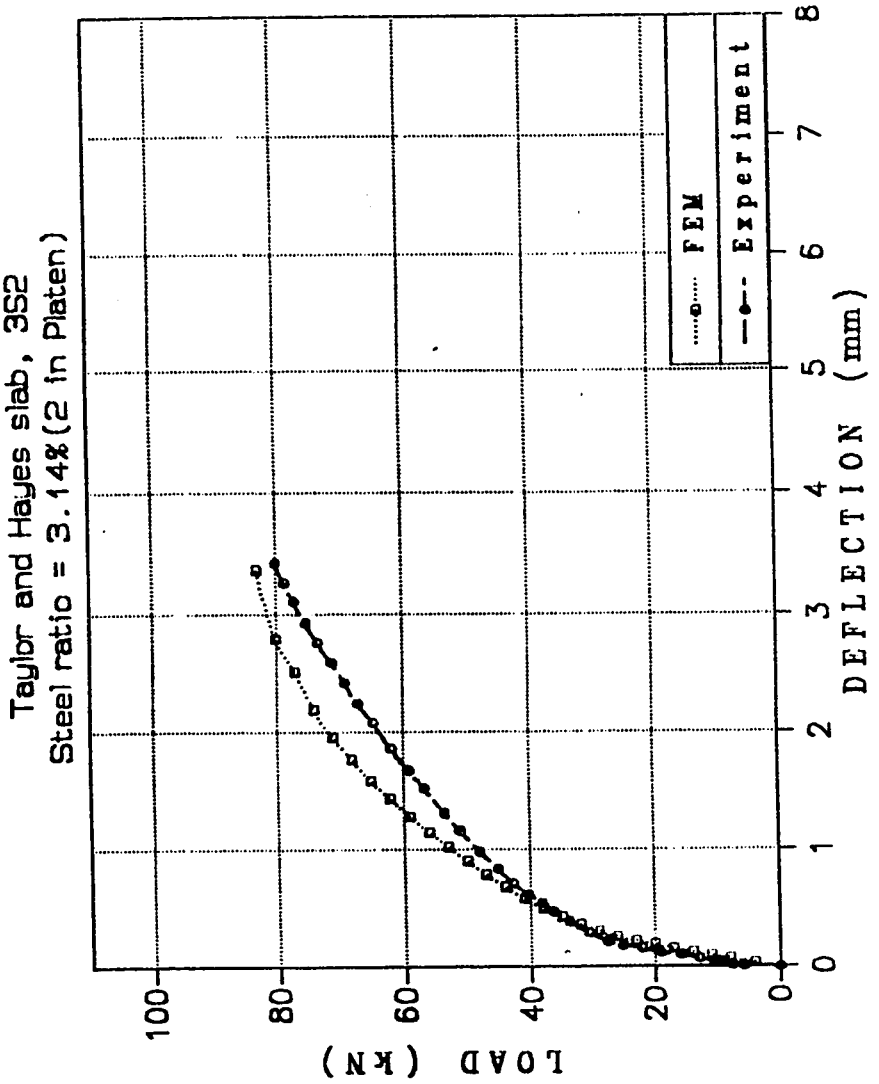

Fig.5.8 Load Deflection curve for slab 3S2

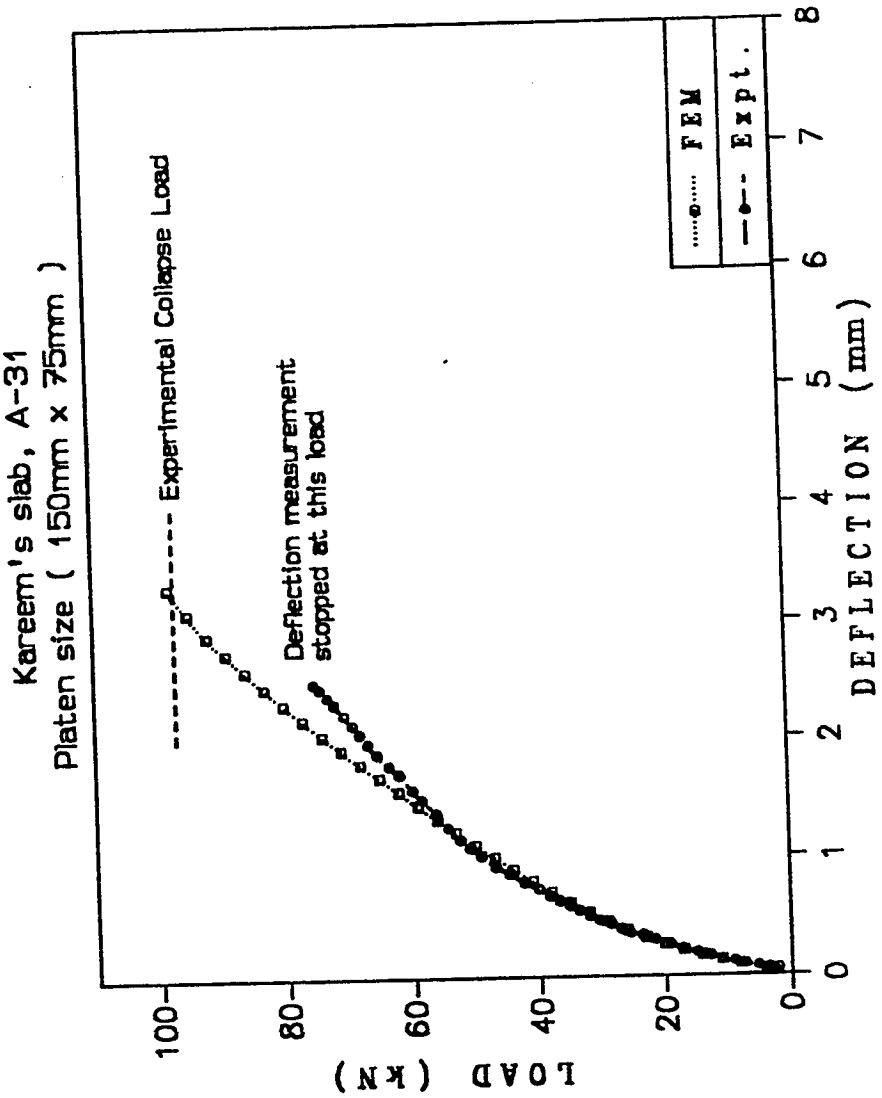

Fig.5.9 Load Deflection curve for slab A-31

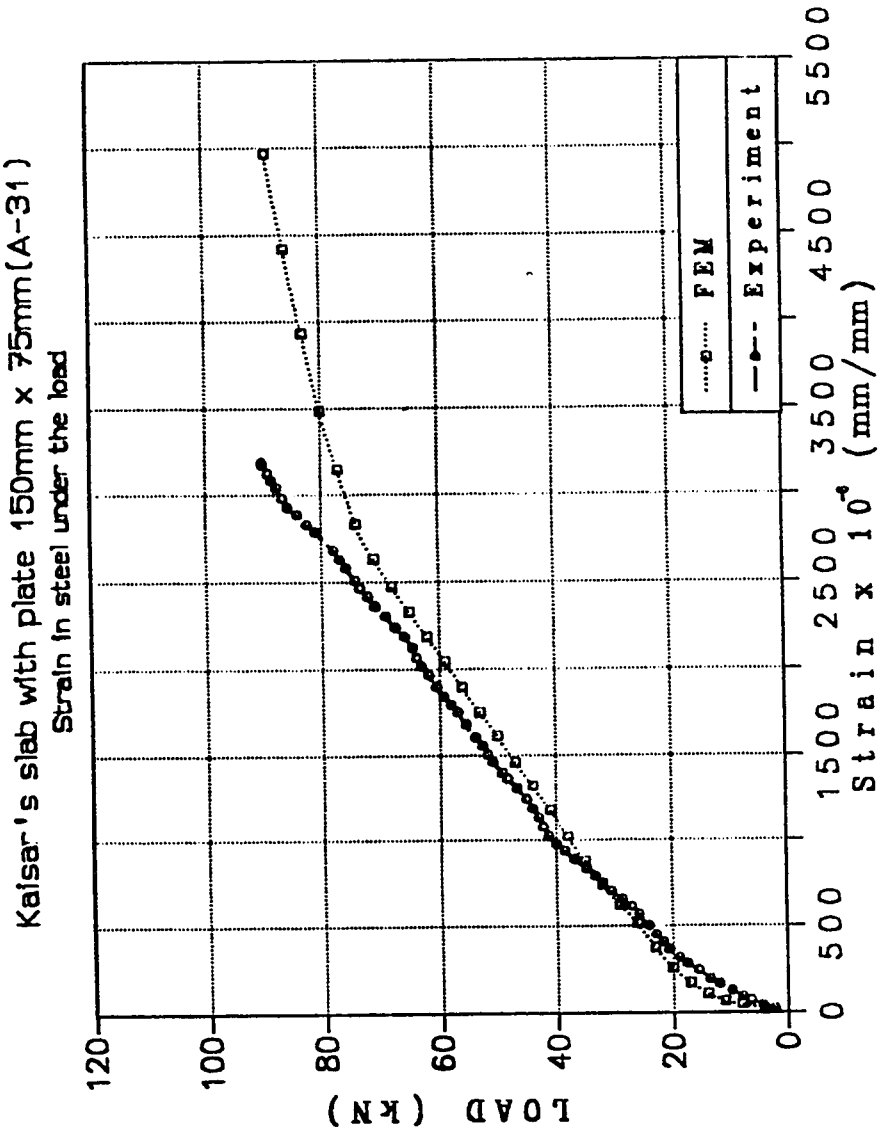

Fig.5.10 Load vs. strain in steel for slab A-31

numerical kink (point of departure from the linear elastic solution) marking the first cracking load matched the experimental first kink quite satisfactorily for the various cases. As the cracking proceeds, the model predicts slightly stiffer results. This deviation is ascribed to the assumed material modelling parameters including tension stiffening parameters α and ε_m and shear degradation parameter ε_c. The influence of these parameters on the various components of response of the reinforced concrete slab is detailed in the next chapter where the stiffness of the slab is noted to be sensitive to these parameters to varying degrees.

5.3.3 Load-Strain (in steel) Curve

Strain in steel reinforcement has been reported by Kareem [2] for the slab tested. One slab (A-31) with loading patch size of 150 mm x 75 mm was selected for comparison. The strains in steel directly under the load are shown in Fig. 5.10. It is evident that the reinforcement strains as obtained from the model compare favourably with the experimentally measured values over the range of loading.

Chapter 6

PARAMETRIC STUDY OF THE MODEL

6.1 INTRODUCTION

In Chapter 5 the validity, accuracy and efficiency of the computational model have been proven by comparing the numerical results with data available from experimentation. In this Chapter, numerical experiments have been conducted in order to highlight the influence of various factors on the behavior of R/C slabs.

There are three aspects of such a study; (i) the sensitivity study of material parameters on the response of R/C slabs, (ii) the influence of structural factors on the failure modes of R/C slabs and (iii) the sensitivity of the solution to finite element discretization parameters. The developed software produces an all encompassing output describing the material state and stress state of each Gauss point, which leads to an indepth understanding of the behavior of the structure and the mechanism of failure modes. The geometry corresponding to the slabs considered by Taylor and Hayes for their experiments [29] has been chosen for the parametric study.

6.2 MATERIAL PARAMETRIC VARIATION STUDY

This study highlights the sensitivity of the slab response to various components embedded in the material model. The following variations in the material modelling were considered:

(i) Perfectly plastic models versus hardening models

(ii) The role of crushing condition on collapse load

(iii) Influence of dowel effect on punching capacity

(iv) Parametric variation of tension stiffening parameter α

(v) Parametric variation of degraded shear modulus

(vi) Role of yield criterion

6.2.1 Perfect Plastic Models Versus Hardening Models

Several researchers use perfect plastic models for prediction of response of reinforced concrete structures, primarily for ease in numerical implementation. In order to investigate the influence of consideration of non-hardening model, comparison is made on basis of Mohr-Coulomb criterion used both as a perfect plastic model and as an isotopic hardening model.

The load-deflection relationship (Fig.6.1) shows a significantly increased structural stiffness and also an increase in collapse load for the perfect plastic model. Results presented in [53] using a perfect plastic model for punching of axisymmetric slabs indicated very similar trends in comparison to experimental results, but were attributed to other factors rather than a limitation in the model itself. It is only but natural that assuming linear elastic behavior for concrete up-to the

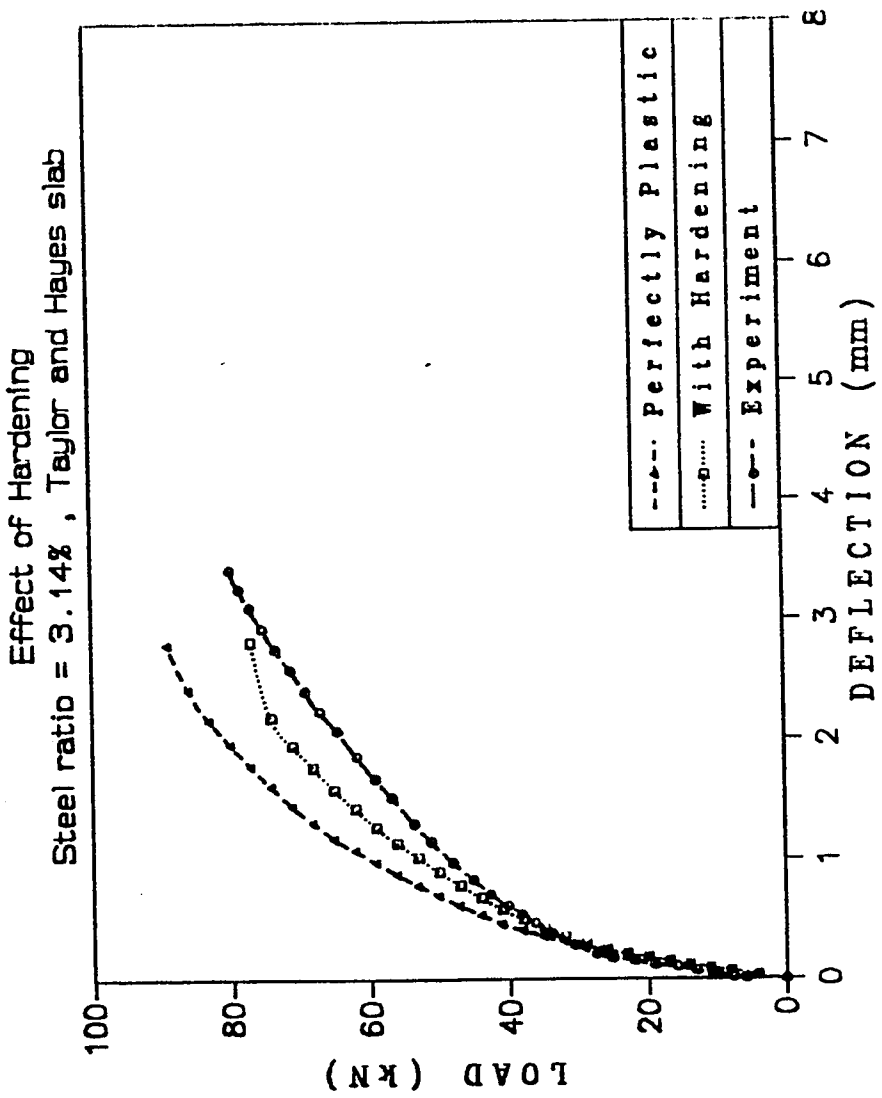

Fig. 6.1 Load deflection curves showing the effect of hardening

failure surface will lead to reduced strains and deflections at corresponding load magnitudes, leading to increased stiffness. A very important observation is made here that a lot of attention is devoted to development of sophisticated constitutive models and their use as failure surfaces in perfect plastic modelling, but their use will inevitably lead to stiffened responses and increased collapse loads. Such constitutive laws become very difficult to incorporate in isotropic hardening models, inasmuch as they cannot be expressed in explicit form. Thus a model like Mohr-Coulomb becomes more useful because of the ease with which it can be expressed in explicit form for implementation in the computational model taking into account isotropic hardening.

Figs. 6.2 and 6.3 are shown to illustrate redistribution of stresses due to cracking at Gauss point, a phenomenon common to both perfect plastic models and strain hardening models. Fig. 6.2 shows dominant stresses σ_{xx} and σ_{yy} , in extreme bottom layers and directly under the load, reaching values very close to the concrete tensile strength f'_t at a load of 14kN. In the subsequent increment of load (P=17kN), there has been a release of these two stresses due to cracking according to the tensile constitutive law, and this can be seen in Fig. 6.3 for points directly under the load. It may be noted that cracking also causes a redistribution of the shear stress, as evidenced by comparing the transverse shear stress τ_{xz} prior to and after first cracking and as shown in Figs. 6.2 and 6.3. Fig. 6.4 shows the strain distribution in the bottom layer at P=17kN.

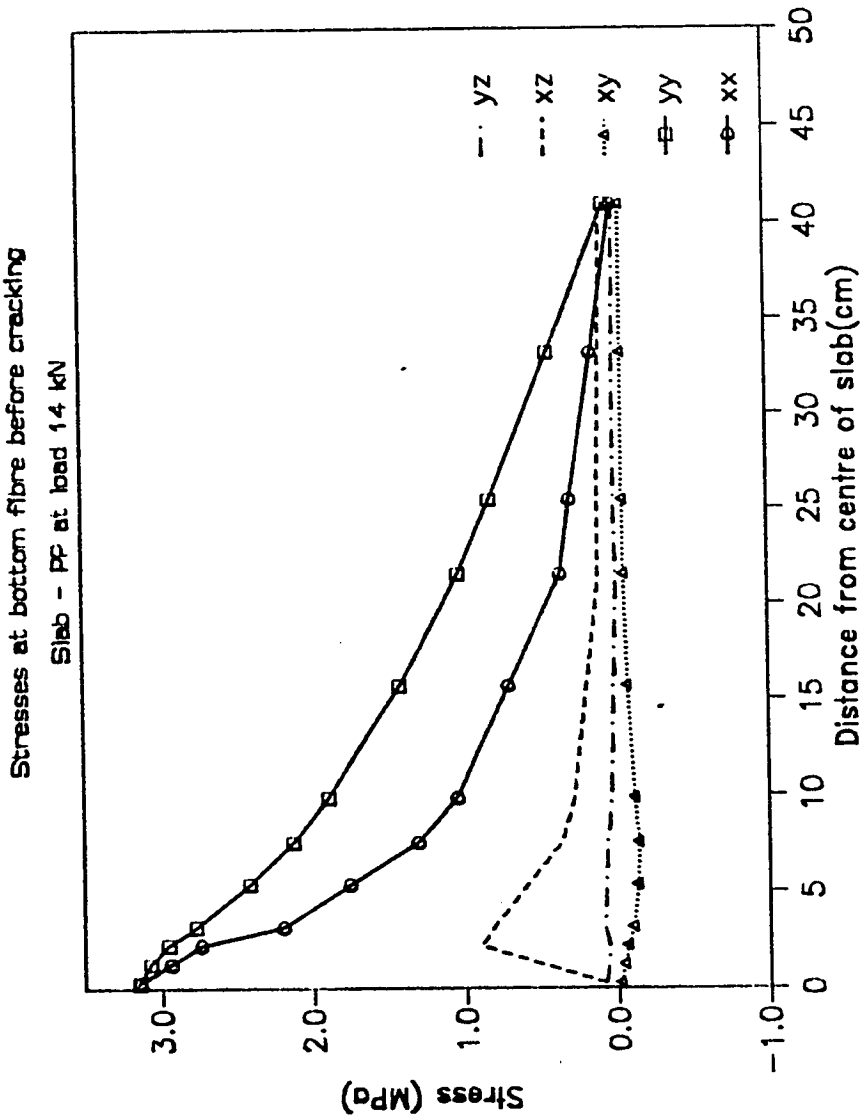

Fig. 6.2 Stresses in bottom layer before cracking at load P= 14 kN

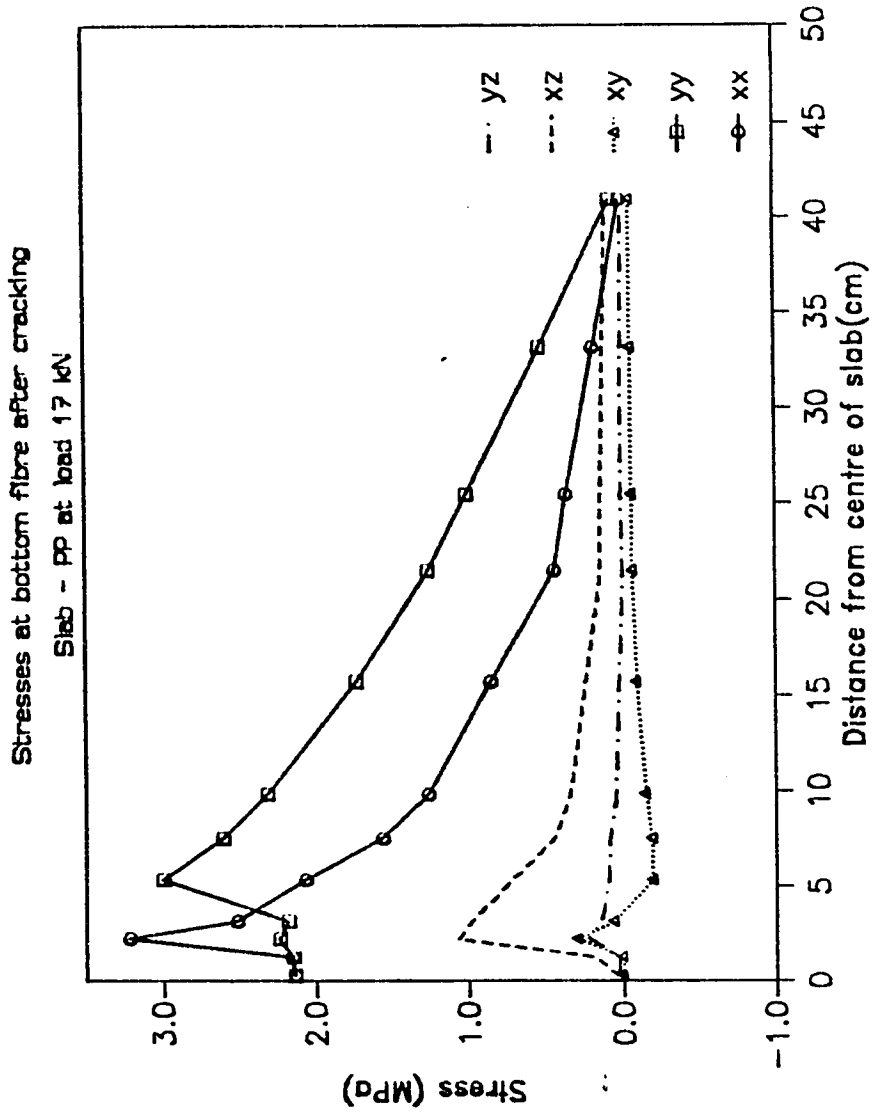

Fig. 6.3 Stresses in bottom layer after cracking at load P = 17 kN

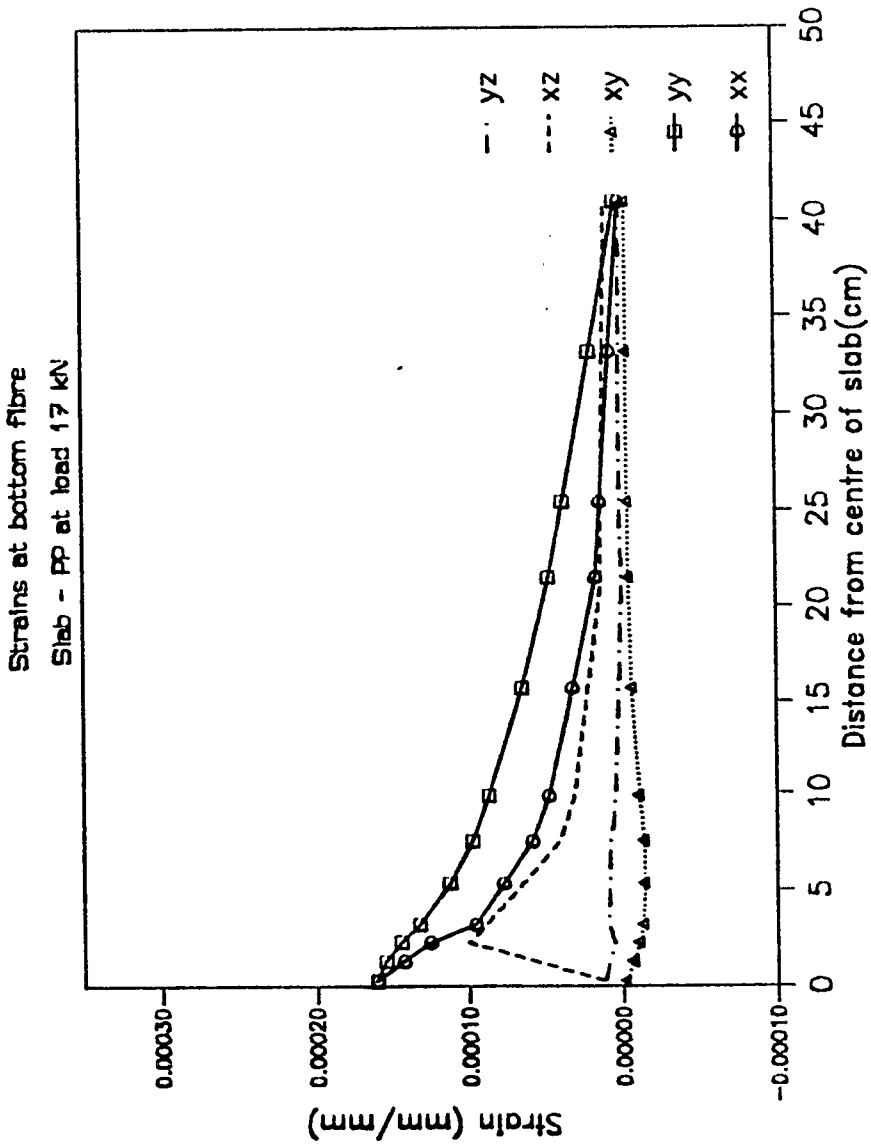

Fig 6.4 Strains in bottom layer after cracking at load P = 17 kN

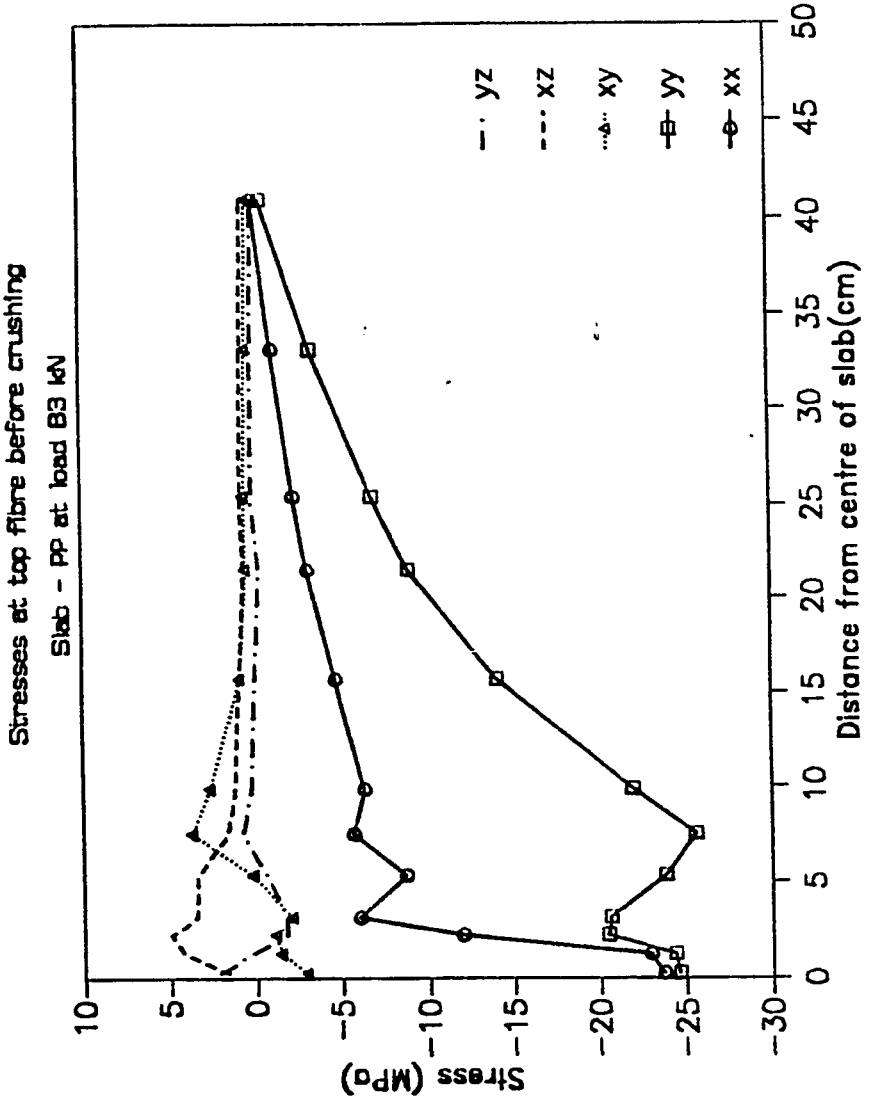

Fig. 6.5 Stresses in top layer before crushing at load P = 83 kN for perfectly plastic case

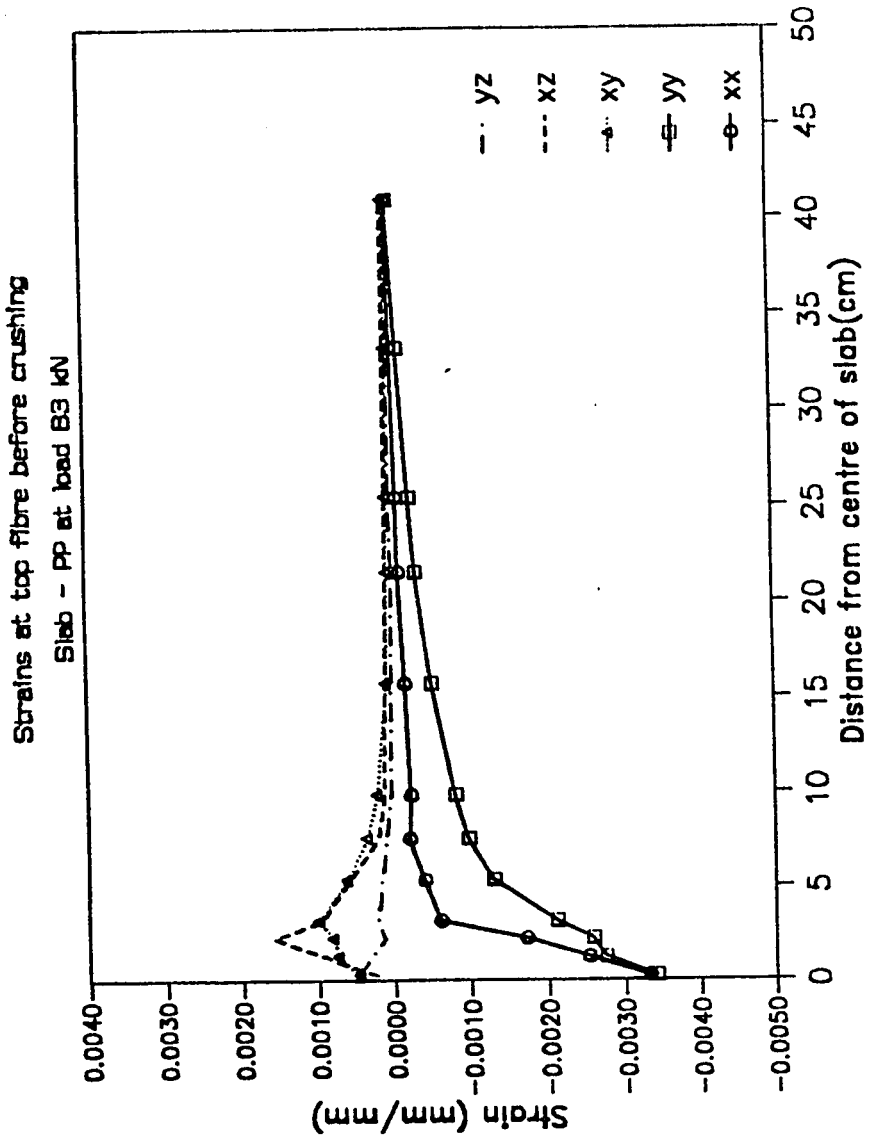

Fig. 6.6 Strains in top layer before crushing at load P= 83 kN for perfectly plastic case

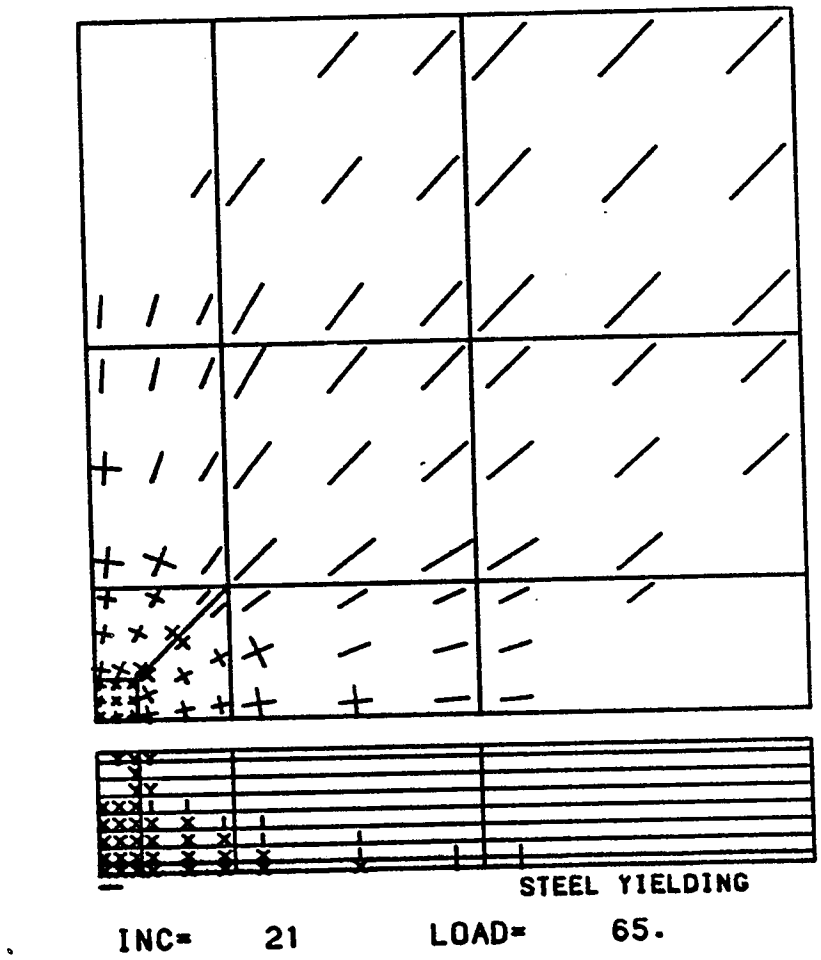

Fig. 6.7 Cracking in bottom of slab and section profile at load P = 65 kN

|	one way cracking
×	two way cracking
Y	yielding of concrete
●	crushing of concrete
——	extent of steel yielding

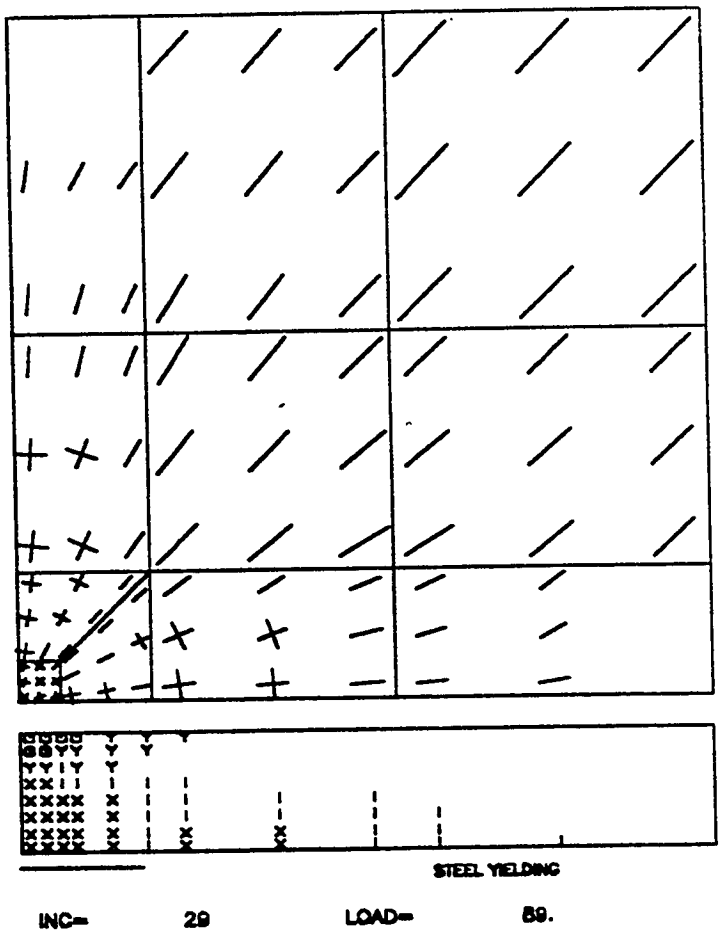

Fig. 6.8 Cracking in bottom of slab and section profile at collapse load $P_u = 89kN$

Figs. 6.5 and 6.6 illustrate the stress and strain distribution along section y = constant and across the centre of the slab, for layers in the extreme top just prior to collapse. Figs. 6.7 and 6.8 are section profiles illustrating status of Gauss points in various layers through the length of the slab at first yield and at the collapse load, respectively.

6.2.2 The Role of Crushing Condition on Collapse Load

The crushing criterion effectively delineates the culmination of the load-deflection curve, with the loading surface at a given Gauss point meeting with the crushing surface expressed in terms of strains and the stresses and stiffnesses correspondingly reduced to zero. This phase of the parametric modelling investigates the behavior of the slab in the event that the loading surfaces were to be allowed to expand uninhibitedly.

Results were obtained to focus on (i) load-deflection (P- Δ variation) (ii) stresses and strains in the top layer at several increments of load ranging from 29kN to 137kN.

The P- Δ curve (Fig. 6.9) shows that with crushing 'silenced', the slab attained a collapse load of 137 kN, approaching the solution that is predicted by the yield line solution (174 kN). The extent of steel yielding is increased dramatically, as indicated in Fig. 6.10, with largest extent of steel yield being along the diagonal (line of symmetry), drawn from the edge of the loaded area to the corner of the slab, much in the fashion of a yield line location in a square slab. The stress variation along a section through the centre of the slab for various load

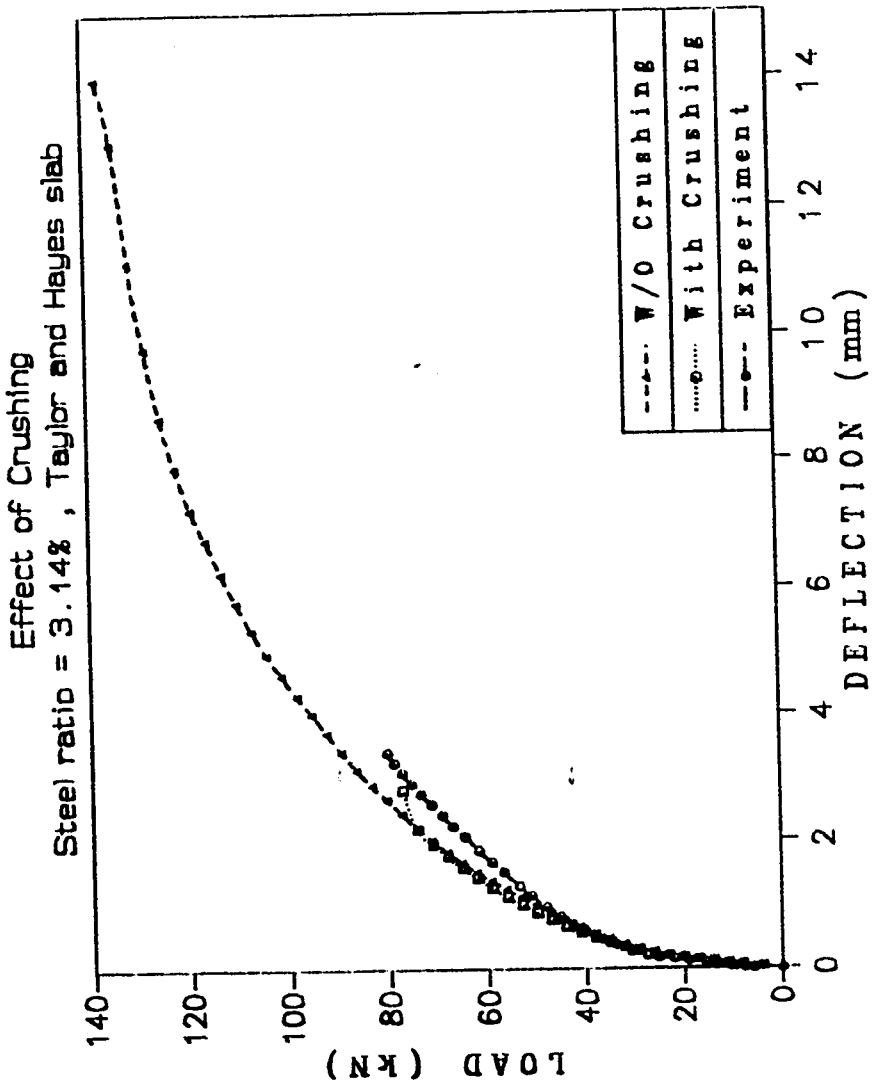

Fig. 6.9 Load deflection curves showing the effect of crushing

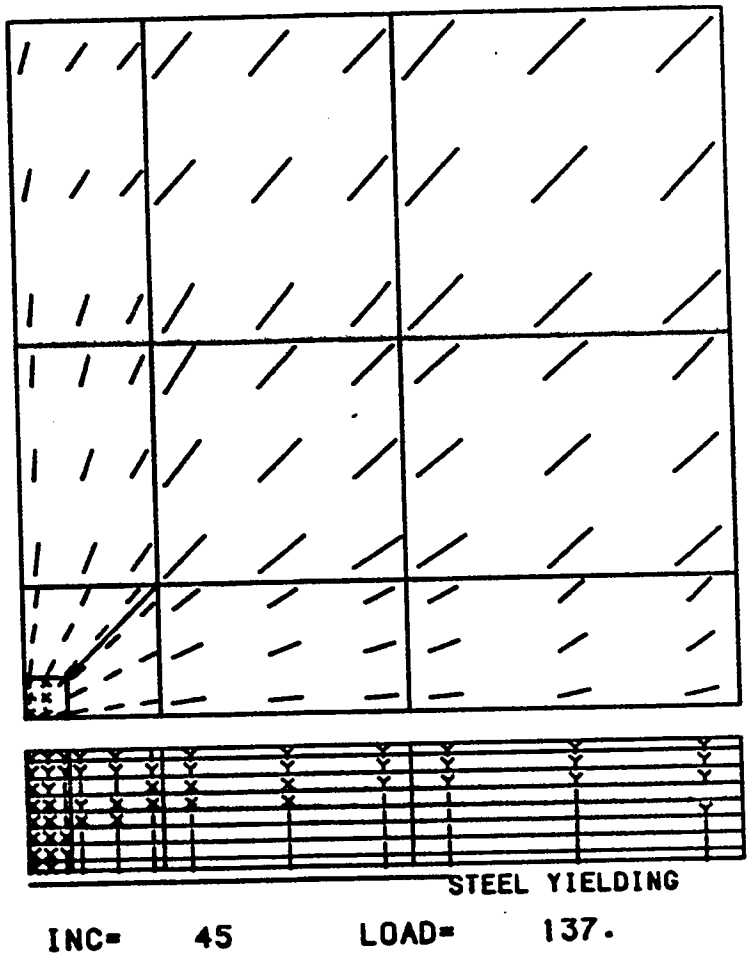

Fig. 6.10 Cracking in bottom of slab and section profile at collapse load $P_u = 137kN$

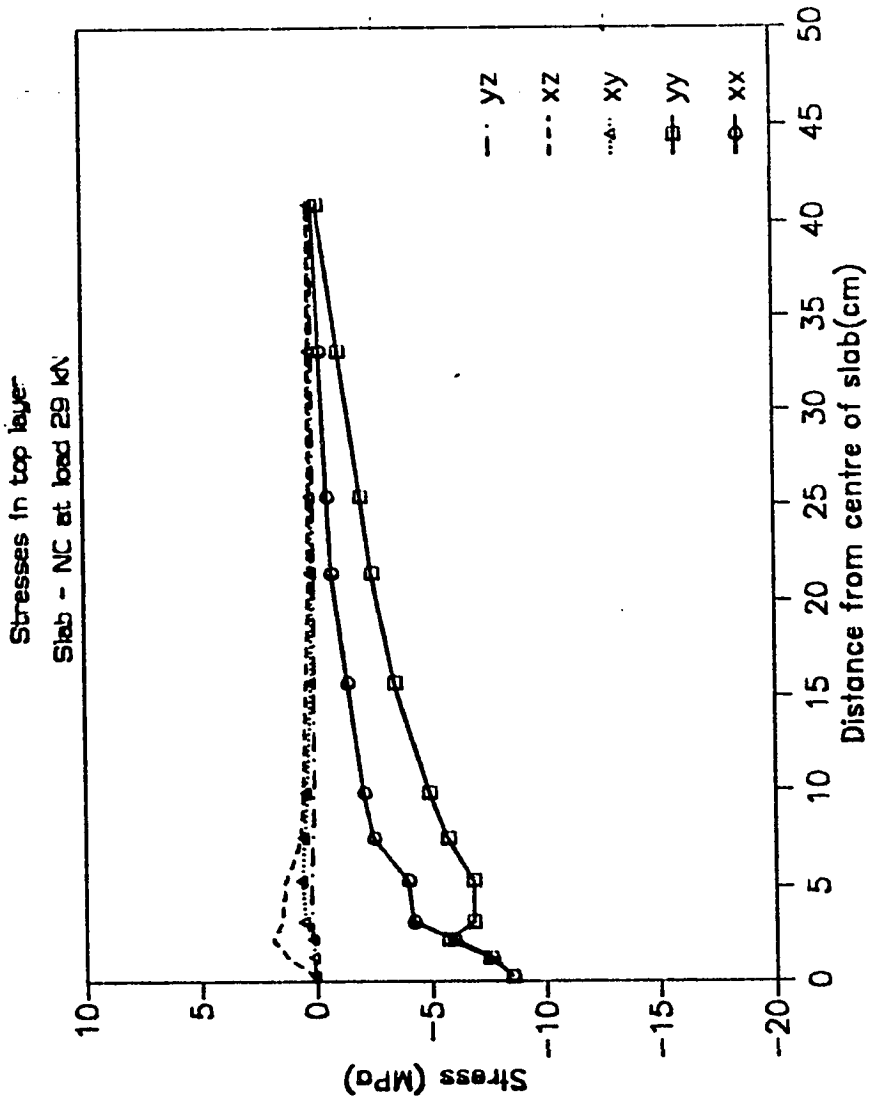

Fig. 6.11 Stresses in top layer at load P = 29 kN for crushing 'silenced'

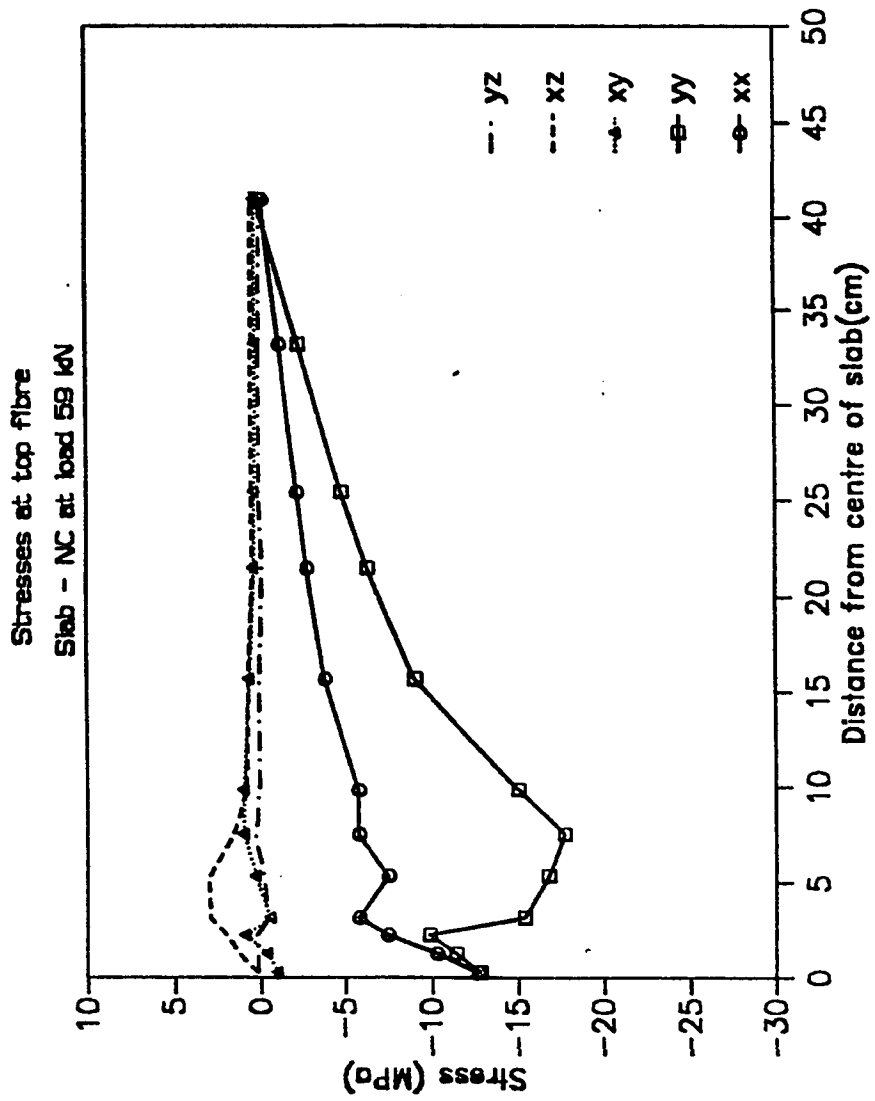

Fig. 6.12 Stresses in top layer at load P = 59 kN for crushing 'silenced'

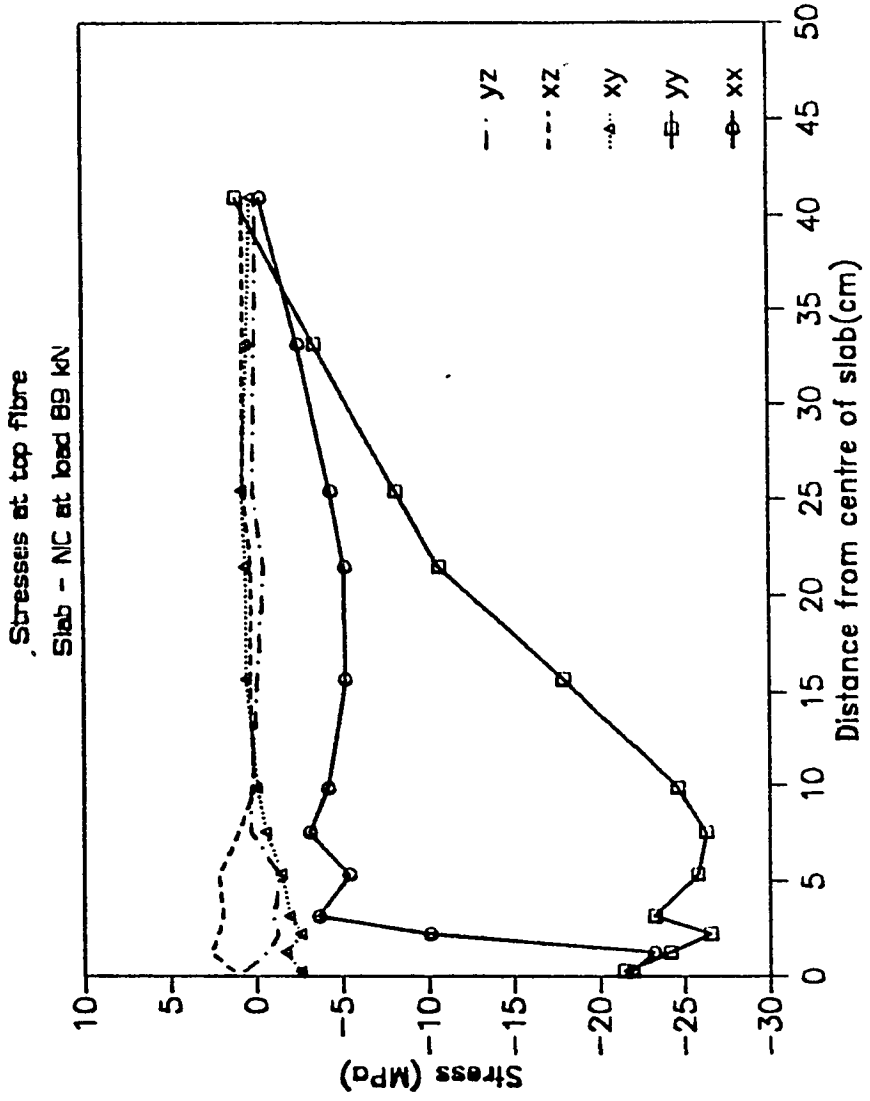

Fig. 6.13 Stresses in top layer at load P = 89 kN for crushing 'silenced'

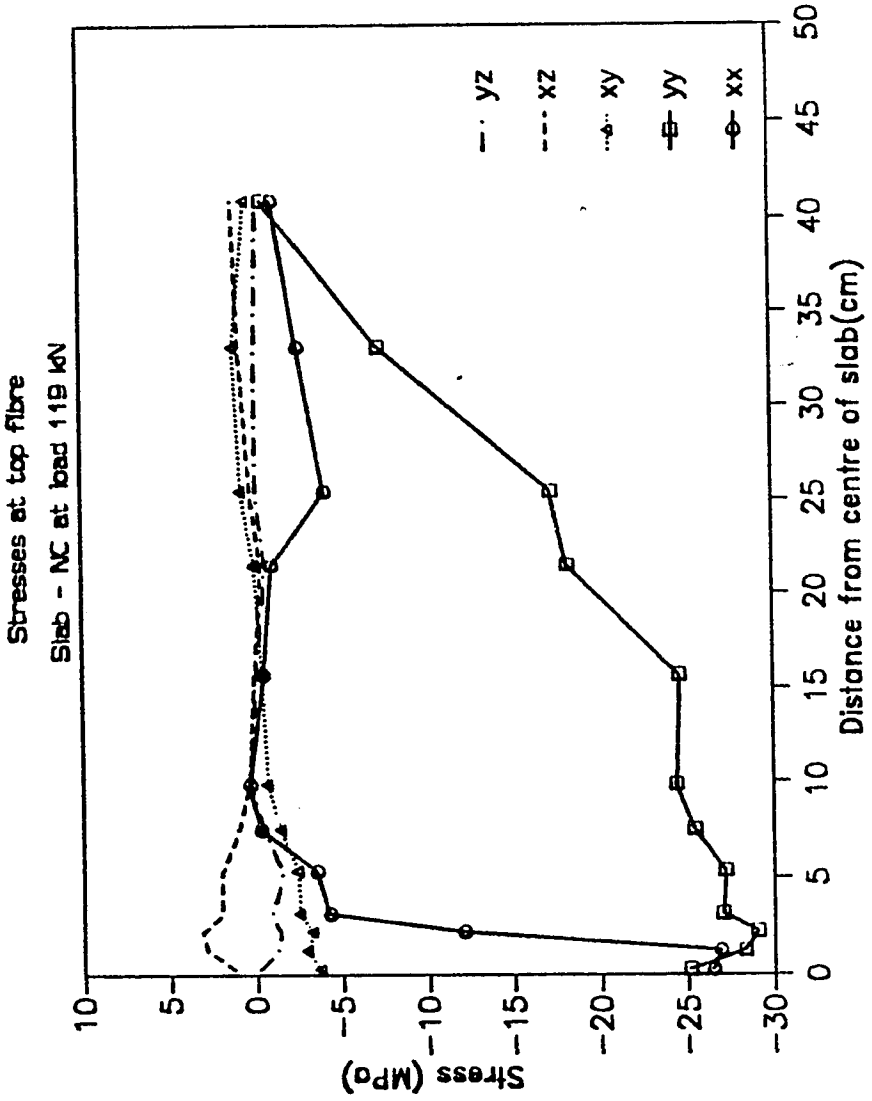

Fig. 6.14 Stresses in top layer at load P = 119 kN for crushing 'silenced'

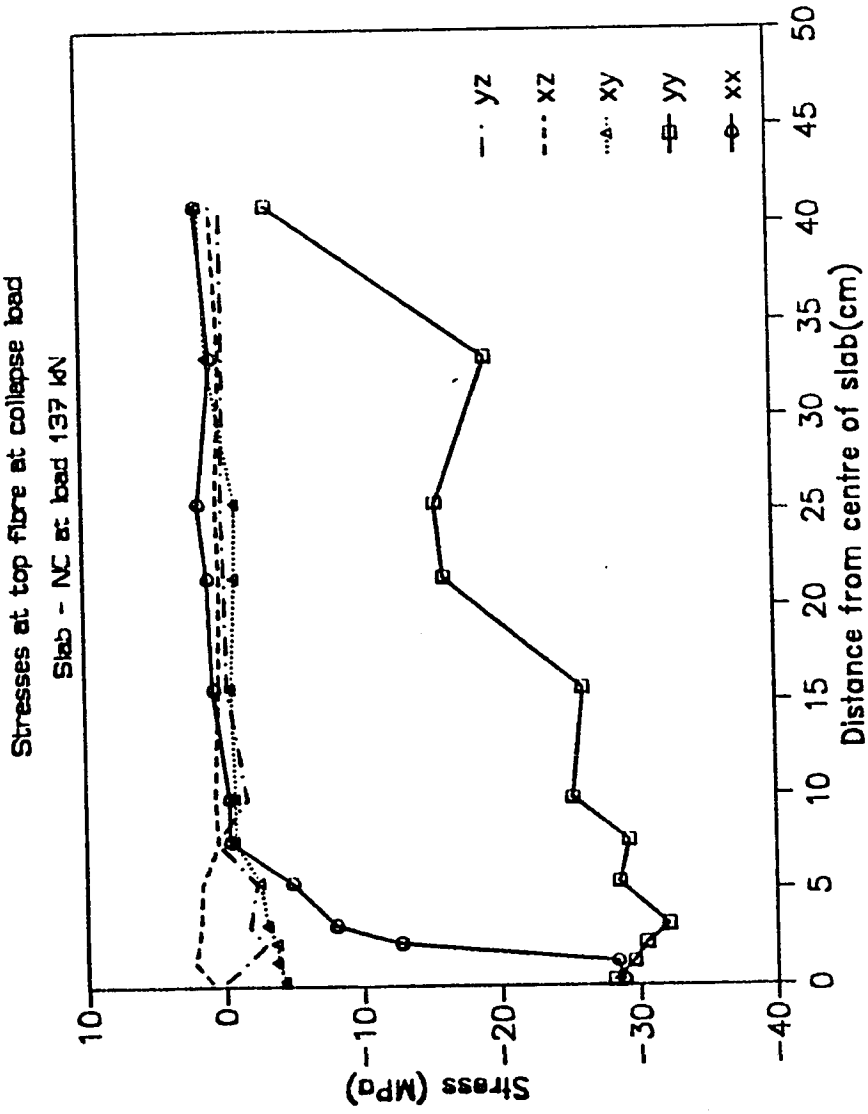

Fig. 6.15 Stresses in top layer at collapse load P_c = 137kN for crushing 'si-lenced'

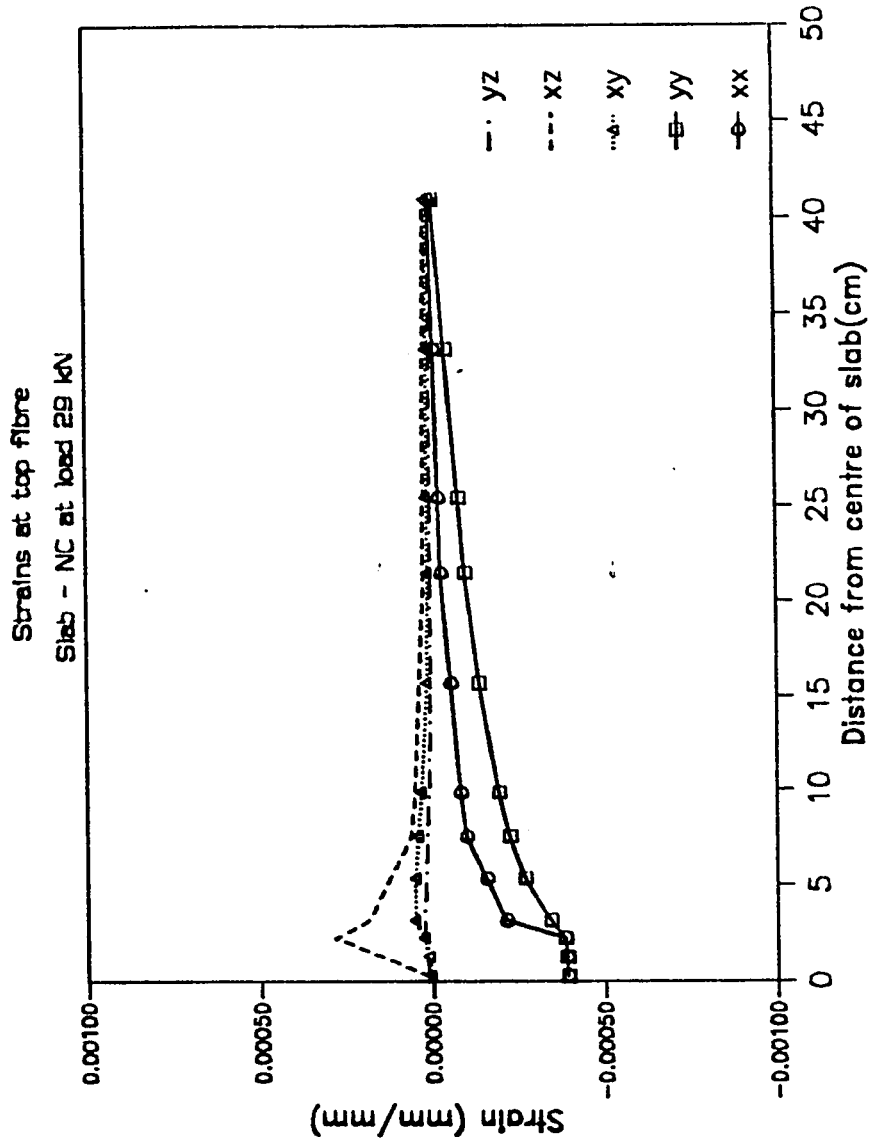

Fig. 6.16 Strains in top layer at load P = 29 kN for crushing 'silenced'

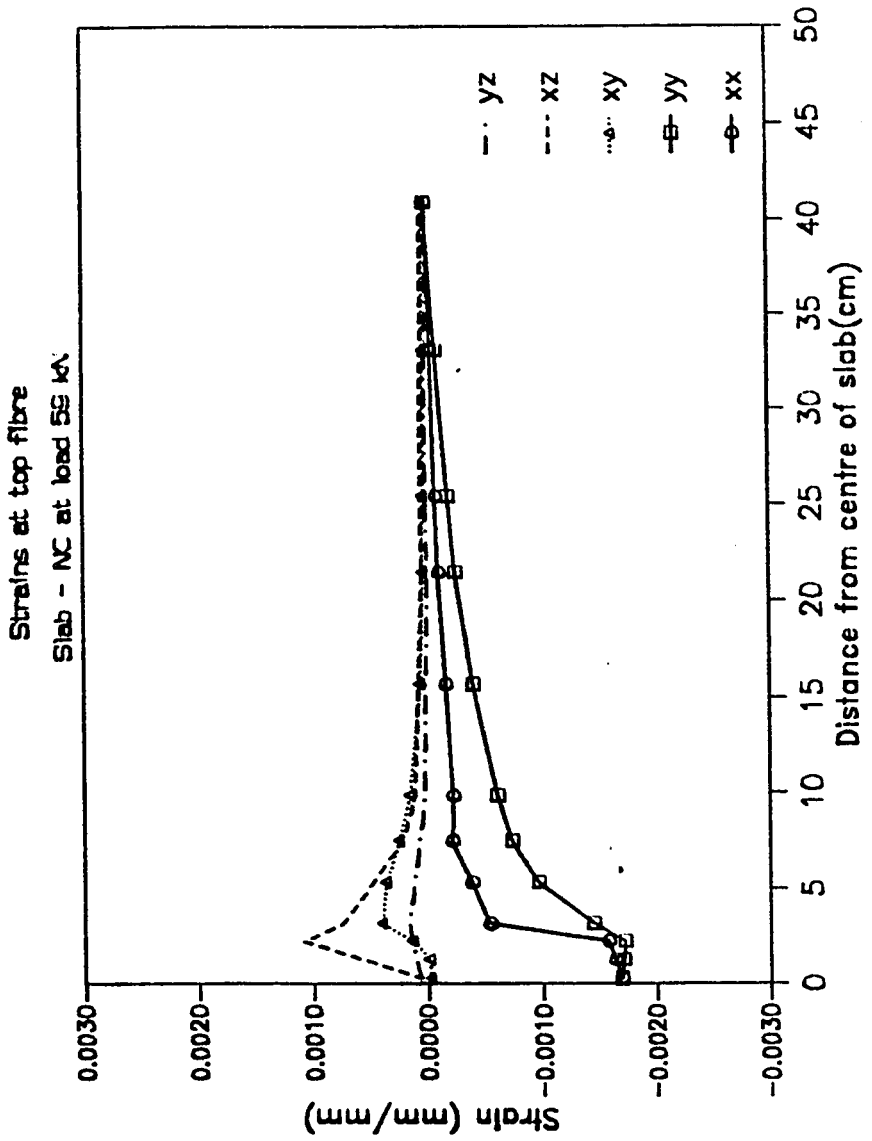

Fig. 6.17 Strains in top layer at load P= 59 kN for crushing 'silenced'

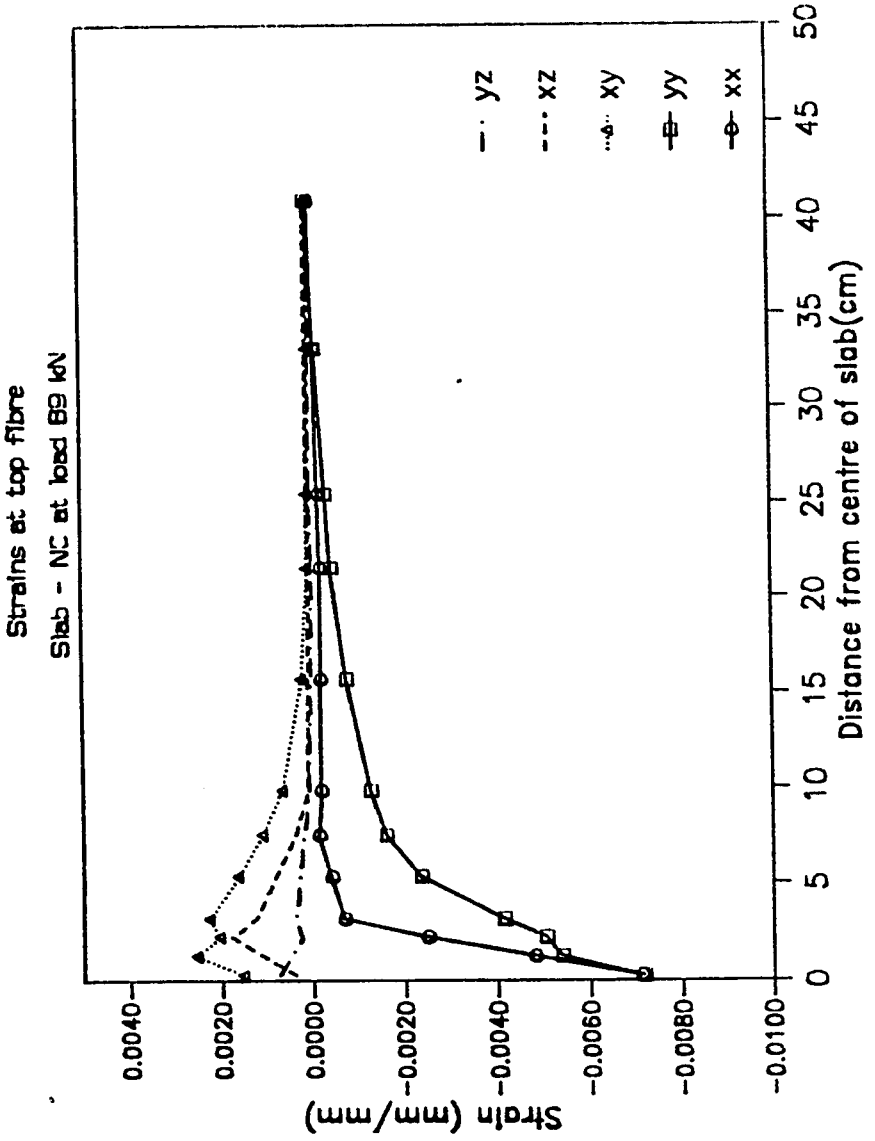

Fig. 6.18 Strains in top layer at load P= 89 kN for crushing 'silenced'

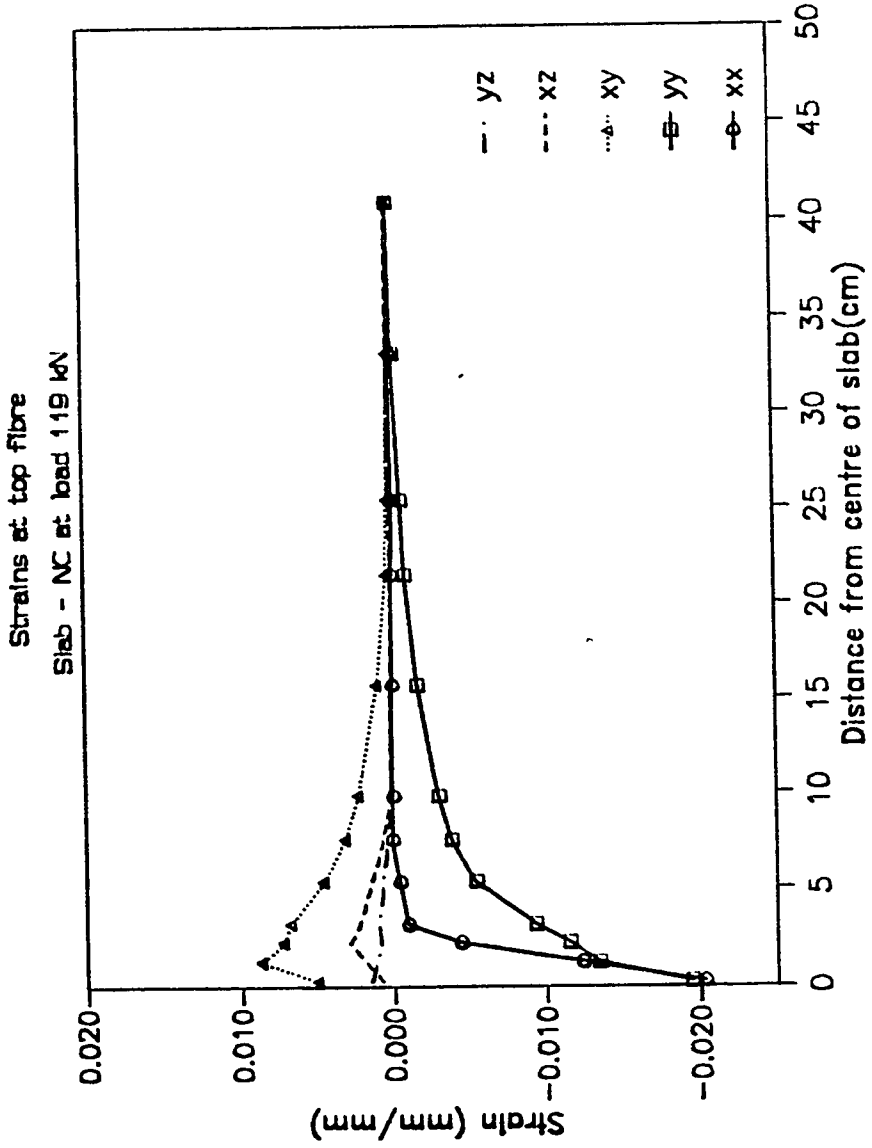

Fig. 6.19 Strains in top layer at load P = 119 kN for crushing 'silenced'

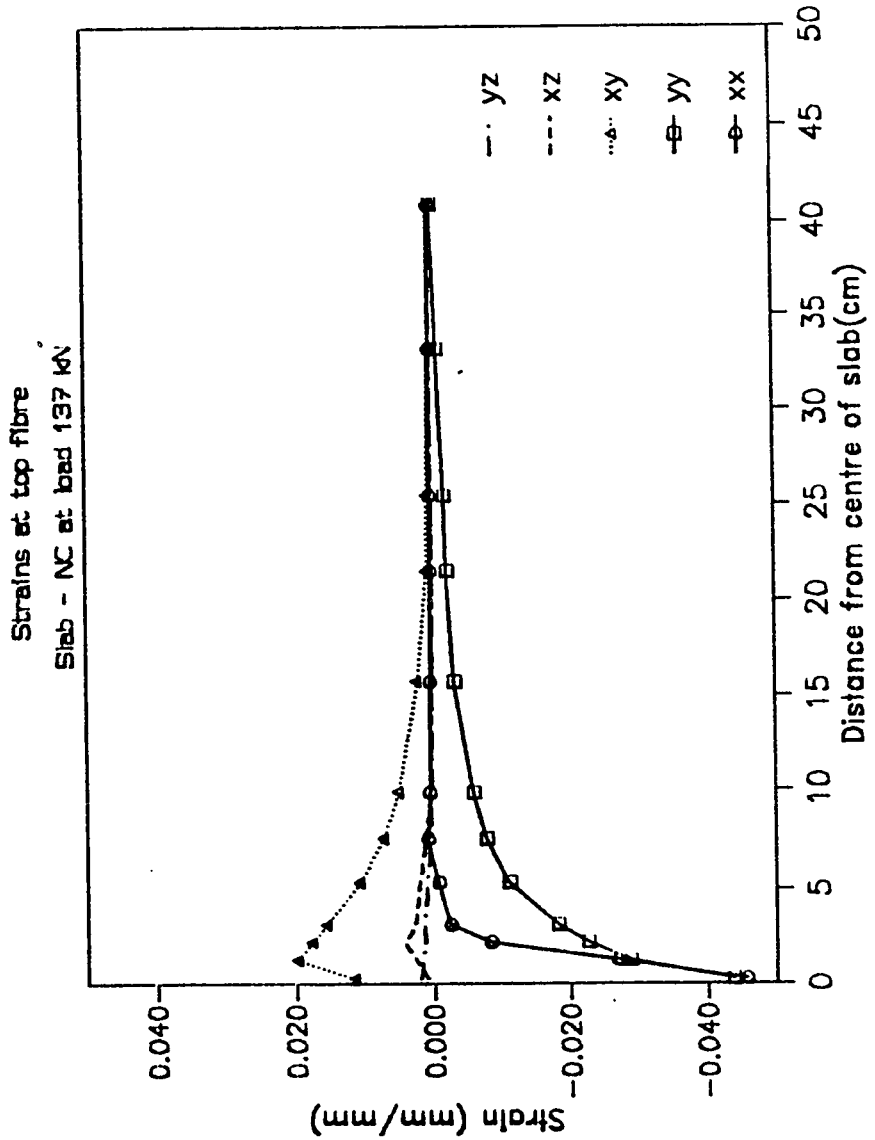

Fig. 6.20 Strains in top layer at collapse load P_u = 137kN for crushing 'si-lenced'

increments is shown in Figs. 6.11 through 6.15 with corresponding strain variations shown in Figs. 6.16 through 6.20. In the absence of a crushing criterion, the strains build up to over 4%, with corresponding increase in the dominant bending stresses σ_y and σ_x.

Each Gauss point in the compression zone is allowed to reach a yield surface, and in the absence of the constraint of a crushing criterion, a highly ductile response is elucidated from the slab.

This parametric study shows the importance of selecting a crushing criterion that neither causes a premature collapse nor allows the slab to extend into a mode not borne out by experimental findings.

6.2.3 Influence of Dowel Effect on Punching Capacity

In order to model the influence of dowel effect on the behavior of the R/C slab, the steel in any given direction was considered to not only have an axial stiffness but also a transverse shear stiffness such that (i) the reinforcement in the x-direction would sustain not only σ_x stresses but also transverse shear τ_{xz} stresses (yielding a dowel resultant force) and (ii) the reinforcement in the y-direction would resist transverse shear stress τ_{yz} in addition to σ_y stresses.

In view of the incorporation of dowel effect, the elasto-plastic constitutive law is taken as a general von-Mises yield criterion rather than a one-dimensional Rankine yield criterion appropriate where the dowel effect is neglected. Results were obtained in order to focus on the

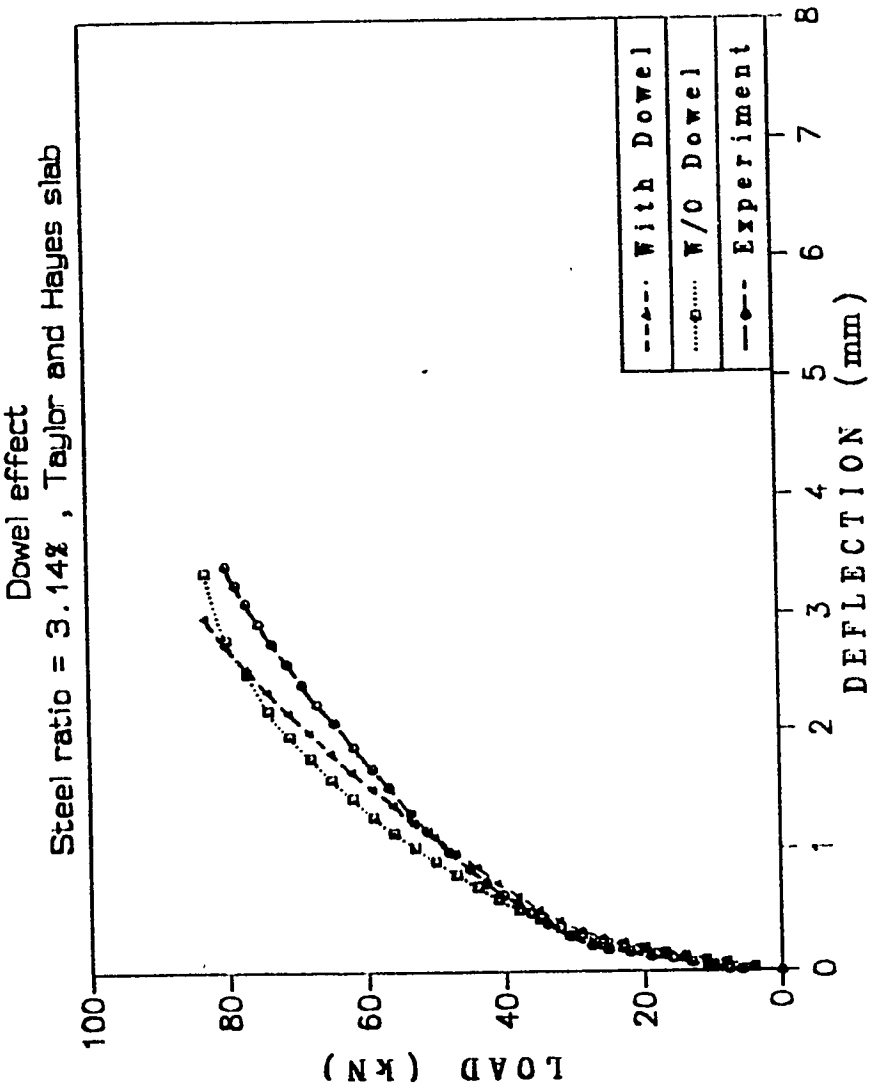

Fig. 6.21 Load deflection curves showing the dowel effect

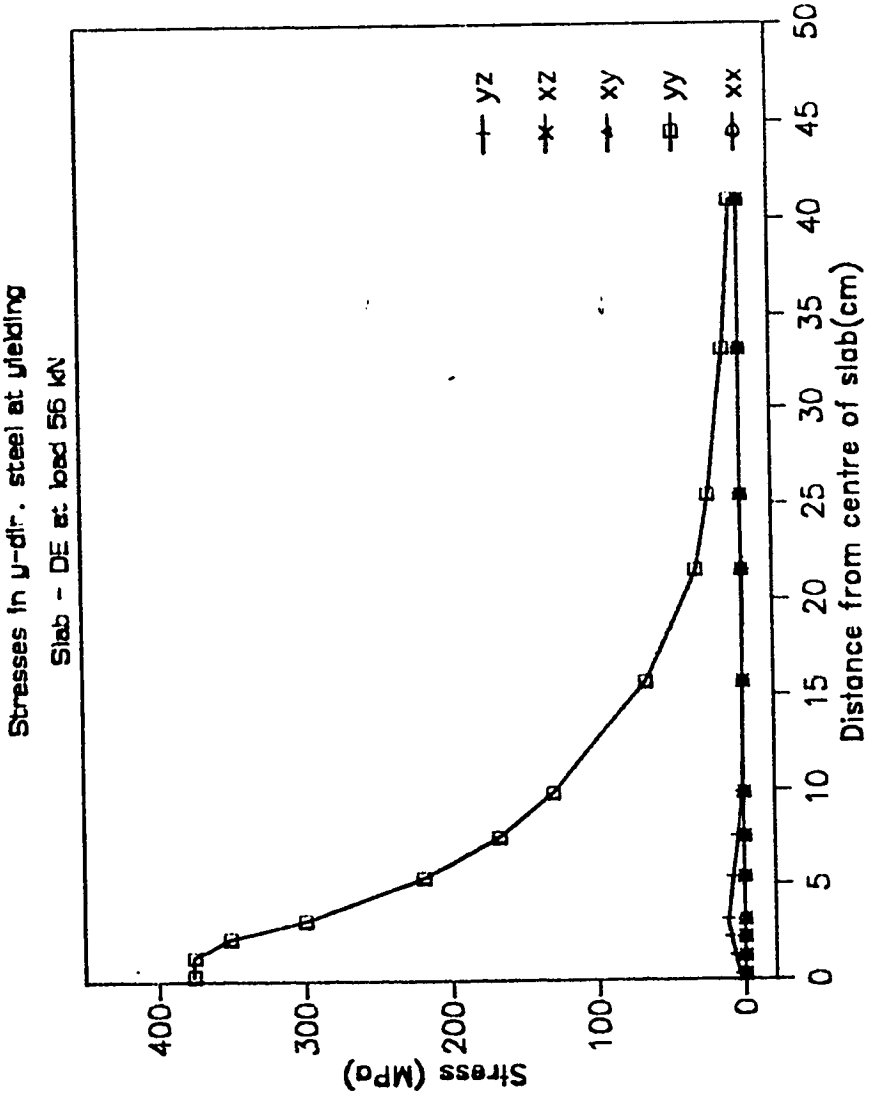

Fig.6.22 Stresses in y-dir. steel under the load at steel yielding at load P = 56 kN

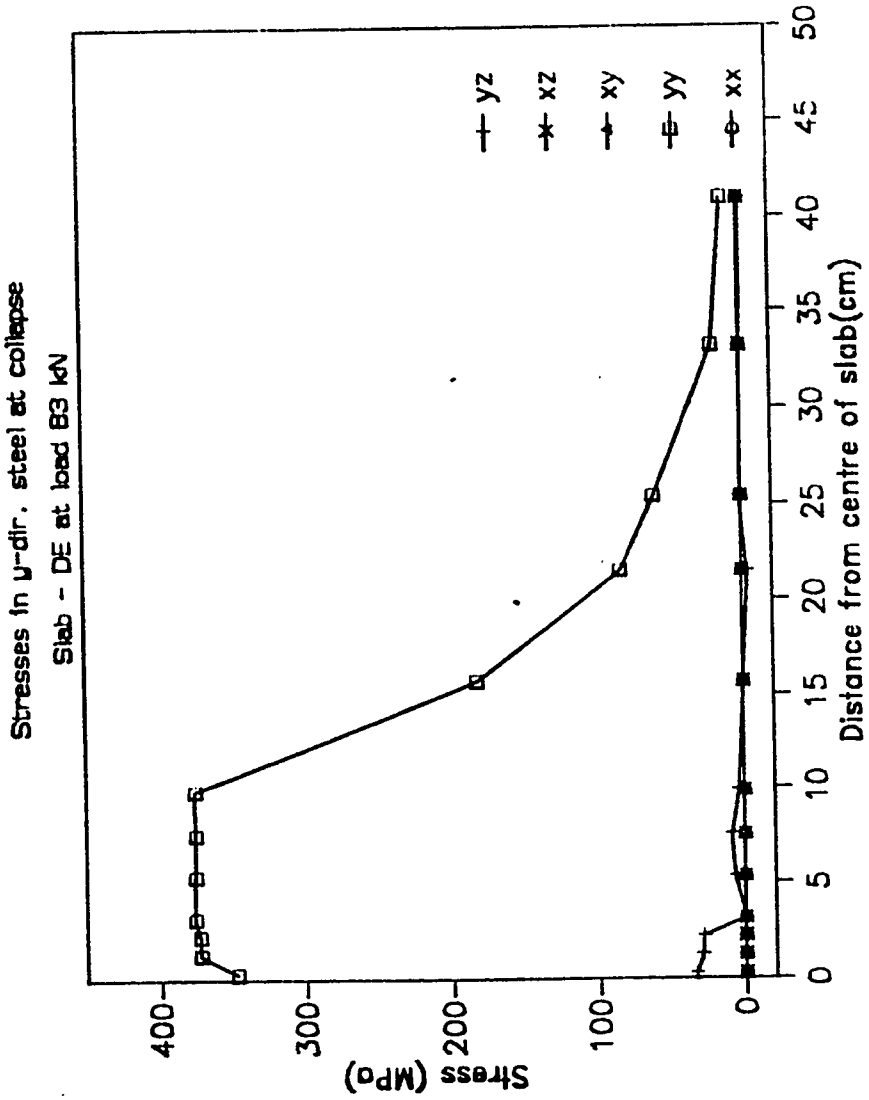

Fig. 6.23 Stresses in y-dir. steel under the load at at collapse load $P_u = 83kN$

modified response of the load-deflection curve due to inclusion of the dowel effect. Fig. 6.21 shows that whilst the structural stiffness of the slab remains virtually unaffected, the collapse load registered an increase of 8 percent due to inclusion of dowel effect. This had a net effect of bringing the collapse load closer to the experimental value.

Stress distribution in the reinforcement in the y-direction at first yield and at collapse load is shown in Figs. 6.22 and 6.23, respectively. It may be noted that the reinforcement has a build up of τ_{yz} shear stress prior to collapse, which in turn leads to a moderate increase in the capacity of the R/C slab.

The overall effect of incorporation of dowel action is to improve the predictability characteristics of the computational model.

6.2.4 Parametric Variation of Tension Stiffening Parameter α

In order to study the influence of the tension stiffening parameter α on the response of the reinforced concrete slab, numerical experiments are carried out for $\alpha=0$ (sudden release of stress on cracking), $\alpha=0.7$ (partial release of stress on cracking) and $\alpha=1.0$ (nominal release of stress on cracking). The slab selected for study had a total reinforcement ratio of 1.57%, with the α effect being more pronounced for weakly reinforced members. Results have been presented so as to focus on

(i) load-deflection patterns

(ii) stresses and strains in the extreme bottom layer at a load greater than the first cracking load

(iii) selected profiles illustrating status of Gauss points at yield and collapse.

Fig 6.24 shows the variation in load-deflection ($P-\Delta$) for the three cases under study. A striking manifestation is the marked effect that α has on the overall stiffness of the slab, with $\alpha=1.0$ exhibiting a highly stiffened system relative to the experimental $P-\Delta$ curve. Although $\alpha=0$ simulates the stiffness of the structure quite accurately at lower load levels, it suffers premature failure at 54% of the experimental load. The use of $\alpha=0.7$ leads to a $P-\Delta$ that is somewhat stiffer than the experimental one, but yields a collapse load which is 89% of the experimental load.

In order to study effect of tension modelling of concrete for slabs moderately reinforced, numerical experiment was reconducted with total $\rho=3.14$. The load reduction with $\alpha=0.0$ was recorded as only 11% (Fig. 6.25) in contrast to 46% for the case of $\rho=1.57$. This result demonstrates that tension modelling of concrete assumes greater importance for weakly reinforced members.

Figs. 6.26 through 6.28 show the stress distribution in the extreme bottom layer for $\alpha=1$, 0.7 and 0.0, respectively, at a load level of 32kN, which is greater than the first cracking load (17 kN). The variations reveal the influence of α on the stress patterns, with σ_{xx}, σ_{yy} maintaining values closer to f_t (3.5 MPa) for $\alpha=1$ than in the cases for $\alpha=0.0$ and $\alpha=0.7$. As Fig. 6.28 reveals, for the case of $\alpha=0.0$ cracking at load level of 32kN has significantly reduced σ_{xx} and σ_{yy} for a distance of 10 cm from the slab centre in contrast to levels of σ_{xx} and

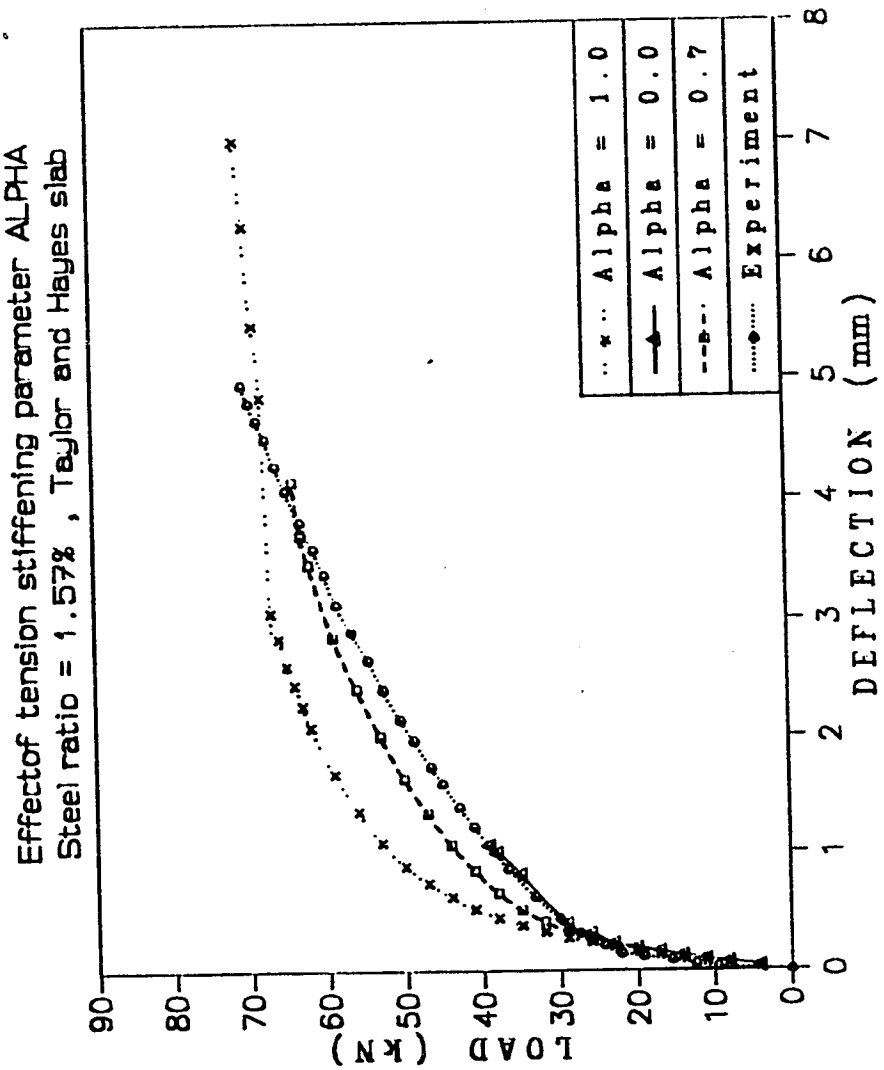

Fig. 6.24 Load deflection curves showing the effect of α for $\rho = 1.57\%$

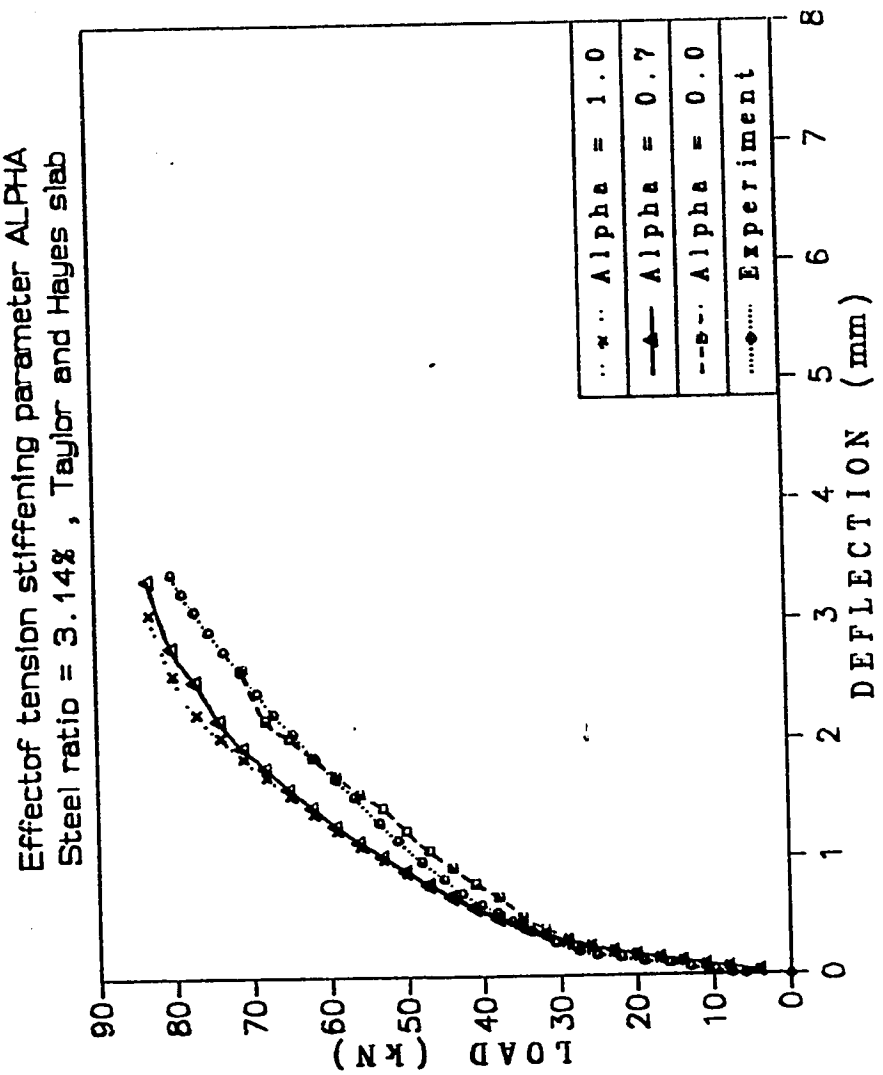

Fig. 6.25 Load deflection curves showing the effect of α for $\rho = 3.14\%$

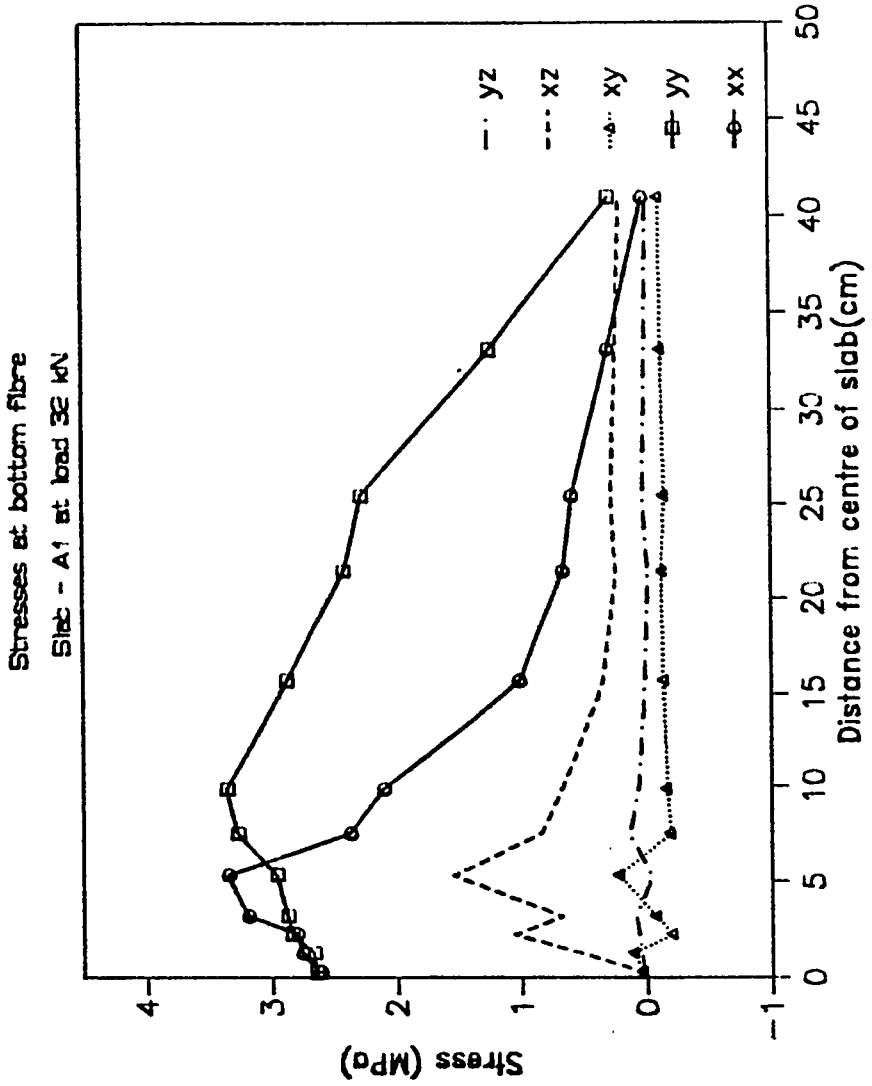

Fig. 6.26 Stresses in bottom layer at load P = 32 kN for $\alpha = 1$.

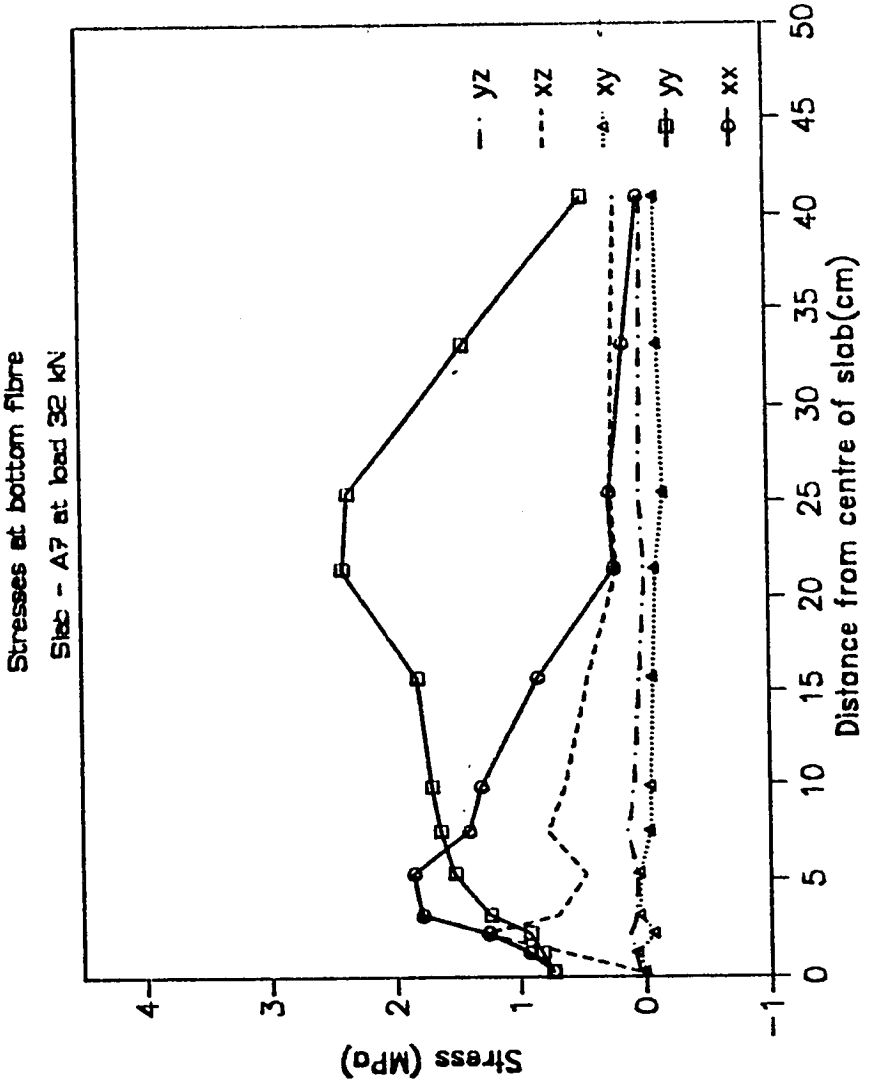

Fig. 6.27 Stresses in bottom layer at load P = 32 kN for $\alpha = 0.7$

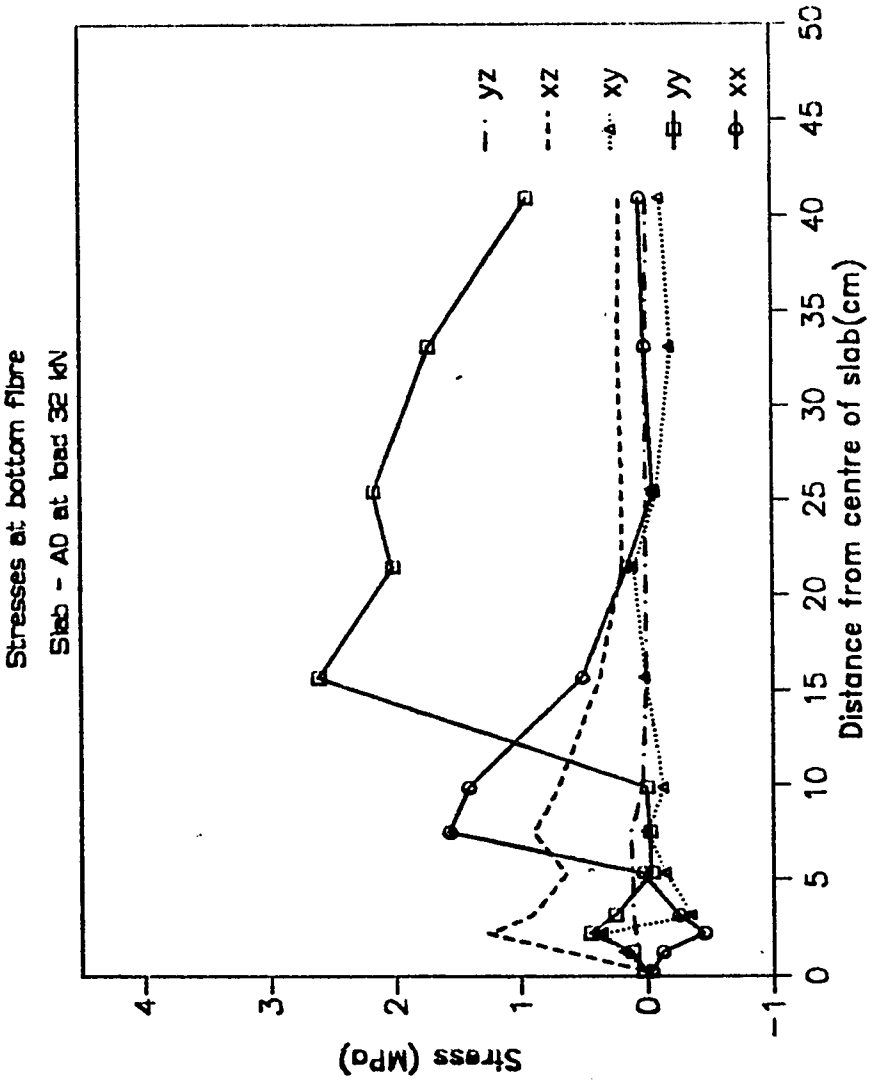

Fig. 6.28 Stresses in bottom layer at load P = 32 kN for $\alpha = 0.0$

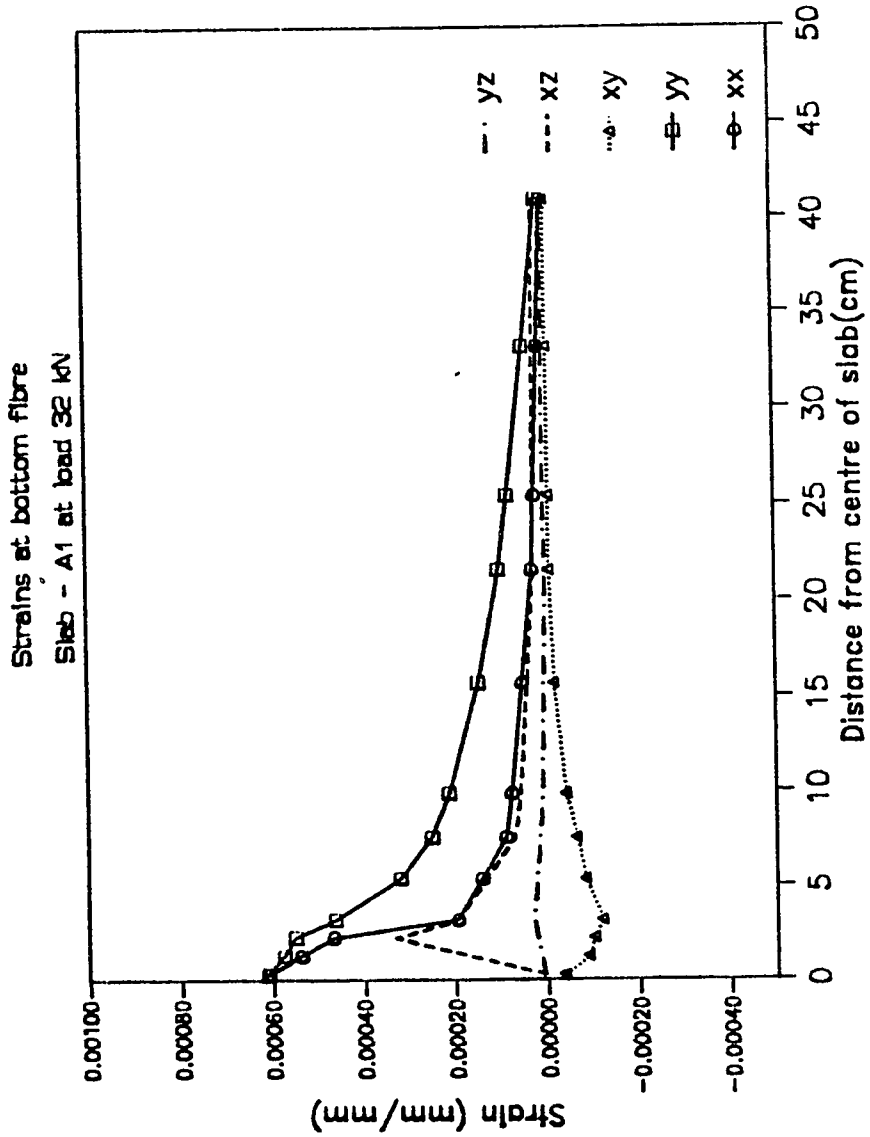

Fig. 6.29 Strains in bottom layer at load P = 32 kN for $\alpha = 1$.

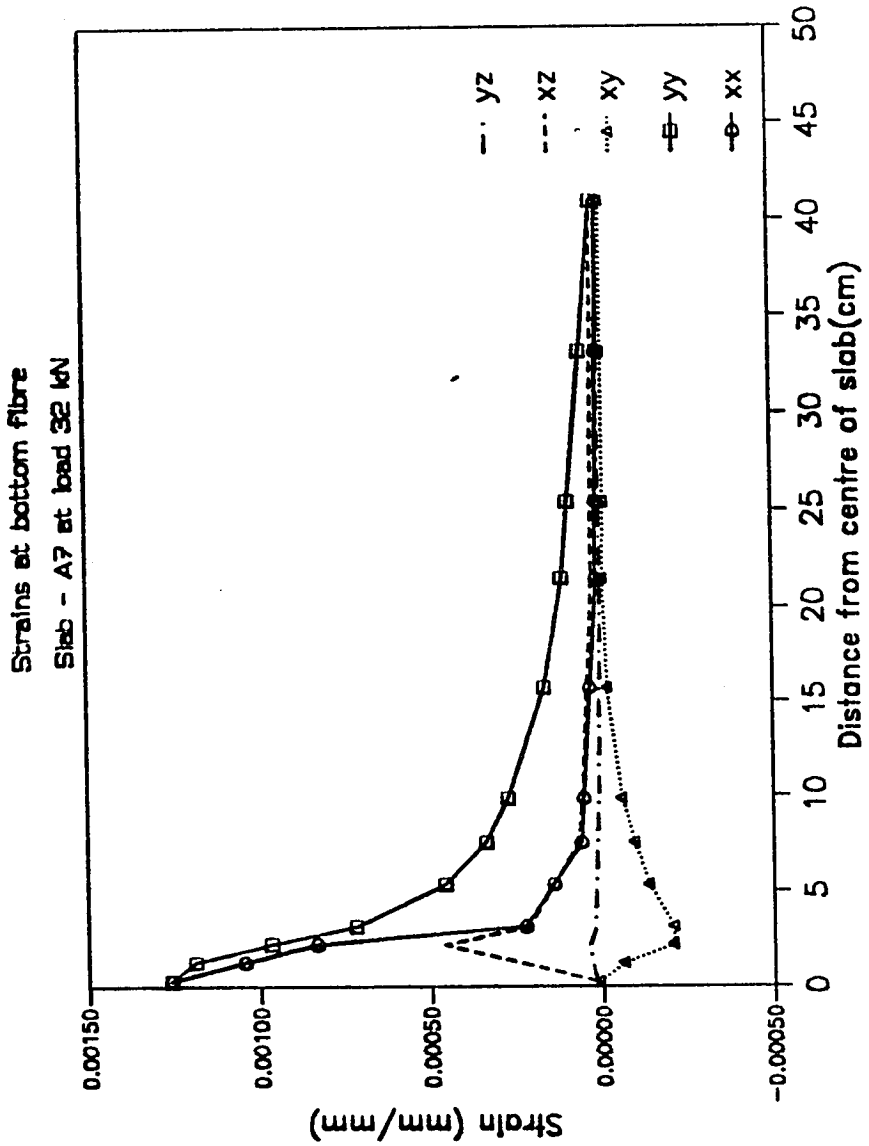

Fig. 6.30 Strains in bottom layer at load P = 32 kN for $\alpha = 0.7$

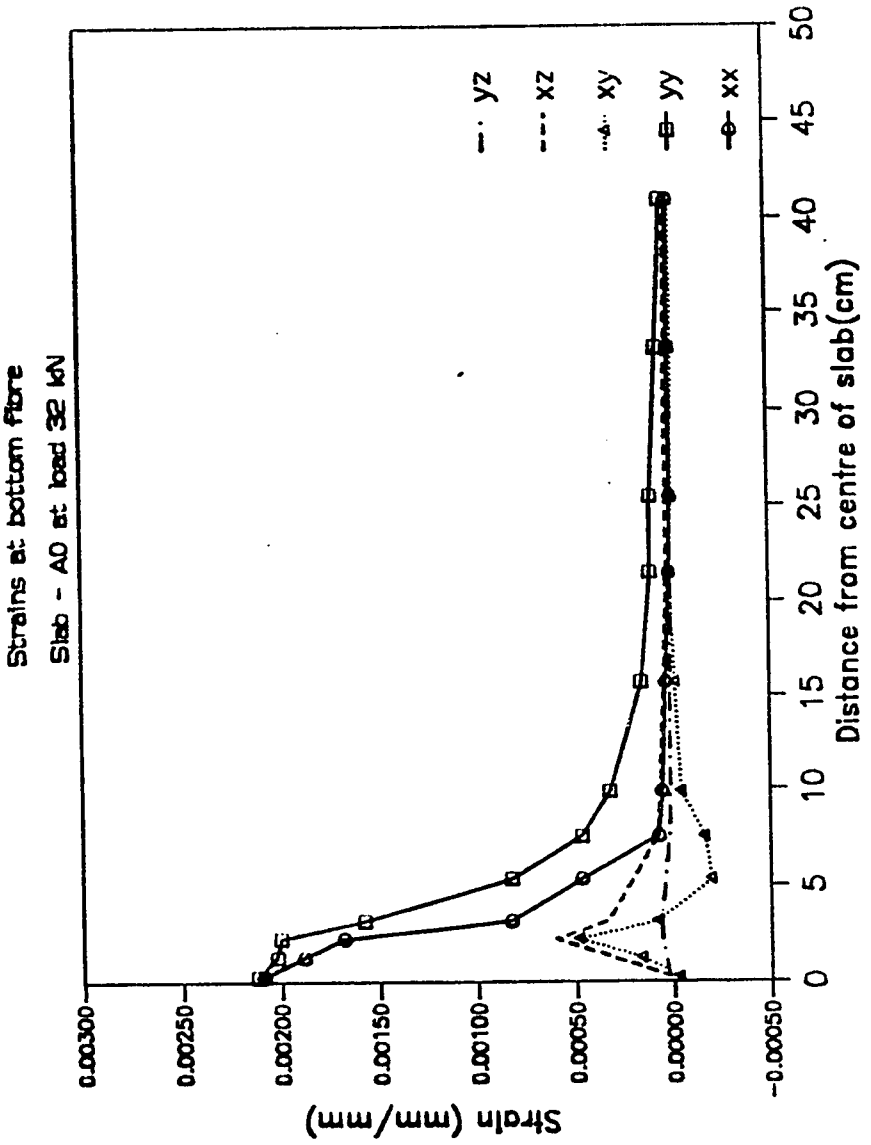

Fig. 6.31 Strains in bottom layer at load P = 32 kN for $\alpha = 0.0$

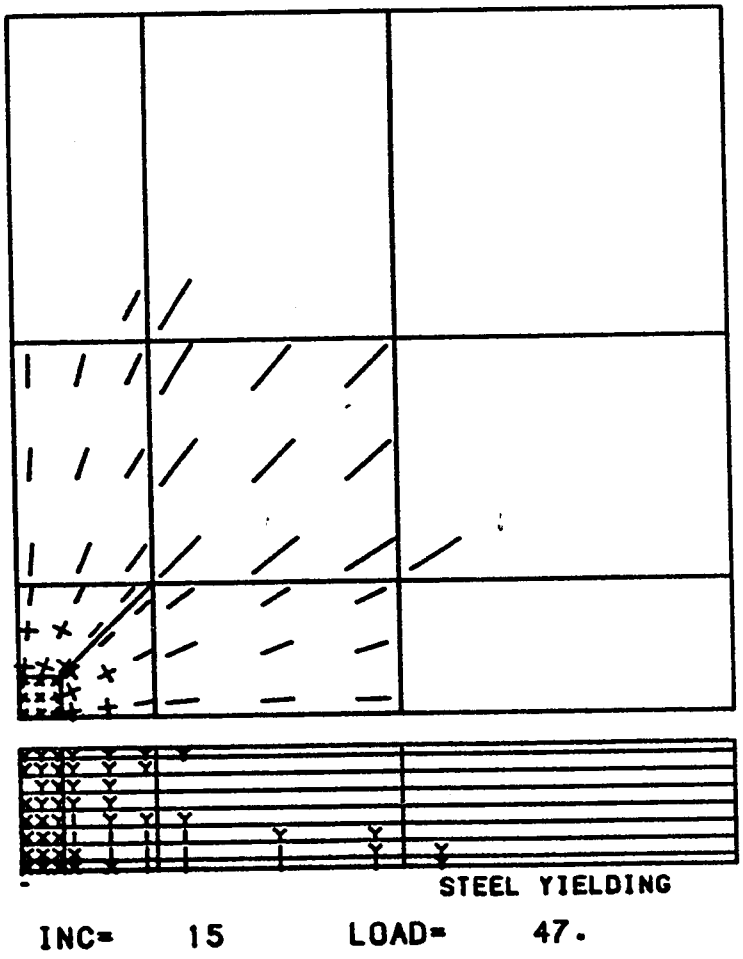

Fig. 6.32 Cracking in bottom of slab and section profile at steel yielding at load P = 47 kN for $\alpha = 1$.

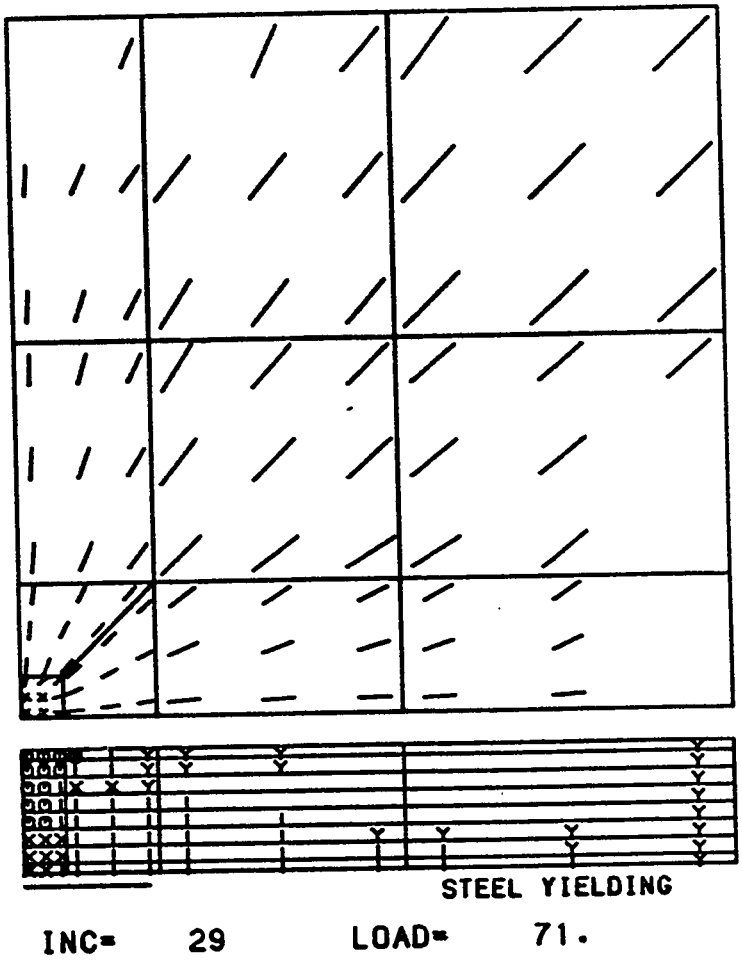

Fig. 6.33 Cracking in bottom of slab and section profile at collapse load $P_u = 71kN$ for $\alpha = 1$.

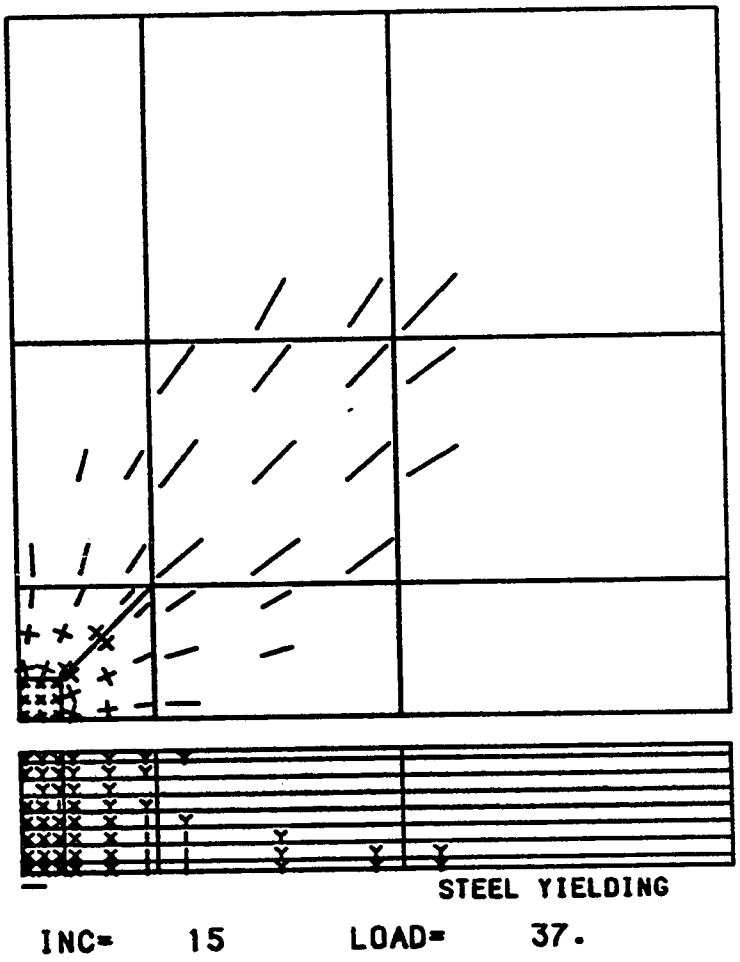

Fig. 6.34 Cracking in bottom of slab and section profile at steel yielding at load P = 37 kN for $\alpha = 0.0$

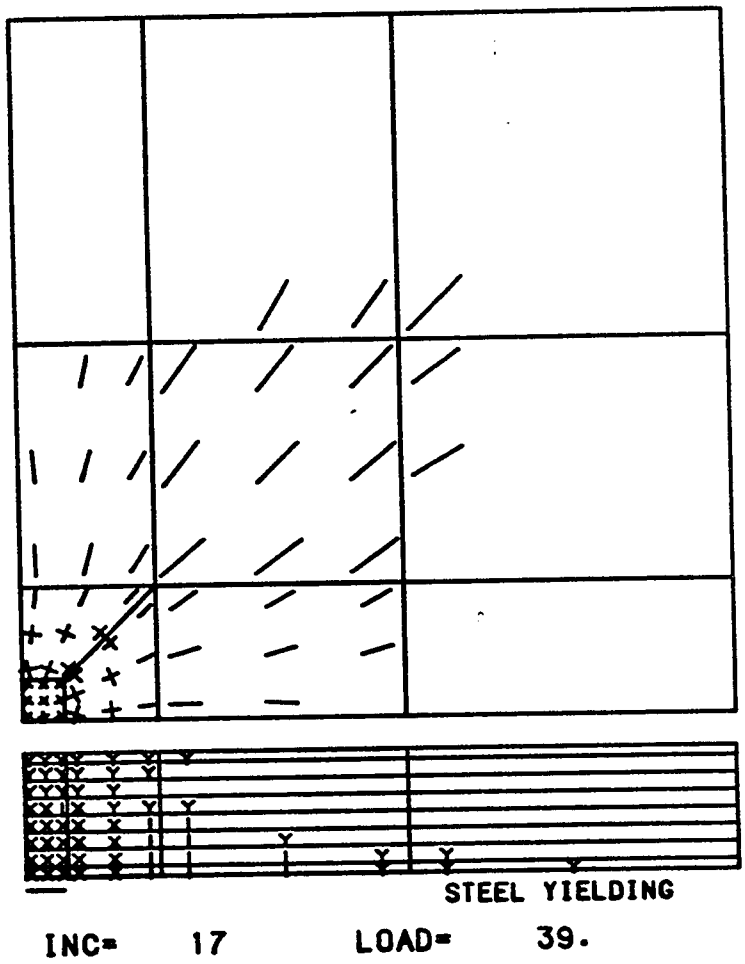

Fig. 6.35 Cracking in bottom of slab and section profile at collapse load $P_u = 39kN$ for $\alpha = 0.0$

σ_{yy} in the same zone for $\alpha=1$ (Fig. 6.26).

Figs. 6.29 through 6.31 show the strain variation in the extreme bottom fibre for the three different values of α under consideration. Dominant strains ε_x and ε_y are much higher for the case of $\alpha=0.0$ (Fig. 6.31) in comparison to the case of $\alpha=1.0$ (Fig. 6.29). This is due to reduced stiffness of relevant Gauss points for the case of $\alpha=0.0$ in contrast to the stiffness for the case of $\alpha=1.0$. Increased strains in turn lead to increased flexibility, which was earlier reflected in the P−Δ variation as illustrated in Fig. 6.24.

Figs. 6.32 and 6.33 show section profiles with status of Gauss point cross section for first steel yield load and collapse load for the case of $\alpha=1$. Similar plots for the case of $\alpha=0$ are shown in Figs. 6.34 and 6.35. Selection of α not only affects the collapse load, but the first steel yield load is also significantly altered. Fig. 6.33 shows that collapse for $\alpha=1$ slab is initiated and culminated by crushing of Gauss points, where Fig. 6.35 shows collapse for $\alpha=0$ slab is precipitated primarily by two way cracking.

6.2.5 Parametric Variation of Degraded Shear Modulus

The computational model uses a degraded shear modulus (G^c) when the tensile strain ε_1 becomes greater than the cracking strain of $\varepsilon_t=f_t/E_c$ according to the rule

$G^c = 0.25\ G(1-\varepsilon_1/0.005)$

with G^c set equal to zero when $\varepsilon_1 \geq 0.005$. This loss of shear stiffness due to cracking reflects aggregate interlock reduction.

The parametric variation studied in this section considered three possible modes of degradation namely (a) normal degradation (b) full degradation which sets G immediately to zero on first cracking and (c) no degradation which retains the full magnitude of G regardless of the cracking strain.

Fig 6.36 shows the load-deflection plot ($P-\Delta$) for the three cases, together with the experimental $P-\Delta$ relationship. It is noted that the stiffness of the structure is not appreciably altered by the variations in assumed degraded modulus but the collapse load for the zero degradation case is appreciably higher than the full degradation case. Of the three possibilities considered, the model making use of normal degradation simulates best the experimental $P-\Delta$.

Shown in Fig. 6.37 is the variation in the transverse shear stress τ_{xz} in the third from bottom layer, along a section taken through the middle of the plate. The stress variation is shown at a load of 50 kN and results for all three cases of varying degradation are superimposed on the same plot. A significant redistribution is noted due to variance in the shear stiffness, with the case of no degradation showing appreciably higher magnitude of the shear stress in cracked zones as compared to normally degraded and fully degraded slabs. Figs. 6.38 through 6.40 show sectional profiles at collapse load for the three cases

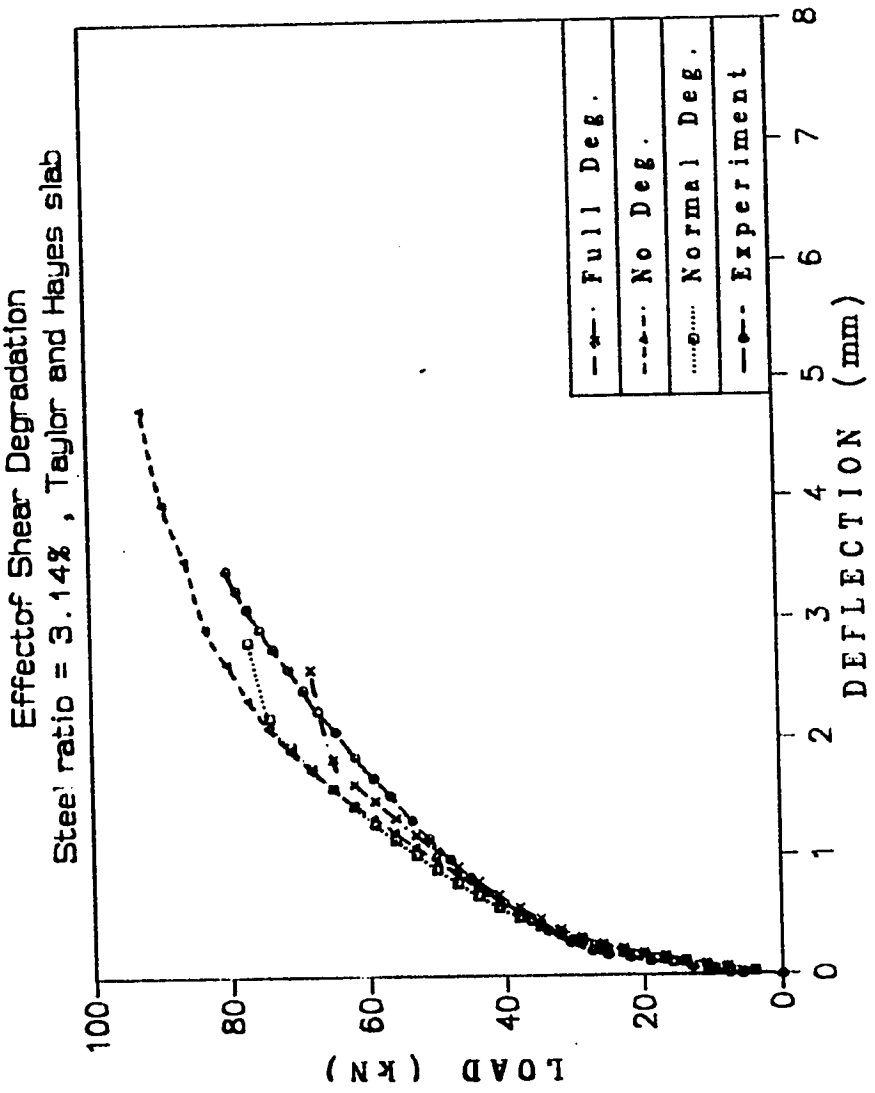

Fig. 6.36 Load deflection curves showing the effect of degree of degraded shear modulus

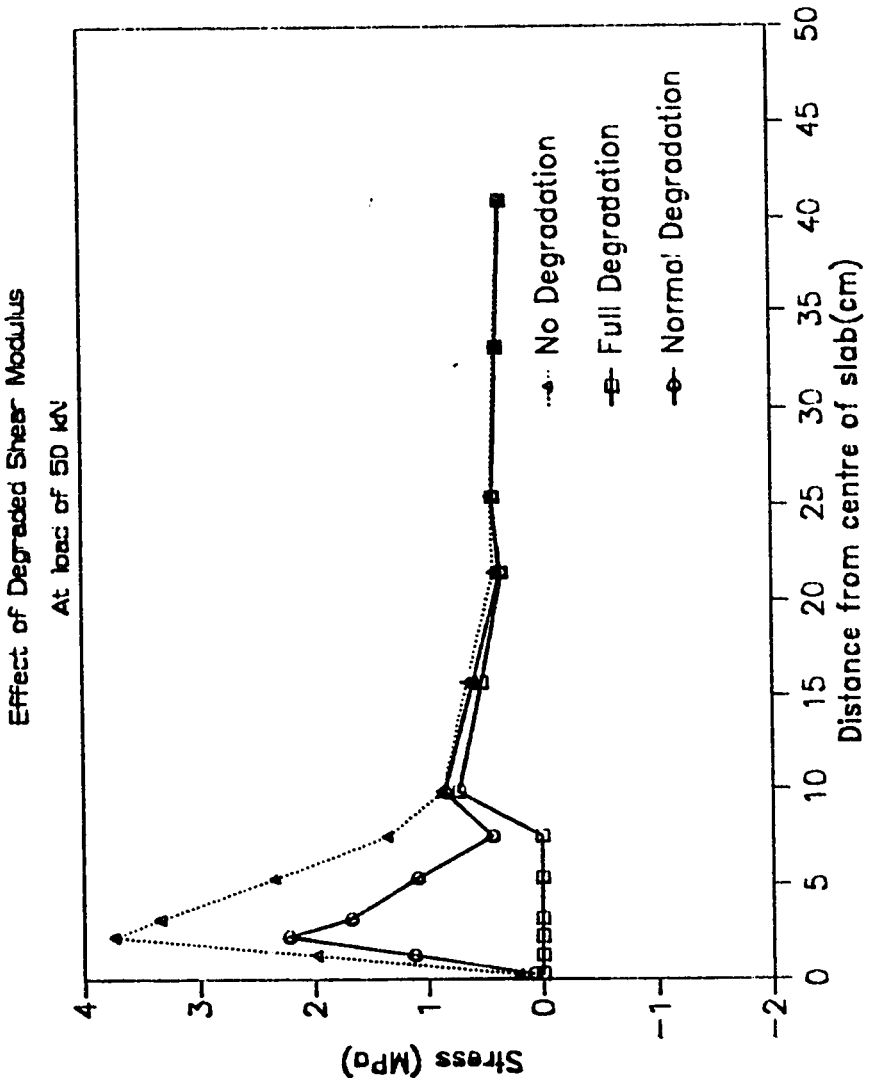

Fig. 6.37 Stresses in third bottom layer at load P = 50 kN

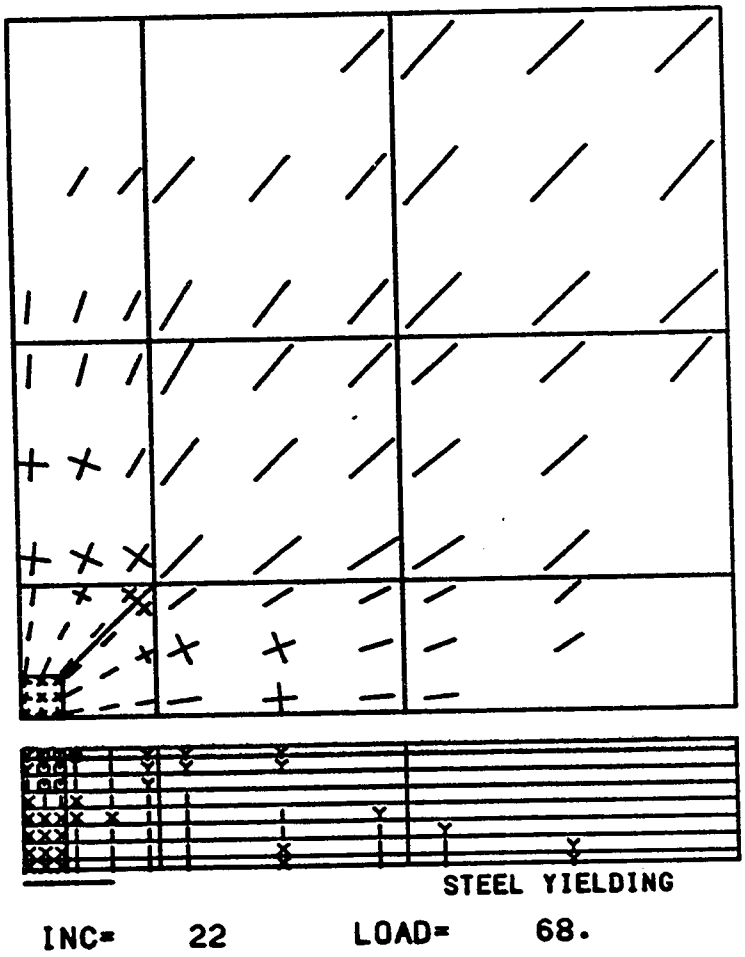

Fig. 6.38 Cracking in bottom of slab and section profile at collapse load $P_u = 68kN$ for fully degraded shear modulus

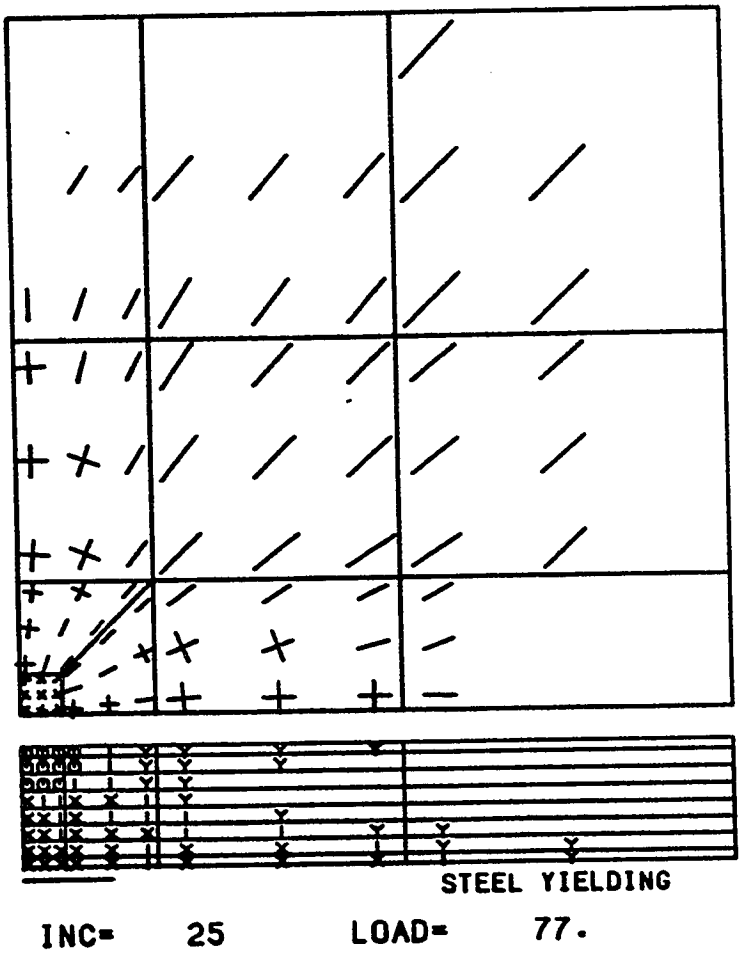

Fig. 6.39 Cracking in bottom of slab and section profile at collapse load $P_u = 77kN$ for normally degraded shear modulus

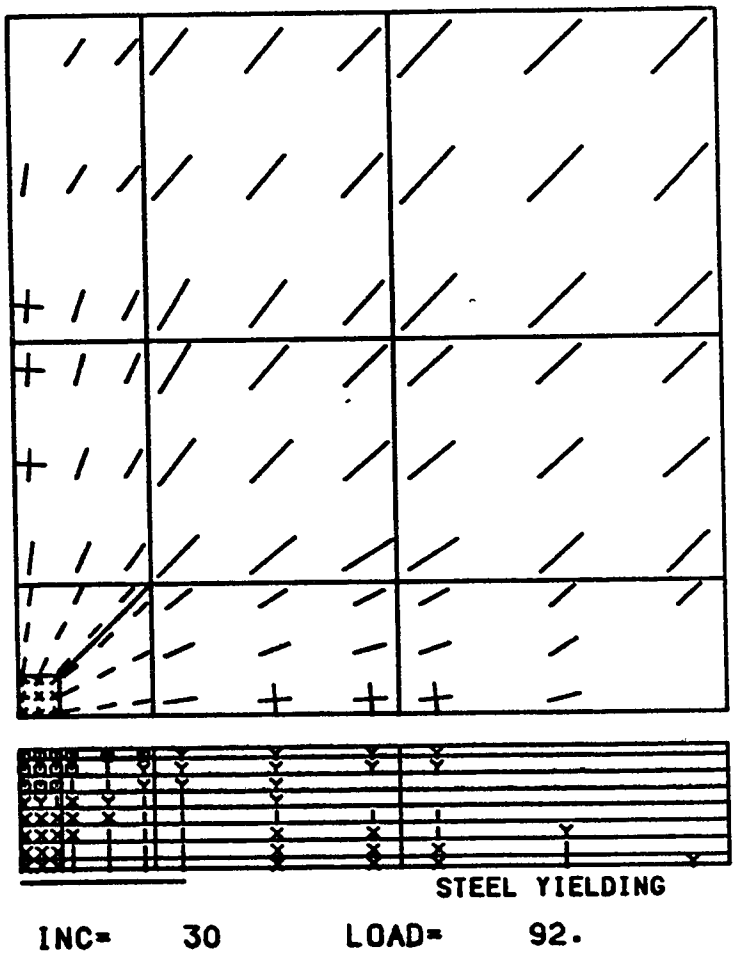

Fig. 6.40 Cracking in bottom of slab and section profile at collapse load $P_u = 92kN$ for no shear degradation

considered, illustrating the material status of the Gauss point in the various layers taking through the depth. In all cases, failure is initiated by crushing at the interface of the loaded element and the adjacent element under a predominantly biaxial stress state.

6.2.6 Role of Yield Criterion

The intent of this segment of the parametric study is to investigate the role of the selected yield criterion on the behavior of the reinforced concrete slab, and this effect is considered by comparison of response of slab modelled using a Mohr-Coulomb yield criterion, proposed yield criterion and Drucker-Prager yielding rule.

Figs. 6.41 and 6.42 show the load-deflection plots for slabs with two different steel percentages - one with a total steel ratios of 1.57% and the other with a steel ratio of 3.14%. For the case of lower steel percentage, the three yield criteria resulted in very similar P-Δ characteristics, with the Drucker-Prager being slightly stiffer. However, for the case of the higher steel percentage, the Drucker-Prager yield criterion yielded a significantly stiffer slab and an increased collapse load in comparison to Mohr-Coulomb and proposed yield criteria, with the latter being closer to the experimental behavior both in terms of stiffness and collapse load. The three yield criteria appear to converge in the case of a structure whose response is dominated by cracking damage and what may be said to constitute a flexural failure. The zones that undergo compression associated yielding are limited in size in comparison to the heavier reinforced slab. For the latter, the tension asso-

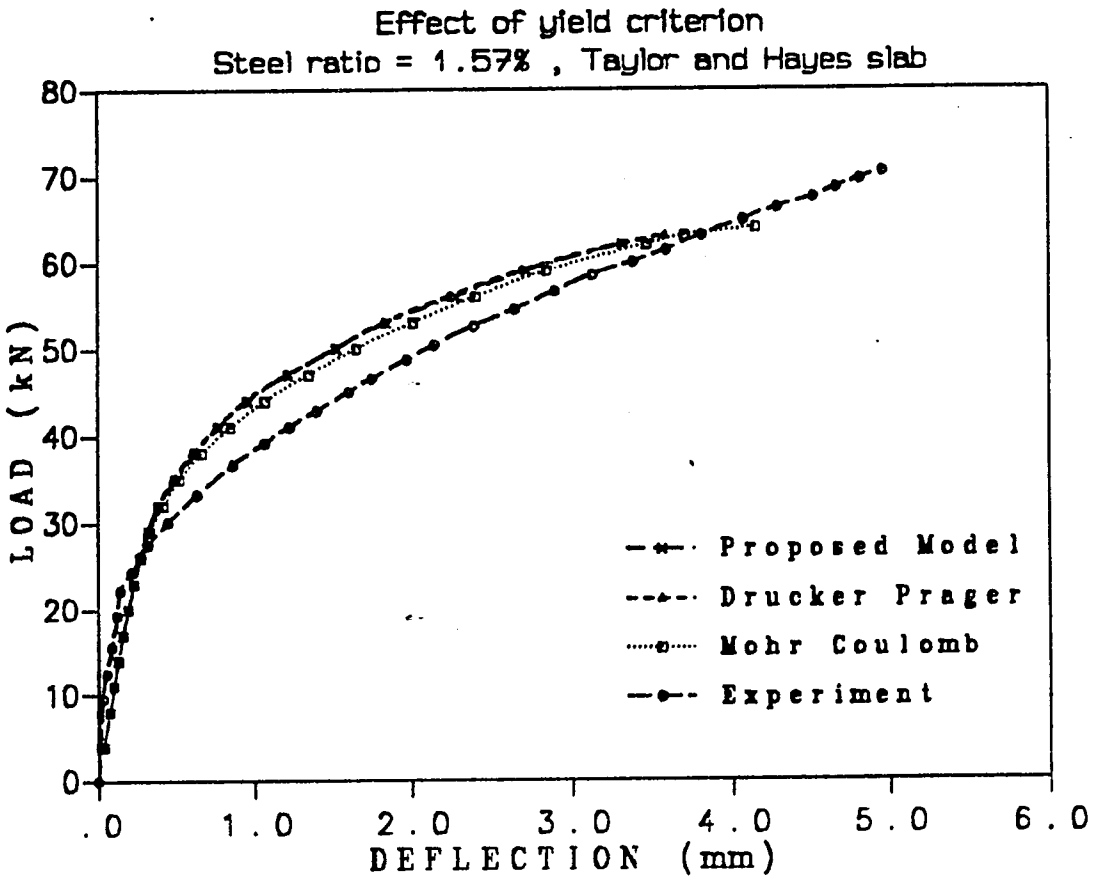

Fig. 6.41 Load deflection curves showing the effect of yield criterion for steel ratio = 1.57%

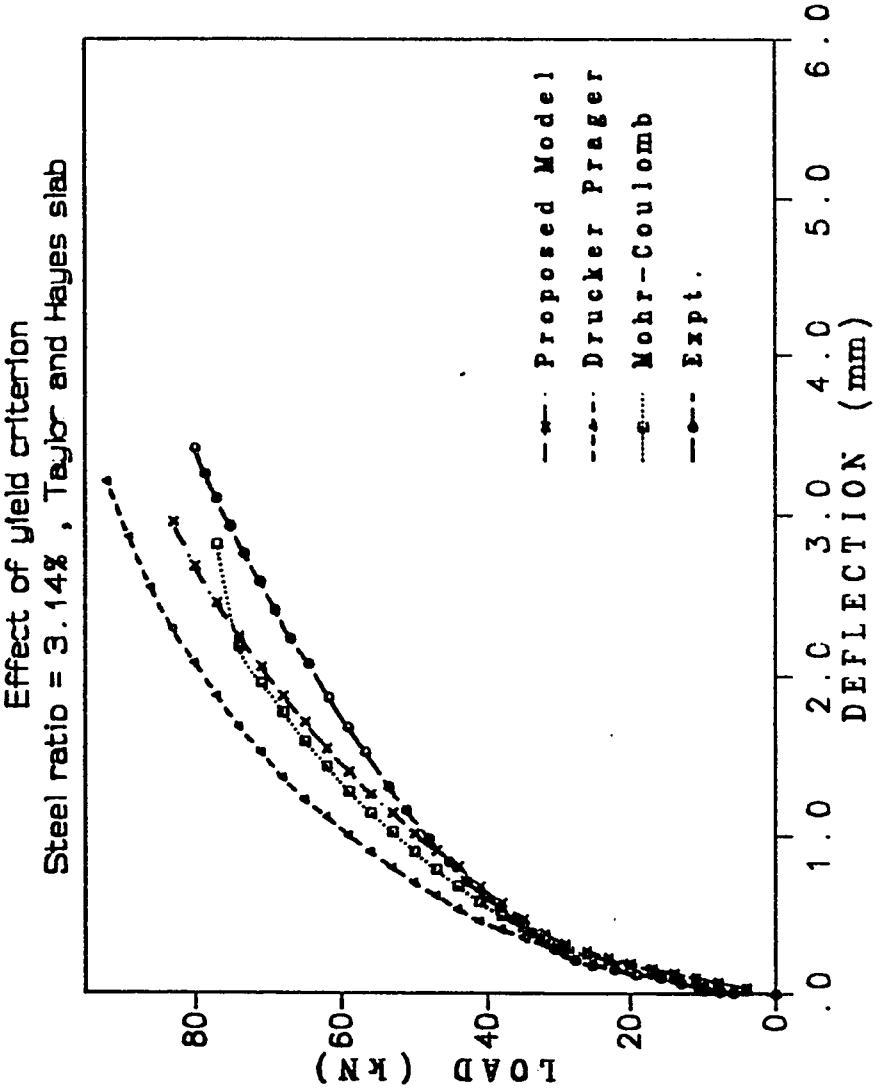

Fig. 6.42 Load deflection curves showing the effect of yield criterion for steel ratio = 3.14%

ciated cracking is arrested at shallower depths and greater zones are susceptible to compression yielding, i.e, the overall response of the structure would reflect greater sensitivity to type of yield criterion selected, and the failure pattern could be classified as being shear dominant, which is also reflected in reduced ductility of the structure. Thus the Mohr-Coulomb yield criterion, in addition to its simplicity and its adaptability to the explicit form of expression, possesses the versatility of tracing both flexure and flexure/shear dominated failures. Mohr-Coulomb and proposed yield criteria gave exactly same numerical collapse load. The model with proposed yield criterion compares very well with experiment initially and later it gets slightly stiffer. This can be further improved by choosing different set of data of concrete tests in order to calculate the model parameters A, B and C. Also the inter-layer variation of tension stiffening parameter α may improve the results further.

Figs. 6.43 and 6.44 show the stress and strain distribution at Gauss point in the top layer prior to crushing (P=68 KN), using the Mohr-Coulomb yield criterion with total steel reinforcement ρ=3.14 . Crushing was initiated in the subsequent increment at the interface of the loaded element and the adjacent element, and the redistribution of stresses with accompanying strains is shown in Figs. 6.45 and 6.46, respectively. Figs 6.47 and 6.48 illustrate the stress and strain distribution in the same slab using Drucker-Prager yield criterion, but the load prior to interaction of crushing is now increased to P=86 kN, with correspondingly higher stresses in the vicinity of the interface of the loaded and unloaded elements.

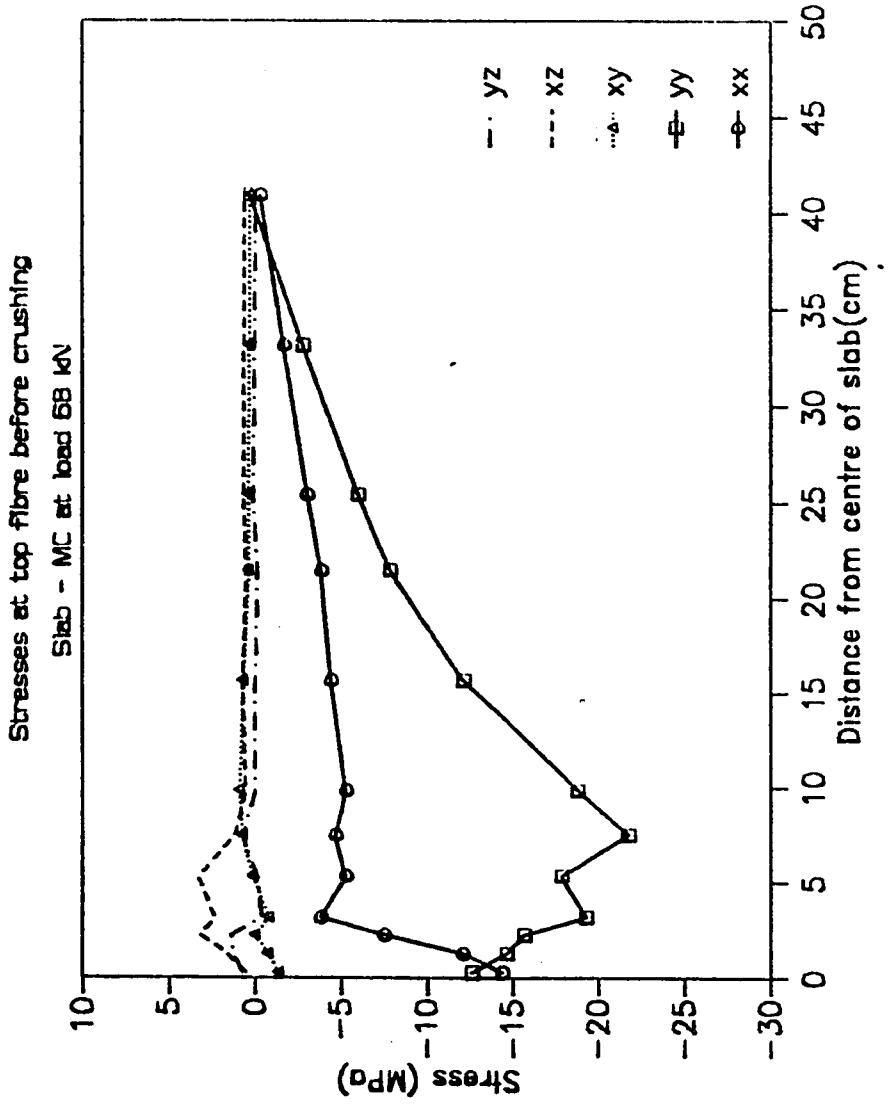

Fig. 6.43 Stresses in top layer before crushing for Mohr-Coulomb yield criterion at load P = 68 kN

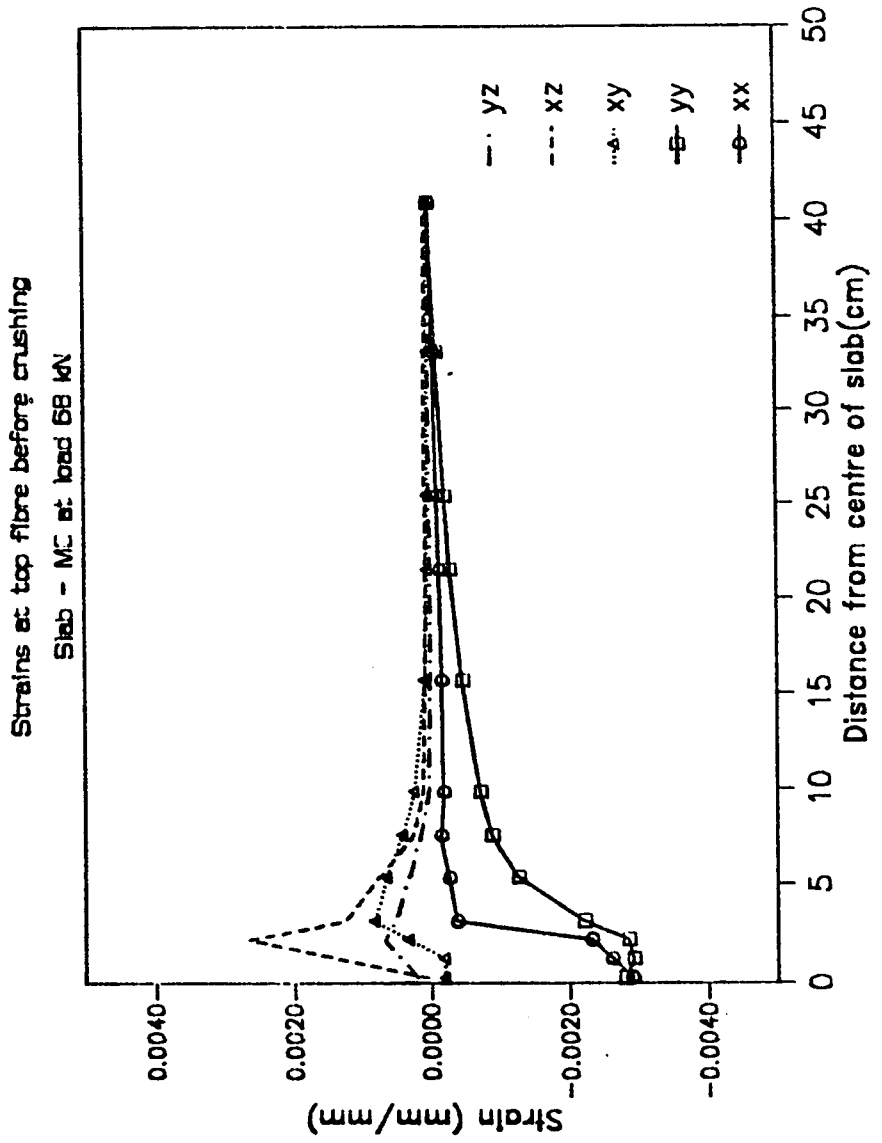

Fig. 6.44 Strains in top layer before crushing for Mohr-Coulomb yield criterion at load P = 68 kN

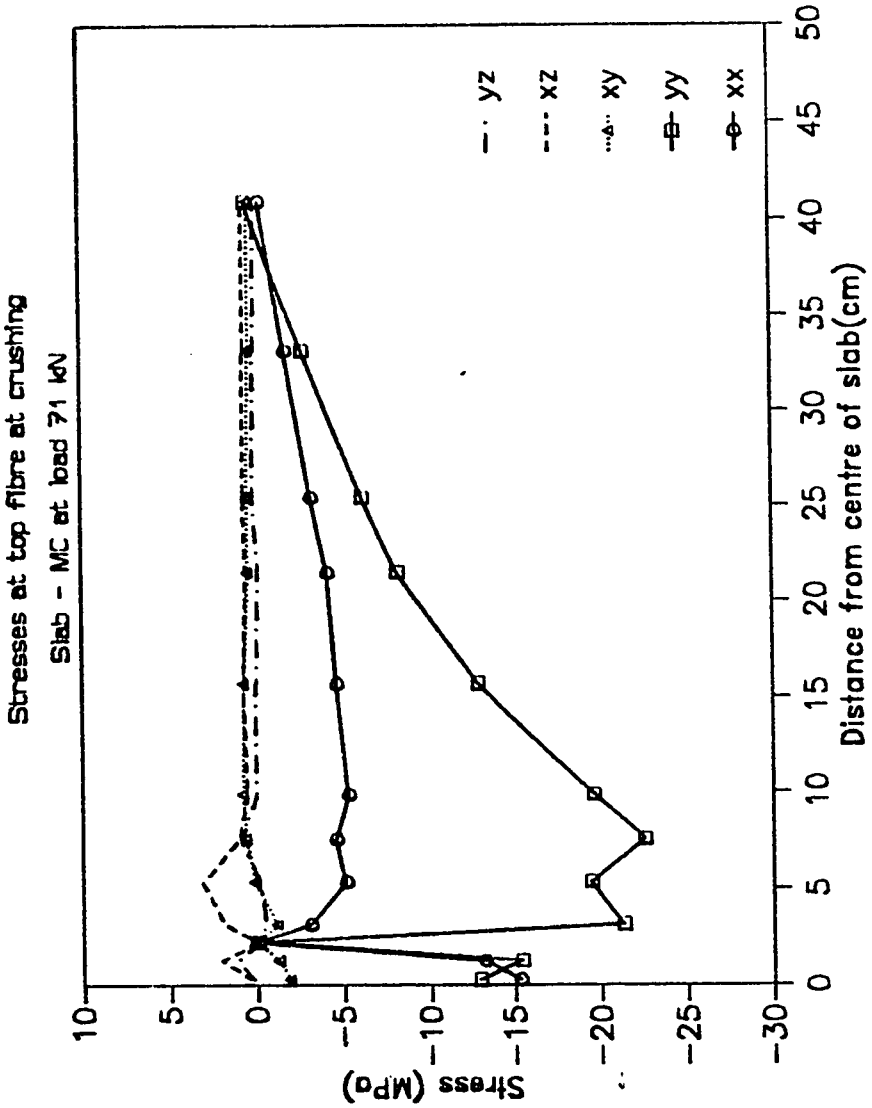

Fig. 6.45 Stresses in top layer at crushing for Mohr-Coulomb yield criterion at load P = 71 kN

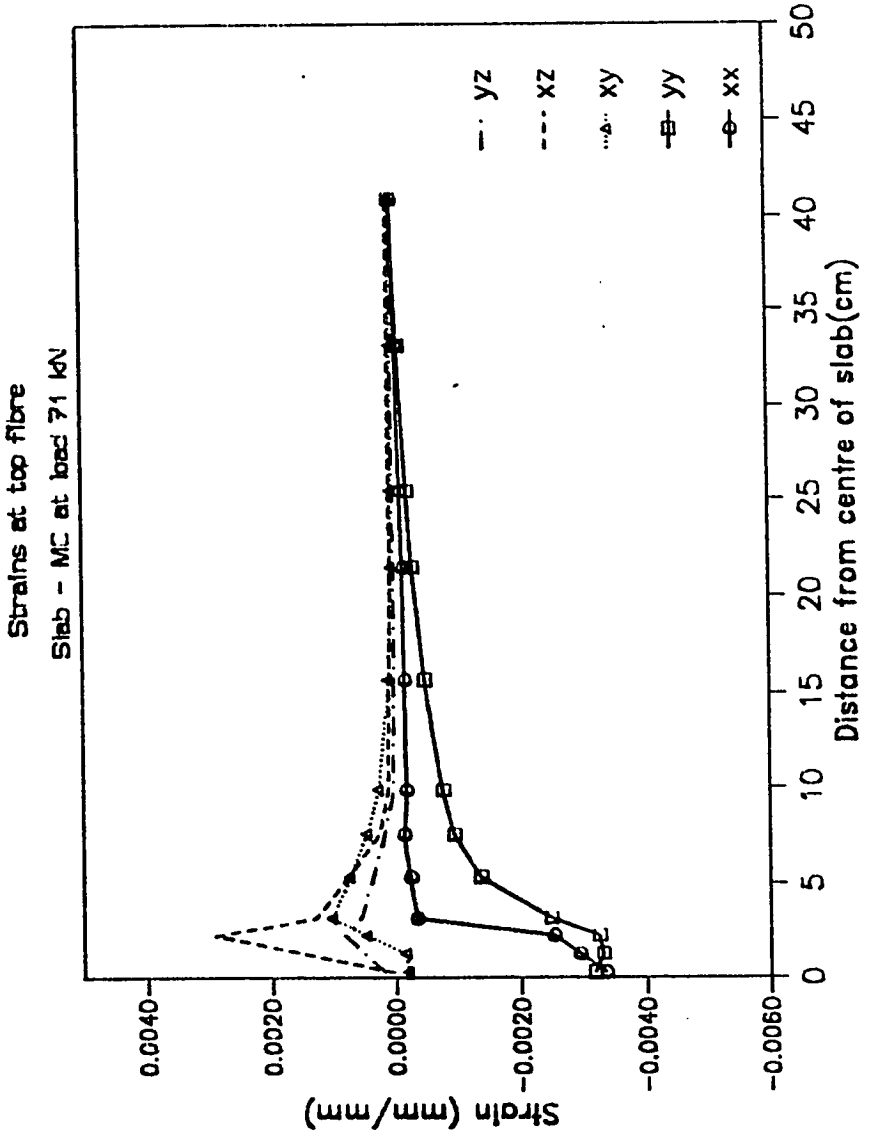

Fig. 6.46 Strains in top layer at crushing for Mohr-Coulomb yield criterion at load P = 71 kN

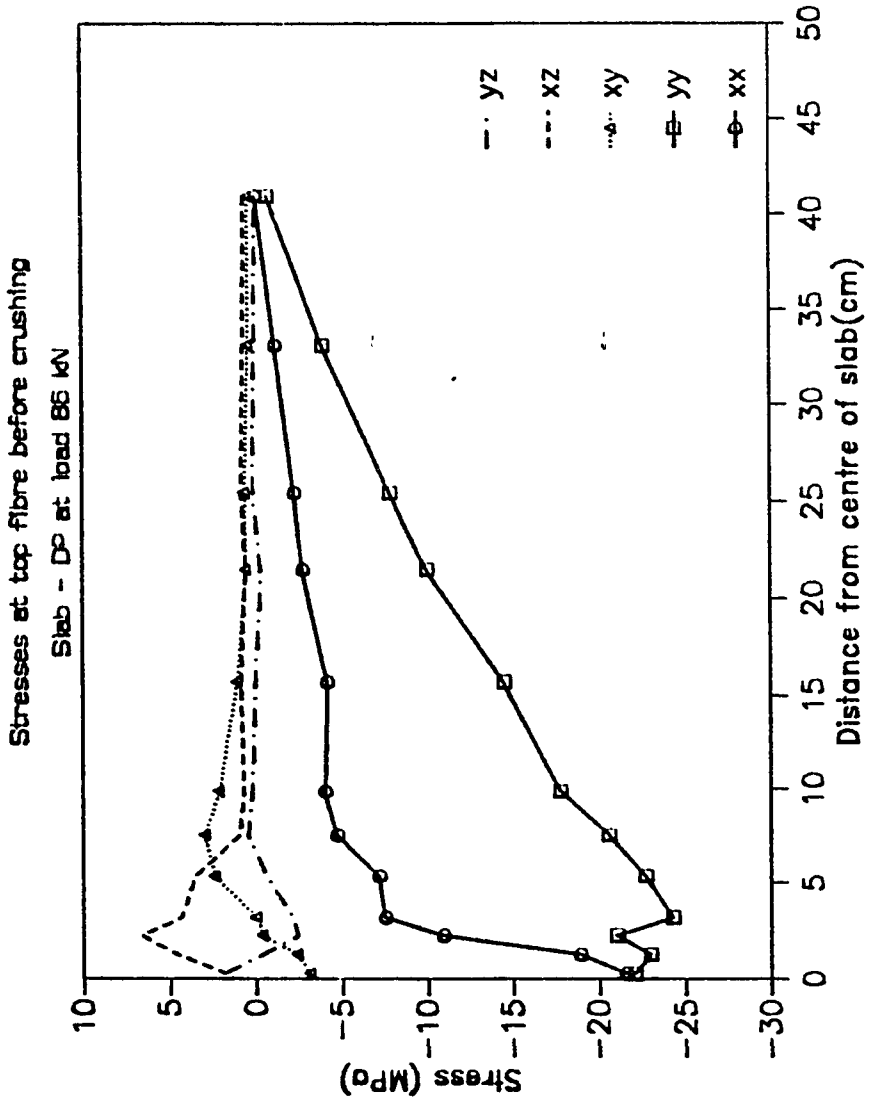

Fig. 6.47 Stresses in top layer before crushing for Drucker-Prager yield criterion at load P = 86 kN

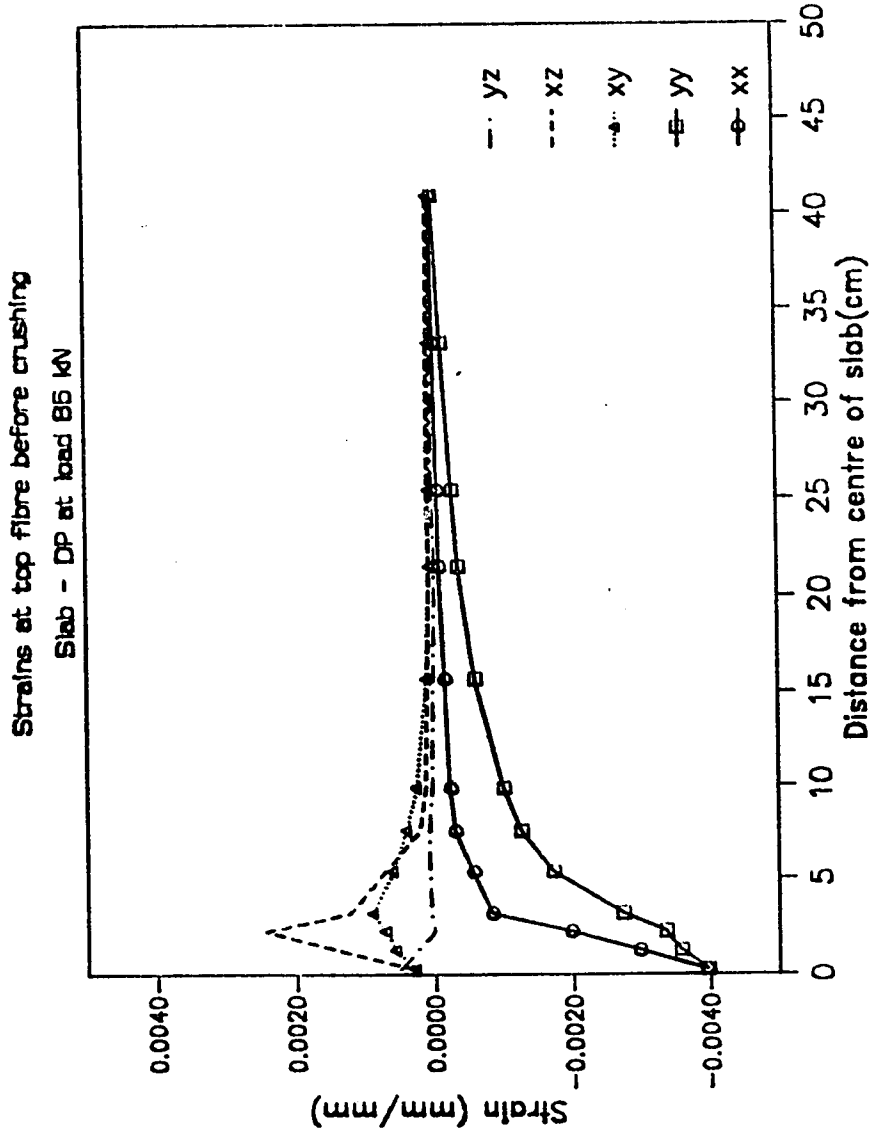

Fig. 6.48 Strains in top layer before crushing for Drucker-Prager yield criterion at load P = 86 kN

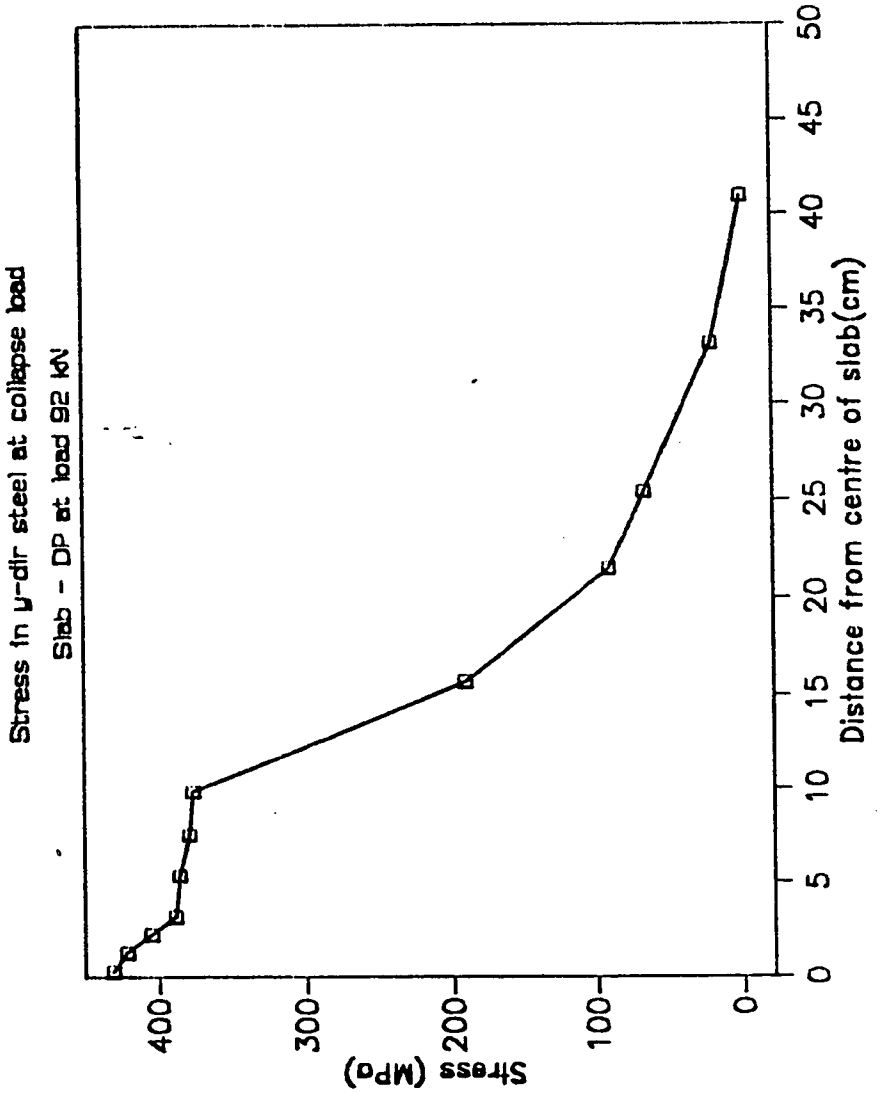

Fig. 6.49 Stresses in y-dir. steel for Drucker-Prager yield criterion at collapse load $P_u = 92kN$

Shown in Fig. 6.49 is the stress distribution in the y-direction reinforcement at the collapse load of 92 KN using the Drucker Prager criterion, with effects of strain hardening in the steel reflected in increased post-yielded steel stress directly under the load.

6.3 INFLUENCE OF STRUCTURAL PARAMETERS

In this section the main structural factors chosen are the reinforcement ratio, support restraint and the size of platen. Some researchers [14,40] highlighted the influence of these parameters on the failure load using perfectly plastic analytic models. This study is based on the progressive material degradation throughout the material of structure as load is increased [114,115].

6.3.1 Influence of Reinforcement Ratio and Patch Size

The influence of main tensile reinforcement on the metamorphosis in failure modes is presented in this section. In order to highlight flexure/shear interactive modes of failure, the slab is analyzed for two patch loads - one with a patch size of 50.8 mm. x 50.8 mm. and the other for a patch size of 101.6 mm. x 101.6 mm.

Shown in Fig. 6.50 is the spectrum of failure loads as obtained for values of total reinforcement in the two directions, ρ, ranging from 0.3% to 6.28%, for a patch load of size 50.8 mm. x 50.8 mm. Also superposed in Fig. 6.50 is the locus of ultimate capacity as obtained from ACI and BS 8110, and experimental values as reported in [6].

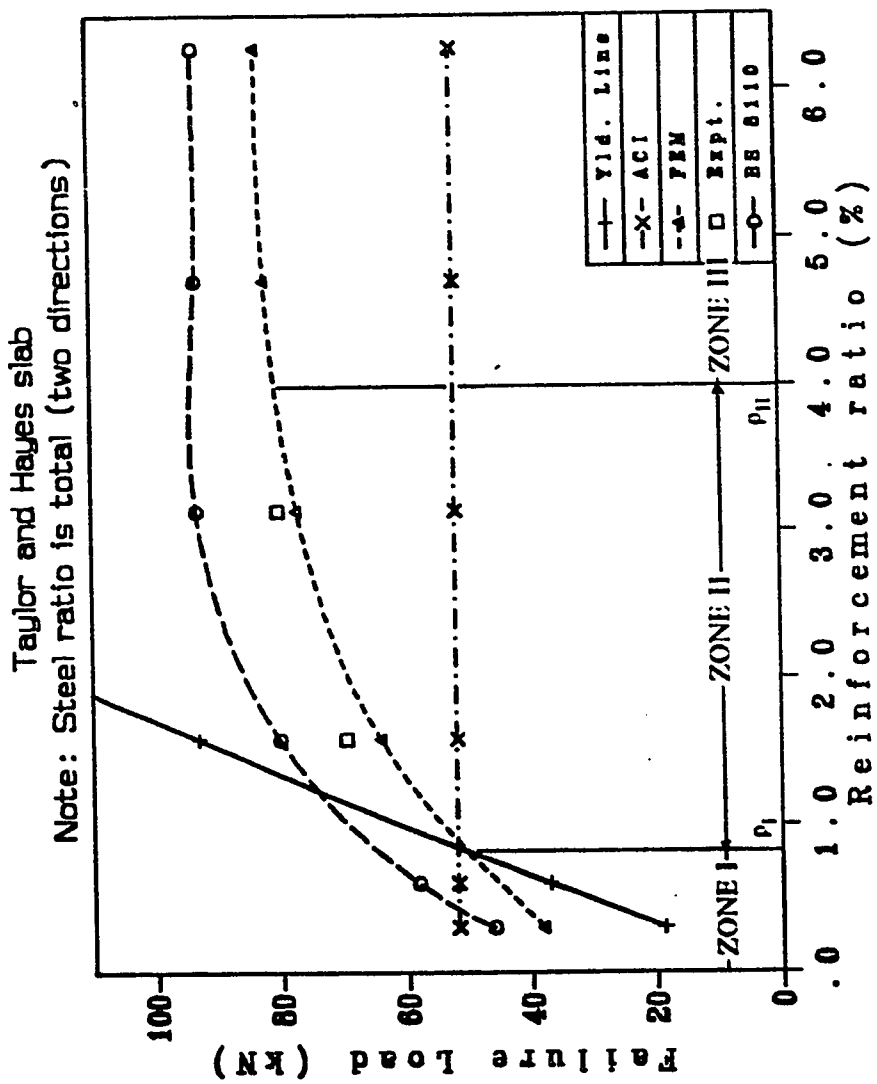

Fig. 6.50 Failure load vs. total reinforcement ratio ρ for patch size 50.8mm x 50.8mm

The behavior may be demarcated into three zones as given by

$0 \leq \rho \leq \rho_I$: Flexure Mode Dominated Failure (Zone I)

$\rho_I \leq \rho \leq \rho_{II}$: Combined Flexure-Shear Mode Failure (Zone II)

$\rho > \rho_{II}$: Shear Mode Failure (Zone III)

For $\rho < \rho_I$ (= 0.75%), the yield line analysis serves as a lower bound estimate to the capacity of the slab. The failure loads as obtained from the model in this zone are somewhat larger than the yield line loads - this is attributed to the load carrying capacity of plain concrete (due to its tensile strength) which is neglected in yield line analysis. Failure in this region (ρ = 0.3%) was marked by deep intrusion of radial cracks, yielding of tension reinforcement along diagonal lines and a measure of ductility.

In zone II (0.75% $\leq \rho \leq$ 4.0%), the failure load continues to be influenced by area of steel reinforcement, albeit at a decreasing rate. Here, the yield line analysis does not reflect the true failure mode of the slab, as ultimate conditions are marked by decreasing ductility and lowered level of yielding of steel reinforcement. Tension cracking damage intrusion is arrested at lower depths by increased steel percentage - leading to increase in ultimate load. In this zone the tangential cracking could grow outwards at increasing load and this in fact forms a trace of potential failure surface in the bottom of slab which for weakly reinforced slab could not be formed. This zone reflects characteristics of a combined flexure-shear failure mode.

In zone III defined by $\rho > 4.0\%$, the failure load as predicted by the model remains by large unaffected by increases in steel percentage and becomes asymptotic to what may be construed to be the true punching capacity. Tension cracking damage intrusion, prior to sudden collapse, is limited to mid-depth. Failure is characterized by gross brittle response, with little yielding of reinforcement. In all the cases considered, it is interesting to note the formation of radial tensile cracks first, followed subsequently by circumferential tensile cracking, although in the case of weakly reinforced slab circumferential cracking is highly limited. It is this two way cracking, accompanied by shear degradation in cracked zones, that forms the failure mechanism of the interactive shear/flexure failure modes in conjunction with crushing of concrete in compression zone.

6.3.2 Failure Modes and Their Mechanisms

Proceeding on a basis that the various failure modes of a reinforced concrete slab subjected to a patch load over a small central zone encompass a spectrum ranging from pure flexural failure (yield line solution) to that of pure shear failure (punching capacity), the primary variable influencing such a transition is the area of main or tensile reinforcement in the slab by virtue of crack arrest factor. This hypothesis may be supported with the following sequence of damage occurring phenomenon in slabs:

(i) at very low levels of main reinforcement (weakly reinforced slabs), initial damage to the slab occurs in the form of tension

cracking in the radial and circumferential directions and such cracks propagate upwards with a low arrest factor.

With increasing load, cracks propagate extensively only in the radial direction, preferentially along the diagonal lines. Also along the diagonal lines reinforcement yields significantly. At the incipience of failure, the cracks extend almost to the full depth and the diagonal cracks extend almost to the corners of the panel. Such a wide distribution of cracks forms a mechanism of global and pure flexural failure similar to that assumed in yield line analysis. This mode of failure is precipitated at low loads and before the formation of potential shear collapse surface, a characteristic of punching shear failure. Results for the slab reinforced with ρ = 0.3% are representative of this behavior, with deep intrusions of tension cracking damage (Fig. 6.51) prior to eventual collapse. The collapse load recorded was only 46% of the full punching shear capacity of the panel, with the latter being defined to be attained for the case of a highly reinforced slab.

Failure of weakly reinforced slabs is typified by a measure of ductility (due to plastic flow of reinforcement) and wide cracks - and can be termed as a soft failure since energy is released gradually. The failure load of such slabs would be close to that given by a yield line analysis.

(ii) at medium levels of main reinforcement, initial damage to the slab again occurs in the form of tension cracking in the radial direc-

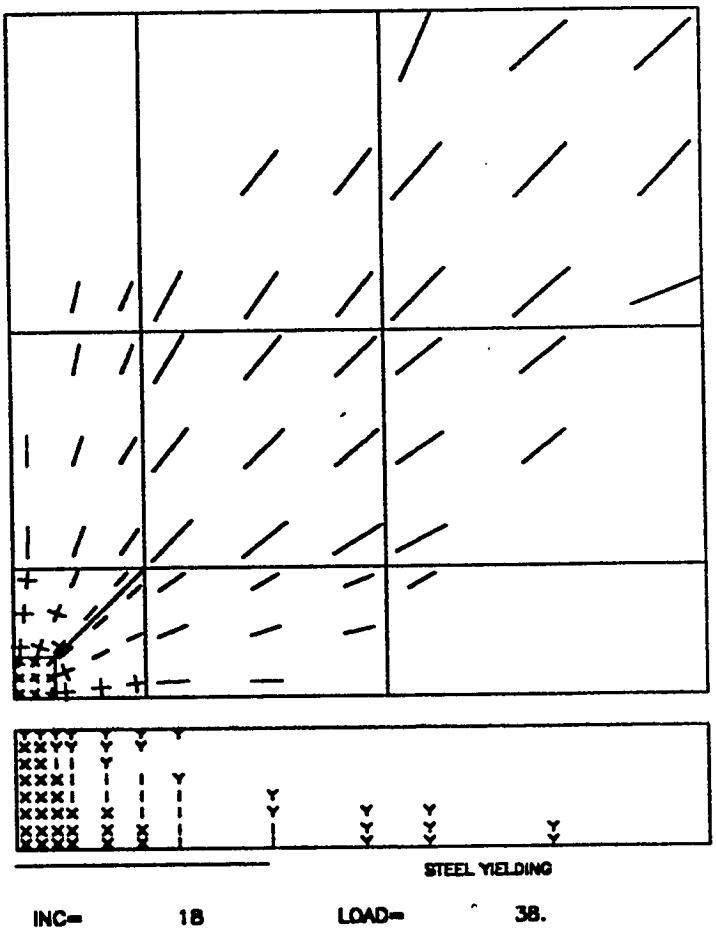

Fig. 6.51 Cracking in bottom of slab and section profile for $\rho = 0.3\%$

tion, but the crack arrest factor is higher due to increased reinforcement. With increasing load, cracks are also formed in the circumferential direction with accompanying degradation in shear transfer mechanism. The damage zone at incipient failure is dominated by two way tension cracking extending to a certain depth, leading to separation along some portion of the potential punching shear collapse surface. By virtue of this separation, failure occurs at a load lower than the true punching or shear capacity of the panel. Results for the slab reinforced with ρ = 3.14% (Fig. 6.37), are representative of this mode of failure. In this case a greater portion of the potential shear collapse surface remains in contact and undegraded in shear transfer. The intact segment of the potential collapse surface is subjected to high shear and compressive stresses, leading to plastic flow.

The plastic flow leads to increased strains in the concrete, which then begins to crush under an appropriate crushing criterion (in the neighborhood of the load). The final event in the collapse mechanism is a sudden displacement of the shear cone relative to the rest of the slab - and it is this phenomenon which has been misconstrued to represent a punching or shear failure. This in reality is a combined flexure/shear failure, with significant damage components from both modes.

Failure of such slabs is typified by decreased ductility - since there is decreased yielding or flow of reinforcement. The failure can be termed as semi-soft, because the displacement of the shear cone at the ultimate event is accompanied by a sudden

release of energy. The failure load of such slabs cannot be predicted by either yield line analysis nor by punching shear analysis.

(iii) at high levels of main reinforcement, initial damage is essentially restricted to minimal tension cracking intrusion, with cracks being arrested prior to any significant growth, yet the circumferential cracking grows outwards at increasing loads. The potential collapse surface is mostly intact by virtue of compressive stresses acting across it. Further damage to the slab can occur only subsequent to plastic flow of the large, undamaged concrete region culminating in crushing of concrete. The final event in this collapse mode is also a sudden displacement of the shear cone relative to the rest of the slab.

Damage zone for panel reinforced with ρ = 6.28% (Fig. 6.52) is shown to be representative of this mode of failure, and the collapse load of P_u = 83.0 kN is taken as a measure of the true punching capacity of the slab and this value is approached asymptotically at ρ = 4.00% (Fig. 6.50). This can be explained as when the cracks are arrested to a certain minimum depth the failure is attributed solely to the mechanism of plastic flow of concrete in compression-shear.

Failure of such slabs is explosive and marked by minimum ductility - since although concrete is in a state of plastic flow, the tension reinforcement is mostly in the elastic region. Thus the degree of plasticity of a composite structure such as a RC

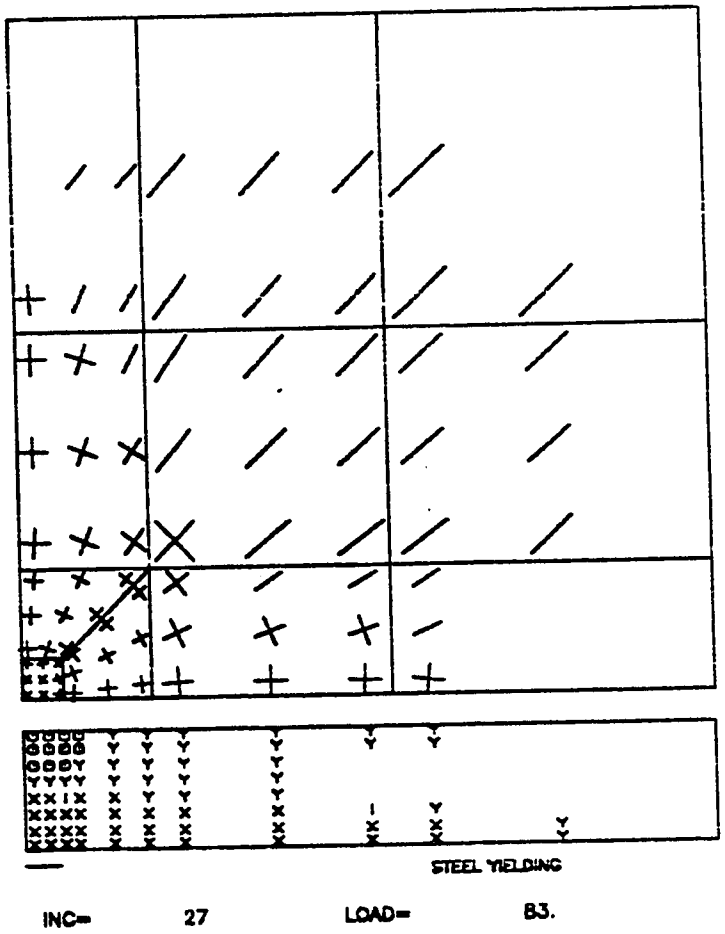

Fig. 6.52 Cracking in bottom of slab and section profile for $\rho = 6.28\%$

slab must be viewed with reference to degree of flow of each material component. This reasoning also explains how punching models based on plasticity formulation [15,16] can predict failure loads of a seemingly overall brittle phenomenon - queried as an apparent dichotomy by certain researchers. The failure load of such slabs can be approximately predicted by punching shear plasticity models [3], in which the basic assumption is an intact potential collapse surface prior to failure and which is realized only in the presence of high main reinforcement. Such failures represent a pure shear or a true punch failure of RC slabs.

Fig. 6.53 shows the failure load-total reinforcement variation for a patch load of size 101.6 mm. x 101.6 mm. One notes that the zones demarcating flexure and shear modes have shifted. This is due to the influence of patch size in transforming the behavior from a localized failure to a relatively global failure. As patch size increases the full punching mechanism corresponding to asymptotic value of failure load requires greater energy to mobilize a larger portion in compression shear, thus allowing the radial cracks to propagate leading to a nearly flexure failure. Also it can be presumed from Fig. 6.53 that, with the increase of patch size the departure of the locus of failure load from that of yield line is minimized.

For weakly reinforced slabs, failure is precipitated in the model by overall loss of structural stability due to intrusion of radial cracking as evidenced by ill-conditioning of the structural stiffness matrix, leading to divergence.

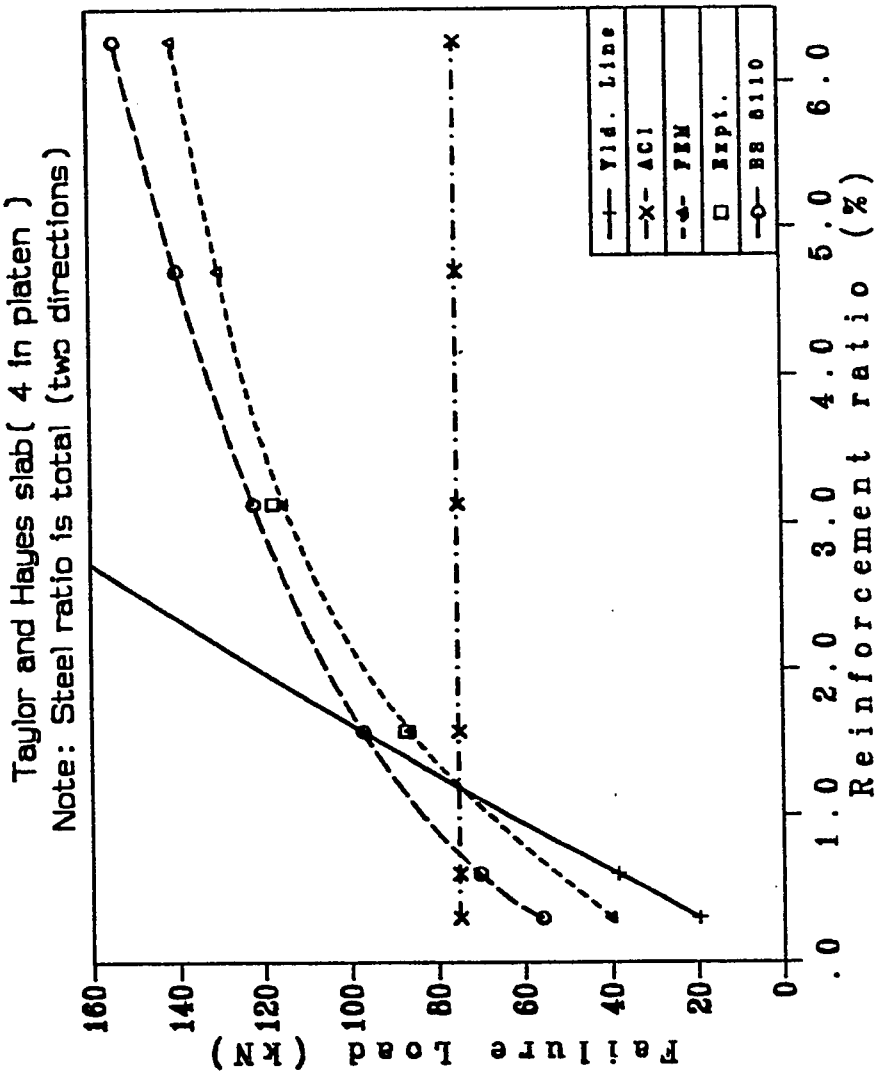

Fig. 6.53 Failure load vs. total reinforcement ratio ρ for patch size 101.6mm x 101.6mm

For moderately to over-reinforced slabs, numerical failure is characterized by crushing of Gauss points, initiated at location of interface between loaded element and the elements adjacent to it. This crushing has a dominant effect, leading to rapid crushing of adjacent Gauss points and culminating in eventual divergence.

The two modes of numerical failure correspond closely to the experimentally observed modes of failures, where weakly reinforced slabs fail 'softly' due to gradual intrusion of flexural cracks where as moderately to over-reinforced slabs fail suddenly, under limited intrusion of cracks, due to crushing of concrete initiated in the vicinity of loaded area.

6.3.3 Influence of Support Restraint

In this section the beneficial effect of edge restraint on punching capacity is highlighted. The effect of support restraint on enhancement of collapse load of the panel was modelled by laterally restraining the four edges of the slab which was loaded with central 50.8 mm. x 50.8 mm. patch ($u = v = 0$). Fig. 6.54 shows the spectrum of failure load of pairs of slabs, one restrained with the other of the pair being unrestrained, with experimental loads reported in [29]. A restrained slab with a given percentage of steel behaves as an unrestrained slab of increased ρ. Moreover the beneficial effect of edge restraint on the collapse load tapers off with increase in main reinforcement percentage, as the two effects basically act in the same way to enhance the capacity, leading to redundancy. This finding corroborates the experimental evi-

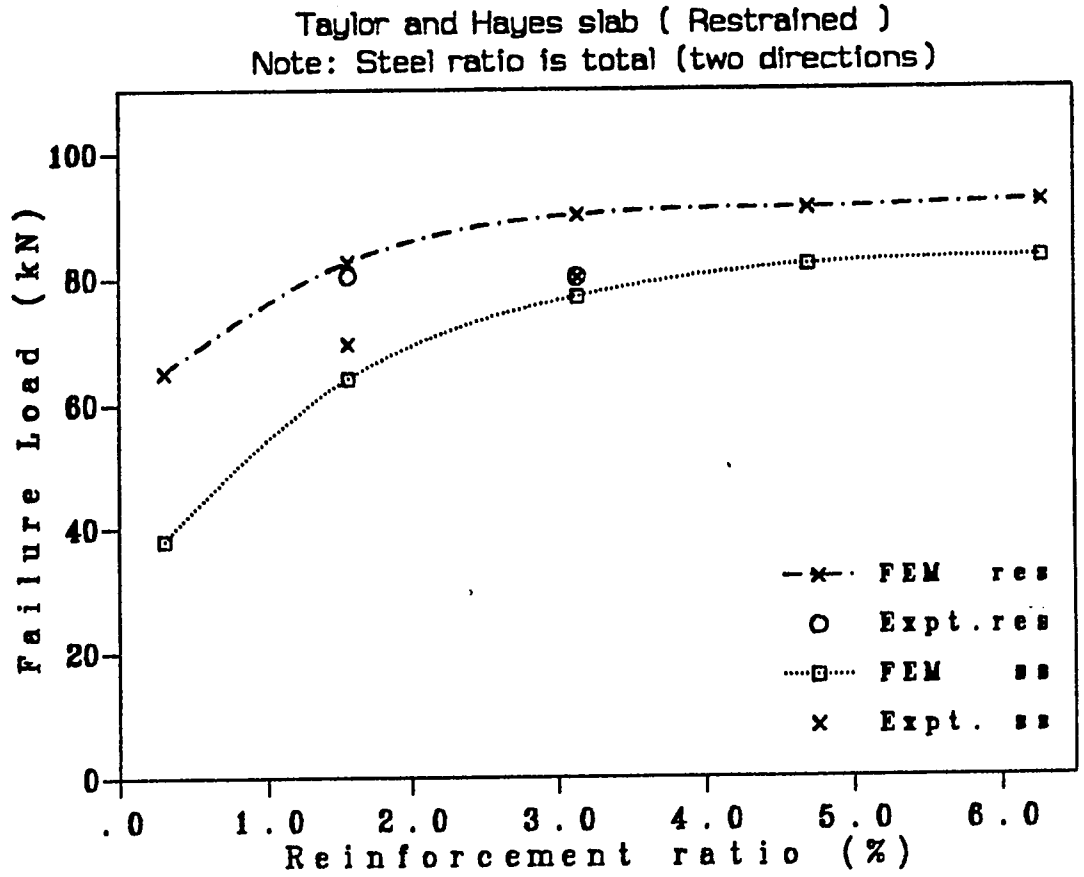

Fig. 6.54 Failure load vs. total reinforcement ratio ρ for restrained slab and unrestrained slab (patch size 50.8mm x 50.8mm)

dence of several research groups [4,29,35]. The weakly reinforced slab when restrained exhibited significant reduction in radial cracking, undergoing a transformation in the behavior from pure flexural mode to a flexure shear mode. Thus the overall effect of support restraint is to reduce the zone of cracking damage (by virtue of in-plane compressive forces) and allow a greater percentage of the true punching capacity to be mobilized. Thus support constraint enhances the punching capacity, yet this beneficial effect tapers off with increasing steel ratio.

6.4 INFLUENCE OF FINITE ELEMENT PARAMETERS

A few finite element parameters such as the number of elements (mesh size), number of layers through thickness and type of elements have been studied in order to ascertain the validity of the test results presented.

6.4.1 Number of Elements and Layers

In order to study the influence of element size on the solution, three cases were chosen; (i) 6 elements, (ii) 11 elements and (iii) 18 elements while using the number of concrete layers equal to 8. In order to investigate the layering effect on the response, three cases were considered; (i) 4 layers, (ii) 8 layers and (iii) 12 layers with the number of elements being 11 in each case.

Fig. 6.55 shows that the collapse load is not as sensitive to the

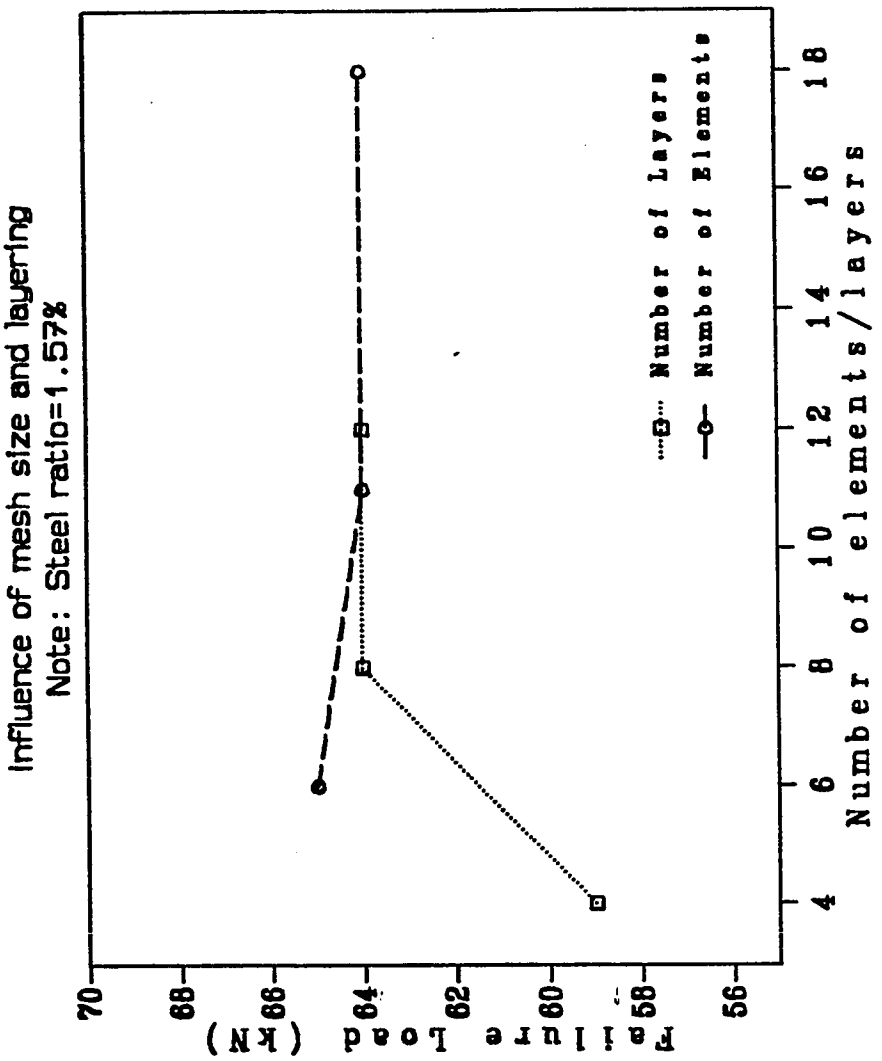

Fig. 6.55 Failure load vs. variation in discretization

mesh size as it is to the number of layers through thickness. Figs. 6.56 and 6.57 illustrate that with the variation of mesh size and number of layers the stiffness of the response remains similar. Thus the layered model with five degrees of freedom and quadratic representation is not as sensitive to the refinement in discretization as has been observed for the case of with non-layered models.

6.4.2 Type of Element

In this work three elements have been incorporated; (i) 9-node Lagrangian, (ii) 8-node Serendipity and (iii) Heterosis. Fig. 6.58 shows that 9-node Lagrangian, Heterosis and 8-node Serendipity elements yielded similar solution with 8-node Serendipity element reflecting a more ductile behavior. This may be ascribed to using selective integration rule with 8-node Serendipity element rather than the reduced integration rule. The results proved that 9-node Lagrangian element is an optimal element and this conclusion is corroborated by other researchers [107,108].

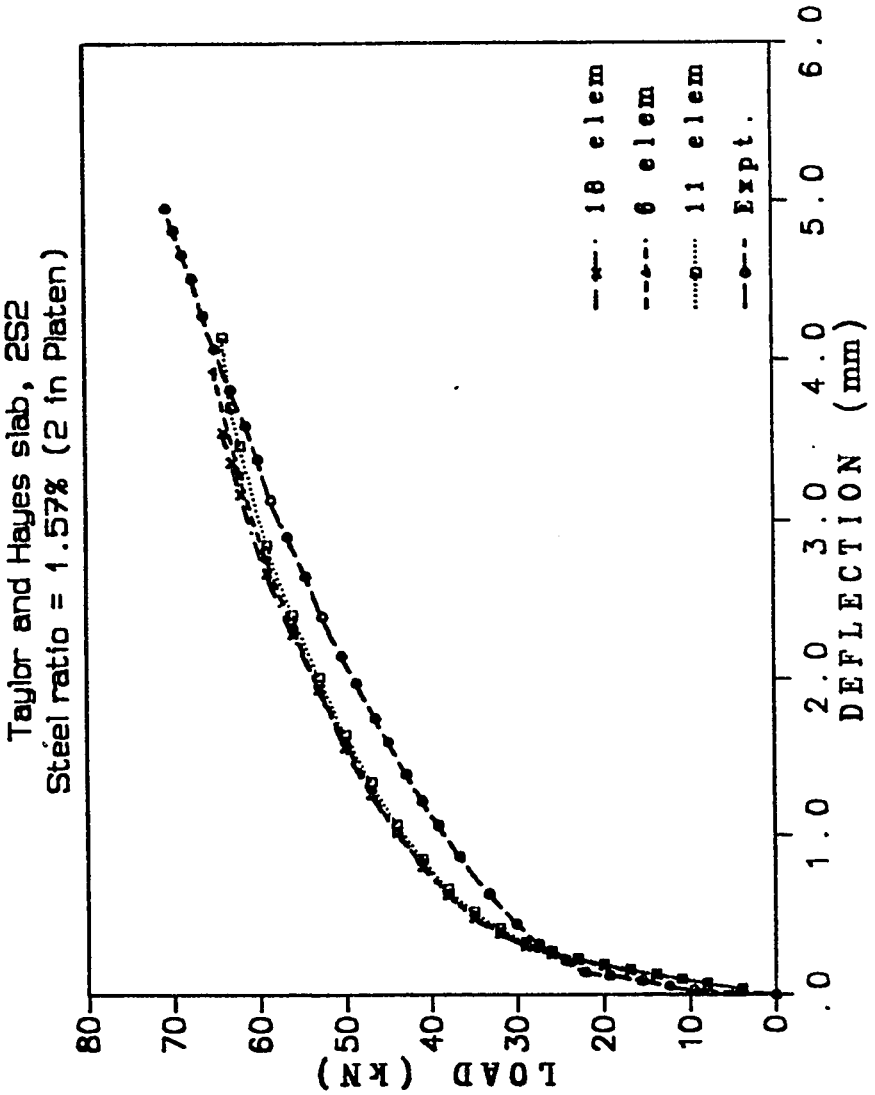

Fig. 6.56 Load deflection curves showing the effect of mesh size

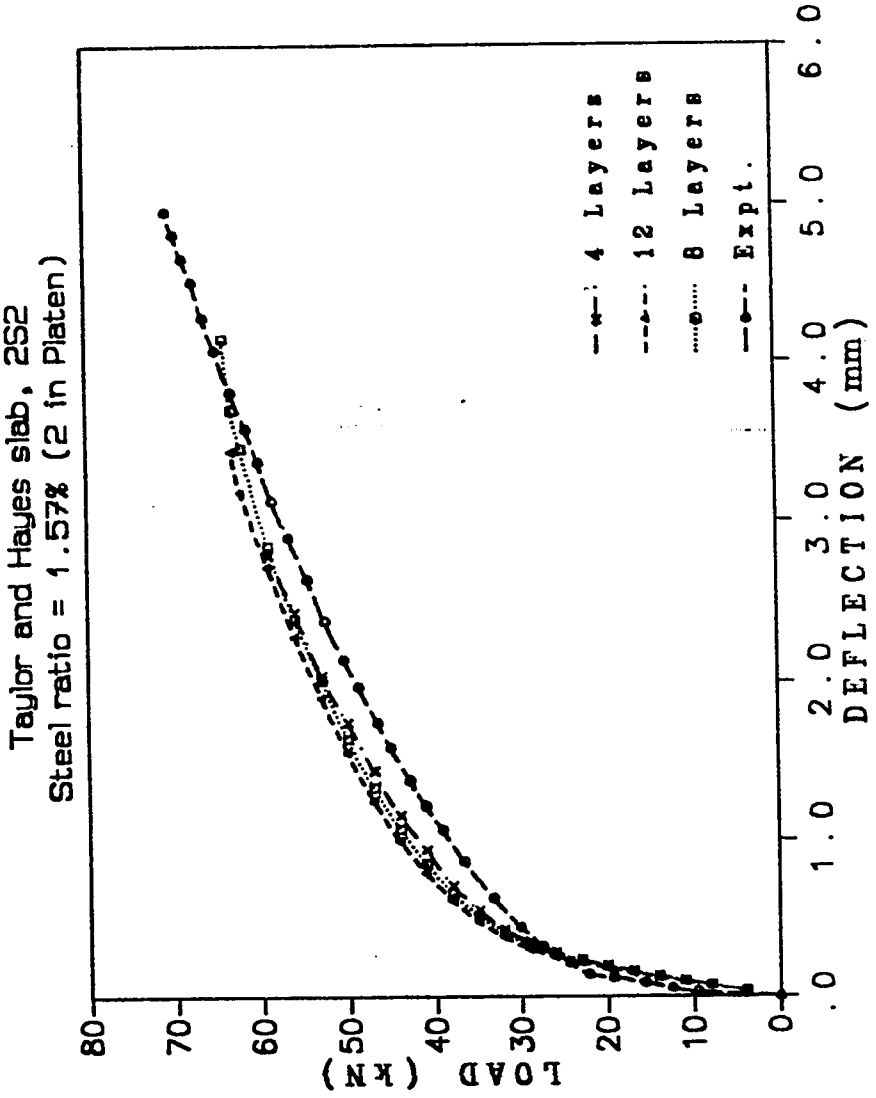

Fig. 6.57 Load deflection curves showing the effect of layering

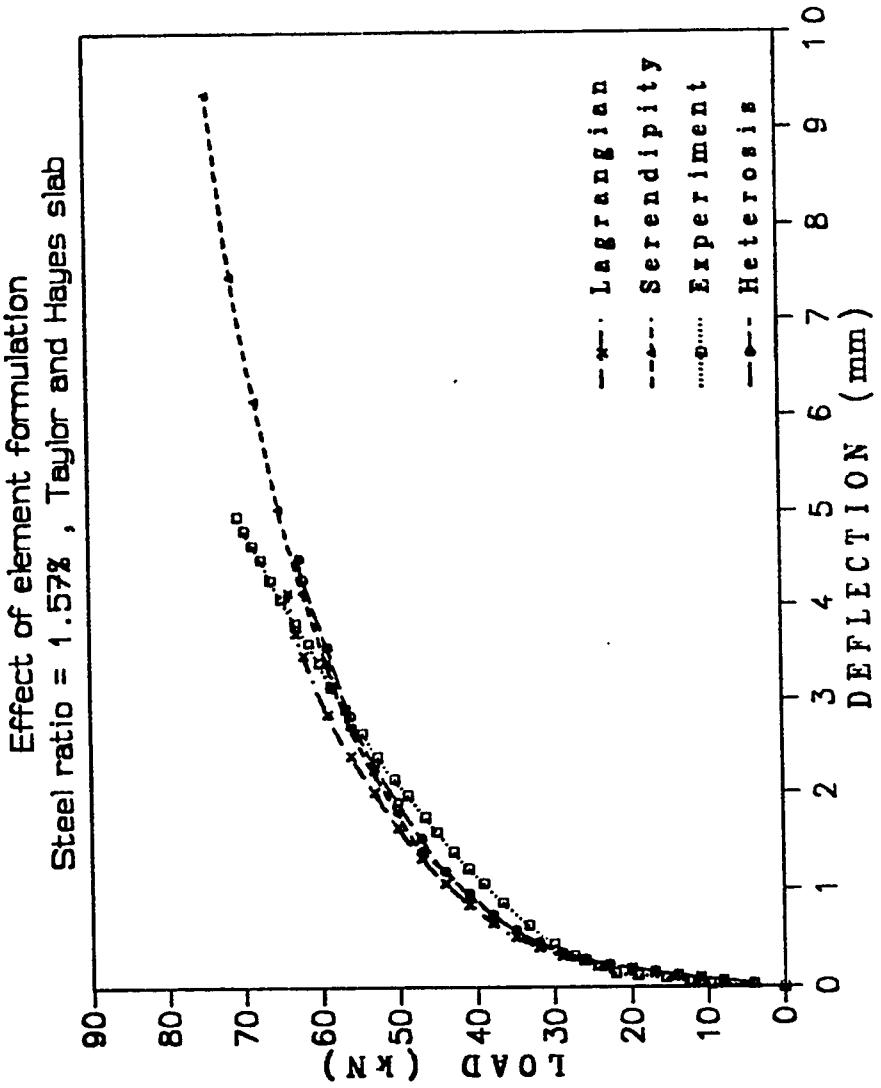

Fig. 6.58 Load deflection curves showing the effect of element type

Chapter 7

CONCLUSIONS

7.1 CONCLUSIONS

The main conclusions drawn from this work are as follows:

1. Computational model developed simulates flexural/shear response of R/C slabs reasonably accurately.
2. The stiffness of the structure is sensitive to tension stiffening parameter α, and more so for cases of under-reinforced slabs.
3. The degree of shear degradation does not affect stiffness of the structure appreciably, but controls the collapse load magnitude.
4. The yield criterion must possess the characteristic of being able to be expressed in explicit form in order to be readily implemented in isotropic hardening model. This is especially important in view of increasing number of sophisticated yield criteria being presented to model concrete in various stages of stressed conditions, but not lending themselves to an explicit formulation.
5. For under-reinforced slabs, the type of yield criterion does not play as important role as for over-reinforced slabs, where greater zones of concrete are subjected to elasto-plastic yielding at higher loads. However, for moderately and over-reinforced slabs, a judicious choice of yield criterion reflecting sensitivity to

expected mode of failure is vital e.g., Mohr-Coulomb for shear related failures.

6. Using elastic perfectly plastic models result in an increased stiffness of the structure, together with an increase in collapse load.

7. The crushing criterion in terms of strains basically affects the magnitude of the collapse load, with virtually no influence on stiffness of the structure. Results have shown that in total absence of a crushing failure surface, the collapse load approaches that as predicted by the yield line solution. An appropriate crushing criterion must incorporate the influence of the first strain invariant and use was made of Drucker-Prager strain criterion.

8. The definition of true punching capacity under central patch loads of small size is enunciated as the phenomenon dominated by plastic yielding of concrete with minimal tension cracking intrusion, and is shown to be approached asymptotically with increasing percentage of main steel reinforcement.

9. On the other end of the spectrum, at very low levels of main reinforcement, failure is seen to be dominated by extensive diagonal tension cracking and reinforcement yielding and constitutes the classical flexural failure. For low to medium levels of reinforcement, the failure modes exhibit damage components defined as a flexure-shear interactive failure.

10. The increase in the patch size reflects in transforming the failure behavior from a localized-punching mode to a global-flexure mode.

11. Effect of support restraint, modelled by constraining mid-plane displacements u, v to be zero, is seen to stiffen the structure,

making a restrained slab with low reinforcement behave as an equivalent slab with higher reinforcement. This effect is noted to taper off with increasing level of reinforcement, a behavioral pattern noted in the experiments of Taylor and Hayes [29].

12. The proposed yield criterion predicted collapse load reasonably accurately. The overall predicted response was somewhat stiffer and this can be improved by modifying the model parameters by fitting other concrete test data.

7.2 RECOMMENDATIONS

Based on the results discussed the following suggestions are given :

1. The philosophy of using minimal main reinforcement in deck slabs [2] should be reconsidered, especially in areas where repeated loads of high magnitude are known to occur. Experience has shown that under heavy service loads, the probable mode of failure in a girder-slab or box girder deck system is the localized "pot hole" type of failure [1]. In the absence of shear reinforcement, sufficient amount of main reinforcement for a given slab thickness should be provided in order to minimize intrusion of two way cracking damage and preclude premature localized failure.

2. The application of more sophisticated models for isotropic hardening can be handled without rendering them to explicit form in the following suggested way:

   If the model is given in the form as

   $F(I_1, J_2, 0, \sigma_o) = \sigma_o$

where it may be noted that σ_o lies on both sides of the equation. If the increment size is reasonably small then σ_o of left side can be assumed to have value of the previous converged increment at that Gauss point. For very small size increments, the difference between effective stresses of subsequent increments is also very small. The extra computation cost for explicit expressions can be balanced by the fine incrementation.

7.3 FUTURE SCOPE OF WORK

The existing model can be further extended/modified to address the following problems of practical significance:

1. Modelling of damaged R/C slab and it's strengthening and repair
2. Modelling of punching shear in prestressed concrete bridge decks
3. Modelling of bottom girder restraint in girder supported bridge decks
4. Modelling of thermal effects on thick plain and R/C slabs

APPENDIX

A.1 YIELD LINE ANALYSIS FOR PATCH LOADING (Figs. 6.50 & 6.53)

Consider a square plate of size 'a' loaded by uniformly distributed load of intensity 'p' over a square patch of size 'b' (Figure A.1)

The effect of patch load is considered by an equivalent moment.

The equivalent moment = $\frac{1}{2}.p.b.\frac{b}{2}.\left|\frac{a}{2}-\frac{2}{3}\frac{b}{2}\right|$

External work due to equivalent moment = $\frac{pb^2}{4}\left(\frac{a}{2}-\frac{b}{3}\right).\frac{2\Delta}{a}$

Internal work due to resisting moment = $2.\frac{m_p}{\sqrt{2}}.\frac{a}{\sqrt{2}}.\frac{\Delta}{a/2}$

$= 2\ m_p\Delta$

Equating external and internal work results in:

$$m_p = \frac{pb^2}{4a}\left(\frac{a}{2}-\frac{b}{3}\right) \qquad (A.1)$$

If P is the total load then,

$$m_p = \frac{P}{4a}\left(\frac{a}{2}-\frac{b}{3}\right) \qquad (A.2)$$

And this equation can be rewritten as:

$$P = \frac{m_p.24a}{3a-2b} \qquad (A.3)$$

where m_p is moment per unit length resisted by reinforcement which is

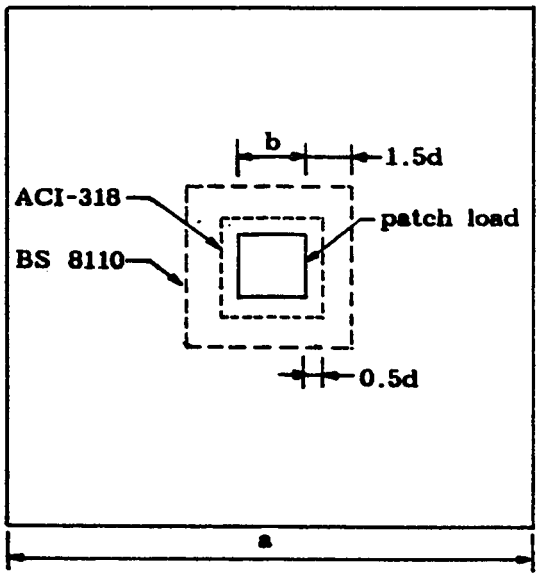

Fig. A.1 Loaded area and control perimeter

given as:

$$m_p = \rho f_y (1 - \rho m/2).12.d^2 \qquad (A.4)$$

where

ρ = A_s/bd (steel ratio in one direction)

f_y = yield strength of reinforcement

$m = f_y/0.85f'_c$

d = effective depth of slab.

A.2 ACI FORMULA FOR PUNCHING COLLAPSE LOAD (Figs. 6.50 & 6.53)

In ACI-318 the control perimeter is taken at a distance of 0.5d from the loaded area (Figure A.1) and the limiting shear stress depends only on the concrete strength. The punching collapse load is given as:

$$P_k = 4\sqrt{f'_c}4(b+d)d \qquad (f'_c \text{ in psi}) \qquad (A.5)$$

A.3 BS 8110 FORMULA FOR PUNCHING COLLAPSE LOAD (Figs. 6.50 & 6.53)

In BS 8110 the control perimeter is assumed at a distance of 1.5d from the loaded area (Figure A.1) and the limiting shear stress not only depends on concrete but also on the reinforcement ratio.

$$P_{ck} = v_{ck} ud \leq 1.2\sqrt{f_{cu}} u_o d \qquad (A.6)$$

where

$v_{ck} = 0.79(100\rho)^{1/3}(f_{cu}/25)^{1/3}(400/d)^{1/4}$

$u = 4(b+3d)$,

$u_o = 4b$

f_{cu} = cube strength in N/sq mm

d = effective depth in mm

A.4 INSTRUCTIONS FOR PREPARING INPUT DATA FOR PROGRAM FATIMA

CARD SET 1 - Title Card (80A1) - one card

Cols. 1-80 Title of the problem, limited to 80 alphanumeric characters

CARD SET 2 - Control Data Card (16I5) - two cards

First Card

Cols. 1- 5 NPOIN Total number of nodal points

Cols. 6-10 NELEM Total number of elements

Cols.11-15 NVFIX Total number of points where one or more degrees of freedoms are prescribed

Cols.16-20 NNODE Number of nodes per element

8- for 8 node Serendipity

9- for 9 node Lagrangian and Heterosis

Cols.21-25 NMATS Total number of different materials

Cols.26-30 NGAUS Number of Gauss points per element
(Bending and Membrane)

Cols.31-35 NGAUZ Number of Gauss points per element (Shear)
NGAUS=3, NGAUZ=3 - Normal integration rule
NGAUS=3, NGAUZ=2 - Selective integration rule
NGAUS=2, NGAUZ=2 - Reduced integration rule

Cols.36-40 NTYPE Type of element:
= 0 - 8 node Serendipity
= 1 - 9 node Lagrangian
= 2 - Heterosis

Cols.41-45 NALGO Nonlinear solution algorithm
= 1 - Initial stiffness method
= 2 - Tangential stiffness method
= 3 - Stiffness matrix is recalculated
in the first iteration of each increment
= 4 - Stiffness matrix is recalculated
in the second iteration of each increment

Cols.46-50 NINCS Total number of load increments

Cols.51-55 NLAYR Total number of layer patterns

Cols.56-60 NCRIT Indicator for concrete yielding criterion
= 1 - Von Mises
= 2 - Tresca

= 3 - Mohr Coulomb

= 4 - Drucker Prager

= 5 - Proposed Yield Criterion

Cols.61-65 NHARD Indicator for hardening of concrete

= 0 - Perfectly Plastic

= 1 - Strain Hardening

Cols.66-70 NREST Restart facility parameter

= 0 - To start the analysis

= 1 - To restart the analysis from the last previously converged load increment

Cols.71-75 NNORM Convergence criterion parameter

= 0 - Displacement norm

= 1 - Residual Force norm

= 2 - Displacements and notations norm

Cols.76-80 NPLOT Indicator for plotting

= 0 - No plotting

= 1 - Plotting of cracking pattern,
material state in sectional view,
and P-Δ curve,
stress and strain distributions etc.

Second Card

Cols. 1- 5 NSDEG Shear degradation parameter

= 0 - Full degradation

= 1 - Normal degradation

= 2 - No degradation

Cols. 6-10 NDOWL Dowel action parameter

= 0 - No dowel action

= 1 - Dowel action included

CARD SET 3 - Gravity Loading Card (4F10.5) - one card

Cols. 1-10 GRAVI(1) Gravitational acceleration in x-direction

Cols.11-20 GRAVI(2) Gravitational acceleration in y-direction

Cols.21-30 GRAVI(3) Gravitational acceleration in z-direction

Cols.31-40 ANVEL Angular velocity (w.r.t. z-axis)

CARD SET 4 - Element Cards (16I5) - one card for each element

Cols. 1- 5 NUMEL Element Number

Cols. 6-10 MATNO(NUMEL) Element layer pattern number

Cols.11-15 LNODS(NUMEL,1) Element node number

: anti-clockwise

: :

: :

: :

: :

Cols. 51-55 LNODS(NUMEL,9) :

CARD SET 5 - Nodal Coordinates Cards (I5,5F10.5)

one card for each node whose coordinates must be

input - finishing with last node.

(Coordinates of the central 9th node and also mid-side nodes whose coordinates are obtained by linear interpolation of the corresponding corner nodes need not be input)

Cols. 1- 5 IPOIN Node number

Cols. 6-15 COORD(IPOIN,1) Mid x-coordinate

Cols.16-25 COORD(IPOIN,2) Mid y-coordinate

Cols.26-35 COORD(IPOIN,3) Mid z-coordinate

Cols.36-45 COORD(IPOIN,4) Top pressure

Cols.46-55 COORD(IPOIN,5) Bottom pressure

CARD SET 6 - Thickness Card (5X,F15.2) one card

Cols. 6-20 THICK Uniform Plate Thickness

CARD SET 7 - Restrained node Cards (1X,I5,5X,I5,5F10.6)
one card for each restrained node

Cols. 2- 5 NOFIX(IVFIX) Restrained node number

Cols.11-15 IFPRE Condition of the degree of freedom:

0 - Free

1 - Restrained

Position 11 - u displacement (x-dir)

Position 12 - v displacement (y-dir)

Position 13 - w displacement (z-dir)

Position 14 - β_1 rotation (about y-axis)

Position 15 - β_2 rotation (about x-axis)

Cols.16-25 PRESC(IVFIX,1) - Prescribed values of nodal
: variables
: :
: :

Cols.56-65 PRESC(IVFIX,5)

CARD SET 8 - Concrete and Steel discretization pattern

Two cards for each layering pattern

First Card (16I5)

Cols. 1- 5 NCLAY(ILAYR) - Number of concrete layers

Cols. 6-10 NSLAY(ILAYR) - Number of steel layers

(ILAYR- Layer pattern identification number)

Second Card (16I5)

Cols. 1- 5 MACON(ILAYR,ICONL)

: Material identification number for each concrete
: layer from bottom to top
: :
: :
: :
: :

: MASTE(ILAYR,ISTEL)

: Material identification number for each steel layer

: layer from bottom to top

: :

: :

CARD SET 9 - Material Cards - Three cards for each different material

First Card (I5)

Cols. 1- 5 NUMAT Material identification number

Second Card (7F10.5) For Concrete Material Only

Cols. 1-10 PROPS(NUMAT,1) E_c Young's Modulus

Cols.11-20 PROPS(NUMAT,2) ν Poisson's ratio

Cols.21-30 PROPS(NUMAT,3) t_ζ Layer thickness expressed in the normalized coordinates

Cols.31-40 PROPS(NUMAT,4) φ Angle of internal friction

Cols.41-50 PROPS(NUMAT,5) f'_t Concrete ultimate tensile strength

Cols.51-60 PROPS(NUMAT,6) f'_c Concrete ultimate compressive strength

Cols.61-70 PROPS(NUMAT,7) ε_u Concrete ultimate compressive strain

Third Card (7F10.5) For Concrete Material Only

Cols. 1-10 PROPS(NUMAT,8) ε_m Tension stiffening parameter

Cols.11-20 PROPS(NUMAT,2) α Tension stiffening parameter

Second Card (7F10.5) For Steel Material Only

Cols. 1-10 PROPS(NUMAT,1) E_s Young's Modulus

Cols.11-20 PROPS(NUMAT,2) E'_s Elastoplastic Young's Modulus

Cols.21-30 PROPS(NUMAT,3) t_ζ Layer thickness expressed in the normalized coordinates

Cols.31-40 PROPS(NUMAT,4) ρ Material density

Cols.41-50 PROPS(NUMAT,5) f_y Steel yield stress

Cols.51-60 PROPS(NUMAT,6) ζ_s Layer position

Cols.61-70 PROPS(NUMAT,7) θ Angle between the reinforcement and the x-axis(measured anti-clockwise)

Third Card (7F10.5) For Steel Material Only - Blank Card

CARD SET 10 - At least one Card for each element

First Card (3I5)

Cols. 1- 5 NPRES Distributed load indicator

=0 no distributed loads on this element

=1 distributed loads to be input

Cols. 6-10 NUCLO Number of concentrated loads on this element (=0, no concentrated loads)

Cols.11-15 NBODY Body load indicator (gravity and/or centrifugal)
=0 no body loads on this element
=1 body loads to be input

Second Card (I5,F5.1,2F15.5) Only exists if NPRES=1

Cols. 1- 5 KPRES Distributed load type indicator
=0 Uniformly distributed load
=1 Hydrostatic load
=2 Load specified at nodes

Cols. 6-10 CFACE = +1.0 Pressure is on top surface
= -1.0 Pressure is on bottom surface

Cols.11-25 PREVA Uniformly distributed load if KPRES = 0
Hydrostatic load --------- if KPRES = 1

Cols.26-40 SURFA z coordinate of zero pressure if KPRES = 1

Third Set of Cards (2I5,2F10.5) Only exists if NUCLO > 0
NUCLO number of cards

Cols. 1- 5 LPOIN Local node number at which the load is applied

Cols. 6-10 LDOFN Nodal variable number corresponding to the

applied load

=1 x displacement

=2 y displacement

=3 z displacement

=4 β_1 rotation

=5 β_2 rotation

Cols.11-20 CARGA Concentrated load value

CARD SET 11 - Load increment control cards (2F10.5,315)

NINCS cards

Cols. 1-10 FACTO Applied load factor for the current increment

Cols.11-20 TOLER Convergence tolerance factor

Cols.21-25 MITER Maximum number of iterations allowed

Cols.26-30 NOUTP(1) Controls output parameter of the unconverged results after the first iteration

=1 print displacement only

=2 print displacement and reactions

=3 print displacement, reactions and stresses

Cols.31-35 NOUTP(2) Controls output parameter of the converged results

=1 print displacement only

=2 print displacement and nodal reactions

=3 print displacement, reactions and stresses

A.5 SAMPLE INPUT DATA AND LINE PRINTER OUTPUT FOR PROGRAM FATIMA

In this appendix the input data and line printer output are provided for the slab tested by Taylor and Hayes 2S2 [29] discussed in Chapter 5 (Figure 5.1)

Input data:

```
   TAYLOR AND HAYES 2 IN SLAB UNRESTRAINED WITH STEEL=1.57%
59   11   28    9    4    3    2    2    4    6    1    5    1    0
 2    1    1    1
     0.0       0.0       0.0       0.0
 1    1    1   10   15   16   17   11    3    2   49
 2    1   15   18   20   21   22   19   17   16   53
 3    1   20   27   31   32   33   28   22   21   54
 4    1   31   38   42   43   44   39   33   32   57
 5    1    3   11   17   19   22   12    5    4   50
 6    1    5   12   22   23   24   13    7    6   51
 7    1   22   28   33   34   35   29   24   23   55
 8    1   33   39   44   45   46   40   35   34   58
 9    1    7   13   24   25   26   14    9    8   52
10    1   24   29   35   36   37   30   26   25   56
11    1   35   40   46   47   48   41   37   36   59
 1        0.0       0.0
 3        0.0      2.54
 5        0.0      8.20
 7        0.0      23.2
 9        0.0      43.2
15       2.54       0.0
17       2.54      2.54
20       8.20      00.0
22       8.20      8.20
24       8.20      23.2
26       8.20      43.2
31       23.2       0.0
33       23.2      8.20
35       23.2      23.2
```

```
37      23.2        43.2
42      43.2         0.0
44      43.2        8.20
46      43.2        23.2
48      43.2        43.2
59       0.0         0.0
                7.62
 1      11011              0.0        0.0        0.0        0.0        0.0
 2      10010              0.0        0.0        0.0        0.0        0.0
 3      10010              0.0        0.0        0.0        0.0        0.0
 4      10010              0.0        0.0        0.0        0.0        0.0
 5      10010              0.0        0.0        0.0        0.0        0.0
 6      10010              0.0        0.0        0.0        0.0        0.0
 7      10010              0.0        0.0        0.0        0.0        0.0
 8      10010              0.0        0.0        0.0        0.0        0.0
 9      10110              0.0        0.0        0.0        0.0        0.0
10      01001              0.0        0.0        0.0        0.0        0.0
14      00110              0.0        0.0        0.0        0.0        0.0
15      01001              0.0        0.0        0.0        0.0        0.0
18      01001              0.0        0.0        0.0        0.0        0.0
20      01001              0.0        0.0        0.0        0.0        0.0
26      00110              0.0        0.0        0.0        0.0        0.0
27      01001              0.0        0.0        0.0        0.0        0.0
30      00110              0.0        0.0        0.0        0.0        0.0
31      01001              0.0        0.0        0.0        0.0        0.0
37      00110              0.0        0.0        0.0        0.0        0.0
38      01001              0.0        0.0        0.0        0.0        0.0
41      00110              0.0        0.0        0.0        0.0        0.0
42      01101              0.0        0.0        0.0        0.0        0.0
43      00101              0.0        0.0        0.0        0.0        0.0
44      00101              0.0        0.0        0.0        0.0        0.0
45      00101              0.0        0.0        0.0        0.0        0.0
46      00101              0.0        0.0        0.0        0.0        0.0
47      00101              0.0        0.0        0.0        0.0        0.0
48      00111              0.0        0.0        0.0        0.0        0.0
 8   2
 1   2   2   2   2   2   2   1   3   4
 1
 2694.4        0.0     .16500       37.0      0.283       3.24    0.00350
 0.0020     0.7000
 2
 2694.4        0.0     .27800       37.0      0.283       3.24    0.00350
 0.0020     0.7000
 3
20000.0      300.0    .013100        0.0      40.00    -0.6667        0.0

 4
20000.0      300.0    .013100        0.0      40.00    -0.6667     1.5708
```

```
1    0    0
0  1.0          3.875                0.0
0    0    0
0    0    0
0    0    0
0    0    0
0    0    0
0    0    0
0    0    0
0    0    0
0    0    0
0    0    0
  0.04       1.00    30    0    1
  0.04       1.00    30    0    1
  0.03       1.00    30    0    1
  0.03       1.00    30    0    1
  0.03       1.00    30    0    1
  0.03       1.00    30    0    3
  0.03       1.00    30    0    1
  0.03       1.00    30    0    1
 0.030       1.00    30    0    1
 0.030       1.00    30    0    1
  0.03       1.00    30    0    1
  0.03       1.00    30    0    1
  0.03       1.00    30    0    1
  0.03       1.00    30    0    1
  0.03       1.00    30    0    1
  0.03       1.00    30    0    1
 0.030       1.00    30    0    1
 0.030       1.00    30    0    1
  0.03       1.00    30    0    1
  0.03       1.00    30    0    1
  .030       1.00    30    0    1
  .030       1.00    30    0    1
  .030       1.00    30    0    1
  .030       1.00    30    0    1
  .030       1.00    30    0    1
  .030       1.00    30    0    1
  .030       1.00    30    0    1
  .030       1.00    30    0    1
  .030       1.00    30    0    1
  .030       1.00    30    0    1
  .030       1.00    30    0    1
  .030       1.00    30    0    1
  .030       1.00    30    0    1
  .030       1.00    30    0    1
  .030       1.00    30    0    1
  .030       1.00    30    0    1
  .030       1.00    30    0    1
  .030       1.00    30    0    1
  .030       1.00    30    0    1
  0.03       1.00    30    0    1
  0.03       1.00    30    0    1
  0.03       1.00    30    0    1
  0.03       1.00    30    0    1
```

Line printer output:

TAYLOR AND HAYES 2 IN SLAB UNRESTRAINED WITH STEEL=1.57%

NPOIN = 59
NELEM = 11
NVFIX = 28
NNODE = 9
NMATS = 4
NGAUS = 3
NGAUZ = 2
NEVAB = 45
NTYPE = 2
NALGO = 4
NINCS = 6
NLAYR = 1
NCRIT = 5
NHARD = 1
NREST = 0
NNORM = 2
NPLOT = 1
NSDEG = 1
NDOWL = 1

X-GRAVITY	Y-GRAVITY	Z-GRAVITY	ANG VEL/
0.00000	0.00000	0.00000	0.00000

ELEMENT	PROPERTY	NODE NUMBERS								
1	1	1	10	15	16	17	11	3	2	49
2	1	15	18	20	21	22	19	17	16	53
3	1	20	27	31	32	33	28	22	21	54
4	1	31	38	42	43	44	39	33	32	57
5	1	3	11	17	19	22	12	5	4	50
6	1	5	12	22	23	24	13	7	6	51
7	1	22	28	33	34	35	29	24	23	55
8	1	33	39	44	45	46	40	35	34	58
9	1	7	13	24	25	26	14	9	8	52
10	1	24	29	35	36	37	30	26	25	56
11	1	35	40	46	47	48	41	37	36	59

NODE	X	Y	Z	PRESSURE AT TOP AND BOT	
1	0.00	0.00	0.00	0.00	0.00
2	0.00	1.27	0.00	0.00	0.00
3	0.00	2.54	0.00	0.00	0.00
4	0.00	5.37	0.00	0.00	0.00
5	0.00	8.20	0.00	0.00	0.00
6	0.00	15.70	0.00	0.00	0.00
7	0.00	23.20	0.00	0.00	0.00

8	0.00	33.20	0.00	0.00	0.00
9	0.00	43.20	0.00	0.00	0.00
10	1.27	0.00	0.00	0.00	0.00
11	1.27	2.54	0.00	0.00	0.00
12	4.10	8.20	0.00	0.00	0.00
13	4.10	23.20	0.00	0.00	0.00
14	4.10	43.20	0.00	0.00	0.00
15	2.54	0.00	0.00	0.00	0.00
16	2.54	1.27	0.00	0.00	0.00
17	2.54	2.54	0.00	0.00	0.00
18	5.37	0.00	0.00	0.00	0.00
19	5.37	5.37	0.00	0.00	0.00
20	8.20	0.00	0.00	0.00	0.00
21	8.20	4.10	0.00	0.00	0.00
22	8.20	8.20	0.00	0.00	0.00
23	8.20	15.70	0.00	0.00	0.00
24	8.20	23.20	0.00	0.00	0.00
25	8.20	33.20	0.00	0.00	0.00
26	8.20	43.20	0.00	0.00	0.00
27	15.70	0.00	0.00	0.00	0.00
28	15.70	8.20	0.00	0.00	0.00
29	15.70	23.20	0.00	0.00	0.00
30	15.70	43.20	0.00	0.00	0.00
31	23.20	0.00	0.00	0.00	0.00
32	23.20	4.10	0.00	0.00	0.00
33	23.20	8.20	0.00	0.00	0.00
34	23.20	15.70	0.00	0.00	0.00
35	23.20	23.20	0.00	0.00	0.00
36	23.20	33.20	0.00	0.00	0.00
37	23.20	43.20	0.00	0.00	0.00
38	33.20	0.00	0.00	0.00	0.00
39	33.20	8.20	0.00	0.00	0.00
40	33.20	23.20	0.00	0.00	0.00
41	33.20	43.20	0.00	0.00	0.00
42	43.20	0.00	0.00	0.00	0.00
43	43.20	4.10	0.00	0.00	0.00
44	43.20	8.20	0.00	0.00	0.00
45	43.20	15.70	0.00	0.00	0.00
46	43.20	23.20	0.00	0.00	0.00
47	43.20	33.20	0.00	0.00	0.00
48	43.20	43.20	0.00	0.00	0.00
49	1.27	1.27	0.00	0.00	0.00
50	2.68	5.37	0.00	0.00	0.00
51	4.10	15.70	0.00	0.00	0.00
52	4.10	33.20	0.00	0.00	0.00
53	5.37	2.68	0.00	0.00	0.00
54	15.70	4.10	0.00	0.00	0.00
55	15.70	15.70	0.00	0.00	0.00

56	15.70	33.20	0.00	0.00	0.00
57	33.20	4.10	0.00	0.00	0.00
58	33.20	15.70	0.00	0.00	0.00
59	33.20	33.20	0.00	0.00	0.00

THICKNESS OF PLATE= 7.62

NODE	CODE	FIXED VALUES				
1	11011	0.000000	0.000000	0.000000	0.000000	0.000000
2	10010	0.000000	0.000000	0.000000	0.000000	0.000000
3	10010	0.000000	0.000000	0.000000	0.000000	0.000000
4	10010	0.000000	0.000000	0.000000	0.000000	0.000000
5	10010	0.000000	0.000000	0.000000	0.000000	0.000000
6	10010	0.000000	0.000000	0.000000	0.000000	0.000000
7	10010	0.000000	0.000000	0.000000	0.000000	0.000000
8	10010	0.000000	0.000000	0.000000	0.000000	0.000000
9	10110	0.000000	0.000000	0.000000	0.000000	0.000000
10	1001	0.000000	0.000000	0.000000	0.000000	0.000000
14	110	0.000000	0.000000	0.000000	0.000000	0.000000
15	1001	0.000000	0.000000	0.000000	0.000000	0.000000
18	1001	0.000000	0.000000	0.000000	0.000000	0.000000
20	1001	0.000000	0.000000	0.000000	0.000000	0.000000
26	110	0.000000	0.000000	0.000000	0.000000	0.000000
27	1001	0.000000	0.000000	0.000000	0.000000	0.000000
30	110	0.000000	0.000000	0.000000	0.000000	0.000000
31	1001	0.000000	0.000000	0.000000	0.000000	0.000000
37	110	0.000000	0.000000	0.000000	0.000000	0.000000
38	1001	0.000000	0.000000	0.000000	0.000000	0.000000
41	110	0.000000	0.000000	0.000000	0.000000	0.000000
42	1101	0.000000	0.000000	0.000000	0.000000	0.000000
43	101	0.000000	0.000000	0.000000	0.000000	0.000000
44	101	0.000000	0.000000	0.000000	0.000000	0.000000
45	101	0.000000	0.000000	0.000000	0.000000	0.000000
46	101	0.000000	0.000000	0.000000	0.000000	0.000000
47	101	0.000000	0.000000	0.000000	0.000000	0.000000
48	111	0.000000	0.000000	0.000000	0.000000	0.000000

LAYER PAT.	NCONL	NSTEL	MATERIAL NUMBER PER CONCRETE AND STEEL LAYER
1	8	2	1 2 2 2 2 2 2 1 3 4

NUMAT ELEMENT PROPERTIES

1 0.2694E+04 0.0000E+00 0.1650E+00 0.3700E+02 0.2830E+00
0.3240E+01 0.3500E-02 0.2000E-02 0.7000E+00

2 0.2694E+04 0.0000E+00 0.2780E+00 0.3700E+02 0.2830E+00
0.3240E+01 0.3500E-02 0.2000E-02 0.7000E+00

3 0.2000E+05 0.3000E+03 0.1310E-01 0.0000E+00 0.4000E+02
-0.6667E+00 0.0000E+00 0.0000E+00 0.0000E+00

4 0.2000E+05 0.3000E+03 0.1310E-01 0.0000E+00 0.4000E+02
-0.6667E+00 0.1571E+01 0.0000E+00 0.0000E+00

```
MAXIMUM FRONTWIDTH ENCOUNTERED =   75
NPRES =    1      NUCLO =    0      NBODY =    0
   0  1.0        3.87500         0.00000
NPRES =    0      NUCLO =    0      NBODY =    0
NPRES =    0      NUCLO =    0      NBODY =    0
NPRES =    0      NUCLO =    0      NBODY =    0
NPRES =    0      NUCLO =    0      NBODY =    0
NPRES =    0      NUCLO =    0      NBODY =    0
NPRES =    0      NUCLO =    0      NBODY =    0
NPRES =    0      NUCLO =    0      NBODY =    0
NPRES =    0      NUCLO =    0      NBODY =    0
NPRES =    0      NUCLO =    0      NBODY =    0
NPRES =    0      NUCLO =    0      NBODY =    0

0     INCREMENT NUMBER     1
0     LOAD FACTOR =   0.04000      CONVERGENCE TOLERANCE =   1.00000
     MAX. NO. OF ITERATIONS =   30 .

 INITIAL OUTPUT PARAMETER =    0
     FINAL OUTPUT PARAMETER =    1
0   DISPLACEMENTS   CONVERGENCE CODE =   1
   NORM OF RESIDUAL SUM RATIO =  0.105083E+01
    ROTATIONS       CONVERGENCE CODE =   1
   NORM OF RESIDUAL SUM RATIO =  0.106744E+01
0   DISPLACEMENTS   CONVERGENCE CODE =   0
   NORM OF RESIDUAL SUM RATIO =  0.119530E-01
    ROTATIONS       CONVERGENCE CODE =   0
   NORM OF RESIDUAL SUM RATIO =  0.121674E-01
0     DISPLACEMENTS
0      NODE      DISP.          Y-DISP         Z-DISP         AF-ROT         BT-ROT
         1  0.000000E+00  0.000000E+00 -0.364738E-02  0.000000E+00  0.000000E+00
         2  0.000000E+00 -0.117580E-05 -0.363119E-02  0.000000E+00  0.129765E-04
         3  0.000000E+00 -0.223382E-05 -0.358516E-02  0.000000E+00  0.248053E-04
         4  0.000000E+00 -0.384931E-05 -0.343868E-02  0.000000E+00  0.438771E-04
         5  0.000000E+00 -0.495346E-05 -0.326631E-02  0.000000E+00  0.574001E-04
         6  0.000000E+00 -0.674089E-05 -0.269800E-02  0.000000E+00  0.798449E-04
         7  0.000000E+00 -0.762995E-05 -0.202202E-02  0.000000E+00  0.916070E-04
         8  0.000000E+00 -0.829498E-05 -0.103307E-02  0.000000E+00  0.996732E-04
         9  0.000000E+00 -0.847930E-05  0.000000E+00  0.000000E+00  0.101559E-03
        10 -0.117583E-05  0.000000E+00 -0.363120E-02 -0.129766E-04  0.000000E+00
        11 -0.113450E-05 -0.221173E-05 -0.357254E-02 -0.120173E-04  0.242425E-04
        12 -0.269500E-05 -0.491656E-05 -0.320071E-02 -0.265747E-04  0.542378E-04
        13 -0.163068E-05 -0.763578E-05 -0.199343E-02 -0.128414E-04  0.901236E-04
        14 -0.110225E-05 -0.847789E-05  0.000000E+00  0.000000E+00  0.100323E-03
        15 -0.223386E-05  0.000000E+00 -0.358515E-02 -0.248055E-04  0.000000E+00
        16 -0.221175E-05 -0.113449E-05 -0.357254E-02 -0.242424E-04  0.120174E-04
        17 -0.215139E-05 -0.215138E-05 -0.353709E-02 -0.230110E-04  0.230112E-04
        18 -0.384936E-05  0.000000E+00 -0.343868E-02 -0.438773E-04  0.000000E+00
        19 -0.365642E-05 -0.365641E-05 -0.330581E-02 -0.383098E-04  0.383099E-04
        20 -0.495350E-05  0.000000E+00 -0.326631E-02 -0.574002E-04  0.000000E+00
        21 -0.491660E-05 -0.269500E-05 -0.320071E-02 -0.542377E-04  0.265749E-04
        22 -0.470213E-05 -0.470213E-05 -0.302821E-02 -0.478963E-04  0.478967E-04
```

```
        23 -0.391677E-05 -0.670511E-05 -0.253849E-02 -0.359459E-04  0.727994E-04
        24 -0.314462E-05 -0.762073E-05 -0.191205E-02 -0.248527E-04  0.859437E-04
        25 -0.243797E-05 -0.826428E-05 -0.981161E-03 -0.121905E-04  0.944378E-04
        26 -0.218114E-05 -0.845640E-05  0.000000E+00  0.000000E+00  0.966296E-04
        27 -0.674098E-05  0.000000E+00 -0.269801E-02 -0.798454E-04  0.000000E+00
        28 -0.670512E-05 -0.391674E-05 -0.253850E-02 -0.727994E-04  0.359457E-04
        29 -0.533093E-05 -0.734008E-05 -0.164632E-02 -0.427574E-04  0.725899E-04
        30 -0.400551E-05 -0.825106E-05  0.000000E+00  0.000000E+00  0.839319E-04
        31 -0.763008E-05  0.000000E+00 -0.202203E-02 -0.916078E-04  0.000000E+00
        32 -0.763587E-05 -0.163070E-05 -0.199344E-02 -0.901241E-04  0.128415E-04
        33 -0.762078E-05 -0.314465E-05 -0.191206E-02 -0.859439E-04  0.248531E-04
        34 -0.734008E-05 -0.533097E-05 -0.164632E-02 -0.725898E-04  0.427577E-04
        35 -0.669993E-05 -0.669997E-05 -0.126671E-02 -0.547497E-04  0.547499E-04
        36 -0.566674E-05 -0.754748E-05 -0.659415E-03 -0.279739E-04  0.630062E-04
        37 -0.543910E-05 -0.775666E-05  0.000000E+00  0.000000E+00  0.652854E-04
        38 -0.829508E-05  0.000000E+00 -0.103308E-02 -0.996741E-04  0.000000E+00
        39 -0.826434E-05 -0.243799E-05 -0.981166E-03 -0.944383E-04  0.121904E-04
        40 -0.754744E-05 -0.566680E-05 -0.659416E-03 -0.630063E-04  0.279737E-04
        41 -0.637801E-05 -0.694060E-05  0.000000E+00  0.000000E+00  0.343040E-04
        42 -0.847948E-05  0.000000E+00  0.000000E+00 -0.101559E-03  0.000000E+00
        43 -0.847806E-05 -0.110227E-05  0.000000E+00 -0.100323E-03  0.000000E+00
        44 -0.845652E-05 -0.218117E-05  0.000000E+00 -0.966303E-04  0.000000E+00
        45 -0.825101E-05 -0.400559E-05  0.000000E+00 -0.839321E-04  0.000000E+00
        46 -0.775654E-05 -0.543915E-05  0.000000E+00 -0.652853E-04  0.000000E+00
        47 -0.694046E-05 -0.637808E-05  0.000000E+00 -0.343041E-04  0.000000E+00
        48 -0.655032E-05 -0.655044E-05  0.000000E+00  0.000000E+00  0.000000E+00
        49 -0.116235E-05 -0.116233E-05 -0.361723E-02 -0.126524E-04  0.126522E-04
        50 -0.203389E-05 -0.380686E-05 -0.340258E-02 -0.207257E-04  0.418575E-04
        51 -0.209396E-05 -0.675777E-05 -0.265696E-02 -0.189680E-04  0.779314E-04
        52 -0.124812E-05 -0.829086E-05 -0.101994E-02 -0.626323E-05  0.983271E-04
        53 -0.380690E-05 -0.203389E-05 -0.340258E-02 -0.418576E-04  0.207258E-04
        54 -0.675783E-05 -0.209394E-05 -0.265697E-02 -0.779318E-04  0.189678E-04
        55 -0.616765E-05 -0.616764E-05 -0.216163E-02 -0.588240E-04  0.588239E-04
        56 -0.430813E-05 -0.805400E-05 -0.850492E-03 -0.213687E-04  0.815537E-04
        57 -0.829093E-05 -0.124812E-05 -0.101995E-02 -0.983277E-04  0.626316E-05
        58 -0.805398E-05 -0.430814E-05 -0.850492E-03 -0.815541E-04  0.213685E-04
        59 -0.666159E-05 -0.666168E-05 -0.345600E-03 -0.328680E-04  0.328678E-04
0      INCREMENT NUMBER      2
0      LOAD FACTOR =    0.08000       CONVERGENCE TOLERANCE =    1.00000
      MAX. NO. OF ITERATIONS =    30

 INITIAL OUTPUT PARAMETER =     0
     FINAL OUTPUT PARAMETER =     1
0    DISPLACEMENTS    CONVERGENCE CODE =    0
    NORM OF RESIDUAL SUM RATIO =  0.524609E+00
     ROTATIONS        CONVERGENCE CODE =    0
    NORM OF RESIDUAL SUM RATIO =  0.532893E+00
0      DISPLACEMENTS
0       NODE       DISP.          Y-DISP          Z-DISP          AF-ROT          BT-ROT
          1  0.000000E+00  0.000000E+00 -0.729430E-02  0.000000E+00  0.000000E+00
          2  0.000000E+00 -0.235155E-05 -0.726192E-02  0.000000E+00  0.259520E-04
          3  0.000000E+00 -0.446751E-05 -0.716985E-02  0.000000E+00  0.496086E-04
          4  0.000000E+00 -0.769835E-05 -0.687690E-02  0.000000E+00  0.877500E-04
          5  0.000000E+00 -0.990653E-05 -0.653218E-02  0.000000E+00  0.114794E-03
```

6	0.000000E+00	-0.134811E-04	-0.539562E-02	0.000000E+00	0.159680E-03
7	0.000000E+00	-0.152590E-04	-0.404375E-02	0.000000E+00	0.183202E-03
8	0.000000E+00	-0.165888E-04	-0.206600E-02	0.000000E+00	0.199332E-03
9	0.000000E+00	-0.169575E-04	0.000000E+00	0.000000E+00	0.203102E-03
10	-0.235157E-05	0.000000E+00	-0.726193E-02	-0.259523E-04	0.000000E+00
11	-0.226893E-05	-0.442334E-05	-0.714462E-02	-0.240340E-04	0.484830E-04
12	-0.538973E-05	-0.983275E-05	-0.640099E-02	-0.531465E-04	0.108470E-03
13	-0.326121E-05	-0.152706E-04	-0.398658E-02	-0.256812E-04	0.180235E-03
14	-0.220435E-05	-0.169546E-04	0.000000E+00	0.000000E+00	0.200631E-03
15	-0.446755E-05	0.000000E+00	-0.716984E-02	-0.496091E-04	0.000000E+00
16	-0.442335E-05	-0.226893E-05	-0.714462E-02	-0.484832E-04	0.240339E-04
17	-0.430265E-05	-0.430266E-05	-0.707373E-02	-0.460204E-04	0.460207E-04
18	-0.769837E-05	0.000000E+00	-0.687691E-02	-0.877506E-04	0.000000E+00
19	-0.731249E-05	-0.731253E-05	-0.661118E-02	-0.766157E-04	0.766158E-04
20	-0.990647E-05	0.000000E+00	-0.653219E-02	-0.114794E-03	0.000000E+00
21	-0.983270E-05	-0.538980E-05	-0.640100E-02	-0.108470E-03	0.531469E-04
22	-0.940372E-05	-0.940377E-05	-0.605601E-02	-0.957869E-04	0.957875E-04
23	-0.783313E-05	-0.134095E-04	-0.507663E-02	-0.718875E-04	0.145590E-03
24	-0.628890E-05	-0.152405E-04	-0.382383E-02	-0.497019E-04	0.171876E-03
25	-0.487565E-05	-0.165275E-04	-0.196218E-02	-0.243795E-04	0.188862E-03
26	-0.436198E-05	-0.169117E-04	0.000000E+00	0.000000E+00	0.193245E-03
27	-0.134811E-04	0.000000E+00	-0.539565E-02	-0.159681E-03	0.000000E+00
28	-0.134095E-04	-0.783312E-05	-0.507664E-02	-0.145590E-03	0.718873E-04
29	-0.106613E-04	-0.146793E-04	-0.329241E-02	-0.855091E-04	0.145170E-03
30	-0.801046E-05	-0.165010E-04	0.000000E+00	0.000000E+00	0.167851E-03
31	-0.152591E-04	0.000000E+00	-0.404377E-02	-0.183203E-03	0.000000E+00
32	-0.152707E-04	-0.326125E-05	-0.398660E-02	-0.180236E-03	0.256814E-04
33	-0.152405E-04	-0.628898E-05	-0.382384E-02	-0.171876E-03	0.497027E-04
34	-0.146793E-04	-0.106614E-04	-0.329242E-02	-0.145170E-03	0.855095E-04
35	-0.133991E-04	-0.133992E-04	-0.253324E-02	-0.109492E-03	0.109492E-03
36	-0.113328E-04	-0.150941E-04	-0.131873E-02	-0.559439E-04	0.126003E-03
37	-0.108774E-04	-0.155123E-04	0.000000E+00	0.000000E+00	0.130561E-03
38	-0.165890E-04	0.000000E+00	-0.206602E-02	-0.199334E-03	0.000000E+00
39	-0.165275E-04	-0.487573E-05	-0.196219E-02	-0.188863E-03	0.243793E-04
40	-0.150940E-04	-0.113330E-04	-0.131874E-02	-0.126003E-03	0.559436E-04
41	-0.127551E-04	-0.138804E-04	0.000000E+00	0.000000E+00	0.686029E-04
42	-0.169577E-04	0.000000E+00	0.000000E+00	-0.203104E-03	0.000000E+00
43	-0.169548E-04	-0.220441E-05	0.000000E+00	-0.200632E-03	0.000000E+00
44	-0.169118E-04	-0.436207E-05	0.000000E+00	-0.193247E-03	0.000000E+00
45	-0.165010E-04	-0.801067E-05	0.000000E+00	-0.167852E-03	0.000000E+00
46	-0.155122E-04	-0.108777E-04	0.000000E+00	-0.130561E-03	0.000000E+00
47	-0.138801E-04	-0.127555E-04	0.000000E+00	-0.686031E-04	0.000000E+00
48	-0.130997E-04	-0.131002E-04	0.000000E+00	0.000000E+00	0.000000E+00
49	-0.232461E-05	-0.232460E-05	-0.723400E-02	-0.253037E-04	0.253035E-04
50	-0.406761E-05	-0.761347E-05	-0.680472E-02	-0.414495E-04	0.837110E-04
51	-0.418771E-05	-0.135149E-04	-0.531356E-02	-0.379336E-04	0.155854E-03
52	-0.249610E-05	-0.165806E-04	-0.203974E-02	-0.125256E-04	0.196640E-03
53	-0.761346E-05	-0.406766E-05	-0.680472E-02	-0.837113E-04	0.414497E-04
54	-0.135148E-04	-0.418770E-05	-0.531358E-02	-0.155854E-03	0.379333E-04
55	-0.123346E-04	-0.123346E-04	-0.432296E-02	-0.117640E-03	0.117640E-03
56	-0.861571E-05	-0.161070E-04	-0.170086E-02	-0.427345E-04	0.163096E-03
57	-0.165807E-04	-0.249612E-05	-0.203975E-02	-0.196642E-03	0.125255E-04
58	-0.161069E-04	-0.861582E-05	-0.170086E-02	-0.163096E-03	0.427341E-04
59	-0.133223E-04	-0.133226E-04	-0.691149E-03	-0.657312E-04	0.657309E-04

0 INCREMENT NUMBER 3
0 LOAD FACTOR = 0.11000 CONVERGENCE TOLERANCE = 1.00000
MAX. NO. OF ITERATIONS = 30

INITIAL OUTPUT PARAMETER = 0
FINAL OUTPUT PARAMETER = 1
0 DISPLACEMENTS CONVERGENCE CODE = 0
NORM OF RESIDUAL SUM RATIO = 0.287875E+00
ROTATIONS CONVERGENCE CODE = 0
NORM OF RESIDUAL SUM RATIO = 0.292377E+00
0 DISPLACEMENTS

0 NODE	DISP.	Y-DISP	Z-DISP	AF-ROT	BI-ROT
1	0.000000E+00	0.000000E+00	-0.100300E-01	0.000000E+00	0.000000E+00
2	0.000000E+00	-0.323345E-05	-0.998549E-02	0.000000E+00	0.356850E-04
3	0.000000E+00	-0.614299E-05	-0.985888E-02	0.000000E+00	0.682138E-04
4	0.000000E+00	-0.105855E-04	-0.945608E-02	0.000000E+00	0.120660E-03
5	0.000000E+00	-0.136218E-04	-0.898207E-02	0.000000E+00	0.157846E-03
6	0.000000E+00	-0.185372E-04	-0.741926E-02	0.000000E+00	0.219568E-03
7	0.000000E+00	-0.209819E-04	-0.556036E-02	0.000000E+00	0.251912E-03
8	0.000000E+00	-0.228106E-04	-0.284086E-02	0.000000E+00	0.274092E-03
9	0.000000E+00	-0.233175E-04	0.000000E+00	0.000000E+00	0.279276E-03
10	-0.323352E-05	0.000000E+00	-0.998550E-02	-0.356856E-04	0.000000E+00
11	-0.311987E-05	-0.608223E-05	-0.982419E-02	-0.330475E-04	0.666658E-04
12	-0.741110E-05	-0.135204E-04	-0.880168E-02	-0.730784E-04	0.149150E-03
13	-0.448432E-05	-0.209979E-04	-0.548175E-02	-0.353128E-04	0.247832E-03
14	-0.303112E-05	-0.233136E-04	0.000000E+00	0.000000E+00	0.275878E-03
15	-0.614304E-05	0.000000E+00	-0.985888E-02	-0.682142E-04	0.000000E+00
16	-0.608229E-05	-0.311985E-05	-0.982419E-02	-0.666660E-04	0.330474E-04
17	-0.591633E-05	-0.591629E-05	-0.972672E-02	-0.632797E-04	0.632798E-04
18	-0.105856E-04	0.000000E+00	-0.945609E-02	-0.120660E-03	0.000000E+00
19	-0.100550E-04	-0.100550E-04	-0.909070E-02	-0.105349E-03	0.105350E-03
20	-0.136219E-04	0.000000E+00	-0.898208E-02	-0.157847E-03	0.000000E+00
21	-0.135204E-04	-0.741117E-05	-0.880169E-02	-0.149150E-03	0.730790E-04
22	-0.129306E-04	-0.129306E-04	-0.832732E-02	-0.131711E-03	0.131712E-03
23	-0.107709E-04	-0.184387E-04	-0.698063E-02	-0.988485E-04	0.200192E-03
24	-0.864755E-05	-0.209565E-04	-0.525796E-02	-0.683427E-04	0.236338E-03
25	-0.670428E-05	-0.227261E-04	-0.269811E-02	-0.335230E-04	0.259695E-03
26	-0.599797E-05	-0.232545E-04	0.000000E+00	0.000000E+00	0.265723E-03
27	-0.185372E-04	0.000000E+00	-0.741929E-02	-0.219569E-03	0.000000E+00
28	-0.184387E-04	-0.107709E-04	-0.698065E-02	-0.200193E-03	0.988481E-04
29	-0.146598E-04	-0.201848E-04	-0.452724E-02	-0.117579E-03	0.199616E-03
30	-0.110149E-04	-0.226897E-04	0.000000E+00	0.000000E+00	0.230805E-03
31	-0.209821E-04	0.000000E+00	-0.556039E-02	-0.251913E-03	0.000000E+00
32	-0.209980E-04	-0.448438E-05	-0.548178E-02	-0.247833E-03	0.353132E-04
33	-0.209566E-04	-0.864766E-05	-0.525798E-02	-0.236338E-03	0.683436E-04
34	-0.201848E-04	-0.146599E-04	-0.452724E-02	-0.199616E-03	0.117580E-03
35	-0.184245E-04	-0.184246E-04	-0.348334E-02	-0.150557E-03	0.150558E-03
36	-0.155832E-04	-0.207551E-04	-0.181333E-02	-0.769259E-04	0.173261E-03
37	-0.149571E-04	-0.213303E-04	0.000000E+00	0.000000E+00	0.179528E-03
38	-0.228108E-04	0.000000E+00	-0.284089E-02	-0.274095E-03	0.000000E+00
39	-0.227263E-04	-0.670433E-05	-0.269812E-02	-0.259697E-03	0.335226E-04
40	-0.207551E-04	-0.155834E-04	-0.181333E-02	-0.173262E-03	0.769254E-04
41	-0.175392E-04	-0.190862E-04	0.000000E+00	0.000000E+00	0.943329E-04
42	-0.233178E-04	0.000000E+00	0.000000E+00	-0.279279E-03	0.000000E+00
43	-0.233139E-04	-0.303118E-05	0.000000E+00	-0.275880E-03	0.000000E+00

```
        44 -0.232548E-04 -0.599806E-05  0.000000E+00 -0.265724E-03  0.000000E+00
        45 -0.226898E-04 -0.110150E-04  0.000000E+00 -0.230806E-03  0.000000E+00
        46 -0.213301E-04 -0.149573E-04  0.000000E+00 -0.179528E-03  0.000000E+00
        47 -0.190859E-04 -0.175394E-04  0.000000E+00 -0.943332E-04  0.000000E+00
        48 -0.180130E-04 -0.180132E-04  0.000000E+00  0.000000E+00  0.000000E+00
        49 -0.319644E-05 -0.319640E-05 -0.994709E-02 -0.347935E-04  0.347931E-04
        50 -0.559314E-05 -0.104688E-04 -0.935682E-02 -0.569945E-04  0.115106E-03
        51 -0.575829E-05 -0.185836E-04 -0.730641E-02 -0.521603E-04  0.214306E-03
        52 -0.343226E-05 -0.227992E-04 -0.280475E-02 -0.172233E-04  0.270390E-03
        53 -0.104688E-04 -0.559317E-05 -0.935682E-02 -0.115106E-03  0.569948E-04
        54 -0.185836E-04 -0.575825E-05 -0.730643E-02 -0.214307E-03  0.521599E-04
        55 -0.169607E-04 -0.169607E-04 -0.594429E-02 -0.161761E-03  0.161761E-03
        56 -0.118471E-04 -0.221479E-04 -0.233878E-02 -0.587622E-04  0.224266E-03
        57 -0.227994E-04 -0.343227E-05 -0.280476E-02 -0.270392E-03  0.172231E-04
        58 -0.221479E-04 -0.118471E-04 -0.233878E-02 -0.224266E-03  0.587616E-04
        59 -0.183190E-04 -0.183192E-04 -0.950368E-03 -0.903840E-04  0.903836E-04
0     INCREMENT NUMBER      4
```

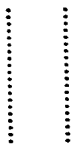

```
0     INCREMENT NUMBER      6
0     LOAD FACTOR =    0.20000      CONVERGENCE TOLERANCE =    1.00000
     MAX. NO. OF ITERATIONS =    30

 INITIAL OUTPUT PARAMETER =     0
    FINAL OUTPUT PARAMETER =     3
0   DISPLACEMENTS   CONVERGENCE CODE =    1
   NORM OF RESIDUAL SUM RATIO =  0.189443E+01
    ROTATIONS       CONVERGENCE CODE =    1
   NORM OF RESIDUAL SUM RATIO =  0.280602E+01
0   DISPLACEMENTS   CONVERGENCE CODE =    0
   NORM OF RESIDUAL SUM RATIO =  0.453904E+00
    ROTATIONS       CONVERGENCE CODE =    0
   NORM OF RESIDUAL SUM RATIO =  0.772652E+00
0     DISPLACEMENTS
0      NODE      DISP.        Y-DISP        Z-DISP        AF-ROT        BT-ROT
         1  0.000000E+00  0.000000E+00 -0.192925E-01  0.000000E+00  0.000000E+00
         2  0.000000E+00  0.656245E-04 -0.191705E-01  0.000000E+00  0.105913E-03
         3  0.000000E+00  0.979237E-04 -0.188418E-01  0.000000E+00  0.188403E-03
         4  0.000000E+00  0.704069E-04 -0.179483E-01  0.000000E+00  0.272953E-03
         5  0.000000E+00  0.471660E-04 -0.169569E-01  0.000000E+00  0.329261E-03
         6  0.000000E+00  0.105488E-04 -0.138832E-01  0.000000E+00  0.422782E-03
         7  0.000000E+00 -0.402270E-05 -0.103634E-01  0.000000E+00  0.474515E-03
         8  0.000000E+00 -0.122598E-04 -0.527912E-02  0.000000E+00  0.510555E-03
         9  0.000000E+00 -0.136849E-04  0.000000E+00  0.000000E+00  0.519002E-03
        10  0.656169E-04  0.000000E+00 -0.191705E-01 -0.105910E-03  0.000000E+00
        11  0.343096E-04  0.812516E-04 -0.187657E-01 -0.843805E-04  0.175975E-03
        12  0.665791E-05  0.335163E-04 -0.165985E-01 -0.146014E-03  0.306571E-03
        13 -0.309578E-05 -0.566644E-05 -0.102152E-01 -0.663591E-04  0.466342E-03
```

14	-0.147511E-05	-0.142915E-04	0.000000E+00	0.000000E+00	0.512612E-03
15	0.979158E-04	0.000000E+00	-0.188418E-01	-0.188400E-03	0.000000E+00
16	0.812472E-04	0.343080E-04	-0.187657E-01	-0.175975E-03	0.843784E-04
17	0.556927E-04	0.556946E-04	-0.185457E-01	-0.155154E-03	0.155154E-03
18	0.704003E-04	0.000000E+00	-0.179483E-01	-0.272953E-03	0.000000E+00
19	0.274578E-04	0.274619E-04	-0.171953E-01	-0.220424E-03	0.220426E-03
20	0.471606E-04	0.000000E+00	-0.169569E-01	-0.329261E-03	0.000000E+00
21	0.335117E-04	0.665963E-05	-0.165986E-01	-0.306571E-03	0.146016E-03
22	0.827276E-05	0.827527E-05	-0.156593E-01	-0.260177E-03	0.260179E-03
23	-0.432595E-05	-0.101485E-04	-0.130524E-01	-0.188587E-03	0.382689E-03
24	-0.661257E-05	-0.897265E-05	-0.979443E-02	-0.128155E-03	0.444029E-03
25	-0.585251E-05	-0.142869E-04	-0.501362E-02	-0.625165E-04	0.483596E-03
26	-0.324583E-05	-0.156499E-04	0.000000E+00	0.000000E+00	0.493695E-03
27	0.105451E-04	0.000000E+00	-0.138833E-01	-0.422784E-03	0.000000E+00
28	-0.101761E-05	-0.432535E-05	-0.130525E-01	-0.382691E-03	0.188587E-03
29	-0.124540E-04	-0.145895E-04	-0.842584E-02	-0.220133E-03	0.373863E-03
30	-0.746160E-05	-0.185104E-04	0.000000E+00	0.000000E+00	0.428685E-03
31	-0.402589E-05	0.000000E+00	-0.103634E-01	-0.474518E-03	0.000000E+00
32	-0.566937E-05	-0.309564E-05	-0.102153E-01	-0.466345E-03	0.663603E-04
33	-0.897515E-05	-0.661232E-05	-0.979446E-02	-0.444030E-03	0.128156E-03
34	-0.145912E-04	-0.124535E-04	-0.842585E-02	-0.373863E-03	0.220133E-03
35	-0.166576E-04	-0.166568E-04	-0.647612E-02	-0.281034E-03	0.281034E-03
36	-0.147196E-04	-0.192636E-04	-0.336709E-02	-0.143111E-03	0.322149E-03
37	-0.120823E-04	-0.199893E-04	0.000000E+00	0.000000E+00	0.333278E-03
38	-0.122626E-04	0.000000E+00	-0.527918E-02	-0.510561E-03	0.000000E+00
39	-0.142895E-04	-0.585253E-05	-0.501364E-02	-0.483599E-03	0.625160E-04
40	-0.192645E-04	-0.147198E-04	-0.336709E-02	-0.322148E-03	0.143110E-03
41	-0.161487E-04	-0.188041E-04	0.000000E+00	0.000000E+00	0.175053E-03
42	-0.136877E-04	0.000000E+00	0.000000E+00	-0.519008E-03	0.000000E+00
43	-0.142943E-04	-0.147534E-05	0.000000E+00	-0.512615E-03	0.000000E+00
44	-0.156524E-04	-0.324630E-05	0.000000E+00	-0.493697E-03	0.000000E+00
45	-0.185122E-04	-0.746251E-05	0.000000E+00	-0.428686E-03	0.000000E+00
46	-0.199902E-04	-0.120833E-04	0.000000E+00	-0.333279E-03	0.000000E+00
47	-0.188036E-04	-0.161500E-04	0.000000E+00	-0.175054E-03	0.000000E+00
48	-0.173613E-04	-0.173627E-04	0.000000E+00	0.000000E+00	0.000000E+00
49	0.538550E-04	0.538528E-04	-0.190679E-01	-0.978677E-04	0.978654E-04
50	0.167549E-04	0.547601E-04	-0.177437E-01	-0.120868E-03	0.254066E-03
51	-0.203786E-05	0.713823E-05	-0.136699E-01	-0.995029E-04	0.412106E-03
52	-0.295620E-05	-0.127994E-04	-0.521199E-02	-0.321278E-04	0.503643E-03
53	0.547547E-04	0.167570E-04	-0.177437E-01	-0.254066E-03	0.120870E-03
54	0.713468E-05	-0.203755E-05	-0.136699E-01	-0.412108E-03	0.995020E-04
55	-0.103039E-04	-0.103026E-04	-0.110903E-01	-0.305614E-03	0.305614E-03
56	-0.107963E-04	-0.176115E-04	-0.434473E-02	-0.109452E-03	0.417315E-03
57	-0.128020E-04	-0.295619E-05	-0.521200E-02	-0.503646E-03	0.321274E-04
58	-0.176133E-04	-0.107963E-04	-0.434473E-02	-0.417317E-03	0.109451E-03
59	-0.178423E-04	-0.178425E-04	-0.176378E-02	-0.167866E-03	0.167864E-03

0 REACTIONS

0 NODE	X-REAC	Y-REAC	Z-REAC	AF-MOM	BI-MOM
1	0.385175E-01	0.385077E-01	0.000000E+00	0.213923E+01	-0.213923E+01
2	0.164940E+00	0.000000E+00	0.000000E+00	0.823193E+01	0.000000E+00
3	0.204671E+00	0.000000E+00	0.000000E+00	0.611642E+01	0.000000E+00
4	0.309444E+00	0.000000E+00	0.000000E+00	0.145397E+02	0.000000E+00
5	-0.503448E-01	0.000000E+00	0.000000E+00	0.118753E+02	0.000000E+00
6	-0.462838E+00	0.000000E+00	0.000000E+00	0.257244E+02	0.000000E+00
7	-0.153498E+00	0.000000E+00	0.000000E+00	0.973464E+01	0.000000E+00
8	-0.820208E-01	0.000000E+00	0.000000E+00	0.110193E+02	0.000000E+00
9	0.311382E-01	0.000000E+00	0.149072E+00	-0.626330E-01	0.000000E+00
10	0.000000E+00	0.164973E+00	0.000000E+00	0.000000E+00	-0.823166E+01
14	0.000000E+00	0.000000E+00	0.516160E+00	0.154721E+01	0.000000E+00
15	0.000000E+00	0.204686E+00	0.000000E+00	0.000000E+00	-0.611629E+01
18	0.000000E+00	0.309427E+00	0.000000E+00	0.000000E+00	-0.145402E+02
20	0.000000E+00	-0.503674E-01	0.000000E+00	0.000000E+00	-0.118754E+02
26	0.000000E+00	0.000000E+00	0.337491E+00	0.234474E+01	0.000000E+00
27	0.000000E+00	-0.462855E+00	0.000000E+00	0.000000E+00	-0.257246E+02
30	0.000000E+00	0.000000E+00	0.751821E+00	0.104041E+02	0.000000E+00
31	0.000000E+00	-0.153500E+00	0.000000E+00	0.000000E+00	-0.973473E+01
37	0.000000E+00	0.000000E+00	0.341800E+00	0.839968E+01	0.000000E+00
38	0.000000E+00	-0.820194E-01	0.000000E+00	0.000000E+00	-0.110192E+02
41	0.000000E+00	0.000000E+00	0.398510E+00	0.217537E+02	0.000000E+00
42	0.000000E+00	0.311426E-01	0.149084E+00	0.000000E+00	0.625920E-01
43	0.000000E+00	0.000000E+00	0.516274E+00	0.000000E+00	-0.154698E+01
44	0.000000E+00	0.000000E+00	0.337408E+00	0.000000E+00	-0.234455E+01
45	0.000000E+00	0.000000E+00	0.751824E+00	0.000000E+00	-0.104039E+02
46	0.000000E+00	0.000000E+00	0.341778E+00	0.000000E+00	-0.839959E+01
47	0.000000E+00	0.000000E+00	0.398461E+00	0.000000E+00	-0.217544E+02
48	0.000000E+00	0.000000E+00	0.983945E-02	0.593378E+01	-0.593390E+01

0 STRESSES

OKLAYR	XX-STR	YY-STR	XY-STR	XZ-STR	YZ-STR	EFF.STRES	EFF.STN1	EFF.STN2	DIR-1	DIR-2	STAT
0					ELEMENT NO. = 1						
G.P. NO. = 1											
CONCRETE LAYERS											
1	0.1622E+00	0.1622E+00	0.6769E-03	0.5738E-02	0.5747E-02	0.1615E+00	0.3690E-03	0.3554E-03	-45.24	0.00	3
2	0.1695E+00	0.1695E+00	0.5627E-03	0.5827E-02	0.5837E-02	0.1701E+00	0.2829E-03	0.2942E-03	44.97	0.00	3
3	0.1787E+00	0.1787E+00	0.4193E-03	0.5940E-02	0.5950E-02	0.1783E+00	0.2003E-03	0.1919E-03	-45.02	0.00	3
4	0.2297E+00	0.2296E+00	0.4213E-01	0.2061E-01	0.2061E-01	0.1876E+00	0.1064E-03	0.0000E+00	-45.02	0.00	2
5	0.3024E-01	0.3025E-01	-0.3600E-02	0.2059E-01	0.2059E-01	0.6405E-01	0.0000E+00	0.0000E+00	0.00	0.00	1
6	-0.2188E+00	-0.2188E+00	0.3023E-03	0.2059E-01	0.2059E-01	0.2261E+00	0.0000E+00	0.0000E+00	0.00	0.00	1
7	-0.4679E+00	-0.4679E+00	0.4204E-02	0.2059E-01	0.2059E-01	0.4739E+00	0.0000E+00	0.0000E+00	0.00	0.00	1
8	-0.6663E+00	-0.6663E+00	0.7314E-02	0.2059E-01	0.2059E-01	0.6749E+00	0.0000E+00	0.0000E+00	0.00	0.00	1
STEEL LAYERS											
1	0.5576E+01	0.0000E+00	0.0000E+00	0.1529E+00	0.0000E+00	0.5582E+01	0.0000E+00	0.0000E+00	0.00	0.00	5
2	0.6834E-10	0.5576E+01	-0.1952E-04	-0.5351E-06	0.1528E+00	0.5582E+01	0.0000E+00	0.0000E+00	90.00	0.00	5

STRESS RESULTANTS = N-XX =-0.12180E+00 M-XX = 0.50928E+01
N-YY =-0.12189E+00 M-YY = 0.50926E+01
N-XY = 0.51643E-01 M-XY = 0.12583E-02
Q-XZ = 0.12391E+00 Q-YZ = 0.12393E+00

G.P. NO. = 2

CONCRETE LAYERS											
1	0.1640E+00	0.1702E+00	-0.2262E-04	0.3945E-02	0.2456E-01	0.1645E+00	0.3393E-03	0.2869E-03	-16.14	0.00	3
2	0.1709E+00	0.1762E+00	-0.1567E-03	0.3988E-02	0.2488E-01	0.1714E+00	0.2695E-03	0.2262E-03	-15.81	0.00	3
3	0.1797E+00	0.1836E+00	-0.1942E-03	0.4045E-02	0.2528E-01	0.1801E+00	0.1819E-03	0.1500E-03	-15.67	0.00	3
4	0.2466E+00	0.2061E+00	-0.2023E-01	0.1384E-01	0.8689E-01	0.2912E+00	0.0000E+00	0.0000E+00	0.00	0.00	1
5	0.1445E-01	-0.3213E-02	-0.9662E-02	0.1384E-01	0.8689E-01	0.1766E+00	0.0000E+00	0.0000E+00	0.00	0.00	1
6	-0.2177E+00	-0.2126E+00	0.9094E-03	0.1384E-01	0.8689E-01	0.2758E+00	0.0000E+00	0.0000E+00	0.00	0.00	1
7	-0.4498E+00	-0.4219E+00	0.1148E-01	0.1384E-01	0.8689E-01	0.4727E+00	0.0000E+00	0.0000E+00	0.00	0.00	1
8	-0.6347E+00	-0.5887E+00	0.1990E-01	0.1384E-01	0.8689E-01	0.6557E+00	0.0000E+00	0.0000E+00	0.00	0.00	1
STEEL LAYERS											
1	0.5095E+01	0.0000E+00	0.0000E+00	0.1027E+00	0.0000E+00	0.5098E+01	0.0000E+00	0.0000E+00	0.00	0.00	5
2	0.5484E-10	0.4474E+01	-0.1566E-04	-0.2258E-05	0.6450E+00	0.4612E+01	0.0000E+00	0.0000E+00	90.00	0.00	5

STRESS RESULTANTS = N-XX =-0.10074E+00 M-XX = 0.49376E+01
N-YY =-0.11583E+00 M-YY = 0.46935E+01
N-XY =-0.64157E-02 M-XY =-0.84195E-01
Q-XZ = 0.83430E-01 Q-YZ = 0.52353E+00

G.P. NO. = 3

CONCRETE LAYERS											
1	0.1680E+00	0.1774E+00	-0.2717E-03	0.2178E-02	0.4392E-01	0.1687E+00	0.2969E-03	0.2165E-03	-14.52	0.00	3
2	0.1746E+00	0.1818E+00	0.4929E-03	0.2191E-02	0.4437E-01	0.1749E+00	0.2346E-03	0.1675E-03	-16.19	0.00	3
3	0.1825E+00	0.1877E+00	0.5192E-03	0.2185E-02	0.4494E-01	0.1827E+00	0.1559E-03	0.1064E-03	-16.85	0.00	3
4	0.1974E+00	0.1330E+00	-0.2874E-01	0.7081E-02	0.1532E+00	0.3448E+00	0.0000E+00	0.0000E+00	0.00	0.00	1
5	-0.9479E-02	-0.3668E-01	-0.1351E-01	0.7081E-02	0.1532E+00	0.3100E+00	0.0000E+00	0.0000E+00	0.00	0.00	1
6	-0.2164E+00	-0.2063E+00	0.1713E-02	0.7081E-02	0.1532E+00	0.3696E+00	0.0000E+00	0.0000E+00	0.00	0.00	1
7	-0.4233E+00	-0.3760E+00	0.1694E-01	0.7081E-02	0.1532E+00	0.4959E+00	0.0000E+00	0.0000E+00	0.00	0.00	1
8	-0.5881E+00	-0.5111E+00	0.2907E-01	0.7081E-02	0.1532E+00	0.6452E+00	0.0000E+00	0.0000E+00	0.00	0.00	1

STEEL LAYERS

1	0.4375E+01	0.0000E+00	0.0000E+00	0.5256E-01	0.0000E+00	0.4376E+01	0.0000E+00	0.0000E+00	0.00	0.00	5
2	0.4134E-10	0.3373E+01	-0.1181E-04	-0.3981E-05	0.1137E+01	0.3906E+01	0.0000E+00	0.0000E+00	90.00	0.00	5

STRESS RESULTANTS = N-XX =-0.14602E+00 M-XX = 0.46771E+01
N-YY =-0.16486E+00 M-YY = 0.42604E+01
N-XY =-0.58225E-02 M-XY =-0.12112E+00
Q-XZ = 0.43079E-01 Q-YZ = 0.92424E+00

G.P. NO. = 4

CONCRETE LAYERS

1	0.1702E+00	0.1640E+00	-0.3775E-04	0.2456E-01	0.3945E-02	0.1645E+00	0.3393E-03	0.2869E-03	-73.90	0.00	3
2	0.1762E+00	0.1709E+00	-0.1556E-03	0.2488E-01	0.3989E-02	0.1714E+00	0.2695E-03	0.2262E-03	-74.19	0.00	3
3	0.1836E+00	0.1797E+00	-0.1951E-03	0.2528E-01	0.4045E-02	0.1801E+00	0.1819E-03	0.1500E-03	-74.34	0.00	3
4	0.2061E+00	0.2466E+00	-0.2022E-01	0.8689E-01	0.1385E-01	0.2912E+00	0.0000E+00	0.0000E+00	0.00	0.00	1
5	-0.3220E-02	0.1445E-01	-0.9654E-02	0.8689E-01	0.1385E-01	0.1766E+00	0.0000E+00	0.0000E+00	0.00	0.00	1
6	-0.2126E+00	-0.2177E+00	0.9104E-03	0.8689E-01	0.1385E-01	0.2758E+00	0.0000E+00	0.0000E+00	0.00	0.00	1
7	-0.4219E+00	-0.4498E+00	0.1148E-01	0.8689E-01	0.1385E-01	0.4727E+00	0.0000E+00	0.0000E+00	0.00	0.00	1
8	-0.5887E+00	-0.6347E+00	0.1989E-01	0.8689E-01	0.1385E-01	0.6557E+00	0.0000E+00	0.0000E+00	0.00	0.00	1

STEEL LAYERS

1	0.4474E+01	0.0000E+00	0.0000E+00	0.6450E+00	0.0000E+00	0.4612E+01	0.0000E+00	0.0000E+00	0.00	0.00	5
2	0.6243E-10	0.5094E+01	-0.1783E-04	-0.3598E-06	0.1028E+00	0.5097E+01	0.0000E+00	0.0000E+00	90.00	0.00	5

STRESS RESULTANTS = N-XX =-0.11586E+00 M-XX = 0.46935E+01
N-YY =-0.10074E+00 M-YY = 0.49375E+01
N-XY =-0.64119E-02 M-XY =-0.84183E-01
Q-XZ = 0.52354E+00 Q-YZ = 0.83488E-01

G.P. NO. = 5

CONCRETE LAYERS

1	0.1710E+00	0.1709E+00	0.4156E-02	0.1976E-01	0.1975E-01	0.1668E+00	0.3161E-03	0.2322E-03	-45.03	0.00	3
2	0.1767E+00	0.1767E+00	0.3448E-02	0.1997E-01	0.1996E-01	0.1733E+00	0.2505E-03	0.1809E-03	-45.02	0.00	3
3	0.1840E+00	0.1840E+00	0.2558E-02	0.2024E-01	0.2023E-01	0.1814E+00	0.1682E-03	0.1165E-03	-45.01	0.00	3
4	0.1858E+00	0.1858E+00	-0.4540E-01	0.6906E-01	0.6906E-01	0.2812E+00	0.0000E+00	0.0000E+00	0.00	0.00	1
5	-0.1196E-01	-0.1196E-01	-0.2121E-01	0.6906E-01	0.6906E-01	0.1981E+00	0.0000E+00	0.0000E+00	0.00	0.00	1
6	-0.2097E+00	-0.2097E+00	0.2987E-02	0.6906E-01	0.6906E-01	0.2844E+00	0.0000E+00	0.0000E+00	0.00	0.00	1
7	-0.4074E+00	-0.4074E+00	0.2718E-01	0.6906E-01	0.6906E-01	0.4582E+00	0.0000E+00	0.0000E+00	0.00	0.00	1
8	-0.5649E+00	-0.5649E+00	0.4646E-01	0.6906E-01	0.6906E-01	0.6292E+00	0.0000E+00	0.0000E+00	0.00	0.00	1

STEEL LAYERS

1	0.4159E+01	0.0000E+00	0.0000E+00	0.5126E+00	0.0000E+00	0.4253E+01	0.0000E+00	0.0000E+00	0.00	0.00	5
2	0.5098E-10	0.4159E+01	-0.1456E-04	-0.1795E-05	0.5126E+00	0.4253E+01	0.0000E+00	0.0000E+00	90.00	0.00	5

STRESS RESULTANTS = N-XX =-0.12749E+00 M-XX = 0.45532E+01
N-YY =-0.12752E+00 M-YY = 0.45530E+01
N-XY =-0.41645E-03 M-XY =-0.17371E+00
Q-XZ = 0.41662E+00 Q-YZ = 0.41658E+00

G.P. NO. = 6

CONCRETE LAYERS

1	0.1741E+00	0.1764E+00	0.5928E-02	0.1506E-01	0.3585E-01	0.1692E+00	0.2915E-03	0.1699E-03	-38.38	0.00	3
2	0.1775E+00	0.1831E+00	0.4288E-02	0.1512E-01	0.3621E-01	0.1753E+00	0.2300E-03	0.1297E-03	-35.65	0.00	3

3	0.1916E+00	0.2044E+00	0.1375E-01	0.6917E-01	0.1113E+00	0.1829E+00	0.1531E-03	0.0000E+00	-35.81	0.00	2
4	0.1569E+00	0.1250E+00	-0.6242E-01	0.5123E-01	0.1243E+00	0.3177E+00	0.0000E+00	0.0000E+00	0.00	0.00	1
5	-0.2355E-01	-0.3836E-01	-0.2791E-01	0.5123E-01	0.1243E+00	0.2761E+00	0.0000E+00	0.0000E+00	0.00	0.00	1
6	-0.2040E+00	-0.2017E+00	0.6603E-02	0.5123E-01	0.1243E+00	0.3337E+00	0.0000E+00	0.0000E+00	0.00	0.00	1
7	-0.3844E+00	-0.3650E+00	0.4111E-01	0.5123E-01	0.1243E+00	0.4697E+00	0.0000E+00	0.0000E+00	0.00	0.00	1
8	-0.5281E+00	-0.4952E+00	0.6861E-01	0.5123E-01	0.1243E+00	0.6222E+00	0.0000E+00	0.0000E+00	0.00	0.00	1
STEEL LAYERS											
1	0.3702E+01	0.0000E+00	0.0000E+00	0.3803E+00	0.0000E+00	0.3760E+01	0.0000E+00	0.0000E+00	0.00	0.00	5
2	0.3952E-10	0.3225E+01	-0.1129E-04	-0.3230E-05	0.9225E+00	0.3599E+01	0.0000E+00	0.0000E+00	90.00	0.00	5

STRESS RESULTANTS = N-XX =-0.12888E+00 M-XX = 0.43524E+01
N-YY =-0.13752E+00 M-YY = 0.41941E+01
N-XY = 0.20831E-01 M-XY =-0.24813E+00
Q-XZ = 0.36697E+00 Q-YZ = 0.82955E+00

G.P. NO. = 7

CONCRETE LAYERS											
1	0.1774E+00	0.1680E+00	-0.2797E-03	0.4393E-01	0.2174E-02	0.1687E+00	0.2969E-03	0.2165E-03	-75.50	0.00	3
2	0.1818E+00	0.1746E+00	0.4879E-03	0.4437E-01	0.2186E-02	0.1749E+00	0.2346E-03	0.1675E-03	-73.82	0.00	3
3	0.1877E+00	0.1825E+00	0.5162E-03	0.4494E-01	0.2180E-02	0.1827E+00	0.1559E-03	0.1064E-03	-73.16	0.00	3
4	0.1330E+00	0.1974E+00	-0.2873E-01	0.1532E+00	0.7064E-02	0.3448E+00	0.0000E+00	0.0000E+00	0.00	0.00	1
5	-0.3668E-01	-0.9484E-02	-0.1351E-01	0.1532E+00	0.7064E-02	0.3100E+00	0.0000E+00	0.0000E+00	0.00	0.00	1
6	-0.2063E+00	-0.2164E+00	0.1715E-02	0.1532E+00	0.7064E-02	0.3696E+00	0.0000E+00	0.0000E+00	0.00	0.00	1
7	-0.3760E+00	-0.4233E+00	0.1694E-01	0.1532E+00	0.7064E-02	0.4959E+00	0.0000E+00	0.0000E+00	0.00	0.00	1
8	-0.5111E+00	-0.5881E+00	0.2907E-01	0.1532E+00	0.7064E-02	0.6451E+00	0.0000E+00	0.0000E+00	0.00	0.00	1
STEEL LAYERS											
1	0.3373E+01	0.0000E+00	0.0000E+00	0.1137E+01	0.0000E+00	0.3906E+01	0.0000E+00	0.0000E+00	0.00	0.00	5
2	0.5362E-10	0.4375E+01	-0.1532E-04	-0.1836E-06	0.5243E-01	0.4376E+01	0.0000E+00	0.0000E+00	90.00	0.00	5

STRESS RESULTANTS = N-XX =-0.16488E+00 M-XX = 0.42604E+01
N-YY =-0.14602E+00 M-YY = 0.46769E+01
N-XY =-0.58218E-02 M-XY =-0.12113E+00
Q-XZ = 0.92421E+00 Q-YZ = 0.42978E-01

G.P. NO. = 8

CONCRETE LAYERS											
1	0.1764E+00	0.1741E+00	0.5920E-02	0.3586E-01	0.1506E-01	0.1692E+00	0.2915E-03	0.1699E-03	-51.66	0.00	3
2	0.1831E+00	0.1775E+00	0.4282E-02	0.3621E-01	0.1512E-01	0.1753E+00	0.2300E-03	0.1297E-03	-54.38	0.00	3
3	0.2045E+00	0.1916E+00	0.1374E-01	0.1114E+00	0.6915E-01	0.1829E+00	0.1531E-03	0.0000E+00	-54.20	0.00	2
4	0.1249E+00	0.1569E+00	-0.6241E-01	0.1243E+00	0.5123E-01	0.3177E+00	0.0000E+00	0.0000E+00	0.00	0.00	1
5	-0.3838E-01	-0.2355E-01	-0.2790E-01	0.1243E+00	0.5123E-01	0.2761E+00	0.0000E+00	0.0000E+00	0.00	0.00	1
6	-0.2017E+00	-0.2040E+00	0.6605E-02	0.1243E+00	0.5123E-01	0.3337E+00	0.0000E+00	0.0000E+00	0.00	0.00	1
7	-0.3650E+00	-0.3844E+00	0.4111E-01	0.1243E+00	0.5123E-01	0.4697E+00	0.0000E+00	0.0000E+00	0.00	0.00	1
8	-0.4951E+00	-0.5281E+00	0.6860E-01	0.1243E+00	0.5123E-01	0.6222E+00	0.0000E+00	0.0000E+00	0.00	0.00	1
STEEL LAYERS											
1	0.3224E+01	0.0000E+00	0.0000E+00	0.9225E+00	0.0000E+00	0.3598E+01	0.0000E+00	0.0000E+00	0.00	0.00	5
2	0.4537E-10	0.3702E+01	-0.1296E-04	-0.1331E-05	0.3803E+00	0.3760E+01	0.0000E+00	0.0000E+00	90.00	0.00	5

STRESS RESULTANTS = N-XX =-0.13752E+00 M-XX = 0.41942E+01
N-YY =-0.12891E+00 M-YY = 0.43523E+01
N-XY = 0.20825E-01 M-XY =-0.24816E+00
Q-XZ = 0.82956E+00 Q-YZ = 0.36695E+00

```
G.P. NO. =    9

CONCRETE LAYERS
  1  0.1780E+00  0.1780E+00  0.8144E-02  0.2792E-01  0.2793E-01  0.1699E+00  0.2852E-03  0.1207E-03 -45.01   0.00   3
  2  0.2089E+00  0.2088E+00  0.3304E-01  0.9539E-01  0.9538E-01  0.1758E+00  0.2251E-03  0.0000E+00 -45.01   0.00   2
  3  0.1602E+00  0.1602E+00 -0.2308E-01  0.9539E-01  0.9538E-01  0.1833E+00  0.1497E-03  0.0000E+00 -45.01   0.00   2
  4  0.1163E+00  0.1163E+00 -0.8399E-01  0.9538E-01  0.9540E-01  0.3200E+00  0.0000E+00  0.0000E+00   0.00   0.00   1
  5 -0.3762E-01 -0.3761E-01 -0.3481E-01  0.9538E-01  0.9540E-01  0.2794E+00  0.0000E+00  0.0000E+00   0.00   0.00   1
  6 -0.1916E+00 -0.1916E+00  0.1438E-01  0.9538E-01  0.9540E-01  0.3228E+00  0.0000E+00  0.0000E+00   0.00   0.00   1
  7 -0.3455E+00 -0.3455E+00  0.6356E-01  0.9538E-01  0.9540E-01  0.4632E+00  0.0000E+00  0.0000E+00   0.00   0.00   1
  8 -0.4682E+00 -0.4682E+00  0.1027E+00  0.9538E-01  0.9540E-01  0.6153E+00  0.0000E+00  0.0000E+00   0.00   0.00   1
STEEL LAYERS
  1  0.3028E+01  0.0000E+00  0.0000E+00  0.7080E+00  0.0000E+00  0.3267E+01  0.0000E+00  0.0000E+00   0.00   0.00   5
  2  0.3712E-10  0.3029E+01 -0.1060E-04 -0.2479E-05  0.7081E+00  0.3268E+01  0.0000E+00  0.0000E+00  90.00   0.00   5

 STRESS RESULTANTS =  N-XX =-0.12589E+00     M-XX = 0.40344E+01
                      N-YY =-0.12590E+00     M-YY = 0.40344E+01
                      N-XY = 0.36976E-01     M-XY =-0.38375E+00
                      Q-XZ = 0.71902E+00     Q-YZ = 0.71909E+00
0                                                  ELEMENT NO. =    2
 G.P. NO. =    1

 CONCRETE LAYERS
   1  0.2722E+00  0.1763E+00  0.1419E-01  0.1118E+00  0.1600E-01  0.1743E+00  0.2403E-03  0.0000E+00 -80.61   0.00   2
   2  0.2009E+00  0.1799E+00  0.2914E-02  0.1115E+00  0.1690E-01  0.1795E+00  0.1876E-03  0.0000E+00 -79.92   0.00   2
   3  0.1125E+00  0.1833E+00 -0.1428E-01  0.1111E+00  0.1826E-01  0.1861E+00  0.1214E-03  0.0000E+00 -78.88   0.00   2
   4  0.2326E-01  0.1438E+00 -0.2507E-01  0.1128E+00  0.9939E-02  0.2556E+00  0.0000E+00  0.0000E+00   0.00   0.00   1
   5 -0.7101E-01 -0.3172E-01 -0.9675E-02  0.1128E+00  0.9939E-02  0.2380E+00  0.0000E+00  0.0000E+00   0.00   0.00   1
   6 -0.1653E+00 -0.2073E+00  0.5717E-02  0.1128E+00  0.9939E-02  0.2802E+00  0.0000E+00  0.0000E+00   0.00   0.00   1
   7 -0.2596E+00 -0.3828E+00  0.2111E-01  0.1128E+00  0.9939E-02  0.4294E+00  0.0000E+00  0.0000E+00   0.00   0.00   1
   8 -0.3347E+00 -0.5227E+00  0.3337E-01  0.1128E+00  0.9939E-02  0.5637E+00  0.0000E+00  0.0000E+00   0.00   0.00   1
 STEEL LAYERS
   1  0.1498E+01  0.0000E+00  0.0000E+00  0.8372E+00  0.0000E+00  0.2085E+01  0.0000E+00  0.0000E+00   0.00   0.00   5
   2  0.4334E-10  0.3536E+01 -0.1238E-04 -0.2583E-06  0.7377E-01  0.3539E+01  0.0000E+00  0.0000E+00  90.00   0.00   5

 STRESS RESULTANTS =  N-XX =-0.13309E+00     M-XX = 0.33331E+01
                      N-YY =-0.16282E+00     M-YY = 0.43153E+01
                      N-XY = 0.94783E-02     M-XY =-0.13540E+00
                      Q-XZ = 0.89667E+00     Q-YZ = 0.99338E-01

 G.P. NO. =    2
               :
               :
 G.P. NO. =    3
               :
               :
0                                                  ELEMENT NO. =    3
                                                         :
0                                                  ELEMENT NO. =    4
                                                        :
                                                        :
                                                        :
                                                        :
```

REFERENCES

1. Al-Mandil, M.Y., Azad, A.K., Baluch, M.H., Pearson-Kirk, D. and Sharif, A.M. *A Study of Cracking of Concrete Bridge Decks in Saudi Arabia*, Vol.I-III, King Abdulaziz City for Science and Technology, Riyadh, Saudi Arabia, June 1989.

2. *Ontario Highway Bridge Design Code*, 2nd Edition, Ministry of Transportation and Communications, Highway Engineering Division, Ontario, Canada, 1983.

3. Kareem, K. *Load Induced Cracking and Failure of Concrete Deck Slabs in Girder-Slab Type Bridges.* M.S. Thesis, Department of Civil Engineering, King Fahd University of Petroleum and Minerals, Dhahran, Saudi Arabia, January 1989.

4. Tong, P.Y. and Batchelor, B. dev. *Compressive Membrane Enhancement in Two-Way Bridge Slabs*, Cracking, Deflection and Ultimate Load of Concrete Slab Systems, ACI SP-30, 1971, pp.271-286.

5. Brotchie, J.F. and Holley, M.H. *Membrane action in slabs*, Cracking, Deflection and Ultimate Load of Concrete Slab Systems, ACI SP-30, 1971, pp.345-377.

6. Eyre, J.R. and Kemp, K.O. *A graphical solution for predicting the increase in strength of concrete slabs*, Magazine of Concrete Research, V.35, No.124, Sept. 1983, pp.151-156.

7. Csagoly, P.F. *Design of Thin Concrete Deck Slabs by the Ontario Highway Bridge Design*, Report SRR79-11, Ministry of Transportation and Communications, Canada, May 1979.

8. Kinnunen, S. and Nylander, H. *Punching of concrete slabs without shear reinforcement*, Transactions of the Royal Institute of Technology, No.158, Stockholm, Sweden, 1960.

9. Kinnunen, S. *Punching of concrete slab with two-way reinforcement*, Kungliga Tekniska Hogskolan, Meddieland 41, Institution for Byggnadsstatik, Stockholm, Sweden, 1963.

10. Nielsen, M. P., et al. *Concrete plasticity- beam shear, punching shear and shear in joints*, Danish Soc. for Struct. Sci. and Engrg., Copenhagen, Denmark, Oct. 1978.

11. Andra, H. *On the strengths of support regions of flat slabs*, Thesis presented to the Univ. of Stuttgart, at Stuttgart, W. Germany, in partial fulfillment of the requirements for the degree of Doctor in Engineering (in German),1982.

12. Van Dusen, M. H. *Unbalanced Moment and Shear Transfer at Slab-Column Connections: A Literature Review*, M.Eng. Thesis, University of Toronto, 1985, 126 pp

13. Hewitt, B.E., and Batchelor, B. de V. *Punching shear strength of restrained slabs*, Journal of the Structural Division, ASCE, Vol.101, No.9, 1975,1837-1852

14. Shehata, I.A.E.M. and Regan, P.E. *Punching in R.C. slabs*, Journal of the Structural Division, ASCE, Vol.115, No.7, July 1989, pp.1726-1740.

15. Braestrup, M.W., Nielsen, M.P., Jensen, B.C. and Bach, F. *Axisymmetric Punching of Plain and Reinforced Concrete*, Lyngby, Technical University of Denmark, Structural Research Laboratory, Report No.R75, 1976, pp. 33.

16. Jiang, D.H. and Shen, J.H., *Strength of concrete slabs in punching shear*, Journal of the Structural Division, ASCE, Vol.112, No.12 Dec.1986, pp.2578-2591.

17. Bortolotti, L. *Punching Shear Strength in Concrete Slabs* ACI Structural

Journal, Vol. 87 No.2, March-April 1990, pp.208-219

18. Bazant,Zdenek P., and Cao, Zhiping *Size Effect in Punching Shear Failure of Slabs*, ACI Structural Journal, Vol.84, No.1, Jan.-Feb.1987, pp.44-51.

19. Alexander S. D. B., Simmonds S. H., *Ultimate Strength of Slab-Column Connections*, ACI Structural Journal, May-June 1987

20. Long A. E. and Bond D., *Punching Failure of Reinforced Concrete Slabs*, Proceedings of Institution of Civil Engineers (London), Vol.37, May 1967,pp. 109-135

21. Long A. E., *A Two-Phase Approach to the Prediction of the Punching Strength of Slabs*, ACI Structural Journal, Feb.1975

22. Gesund, Hans, and Dikshit, O. P., *Yield Line Analysis of the Punching Problem at slab/Column Intersections*, Cracking, Deflection, and Ultimate Load of Concrete Slab Systems, ACI SP-30, 1971, pp. 177-201.

23. Yitzhaki,David *Punching Strength of Reinforced Concrete Slabs*, ACI Structural Journal, Proceedings Vol.63, No.5, May 1966, pp.527-542

24. Richart, F. E. and Kluge, R. W., *Tests of Reinforced Concrete Slabs Subjected to Concentrated Loads*, Eng. Expt. Stn. Bulletin 314, University of Illinois, June 1939

25. Elstner, R. C., and Hognestad, E. *Shearing strength of reinforced concrete slabs*, Journal of Prestressed Concrete Institute, Vol.28, No.1,1956, pp.29-57

26. Scordelis, A. C.,et al. *Shearing strength of prestressed lift slab*, Journal of American Concrete Institute, Vol.55, No.32,1958,485-506

27. Moe, J. *Shearing strength of reinforced concrete slabs and footings under concentrated load*, Bulletin D47, Portland Cement Assoc.,1961.

28. Andersson, Jan L.: *Punching of Concrete Slabs with Shear Reinforcement*, Transactions, Royal Institute of Technology, Stockholm , No. 212, 1963, 59 pp.

29. Taylor, R. and Hayes, B. *Some tests on the effect of edge restraint on punching shear in reinforced concrete slabs*, Magazine of Concrete Research, Vol.17, No.50, March 1965, pp.39-44.

30. Mowrer, R.D., and Vanderbilt, M.D. *Shearing Strength of Lightweight Aggregate Reinforced Concrete Flat Plates*, ACI Structural Journal, Proceedings Vol.64, No.11, Nov. 1967,pp.722-729

31. Corley, W.Gene, and Hawkins, Neil MM. *Shearhead Reinforcement for Slabs*, ACI Structural Journal, Proceedings Vol.65, No.10, Oct. 1968,pp.8811-824.

32. Criswell, M.E. *Strength and Behavior of Reinforced Concrete Slab-Column Connections subjected to Static and Dynamic Loadings*, Technical Report N-70 U.S. Army Engineer Waterways Experiment Station Vicksburg, Dec. 1970, 170 pp.

33. Gerber, L. L., and Burns, N. H. *Ultimate strength tests of post-tensioned flat slabs*, Journal of Prestressed Concrete Institute, Vol.16, No.6, 1971,pp.40-58

34. Masterson, D. M. *A Study of the Punching Strength of Reinforced Concrete Flat Slabs*, Thesis presented to Queens University, at Kingston, Ontario, Canada, in 1971, in partial fulfillment of the requirements for the degree of Doctor of Philosophy.

35. Aoki, Y. and Seki, H. *Shearing Strength and Flexural Cracking and Capacity of Two-Way Slabs Subjected to Concentrated Load*, Cracking, Deflection and Ultimate Load of Concrete Slab Systems, ACI SP-30, 1971, pp.103-126.

36. Nylander, H., Kinnunen, S., and Ingvarson, H. *Punching of column-supported slab bridges of concrete with prestressed and non-prestressed reinforcement*, Institution for Byggnadsstatik RTH , Meddelande 123, Stockholm, Sweden (in Swedish), 1977.

37. Kinnunen, S., Nylander, H., and Tolf, P. *Investigations of Punching at the Building Statics Division RTH*, Nordisk Betong, 3, Stockholm, Sweden (in

Swedish), 1978.

38. Shehata, I.A. *Punching of prestressed and nonprestressed reinforced concrete flat slabs*, Thesis presented to the Polytechnic of Central London, at London, U.K., in partial fulfillment of the requirements for the degree of Master of Philosophy,1982.

39. Regan, P.E. *The dependence of punching resistance upon the geometry of the failure surface*, Magazine of Concrete Research, Vol.36, No.126, March 1984, pp.3-8.

40. Regan, P.E. *Symmetric punching of reinforced concrete slabs*, Magazine of Concrete Research, Vol.38, No.136, September 1986. pp.115-128.

41. Narayanan, R. *Punching Shear Tests on Steel-Fibre-Reinforced Micro-Concrete Slabs*, Magazine of Concrete Research, Vol.39, No. 138, Mar. 1987, pp. 42-50.

42. Gardner, N. J. *Relationship of the Punching Shear Capacity of Reinforced Concrete Slabs with Concrete Strength*, ACI Structural Journal, Vol.87, No.1,Jan.-Feb.1990

43. Dragosavic, M., and Van den Reukel, A. *Punching Shear*, Heron (Delft), Vol.20,No.2, 1974, 48 pp.

44. Ngo, D., and Scordelis, A,C. *Finite Element Analysis of Reinforced Concrete Beams*, ACI Structural Journal, Vol.64, No.3,March 1967.

45. A. C. Scordelis *Finite Element Analysis of Reinforced Concrete Structures*, Proceedings of the Specialty Conference on Finite Element Method in Civil Engineering Montreal, Canada, June 1-2, 1972.

46. W. C. Schnobrich *Finite Element Determination of Nonlinear Behavior of Reinforced Concrete Plates and Shells*, Proceedings of the Symposium on Nonlinear Techniques and Behavior in Structural Analysis, Transport and road Research Laboratory, United Kingdom, 1974.

47. W. C. Schnobrich *Behavior of Reinforced Concrete Predicted by Finite Element Method*, Proceedings of Second National Symposium on Computerized Structural Analysis and Design, George Washington University, Washington, D.C., March, 1976.

48. R. Wegner *Finite Element Models for Reinforced Concrete*, Proceedings, U.S. - Germany Symposium on Formulations and Computational Methods in Finite Element Analysis, M.I.T., Boston, August 8-13,1976.

49. *State-of-the-Art Report on Finite Element Analysis of Reinforced Concrete*, Task Committee on Concrete and Masonry Structures, ASCE, April 1982.

50. Christian M. and Hajime O., *Finite Element Analysis of Reinforced Concrete Structures*, Proceedings of Seminar, Sponsored by Japan Society for Promotion of Science and U.S. National Science Foundation. Tokyo, Japan, May 21-24,1986.

51. Masterson, D. M., and Long, A. E. *The Punching Strength of Slabs, A Flexural Approach Using Finite Elements*, Shear in Reinforced Concrete,SP 42, American Concrete Institute, Detroit, 1974, pp. 747-768.

52. de Borst R. and Nauta P. *Non-orthogonal Cracks in a smeared finite element model*, Engng. Computations 2, 1985, pp. 35-46

53. Gonzalez-Vidosa F., Kotsovos M. D. and Pavlovic M. N. *Symmetrical Punching of Reinforced Concrete Slabs: An Analytical Investigation Based on Nonlinear Finite Element Modeling*, ACI Structural Journal, May-June, 1988.

54. Aktan, A. E., and Pecknold, D. A. *Response of a Reinforced Concrete Section to Two-Dimensional Curvature Histories*, ACI Structural Journal, Vol.71, No.5, May, 1974, pp. 246-250.

55. Cedolin, L., Crutzen, Y.R.J., and Poli, S. D. *Triaxial Stress Strain Relationship for concrete*, Journal of Engng. Mech. Div., ASCE, Vol.103, No.3, June, 1977, pp. 423-439.

56. Coon, M. D., and Evans, R. J. *Incremental Constitutive Laws and Their Associated Failure Criteria with Application to Plain Concrete*, Int'l. Journal of Solids and Struct., Vol.8, 1972, pp. 1169-1183.

57. Elwi, A. A., and Murray, D. W., *A 3D Hypoelastic Concrete Constitutive Relationship*, Journal of Engng. Mech. Div., ASCE, Vol.105, No.4, Aug., 1979, pp. 623-641.

58. Ottosen, N. S. *Constitutive Model for Short-Time Loading of Concrete*, Journal of Engng. Mech. Div., ASCE, Vol.105, No.1, Feb., 1979, pp. 127-141.

59. Palaniswamy, R., and Shah, S. P., *Fracture and Stress-Strain Relationship of Concrete Under Triaxial Compression*, Journal of the Struct. Div., ASCE, Vol.100, No.5, May, 1974, pp. 901-916.

60. Buyukozturk, O. *Nonlinear Analysis of Reinforced Concrete Structures*, Computers and Structures, Vol.7, Feb., 1977, pp. 149-156.

61. Chen, A. C. T., and Chen, W. F. *Constitutive Relations for Concrete*, Journal of Engng. Mech. Div., ASCE, Vol.101, No.4, Aug., 1975, pp. 465-481.

62. Chen, A. C. T., and Chen, W. F. *Constitutive Equations and Punch-Indentation of Concrete*, Journal of Engng. Mech. Div., ASCE, Vol.101, No.6, Dec., 1975, pp. 889-906.

63. Murray, D. W., Chitnuyanondh, L., Rijub, A. K. Y., and Wong, C. *Concrete Plasticity Theory for Biaxial Stress Analysis*, Journal of Engng. Mech. Div., ASCE, Vol.105, No.6, Dec., 1979, pp. 989-1006.

64. Bazant, Z. P. and Kim, S. S. *Plastic-Fracturing Theory for Concrete*, Journal of Engng. Mech. Div., ASCE, Vol.105, No.3, June, 1979, pp. 407-428 with Errata in Vol.106

65. Han, D. J. and Chen, W. F. *Strain-Space Plasticity Formulation for Hardening-Softening Materials with Elasto-plastic Coupling*, Int'l. Journal of Solids and Struct., Vol.8, 1972, pp. 1169-1183. Vol.22, No.8, 1986, pp.935-950

66. Bazant, Z. P. *Endochronic Inelasticity and Incremental Plasticity*, Int'l. Journal of Solids and Struct., Vol.14, 1978, pp. 619-714.

67. Bazant, Z. P., and Bhat, P. D. *Endochronic Theory of Inelasticity and Failure of Concrete*, Journal of Engng. Mech. Div., ASCE, Vol.102, No.4, Aug., 1976, pp. 701-722.

68. Bazant, Z. P., and Shieh, C. L. *Endochronic Model for Nonlinear Triaxial Behavior of Concrete*, Nuclear Engng. and Design, Vol.47, 1978, pp.305-315.

69. Bazant, Z. P., and Shieh, C. L., *Hysteretic Fracturing Endochronic Theory for Concrete*, Journal of Engng. Mech. Div., ASCE, Vol.106, No.6, Dec., 1980, pp. 929-950.

70. Valanis, K. C. *A Theory of Viscoplasticity Without a Yield Surface*, Afchiwum Mechanik Stossowanej, Vol. 23, 1971,.pp. 517-551.

71. Crisfield, M. A. *Local Instabilities in the Non-Linear Analysis of Reinforced Concrete Beams and Slabs*, Proc. of the Institutions of Civil Engineers, Part 2, Vol. 73, Mar., 1982, PP. 135-145.

72. Gilbert, r. I., and Warner, R. F. *Tension Stiffening in Reinforced Concrete Slabs*, Journal of Struct. Div., ASCE, Vol.104, No.12,Dec.,1978,pp.1885-1900.

73. Greunen, J. V. *Nonlinear Geometric, Material and Time Dependent Analysis of Reinforced and Prestressed Concrete Slabs and Panels*, Thesis presented to the University of California, Berkeley, Calif., in Oct., 1979, in partial fulfillment of the requirements for the Doctor of Philosophy.

74. Lin, C. S., and Scordelis, A. C. *Nonlinear Analysis of RC Shells of General Form*, Journal of Struct. Div., ASCE, Vol.101, No.3,Mar.,1975,pp.523-538.

75. Jimenz, R., Gergely, P., and White, R. N. *Bond and Dowel Capacities of Reinforced Concrete*, ACI Structural Journal, Vol.76, No.1, Jan.,1979, pp. 73-92.

76. Al-Mahaidi, R. S. H., *Non-Linear Finite Element Analysis of Reinforced*

Concrete Deep Members, Thesis presented to Cornell University, Ithaca, N.Y., 1979, in partial fulfillment of the requirements for the Doctor of Philosophy.

77. Cedolin, L., and Poli, S. D. *Finite Element Studies of Shear Critical Beams*, Journal of Engng. Mech. Div., ASCE, Vol.103, No.3, June,1977, pp.423-440

78. Wischers, G. *Application of Effects of Compressive Loads on Concrete*, Betontechnische Berichte, No. 2 and 3, Duesseldorf, Germany, 1978.

79. Kupfer, H. *Das Verhalten des Betons unter Zweiachsigen Beanspruchung*, Bericht Nr. 18, Lehrstuhl fur Massivbau, Technische Hochschule, Munchen, 1969.

80. Richart, R. E., Brandtzaig, A., and Brown, R. L. *A Study of the Failure of Concrete Under Combined Compressive Stresses*, Engng. Experiment Station, University of Illinois, Bulletin No. 185, 1928, 104 pp.

81. Gerstle, K. H., et al. *Strength of Concrete Under Multi-Axial Stress States*, Proc. of the McHenry Symposium on Conc. and Conc. Structures, ACI SP-55, 1978, pp. 103-131.

82. Chen, W. F., and Saleeb, A. F. *Constitutive Equations for Engineering Materials, Elasticity and Modeling*, Vol.1, 1982

83. Argyris, J. H., Faust, G., Szimmat, J., Warnke, E. P., and Willam, K. J. *Recent Developments in the Finite Element Analysis of Prestressed Concrete Reactor Vessels*, Nuclear Engineering and Design, Vol. 28, 1974, pp. 42-75.

84. Eibl, J., and Ivanyi, G. *Studie zum Traggund Verformungs-verhalten von Stahlbeton* (in German with English summary), Dertsher Auschuss fur Stahlveton, Heft 260, Berlin, 1976.

85. Paul, B. *Macroscopic Criteria for Plastic Flow and Brittle Fracture*, Fracture, an Advanced Treatise, Vol. 2, H. Liebowitz, Editor, academic Press, New York, 1968.

86. Chen, W. F. *Plasticity in reinforced Concrete*, McGraw-Hill Book Company,

Inc., New York, 1981.

87. Drucker, D. C., and Prager, W. *Soil Mechanics and Plastic Analysis or Limit Design*, Quarterly of Applied Mathematics, Vol.X, No.2, 1952, pp. 157-165

88. Bresler, B., and Pister, K. S. *Strength of Concrete Under Combined Stresses*, ACI Structural Journal, Sept. 1958, pp. 321-345

89. Willam K. J., and Warnke, E. P. *Constitutive Models for the Triaxial Behavior of Concrete*, Int'l. Association of Bridge and Structural Engineers Seminar on "Concrete Structures Subjected to Triaxial Stresses," Paper III-1, Bergamo, Italy, May 17-19, 1974, pp.1-30.

90. Reimann, H. *Kritische Spannungszustande der Betons bei mehrachsiger, ruhender Kurzzeitbelastung*, Deutscher Auschuss fur Stahlbeton, Vol.175, Berlin, 1965.

91. Ottosen, N. S. *A Failure Criterion for Concrete*, Journal of Engng. Mech. Div., ASCE, Vol.103, No.4, Aug.1977, 527-535.

92. Han, D. J., Chen, W. F., *Constitutive Modeling in Analysis of Concrete Structures*, Journal of Engng. Mech. Div., ASCE, Vol.113, No.4, April,1987, pp.577-593.

93. Figueiras J.A. and Owen D. R. J. *Analysis of elasto-plastic and geometrically nonlinear anisotropic plates and shells*, Finite Element Software for Plates and Shells, Authors Hinton, E. and Owen, D.R.J., Pineridge Press, Swansea, U.K., 1984, pp.235-326.

94. Owen D. R. J. and Hinton E. *Finite Elements in Plasticity Theory and Practice*, Pineridge Press, Swansea, U.K., 1980, pp. 227-228

95. Rashid, Y. R. *Analysis of Prestressed Concrete Pressure Vessels*, Nuclear Engineering and Design, Vol.7, No.4, Apr.,1968, pp.334-344

96. Lin, C. S., and Scordelis, A. C. *Finite Element Study of a Reinforced Concrete Cylindrical Shell Through Elastic, Cracking, and Ultimate Ranges*, ACI

Structural Journal, Vol.72,Nov.,1975, pp. 628-633

97. Liu, T. C. Y., Nilson, A. H., and Slate, F. O. *Biaxial Stress-Strain Relations for Concrete*, Journal of Structural Div., ASCE, Vol.98, No.5, May.,1972,pp. 1025-1034.

98. Bazant, Z. P., and Cedolin, L. *Blunt Crack Band Propagation in Finite Element Analysis*, Journal of Engng. Mech. Div., ASCE, Vol.105, No.2, April,1987, pp.297-315

99. Bazant, Z. P., and Cedolin, L. *Fracture Mechanics of Reinforced Concrete*, Journal of Engng. Mech. Div., ASCE, Vol.106, No.6, Dec.,1980, pp.1287-1306

100. Bazant, Z. P., and Cedolin, L. *Finite Element Modeling of Crack Band Propagation*, Journal of Structural Div., ASCE, Vol.109, No.1, Jan.,1983, pp.69-92.

101. Fenwick, R. C., Paulay, T. *Mechanics of Shear Resistance of Concrete Beams*, Journal of Structural Div., ASCE, Vol.94, No.10, October 1968, pp. 2325-2350

102. Hamadi, Y. D., Regan, P. E. *Behavior in Shear of Beams with Flexural Cracks*, Magazine of Concrete Research, Vol. 32, No. 111, June 1980, pp.67-78

103. Hand, F. R., Pecknold, D. A. and Schnobrich, W. C. *Nonlinear Layered Analysis of RC Plates and Shells*, Journal of Structural Div., ASCE, Vol.99, No.7, Proc. Paper 9860, July, 1973, pp.1491-1505

104. Ahmad S., Irons B. M. and Zienkiewicz O. C. *Analysis of thick and thin shell structures by curved finite elements*, Int'l. Journal Num. Meth. Eng., Vol.2,1970, pp. 419-451.

105. Zienkiewicz O. C., Taylor R. L. and Too J. M. *Reduced integration technique in general analysis of plates and shells*, Int'l. Journal Num. Meth. Eng., Vol.3,1971, pp. 275-290.

106. Pawsey S. F. and Clough R. W. *Improved numerical integration of thick shell*

finite elements, Int'l. Journal Num. Meth. Eng., Vol.3,1971, pp. 575-586.

107. Pugh E. D. L., Hinton E. and Zienkiewicz O. C. *A study of quadrilateral plate bending elements with reduced integration*, Int'l. Journal Num. Meth. Eng., Vol.12,1978, pp. 1059-1079.

108. Hinton E., Salonen E. M. and Bicanic N. *A study of locking phenomena in isoparametric elements*, Conf.on the Mathematics of F.E. and Applications II, Brunel University, 1975, pp. 436-447.

109. Hughes T. J. R., Cohen M. and Haroun M. *Reduced and selective integration techniques in the finite element analysis of plates*, Nuclear Engineering and Design, Vol. 46, 1978, pp. 203-350.

110. Parisch H. *A critical survey of the 9-node degenerated shell element with special emphasis on thin shell applications and reduced integration*, Comp. Meths. Appl. Mech. Eng., Vol.20, 1979, pp. 323-350.

111. Hughes T. J. R. *Nonlinear finite element analysis of shells: part I, three-dimensional shells*, Comp. Meth. Appl. Mech. Eng., Vol.26, 1981,pp. 331-362.

112. Irons, B. M. *A frontal solution program*, Int'l. Journal Num. Meth. Eng., Vol.2,1970, pp. 5-32.

113. Hinton, E. and Owen, D. R. J. *Finite Element Programming*, Academic Press, London, U.K., 1977

114. Abbasi, M.S.A., Baluch, M.H., Azad, A.K. and Abdel Rahman, H.H. *Nonlinear Finite Element Modelling of Punching in Reinforced Concrete Slabs*, Proceedings of SCI-C 1990, Second International Conference held in Zell Am See, Austria, 4th-6th April,1990, pp. 279-290

115. Abbasi, M.S.A., Baluch, M.H., Azad, A.K. and Abdel Rahman, H.H. *Nonlinear Finite Modelling of Failure Modes in R/C Slabs*, Computers and Structures, To be published.